Thèse en cotutelle avec
l'Université technique d'Iasi (Roumanie) et l'Université de Soochow (Chine)

Vêtement de protection pour femmes enceintes contre les rayonnements non ionisants utilisant un écran électromagnétique en textile, issu de fils hybrides électroconducteurs

Protective garment for pregnant women against non-ionizing radiation using textile electromagnetic-shield, from electroconductive hybrid yarns

Présentée par:

Marzieh JAVADI TOGHCHI

pour obtenir le grade de Docteur de l'Université de Lille

Discipline: Mécanique des solides, des matériaux, des structures et des surfaces

Soutenue le 01/09/2020 devant la commission d'examen

Sébastien PRUVOST	Professeur, INSA Lyon, France	President du jury
Olaru SABINA	Professeur associe, Département de design et d'anthropométrie, Roumanie	Rapporteur
Sébastien PRUVOST	Professeur, INSA Lyon, France	Rapporteur
Antonela CURTEZA	Professeur, l'Université technique d'Iasi, Roumanie	Examinateur
Yan CHEN	Professeur, l'Université de Soochow, Chine	Examinateur
Christine CAMPAGNE	Professeur, ENSAIT, France	Directeur
Carmen LOGHIN	Professeur, l'Université technique d'Iasi, Roumanie	Co- directeur
Pascal BRUNIAUX	Professeur, ENSAIT, France	Invité
Irina CRISTIAN	Professeur associe, l'Université technique d'Iasi, Roumanie	Invité

Declaration

All the work presented henceforth was conducted in the three following laboratories:

GEMTEX, École Nationale Supérieure des Arts et Industries Textiles (ENSAIT), Roubaix, France

Faculty of Textile, Leather and Industrial Management, Gheorghe Asachi Technical University, Iasi, Romania

College of Textile and Clothing Engineering, Soochow University, Suzhou, Jiangsu, China

In the papers contributing to this thesis, the candidate (first author) carried out all the experiments, analysis and preparation of the manuscripts. All other authors contributed by proofreading and providing insight on the discussions.

Publications contributing to this thesis

Journal papers

- Javadi Toghchi, M., Campagne C., Cayla A., Bruniaux, P., Loghin, C., Cristian, I., Burgnies, L., and Chen, Y., Electrical conductivity enhancement of hybrid PA6,6 composite containing multiwall carbon nanotube and carbon black for shielding effectiveness application in textiles, Synthetic Metals, 251 (2019), 75–84.
- Javadi Toghchi, M., Loghin, C., Cristian, I., Campagne C., Bruniaux, P., Cayla A., Lucano, N., and Chen, Y., The effects of the structural parameters of three-dimensional warp interlock woven fabrics with silver-based hybrid yarns on electromagnetic shielding behavior, Textile Research Journal, 90, 11-12 (2020), 1354-1371.
- Javadi Toghchi, M., Bruniaux, P., Campagne C., Cayla A., Loghin, C., Cristian, I., Chen, Y., and Wang, L., Virtual mannequin simulation for customized garment manufacturing, MDPI (Designs), 53-3 (2019).

Conference papers

- Javadi Toghchi, M., Loghin, C., Cristian, I., Campagne, C., Bruniaux, P., and Cayla, A., Investigation of woven characteristics on electromagnetic shielding behavior, IOP Conf. Series: Materials, Science, and Engineering, 374 (2018).
- Javadi Toghchi, M., Loghin, C., Campagne, C., Cristian, I., Bruniaux, P., Ciobanu, L., Cayla, A., Chen, Y., and Wang, L., Thermal resistance and water vapor permeability of compound

woven fabrics containing silver multifilament yarns, IOP Conf. Series: Materials, Science, and Engineering, 572 (2019).

- Javadi Toghchi, M., Campagne, C., Loghin, C., Cristian, I., Bruniaux, P., Cayla, A., Lucano, N., and Chen, Y., Electromagnetic shielding woven fabrics made of multifilament silver coated with PA6,6 and PA6,6-based conductive filament, proceedings of the 5th World Congress on New Technologies (NewTech'19), Lisbon, Portugal (2019).

Academic Awards

- Best Paper Award: 5th World Congress on New Technologies (NewTech), Electromagnetic shielding woven fabrics made of multifilament silver coated with PA6,6 and PA6,6-based conductive filament (2019).
- Silver Award: EuroInvent Conference and Exhibition: Investigation of woven characteristics on electromagnetic shielding behavior (2018).

Acknowledgment

I would like to express my appreciation to my dissertation advisors, Professor Christine Campagne, Professor Pascal Bruniaux, Professor Carmen Loghin, Dr. Aurelie Cayla, Dr. Irina Cristian and Professor Yan Chen who provided me the opportunity to do this research. Thank you all for your support, motivation, trust, and encouragement throughout the duration of this research. This work would not have been possible without your support.

This study was funded by the European Commission through the Erasmus Mundus Joint Doctorate Project entitled "SMDTex (Sustainable Management and Design for Textiles" and was carried out at École Nationale Supérieure des Arts et Industries Textiles, GEMTEX, Roubaix, France, Gheorghe Asachi Technical University, Iasi, Romania, and Soochow University, Suzhou, China. I am thankful to all members of the SMDTex project. It was a privilege to be part of SMDTex.

I also would like to express my gratitude to Professor Xianyi Zeng, coordinator of the SMDTex Program, Dr. Ludovic Burgnies, and Dr. Lamine Kone from IEMN lab of Lille University, Mr. Francois Dassonville and Mr. Frédérick Veyet (ENSAIT), Dr. Nicolae Lucano and Dr. Luminita Ciobanu (Gheorghe Asachi Technical University of Iasi). I also want to appreciate Marie Hombert for administrative support in France.

My thanks also go to all my friends and colleagues namely Arezoo, Marjan, Mina, Sara, Neda, Razieh, Sheenam, Sweta, Nett, Mellisa, Mulat, Balkiss, May, Mahboob, Rayehe, Xiang Yan, Yanni Xu, Yannic, Adeline, Ajinkya, Dorin, Emil, Mihaescu, Mirela, Mihaela and Ana Maria.

I would like to express my deepest gratitude to my parents, Maman Ezat and Baba Jan (Mr. Javadi), and my siblings Mehri, Jafar, Maryam, Mohamad and Alireza for their unconditional love and encouragement.

In the end, I would like to express my deepest appreciation to my beloved husband (Dr. Erfan A Esfahani) for his endless love and support.

To My Loving Family

Abstract

Due to the increasing concern of health issues urged by human exposure to radiation, textiles have been massively considered in the application of ElectroMagnetic Shielding Effectiveness (EMSE). Electrically conductive materials produce and transport free charges which result in shielding behaviour. Thus the first generation of shielding materials has been made of metallic yarns and composites due to the high electrical conductivity of metals. However, these products suffer from poor washability and uncomfortability in place of textile wearable applications.

In this study, a polymer-based conductive monofilament is developed and introduced for making personal wearable protection devices with the purpose of declining the limitations of the traditional shielding fabrics containing metal yarns. Hence, the main contribution of this study is the formulation, production, and characterization of conductive polymer nanocomposite (CPC) monofilaments and the integration of the developed monofilaments into the woven fabrics intended for protecting pregnant women and their fetuses against the detrimental effects of the electromagnetic waves in the human living environment.

To begin with, the effects of the structural parameters of woven fabrics (e.g. weave structures, density of the conductive yarns, and waviness degree of the yarns) were studied on the EMSE behaviour. The results suggested that changing the position of conductive yarns by changing the structural parameters such as waviness degree played a significant role in the EMSE of the woven variants. Specifically, increasing only 7% of the waviness degree of the conductive warps led to 17% EMSE improvement due to the increase of the conductive yarns through the thickness of the 3D warp interlock woven variants.

At this point, the CPC monofilaments were produced containing multiwall carbon nanotube and carbon black incorporated into a thermoplastic polymer (PA6,6) using a melt mixing process and the morphological, electrical, and mechanical properties of the nanocomposites were investigated. The results showed that the electrical conductivity of the PA6,6-based nanocomposite monofilament was improved thanks to the synergism between the carbon nanofillers. In addition, the viscosity was in the standard range for the melt extrusion process. The developed monofilament was lightweight, corrosion-resistant and the manufacturing process was very well established in comparison with metal yarns due to the fact that extrusion is an adaptable and cost-effective method for thermoplastic polymers.

The developed nanocomposite monofilament was integrated into the woven fabric structures and the EMSE of the manufactured woven fabrics was evaluated in the frequency range of 1-10 GHz. The results revealed that the shielding of the fabrics weaved using the developed monofilament was promising for personal protection (EMSE≥10dB). Also, incorporating the monofilaments with higher conductivity or applying a bigger density of conductive monofilaments in the fabric structure led to better attenuation.

Moreover, since the ultimate goal of this research is to shield both mother and fetus against the harmful effects of electromagnetic waves, a parametric graphical method was employed to develop a 3D adaptive mannequin based on weight gain during pregnancy. Lastly, the mannequin was applied to design a block pattern for personalized garment making with the manufactured EMSE woven fabrics.

Keywords: Conductive polymer nanocomposites, Multiwall carbon nanotubes, Carbon black, Synergy effects of carbon nanofillers, Compound woven fabrics, Electrical conductivity, Electromagnetic shielding effectiveness, 3D virtual mannequin for pregnancy period, Garment block pattern

Résumé

En raison de l'inquiétude croissante des problèmes de santé provoqués par l'exposition aux rayonnements, les textiles ont été massivement pris en compte dans les applications de blindage électromagnétique (EMSE). Les matériaux électriquement conducteurs permettent le transport des charges électriques qui entraînent un comportement de blindage. La première génération de matériaux textiles destinés au blindage a été constituée de fils métalliques en raison de la conductivité électrique élevée des métaux. Cependant, ces produits souffrent d'une mauvaise lavabilité et d'un inconfort pour les applications textiles souples.

Dans cette étude, un monofilament conducteur à base de polymère thermoplastique a été développé et tissé pour fabriquer des dispositifs de protection individuels portatifs afin de pallier aux limitations des tissus contenants des fils métalliques. Par conséquent, la contribution majeure de cette étude est la formulation, la production et la caractérisation de monofilaments de nanocomposites polymères conducteurs (CPC). L'intégration des monofilaments développés dans des tissus est destinée à protéger les femmes enceintes et leurs fœtus contre les effets néfastes des ondes électromagnétiques dans la vie de tous les jours.

Dans un premier temps, les effets des paramètres structurels des étoffes tissées (par exemple les armures, la densité des fils conducteurs et l'ondulation des fils) ont été étudiés sur le comportement EMSE. Les résultats suggèrent que le changement de position des fils conducteurs en changeant les paramètres structurels telles que l'ondulation des fils a joué un rôle important dans l'efficacité des échantillons tissés. Plus précisément, l'augmentation de seulement 7% de l'ondulation des fils conducteurs a entraîné une amélioration de 17% de l'EMSE en raison de l'augmentation de la quantité de fils conducteurs dans l'épaisseur des échantillons tissés en 3D.

Des monofilaments CPC contenant des nanotubes de carbone multiparois et du noir de carbone incorporés dans un polymère thermoplastique (PA6,6) ont été produits en utilisant un procédé de mélange à l'état fondu (extrusion). De plus, les propriétés morphologiques, électriques et mécaniques des nanocomposites ont été étudiées.

Les résultats ont montré que la conductivité électrique du monofilament nanocomposite à base de PA6,6 était améliorée grâce à la synergie entre les nanocharges carbonées. De plus, la viscosité était dans la plage standard pour le processus d'extrusion à l'état fondu. Le monofilament développé était plus léger, et résistant à la corrosion que les fils métalliques, avec un procédé de mise ne œuvre standard pour les filaments textiles.

Le monofilament nanocomposite développé a été intégré dans les structures de tissu tissé et l'EMSE des tissus fabriqués a été évaluée dans la gamme de fréquences de 1-10 GHz. Les résultats ont révélé que le blindage des tissus à l'aide du monofilament développé était prometteur pour la protection individuelle (EMSE≥10dB). De plus, l'incorporation des monofilaments avec une conductivité plus élevée ou l'application d'une plus grande densité de monofilaments conducteurs dans la structure du tissu a conduit à une meilleure atténuation.

De plus, puisque le but ultime de cette recherche est de protéger la mère et le fœtus contre les effets nocifs des ondes électromagnétiques, une méthode graphique paramétrique a été utilisée pour développer un mannequin adaptatif 3D basé sur la tendance à la prise de poids pendant la grossesse. Enfin, le mannequin a été appliqué pour concevoir un motif en bloc pour la confection de vêtements personnalisés avec les tissus EMSE fabriqués.

Mots clés: Nanocomposites polymères conducteurs, Nanotubes de carbone à multiparois, Noir de carbone, Effet de synergie des nanocharges de carbone, Tissage 3D,, Conductivité électrique, Efficacité du blindage électromagnétique, Mannequin virtuel 3D pour la période de grossesse, Modèle de bloc de vêtement

Rezumat

Datorită preocupărilor crescute privind problemelor de sănătate cauzate de expunerea umană la radiații, în ultimii ani s-au propus numeroase soluții textile cu eficacitate a ecranării electromagnetice (EMSE). Materialele electro-conductive produc și conduc sarcini libere, ceea ce le conferă proprietăți de ecranare electromagnetică.Prima generație de materiale textile de ecranare a fost realizată din fire metalice și compozite, datorită conductivității electrice ridicate a metalelor. Acest tip de produse sunt greu lavabile și incomode, ceea ce le fac neadecvate pentru utilizarea ca îmbrăcăminte.

În acest studiu, a fost propus și dezvoltat un monofilament conductiv pe bază de polimeri pentru realizarea imbracamintei de protecție, cu scopul de a depăși limitările materialelor textile clasice de ecranare, care conțin fire metalice. Prin urmare, contribuția principală a acestui studiu este formularea, producerea și caracterizarea unor monofilamente din materiale compozite polimerice conductive (CPC) și integrarea acestora în materiale țesute destinate protejării femeilor însărcinate și a fetușilor împotriva efectelor dăunătoare ale undelor electromagnetice prezente în mediile de viață ale oamenilor.

În primă fază au fost studiate efectele parametrilor structurali ai țesăturilor (de exemplu legătura, densimea firelor conductive, contracția firelor) asupra comportamentului EMSE. Rezultatele au sugerat că schimbarea poziției firelor conductive prin modificarea parametrilor structurali, cum ar fi gradul de undulare a firelor, a jucat un rol semnificativ în EMSE-ul variantelor țesute. Mai exact, o creștere cu doar 7% a contracției firelor de urzeală conductive a dus la o îmbunătățire a EMSE de 17%, datorită creșterii poziționării firelor conductive pe direcție verticală în varianta țesută 3D warp interlock.

În etapa următoare, monofilamente CPC au fost produse prin încorporarea de nanotuburi de carbon cu pereți multipli și nanoparticule de negru de fum într-un polimer termoplastic (poliamidă PA6,6) folosind un proces de topire și amestecare, după care au fost cercetate proprietățile morfologice, electrice și mecanice ale nanocompozitelor.

Rezultatele au arătat o îmbunătățire a conductivitatății electrice a nanocompozitului bazat pe PA6,6 datorită sinergiei dintre nanoparticulele de carbon. În plus, vâscozitatea soluției de amestec obținute s-a încadrat în intervalul standard pentru procesul de extrudare prin topire. Monofilamentul realizat are masă redusă, est rezistent la coroziune, iar procesul de fabricație este

mai facil în comparație cu cel pentru fire metalice, datorită faptului că extrudarea este o metodă ușor adaptabilă și rentabilă pentru producerea polimerilor termoplastici.

Monofilamentul de nanocompozit dezvoltat a fost integrat în structuri țesute și EMSE-ul țesăturilor fabricate a fost evaluat în intervalul de frecvență de 1-10 GHz. Rezultatele au arătat faptul că proprietatea de ecranare a materialelor produse folosind monofilamentul dezvoltat a fost promițătoare pentru protecția personală (EMSE≥10dB). De asemenea, încorporarea monofilamentelor cu o conductivitate mai mare și creșterea desimii monofilamentelor conductive din țesătură au determinat o atenuare mai bună.

Mai mult, având în vedere că scopul final al acestei cercetări este protejarea, atât a mamei cât și a fetusului, împotriva efectelor nocive ale undelor electromagnetice, a fost utilizată o metodă parametrică grafică pentru a dezvolta un manechin adaptiv 3D bazat pe creșterea în greutate din timpul sarcinii. În cele din urmă, manechinul a fost folosit pentru proiectarea unui tiparelor pentru confecționarea personalizată a articolelor de îmbrăcăminte cu țesăturile EMSE fabricate.

Cuvinte cheie: nanocompozite polimerice conductive, nanotuburi de carbon cu pereți multipli, negru de fum, efectul sinergic al nanoparticulelor de carbon, țesături compuse, conductivitate electrică, eficacitatea ecranării electromagnetice, manechin virtual 3D pentru perioada de sarcină, tipare pentru îmbrăcăminte

导电复合纱织物的电磁辐射防护孕妇服装研究

摘 要

由于人们对辐射引起的健康问题的日益关注，纺织品在电磁屏蔽效能（EMSE）方面的应用得到了广泛的重视。导电材料能够产生和传输自由电荷，从而产生屏蔽功能。由于金属材料具有优良的导电性，第一代屏蔽材料就是由金属丝和复合材料制成。然而，这些产品的耐水洗性差，不适于纺织服装的应用。

为了克服传统金属丝加工的屏蔽织物的不足之处，本研究开发了一种聚合物基导电单丝，并将其应用于制作个人穿戴防护装置。这项研究的主要贡献包括导电聚合物纳米复合材料（CPC）单丝的配方、生产、特性，以及将所开发的单丝集成到用于保护孕妇及其胎儿免受人类生活环境中电磁波有害影响的织物之中。

首先，研究了机织物结构参数（包括组织结构、导电纱密度、纱线屈曲波）对电磁屏蔽效能EMSE的影响。研究结果表明，通过改变织物的屈曲波等结构参数来改变导电纱的位置，对织物变形后的电磁屏蔽效能EMSE起着重要的影响作用。具体地说，只增加7%的导电纱线屈曲波，就能够导致电磁屏蔽效能EMSE提高17%，这是由于导电经线三维交织时屈曲波高度增加，可以达到增加厚度的目的。

本研究中，制备了含有多层碳纳米管和炭黑的CPC单丝，利用熔融混合工艺将碳黑材料与热塑性高聚物（PA6，6）相结合，并对纳米复合材料的形态、电学性能和机械性能进行了研究。

结果表明，由于碳纳米填料之间的协同作用，热塑性高聚物（PA6，6）基纳米复合单丝的导电性有所提高。此外，熔体挤出过程中的粘度也在标准范围内。由于挤出是一种适用于热塑性聚合物且成本效益高的方法，因此，所开发的单丝具有轻质、耐腐蚀的特点，并且与金属丝相比，其制造工艺非常成熟。

将研制的纳米复合单丝加工到机织物中，在1-10GHz频率范围内对所制机织物的电磁屏蔽效能EMSE进行了评价。结果表明，用该单丝制织的织物具有良好的屏蔽性能（EMSE≥10dB）。此外，在织物结构中加入导电率较高的单丝或提高导电单丝的密度，可是电磁辐射强度得到更大程度的衰减。

此外，由于本研究的最终目标是保护母亲和胎儿免受电磁波的有害影响，因此采用参数化制图方法开发了一种基于孕期体重增长趋势的三维自适应人体模型，并将该人体模型应用于电磁辐射防护机织物的个性化成衣设计中。

关键词：导电聚合物纳米复合材料，多层碳纳米管，炭黑，纳米碳填料的协同效应，复合机织物，导电性，电磁屏蔽效果，妊娠期三维虚拟人体模型，服装样板原型

Table of content

List of figures

List of tables

List of Abbreviations

ABS	Acrylonitrile butadiene styrene
BD	Binding depth
CAD	Computer aided deisgn
CB	Carbon black
CF	Cover factor
CNF	Carbon nanofiber
GNP	Graphene Nano plate
CNT	Carbon nanotube
CPC	Conductive polymer nanocomposite
dB	Decibel
DL	Double layer
EMSE	Electromagnetic shielding effectiveness
FDM	Fused deposition modeling
GHz	Gigahertz
GNS	Graphene Nanosheet
ICP	Intrinsic conductive polymer
IR	Infrared
KB	Ketjenblack
MFI	Melt flow index
MHz	Megahertz
MWCNT	Multiwall carbon nanotube
N_m	Metric number
PA	Polyamides
PANI	Polyaniline
PA6,6	Polyamide 6,6
PBT	Polybutylene terephthalate
PE	Polyethylene
PET	Polyethylene terephthalate
PLA	Polylactic acid

PMMA	Polymethyl methacrylate
POM	Polyoxymethylene
PP	Polypropylene
PPS	Polyphenylene sulfide
Ppy	Polypyrrole
RF	Radio frequency
SE	Shielding effectiveness
SWCNT	Single wall carbon nanotube
TEM	Transverse electromagnetic cell method
TEM	Transmission electron microscopy
UV	Ultraviolet
2w	4-wire ohms measurement
4w	2-wire ohms measurement

Introduction

The concern about health issues caused by human exposure to radiation has been currently increased due to the fact that electrical devices (e.g. cell phones and microwave ovens) are commonly used all over the world. As a matter of fact, electromagnetic waves which are emitted by the electrical devices have harmful effects on the human body [1], [2].

The magnitude of the damage on the human body depends on the frequency, intensity, and polarization of electromagnetic waves. For example, ionizing electromagnetic waves (e.g. X-rays and Gamma rays) contains sufficient electromagnetic energy to strip atoms and molecules from body tissues and changes the biochemical reactions in the body.

In contrast, the energy of non-ionizing electromagnetic waves is below the required extent for effects at the atomic level. The specific long-term effects resulting from extensive exposure to non-ionizing radiation are not completely clear at the moment although the body temperature rise is generated by exposure to non-ionizing electromagnetic waves.

However, a number of studies suggested potential health hazards that are linked to the exposure to the non-ionizing radiation. For instance, the effects of mobile phone use on the central nervous system, increasing the skin surface temperature during mobile phone use, and the absorption rate of the electromagnetic field in the vicinity of mobile phone base stations were reviewed by numerous studies [3]–[7]. In addition, the effects of electromagnetic waves have been extensively investigated on the body organs of rats in order to examine the impacts of electromagnetic waves on a living organism [8]–[11].

Moreover, there is a major concern that fetuses and children are more vulnerable than adults to the potential influences of exposure to radiation given the rapid development of neurological and organ systems in early life and the extended impacts over the entire lifetime [12]–[17]. Thus, it is of great importance to protect the pregnant women and their fetuses against likely hazards caused by non-ionizing electromagnetic waves emitted in our living environment in the direction of ensuring a healthier society.

Major efforts have been put forward in the last few years to make electromagnetic shielding effectiveness textiles aimed at different frequency ranges due to the above-mentioned issues caused by human exposure to the electromagnetic waves. It is noted that the electrically conductive materials (e.g. metals) generate and transport free charges which lead to electromagnetic shielding effectiveness.

In the beginning, metallic composites and yarns were used for developing electromagnetic shielding behaviour in the textiles industry. However, the usage of traditional metallic composites and yarns is limited for electromagnetic shielding textiles because of high density (heavyweight), poor mechanical flexibility, and corrosiveness of metals together with expensive processing costs. Also, it is noted that polymer-based materials are broadly found in our daily life, mostly due to reasonably low cost, lightweight, flexibility, and corrosion resistance of polymers while functional polymers advanced providing countless high-value products, for example, antibacterial, reinforcing structures, electromagnetic shielding effectiveness, etc.

Therefore, hereafter, the shielding materials and textiles are principally concentrated on using carbons as the conductive component in the polymeric nanocomposites due to the fact that conductive polymer nanocomposites (CPCs) are mostly lightweight and corrosion-resistant and their manufacturing process is very well established in comparison with metal yarns (e.g. applying the melt mixing method as an adaptable, cost-effective, and environmentally friendly technique) [18].

The main objective of this thesis was to make a scalable wearable device designed for the pregnancy period for shielding against electromagnetic waves in the human living environment. Accordingly, this thesis focused on making a novel conductive thermoplastic monofilament with the potential of mass customization for electromagnetic shielding textile applications. A suitable candidate was suggested in consideration of the required electromagnetic shielding effectiveness performance, monofilament uniformity and acceptable viscosity of the nanocomposite for the monofilament making process using melt extrusion technique.

Thesis framework

This project has been comprehended in the framework of Erasmus Mundus joint doctorate project as a part of SMDTex (sustainable management and design for textiles) program. The thesis work was carried out at three different universities, ENSAIT- GEMTEX, France; Gheorghe Asachi Technical University of Iasi, Romania and Soochow University, China in a period of 48 months.

One of the objectives of this work was to determine the effects of woven characteristics on the shielding performance of the fabrics. Another main objective was to develop a new hybrid electroconductive nanocomposite monofilament using carbon nanofillers with the aim of optimizing the loading of the nanofillers. In addition, the developed hybrid yarn was used to manufacture an electromagnetic shielding woven fabric intended for personal protective clothing during pregnancy period.

The Ph.D. thesis is structured into five different chapters as below:

Chapter 1 deals with the state of the art, the theme of the thesis and covers a comprehensive review of the relevant literature. This chapter presents electromagnetic shielding effectiveness theory and reviews the completed studies of the shielding textiles while the solutions, scope, and limitations of using different electrically conductive materials are described. Also, it presents the proposed strategy to justify the ideas and goals of the thesis.

Chapter 2 presents the effects of structural parameters of the woven fabrics using commercial metal yarns on the performance of the fabrics designed for electromagnetic shielding effectiveness. Details of the materials, manufacturing process and shielding measurements are discussed. The main objective was to clarify in what way fabric properties have effects on the level of protection against radiation.

Chapter 3 introduces an electrically conductive polymer-based monofilament for the reason that conductive polymer nanocomposites (CPCs) are commonly lightweight, corrosion-resistant, and the manufacturing process is well established compared to metal yarns. The morphological and electrical characterizations of the CPCs and the shielding of the developed woven fabrics are also deliberated in a specific frequency range in this chapter.

Chapter 4 presents a 3D virtual mannequin making for pregnancy period intended for electromagnetic shielding garment design with the aim of protecting mothers and fetuses against radiation.

In the last chapter, the general conclusions and contributions of the thesis based on the results and discussions in the above-mentioned chapters are presented. To finish, potential future research directions that would need further investigation are outlined.

Chapter 1: State of the art

This chapter talks about electromagnetic shielding effectiveness theory and completes a review of electromagnetic shielding effectiveness characteristics, measurements, and previous studies of the electromagnetic shielding effectiveness textiles using a range of electrically conductive materials (e.g. metals, intrinsic conductive polymers, and carbon fillers).

Metallic composites and yarns are traditional materials which are used for electromagnetic shielding applications in textiles. However, metals characteristics including high density, poor flexibility, corrosiveness, and expensive processing cost limit the usage of metals for electromagnetic shielding applications.

Alternatively, polymer-based composites are a class of engineering materials containing a blend of two or more components to produce a multiphase system with different properties from the components and they have been extensively used in textile industry for different functions and applications.

For instance, carbon-filled polymer nanocomposites which are known as conductive polymer nanocomposites (CPCs) consist of conductive carbon nanofillers in polymer matrices with the aim of mechanical and electrical properties improvement of the polymer matrix for different applications (e.g. heating textile, electromagnetic shielding applications, etc.).

Carbon nanotube (CNT) including single wall carbon nanotube (SWCNT) and multiwall carbon nanotube (MWCNT) as well as carbon black (CB) have been mostly used as electrically conductive nanofillers in CPCs generating due to the electrical conductivity enhancement in a polymer matrix at low nanofiller content. Accordingly, a summary of completed studies on electrically conductive textiles development using polymer-based nanocomposites filled with carbon nanofillers for different applications including electromagnetic shielding effectiveness is deliberated in the following chapter.

1.1 Electromagnetic shielding effectiveness characteristics and measurement methods

1.1.1 The electromagnetic waves definition

Electromagnetic waves consist of oscillating magnetic field and electric field while the electric field and magnetic field of an electromagnetic wave are at right angles to each other and both are perpendicular to the direction of the electromagnetic wave [19].

These days, electrical devices such as cell phones, microwave ovens, wireless routers, televisions, etc. are used all around the world. These electrical devices emit electromagnetic waves into our living environment. There are two main categories of electromagnetic waves based on the frequency ranges (ionizing and non-ionizing electromagnetic waves) as specified in Figure 1-1 [20].

Ionizing and non-ionizing electromagnetic waves have diverse and unequal effects on human body due to the dissimilar performance of the electromagnetic waves at different frequency from low frequency through radio frequency (RF) and microwaves, to Infrared (IR) light, visible light, ultraviolet (UV) light, X-rays, and Gamma rays.

In recent decades, the concern about health issues caused by human exposure to radiation such as a headache, fatigue, and cancer has been increased [1]–[6]. It should be taken into consideration that fetuses are at higher risk in confronting with the detrimental effects of electromagnetic waves. The reason is correlated to the rapid development of neurological and organ systems in early stage of fetus life [16], [17].

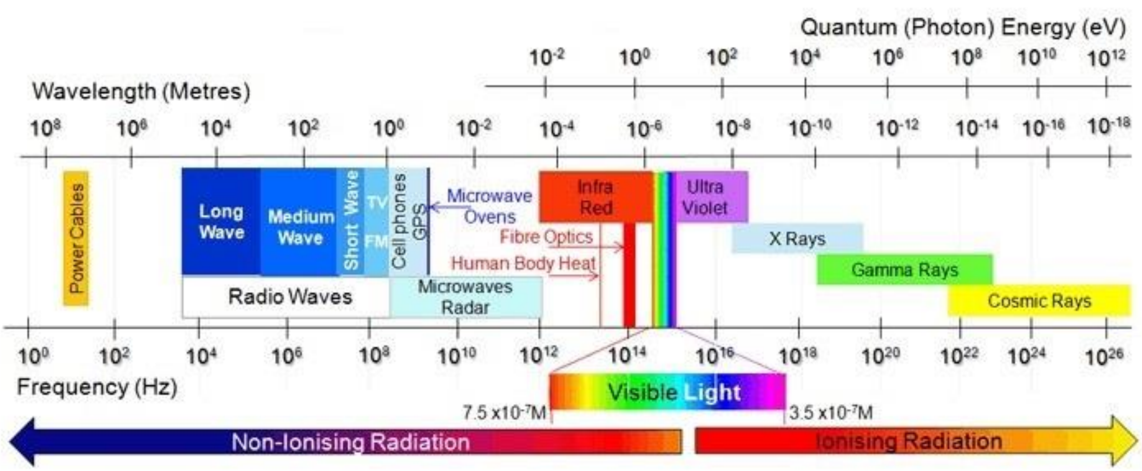

Figure 1-1- Electromagnetic radiation spectrum [20]

1.1.2 Electromagnetic shielding effectiveness theory

The electromagnetic shielding effectiveness (EMSE) can be outlined as the ratio of the energy impinging on a side of the shield to the transmitted energy out the other side. Absorption and reflection occur when an electromagnetic wave passes through a shield and the remaining energy is the energy that emerges out from the shield [19], [21]–[23].

The EMSE is identified in terms of reduction in an electric field (E), magnetic field (H) or plane-wave strength (P) by applying shielding materials. Consequently, EMSE is expressed in decibels (dB) as a function of the logarithmic ratio of the electric, magnetic or plane-wave strength before (E_i, H_i or P_i) and after (E_t, H_t or P_t) attenuation, (equation (1)).

$$\mathrm{EMSE(dB)} = 20\log\frac{E_t}{E_i} = 20\log\frac{H_t}{H_i} = 10\log\frac{P_t}{P_i} \tag{1}$$

1.1.2.1 The correlation between electrical conductivity and electromagnetic shielding effectiveness

Generally speaking, electrically conductive materials generate and transport free charges which lead to EMSE behavior. The electromagnetic shield material attenuates the transmission of electromagnetic waves from one region to another using movable charge carriers (electrons or holes), or electric and magnetic dipoles [24], [25].

The electromagnetic shielding mechanism is strongly associated with the characteristic of the attenuator or shield material where there are three shielding mechanisms by reflection (SE_R), absorption (SE_A), and internal or multiple-reflection (SE_M) as indicated in Figure 1-2. It should be noted that the total electromagnetic shielding effectiveness is the accumulation of the shielding of three different mechanisms as shown in equation (2) [25].

$$\mathrm{EMSE\ (dB)} = SE_R + SE_A + SE_M \tag{2}$$

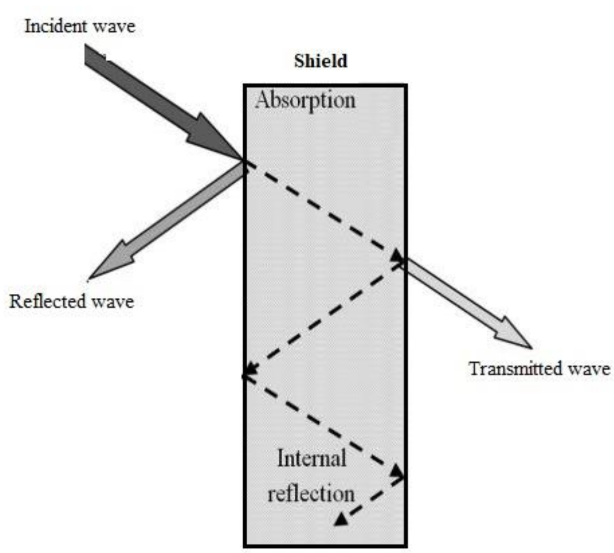

Figure 1-2- Multiple mechanisms which contribute to the attenuation of an incident field [11]

The mobile charge carries interaction with the electromagnetic wave of the shielding material leads to a shielding reflection mechanism (SE_R). In addition, the absorption mechanism (SE_A) occurs when the material has electric and/or magnetic dipoles of the shielding material interact with the electromagnetic field. As a result, absorption arises for materials with high dielectric constant or high magnetic permeability. Also, the multiple-reflection mechanism transpires if the electromagnetic wave reflects from the second inner boundary to the first reflected back and forth within the material. It should be noted that the multi-reflection mechanism is generally negligible and can be ignored when $SE_A \geq 10$ dB.

The SE_R and SE_A can be calculated according to equations (3) and (4) which was suggested by Al-Saleh and Sundararaj [26] where f is the frequency of radiation (Hz), μ is the magnetic permeability of the shield (H/m), σ shows the electrical conductivity (S/m), δ is the skin depth and t is the thickness of the shielding material (m). It should be noted that $\mu=\mu_0\mu_r$ when μ_0 is the permeability of vacuum and μ_r is equal to 1 for carbon-based materials.

$$SE_R = 10\log\left(\frac{\sigma}{2\pi f\mu}\right) + 39.5 \quad (3)$$

$$SE_A = 8.7\frac{t}{\delta} \quad , \; \delta = \frac{1}{\sqrt{\pi f\mu\sigma}} \quad (4)$$

EMSE can be defined experimentally by measuring the amount of power of a reflected (R) or transmitted (T) incident radiation using complex scattering parameters. As a result, the absorbed radiation (A) can be calculated using equation (5) when the incident radiation power is 1 milliwatt. Finally, the EMSE by reflection and absorption mechanisms are defined as given in equation (6) and equation (7) considering the experimental data coefficients of R and T [24]–[28]. Consequently, the EMSE is determined using equation (8) which is the same as equation (1).

$$I=1=R+T+A \quad (5)$$

$$SE_R = 10\log\left(\frac{I}{I-R}\right) \quad (6)$$

$$SE_A = 10\log\left(\frac{I-R}{T}\right) \quad (7)$$

$$EMSE = SE_R + SE_A = 20\log\left(\frac{I}{T}\right) \quad (8)$$

1.1.3 Electromagnetic shielding effectiveness measurement methods

A number of techniques have been established and used by different studies to evaluate the EMSE of planar structures (e.g. fabrics) [29]–[38]. However, different methods of EMSE measurements produce dissimilar performance values which are generally hard to correlate with one another [39]. Some of the common EMSE methods are concisely discussed in the following.

1.1.3.1 Transverse electromagnetic cell method with a circular coaxial holder

Transverse electromagnetic cell method (TEM) with circular coaxial holder for measuring the EMSE of planar materials was primarily developed and published in standard ASTM D4935 when the continuous conductor version is an expanded 50Ω coaxial transmission line [29]. The proposed method is still used to measure the EMSE of planar materials for a plane-wave although this method is no longer a formal standard. A schematic of the EMSE measurement setup based on standard ASTM D4935 is presented in Figure 1-3.

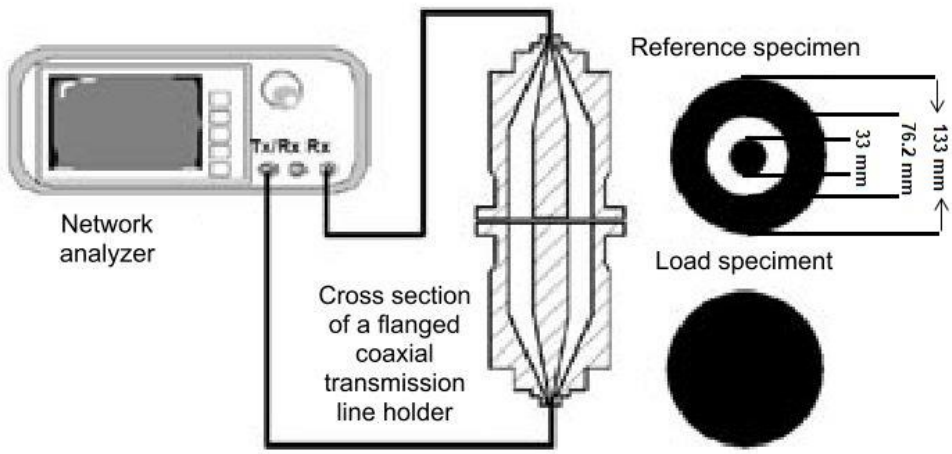

Figure 1-3- Schematic of the EMSE measurement setup based on standard ASTM D4935 [29], [31]

First, a reference sample is located in the test adapter in order to consider the cable losses and the coupling capacitance. Second, the sample of a shield planar material is placed in the test adapter and the logarithmic ratio of these two measurements introduces the EMSE of the shield specimen in dB as presented in equation (1). It should be taken into consideration that the thickness of the specimen should be smaller than 1/100 of the wavelength of the required electromagnetic waves for the EMSE measurement. This method has been applied by several studies to measure the ESME of textile materials [30], [40]–[47].

This measurement setup applies for a frequency range of 30 MHz to 1.5 GHz while it can be applied to measure the EMSE at a lower frequency range or higher frequency range. However, the limitation of the frequency range is based on reducing displacement current as a result of decreased capacitive coupling at lower frequency range or because of the induction of higher order modes in higher frequency which states that the field inside the test adapter is no longer a TEM wave for a specific specimen size.

Also, dual-TEM is a modified TEM method while two cells are linked together for EMSE measurement when they are coupled through an opening in the common wall [39], [48]. However, the frequency range for the dual-TEM method is between 1 and 200 (MHz).

1.1.3.2 MIL-STD-285 standard and the modified methods

The MIL-STD-285 standard method was initially established by the American military standard in 1956 for EMSE measurements [49]. A number of improved methods according to this standard have been developed although the standard was withdrawn years ago. The measuring setup based on this standard includes two screened rooms with one common wall while this wall has an aperture for the sample insertion as shown in Figure 1-4 [31], [39], [48].

This standard is the most common referenced for EMSE measurements in the frequency between a few MHz to 10 GHz [31]. The transmitting and receiving antennas are directed toward one another and are at a specified distance from each other. The receiver antenna measures the transferred power with and without the sample in the opening on the common wall and the EMSE is obtained by the logarithmic ratio between these two measurements. The main negative point of this method is that the measurement is dependent on the antenna distance from the wall along with the reflections of the electromagnetic wave inside the shielded enclosure.

The EMSE measurement method according to standard MIL-STD-285 was replaced by a revised version in order to reduce the complications of the reflections caused by absorbing material in the shielded rooms and as a result, the frequency range extended to 100 GHz [41].

It should be noted that an anechoic chamber has been employed to measure the EMSE of the textile planar materials like fabrics by a number of studies which work according to the standard MIL-STD-285 modified methods [30], [34], [35], [50], [51]. However, such electromagnetic measurements are dependent on the wave polarization and can be different from EMSE in a realistic electromagnetic environment.

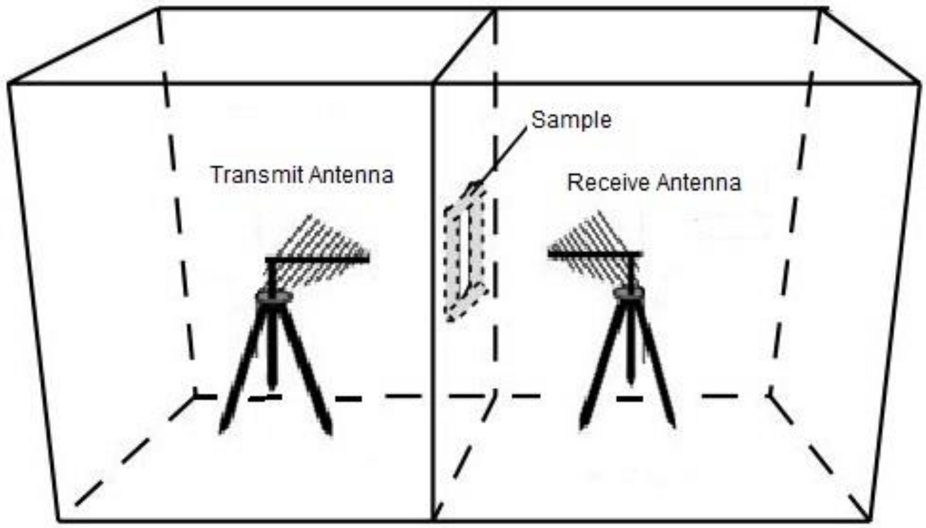

Figure 1-4- The EMSE measurement setup according to the standard MIL-STD-285 [48]

1.1.3.3 Mode-stirred chamber method

The mode-stirred chamber is an alternative method that allows having a better evaluation of the EMSE in a realistic electromagnetic environment, and it is commonly considered by the electromagnetic compatibility community [42].

The dual mode-stirred chamber method was established by the national institute of standards and technology (NIST) of the United States when it includes two mode-stirred chambers next to each other having a common wall with an aperture for sample insertion [52], [53]. A mode stirring arrangement was applied in a shielded enclosure in the dual mode-stirred chamber method to generate electromagnetic fields with a specified number of modes within the chamber [48].

In this method, the placement of antennas is not a critical issue although this method needs equipment to control the mode stirring which can be expensive. The lowest frequency of this method depends on the smallest size of the mode-stirred chambers. In other words, the smallest distance inside a chamber should be seven times the wavelength of the lowest frequency which is almost 500 MHz as reported by related studies [39], [48].

Also, a simple sketch of the nested mode-stirred chamber for shielding effectiveness measurement based on standard IEC61000-4-21 is represented in Figure 1-5 [36]–[38], [54]–[58]. The mode-stirred chamber allows evaluating the EMSE in a realistic electromagnetic environment where the wave polarization cannot be controlled. Specific electromagnetic environment results from the characteristics of the reverberation chamber, stirrers, and antennas, and a statistical study of field arrangement in the chamber produced by different positions of the stirrer.

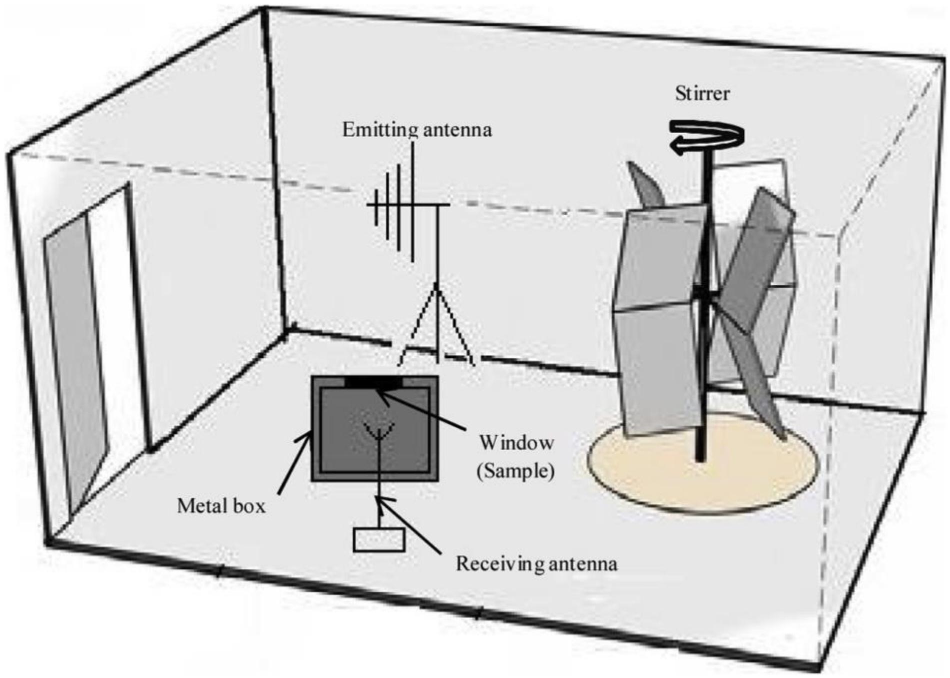

Figure 1-5- Schematic of the mode-stirred chamber for EMSE measurements [59]

The experimental EMSE setup in a reverberation mode-stirred chamber includes an emitting antenna and a mode-stirrer producing the external ambient electromagnetic energy around a closed region formed by a metallic box. On one side of the box, only a window allows to couple a receiving antenna to the ambient electromagnetic energy. The sample under test is introduced in front of the window and the transmitted power to the receiving antenna is measured and the mean value of all the introduced angles is calculated. The EMSE is the ratio of this mean value to the calculated mean value of the EMSE measurement of one complete turn (360 degrees) without sample as a reference measure. It should be taken into consideration that all the wave polarizations can be considered for the measurement thanks to the stirrer rotation.

Furthermore, there are some other methods to evaluate the EMSE of materials which are not widely used (e.g. dual-chamber test fixture (ASTM ES7-83) and free space method) due to the lack of accuracy of the measurement or the frequency range limit [41], [42], [48], [60].

It is concluded that measured values of EMSE in a mode-stirred chamber are close to the values in a realistic electromagnetic environment by averaging the field measured in several stirrer positions corresponding to a large number of field configurations and polarization.

On the other hand, line-of-sight characterization achieved by measurements in an anechoic chamber describes the transmission of the wave through the sample, and it strongly depends on wave polarization and the incidence of the impinging waves. Moreover, methods based on coaxial TEM cells have been experimentally validated in the low frequency range. The wider frequency range can be used by lowering the TEM cell dimensions but in this case, the sample size should be smaller and the mechanical processing could be difficult.

To sum up, all the aforementioned methods can be used for the EMSE measurements of fabrics with regard to the frequency range and types or dimensions of shield materials. Anechoic and mode-stirred chambers are two approaches utilized for EMSE measurements in the present thesis due to the targeted frequency ranges. It is also noted that the measurement in the mode-stirred chamber gives a realistic electromagnetic environment where the wave polarization cannot be controlled (e.g. the human living environments).

1.2 Electromagnetic shielding effectiveness textiles

Textiles have been broadly considered in the applications of electromagnetic shielding effectiveness (EMSE). As explained earlier, electromagnetic shielding effectiveness (EMSE) can be performed using electrically conductive materials to protect the human body against the detrimental effects of electromagnetic waves as the electrically conductive materials can generate and transport free charges which lead to electromagnetic shielding effectiveness [23], [61].

It should be taken into consideration that more often than not, textiles are not intrinsically electrical conductive materials. Therefore, there are various systems to enhance the electrical conductivity for electromagnetic shielding effectiveness applications.

A large number of studies related to the manufacturing of electrical conductive fabrics for EMSE applications have been completed at different frequency ranges. Metals, intrinsic conductive polymers (ICPs), and carbons are three main electrical conductive categories of materials which have been widely used with the purpose of electrically conductive development using different processes for different functions and applications in textiles (e.g. electromagnetic shielding effectiveness).

1.2.1 Electromagnetic shielding textiles using metals as conductive material

One of the widespread techniques for electrical conductivity enhancement in textiles is to coat the surface of textiles with metal layers. In addition, electrical conductivity can be enhanced by integrating metal yarns or fibers inside the fabric structures. There are three main fabric making methods, weaving, knitting, and nonwoven fabric making process when all can be applied to manufacture electrically conductive fabrics for EMSE applications.

It is noted that fabric making methods and characteristics could alter the EMSE of the fabrics and that's is the reason that different fabric making processes have been applied for EMSE development aimed at different frequencies.

1.2.1.1 Commercial textile products

A large number of commercial EMSE textiles have been industrialized to protect the human body or sensitive devices against radiation. Metals (e.g. copper, silver, nickel, and stainless steel) have been widely used for making EMSE commercial textile products due to the high electrical conductivity of metals [62], [63].

For example, FlecTron® is a copper-plated nylon woven fabric with a low surface resistivity while it is recommended to be applied for making shielded enclosures or clothing. Also, FlecTron®-N (Figure 1-6) is another commercial EMSE fabric that has superior tarnish resistance owing to the addition of nickel to the fabric. However, nickel causes skin allergies and cannot be used in direct contact with the human skin [64],[65].

Figure 1-6- FlecTron®-N [64]

In addition, Shieldit® (given in Figure 1-7) is rugged plain weave nylon plated with tin and copper for excellent electromagnetic shielding properties. This fabric is coated with conductive acrylic on one side of the fabric and a hot melt adhesive with polyethylene barrier on another side of the fabric for better washability. It is been stated that the EMSE of this fabric is 80 dB at 100 MHz with the targeted application of shielding the extension cords and computer cables. However, this fabric doesn't breathe well and it can cause skin irritation as a result of plastic coatings which make it inapplicable for clothing applications [62], [64].

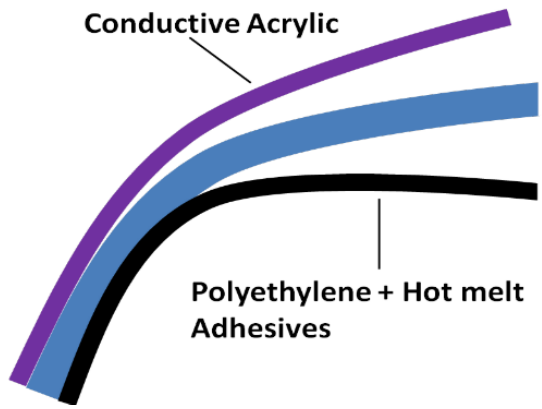

Figure 1-7- Shieldit® fabric structure [64]

As a final point, these products suffer from some weaknesses like heavy weight due to the high density of metals, expensive and uneconomic production processing, inflexibility; poor washability, poor breathability, oxidation or mechanical abrasion.

Therefore, in recent decades, it has been tried to overcome the limitations and difficulties of the available commercial products by proposing better alternatives for EMSE applications.

1.2.1.2 Metal coating on the textile surface

Metals were initially used for decorative purposes in textile industry. Afterward, they have been extensively used due to the high electrical conductivity since the vapor deposition techniques development started in the 1960s [66]. Consequently, a range of metals like copper, silver, tin, stainless steel, nickel, aluminum, and gold has been utilized in order to improve the electrical conductivity of common textiles. One of the techniques to add metals to the common textile materials is metal coating process (e.g. electroless plating, sputtering, and dip coating methods) [53], [67]–[69].

For example, electrically conductivity enhancement by combining silver nanowires and fabric threads using a dip-coating method was generated by Goldthorpe group [67]. They established electrical conductive textiles by coating the surfaces of polyester, polyamide and cotton threads with random networks of solution-synthesized silver nanowires.

In another study, the development of metal-coated fibers for application in textile electrodes was investigated by Gasana *et al.* [68]. They proposed electrical conductivity improvement by a chemical coating of polypyrrole (intrinsic conductive polymer) and copper metallization at polyaramide surfaces. They observed that DC-electroconductive polyaramide structures were attained when the copper was deposited on top of the prior deposited polypyrrole layer.

Moreover, a set of textiles were coated with metal particles to become electrically conductive and electromagnetic shield by Lu *et al.* [69]. They fabricated a compact and continuous silver coating on modified polyethylene terephthalate (PET) fabric using an ultrasonic-assisted electroless plating technique. They declared that the shielding effectiveness of the silver-coated fabrics was about 32 dB at the frequency range of 0.01 MHz -18 GHz.

1.2.1.3 Knitting fabrics made of metal yarns

Few studies have proposed knitted fabrics for electromagnetic shielding effectiveness (EMSE) applications due to the fact that knitted fabrics provide a high degree of flexibility and comfortability for the wearer [50], [70]–[75]. For example, Perumalraj and Dasaradan studied the EMSE of knitted fabrics containing copper core yarns [70]. They knitted a range of knitted structures using copper core yarns when copper wires with different diameters (0.1, 0.11 and 0.12 mm) were used as core and cotton fibers were applied as sheath material. After that, they measured the EMSE of the manufactured fabrics in the frequency range of 20-18000 MHz. They said that an increase in the EMSE values was observed with an increase of wale density, course density and tightness factor of the knitted fabrics. They also suggested that the weft-knitted fabric with interlock structure showed higher attenuation in comparison with the weft-knitted fabric with plain and rib structures. They suggested the manufactured knitted fabrics for the industrial appliances shield, such as industrial electronic gadgets, power lines, mobile radio, TV broadcasts, receivers, and etc.

Also, the EMSE of copper/cotton full milano and 1×1 rib weft-knitted fabrics at a frequency range between 0.03 and 1.5 GHz was studied by Mofarah *et al.* [71]. They observed that the heavier and thicker knitted fabrics with larger stitch density had higher EMSE values. They also described that the knitted fabric with milano knit structure showed higher EMSE values than the one with 1×1 rib knit structure as a result of using more conductive yarns in milano structure.

In another study, Cheng *et al.* manufactured copper/glass knitted fabrics reinforced polypropylene composites and evaluated the EMSE of the developed fabrics [74]. They applied glass fibers as the reinforcement and copper wires as the electrically conductive material for composites making. They suggested that the EMSE of the knitted fabrics was altered by the quantity of copper in the composite which was varied by changing the knit structure, stitch density and linear density of the yarns.

1.2.1.4 Using metal fibers in nonwoven structures

A number of studies have been completed in the field of nonwoven fabrics for electromagnetic shielding effectiveness applications in textiles [76]–[81]. For instance, two layers of nonwoven fabrics and a layer of chopped copper wires were used to make nonwoven fabrics with the aim of producing functional nonwoven insulation material having EMSE properties by Çeken *et al.* [78]. They suggested that the EMSE values were reasonable in the frequency range between 1125 MHz and 2925 MHz. On the other hand, the produced nonwoven fabrics were relatively bulky and the manufactured nonwoven fabrics were recommended for applications in the construction and automotive industry.

In another study, Ozen *et al.* investigated the EMSE of needle-punched nonwoven fabrics made of stainless steel/polyester and polyester fibers [80]. They stated that the EMSE increased at low, medium and high frequencies (15-3000MHz) by increasing the conductive stainless steel fiber content in the manufactured nonwoven structures. However, the porosity of the surfaces was introduced as the main source of the EMSE reduction of the nonwoven fabrics.

As a final point, it should be mentioned that although nonwoven structures have attracted attention for the EMSE applications, they are not capable for wearable applications due to the high thickness and uncomfortability.

1.2.1.5 Woven fabrics containing metal yarns and the effects of the structural characteristics

Woven fabrics are any textiles consist of at least two sets of yarns (warp and weft) that interlace perpendicularly to each other on a weaving machine. Taking into account that a satisfactory level of EMSE can be obtained by arranging the conductive yarns in an orthogonal grid, woven fabrics have been highly considered for EMSE applications in textile industry where the influences of fabric characteristics have been discussed [82]–[87].

For example, Liu and Wang studied the influence of weave structures on the EMSE of the woven fabrics [84]. They declared that the float of the yarns was the key factor in the EMSE level of the woven fabrics. They suggested that the EMSE of the plain-woven fabric was better than that of the twill woven fabric followed by the satin woven fabric while the fabric parameters of density, yarn linear density, and metal content remained unchanged. It should be noted that they studied the EMSE of a number of simple woven fabrics although the information about how the stainless steel yarns placed in the woven structures was not discussed.

In another study, Ozdemir *et al.* made woven fabrics using different weave structures (Figure 1-8) with textured steel yarns as electrically conductive material [85]. They declared that the EMSE was not changed with varying the weave structures due to the diagonally arranged of the yarn floats in the woven samples (2/2 twill, 3/1 twill, whipcord, barathea, and crepe weave structures s). On the other hand, the symmetrical arrangement of the yarn floats led to the EMSE decrease of the woven fabric weaved with herringbone weave structure.

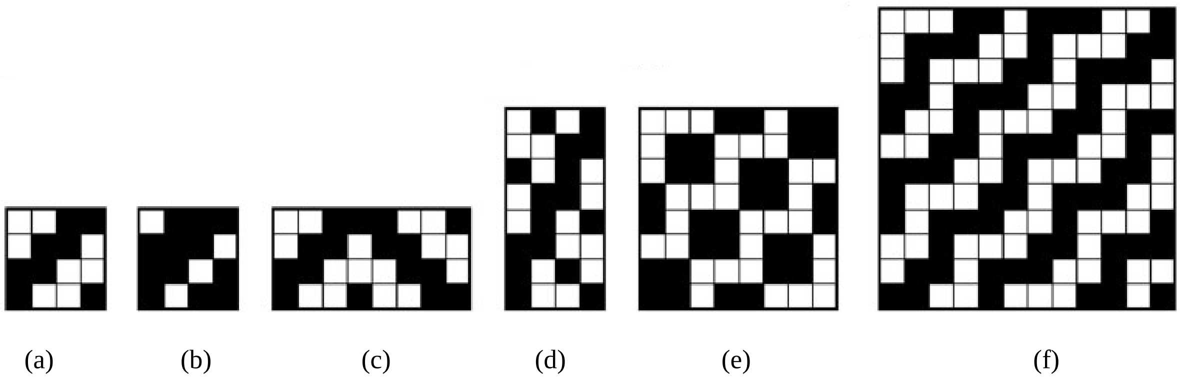

Figure 1-8- (a) 2/2 Twill, (b) 3/1 Twill, (c) Herringbone, (d) Whipcord, (e) Barathea, and (f) Crepe weave patterns [85]

Furthermore, the EMSE of stainless steel/polyester woven fabrics was investigated by Cheng and Lee where the conductive yarns were inserted in both weft and warp directions [86]. They believed that the EMSE of the woven fabrics is influenced by different properties, including fabric structure, yarn density, number of layers, and the amount of conductive material although the influences of these parameters on EMSE were not clearly explained.

Also, the effects of material type, yarn count, yarn density and the number of fabric layers were studied on EMSE by Das *et al.* [87]. They stated that the influence of the conductive yarn density (metal yarns) was negligible on the EMSE of the woven fabrics. They also observed that increasing the yarn count as well as increasing the number of fabric layers led to higher EMSE values. They also suggested that the EMSE values of the woven fabrics made of brass and copper were comparable.

Furthermore, a number of woven fabrics were manufactured for EMSE applications by Ozdemir *et al.* [88]. They inserted the conductive yarns at certain intervals in order to obtain different yarn density in the woven fabric structures. The applied conductive yarns consisted of polyester and stainless steel as core yarns with cotton fibre as a sheath and the EMSE of the woven samples was increased by increasing the conductive weft yarn density while the weft yarns were vertical to the antenna polarization.

In another study, the EMSE of various two-ply conductive woven fabrics composed of cotton and copper yarns was evaluated by Perumalraj and Dasaradan [89]. They believed in an enlargement of the EMSE values with an increase in warp density, weft density and cover factor due to the higher number of copper threads occupied per unit area. They also suggested that using twill weave structure led to a higher EMSE due to the float length and less porosity. In addition, they declared that an increase in the copper wire diameter led to decrease in EMSE as a result of the openness of the fabric caused by the high bending force of the copper threads.

As already indicated, many studies have been completed on the subject of the effects of simple woven fabrics characteristics on the EMSE behavior. On the other hand, there are only a limited number of studies about complex woven fabrics with conductive yarns for EMSE applications.

For instance, the EMSE of five different compound woven fabrics (orthogonal, angle interlock, cell-type spacer, multi-tubular spacer, and contour) using copper-wrapped hybrid yarn was compared in X-band frequency range by Pandey *et al.* [90]. Images of the produced 3D fabrics are represented in Figure 1-9.

They suggested that the poor EMSE results were observed for the fabrics made of 100% cotton yarns as cotton yarns are nonconductive materials. In addition, they stated that tubular contour fabric showed the best EMSE behavior in the vertical plane when orthogonal fabric had the best waves absorption in the horizontal plane. Also, they declared that the produced fabric with an angle-interlock structure had the minimum EMSE values. However, the relationship between the structural characteristics of the 3D woven fabrics and the EMSE values was not clearly explained.

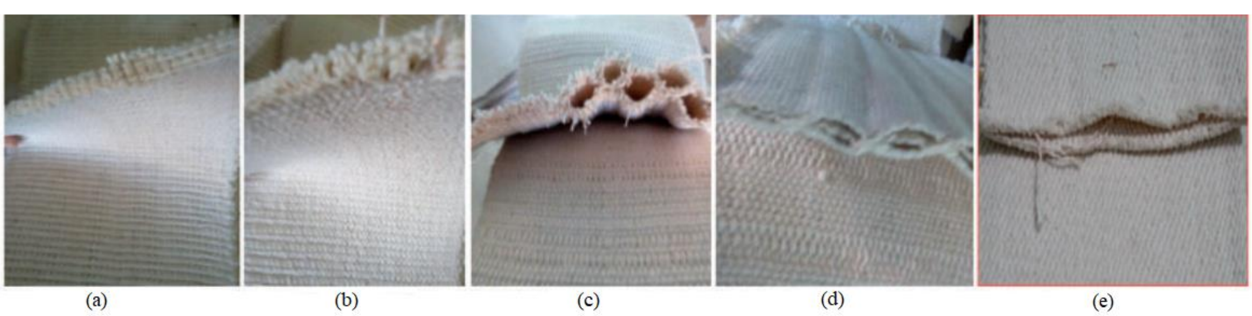

Figure 1-9- Images of the manufactured 3D fabrics (a) Orthogonal, (b) Angle interlock, (c) Cellular spacer, (d) Multi-tubular spacer, (e) Tubular contour [90]

It should be also taken into consideration that several analytical models for EMSE estimation of woven fabrics have been proposed by a number of studies [91],[92].

For example, Liang *et al.* proposed a mathematical model to calculate the EMSE of the metal fiber blended woven fabrics where the model was developed based on the aforesaid shielding equations (equation(1) to equation(8)) [92]. The proposed conductive grid structures composed of two parallel metal yarn systems and the influences of yarn diameter, yarn spacing and weaving angle on the EMSE enhancement were investigated although the simplification assumptions made the proposed model far from real yarn alignment in the woven fabrics.

1.2.2 Electromagnetic shielding textiles using intrinsic conductive polymers

Intrinsically conductive polymers (ICPs) such as polyaniline (PANI) and polypyrrole (Ppy) conduct electricity due to their π-conjugated chain structures [93]. The ICPs are generally not thermoplastic polymers and also, they have weak mechanical properties which make them unlikely to be applied in the traditional textile process. Therefore, coating or polymerizing the conducting solutions of ICPs on the surface of textiles is a practical method to generate conductivity in textiles using ICPs [2], [18], [25], [46], [94]–[96].

For example, Jagatheesan *et al.* reviewed the EMSE properties of electrical conductive composites containing ICPs and stated that the main limitations of ICPs for electrical conductivity enhancement of the composites and fabrics are the rigid characteristics caused by chemical conformation of benzene rings, poor long term stability and lack of processing methods [2].

In another study, polypyrrole (Ppy) was coated on the surface of polyethylene terephthalate (PET) woven fabric to achieve the electrical conductivity for electromagnetic shielding development by Kim *et al.* [94]. They suggested that both Ppy content and the electrical conductivity of the composite were increased with increasing the number of the chemical polymerization. Also, they suggested that the EMSE value was increased from 13 to 36 dB due to the increase in the electrical conductivity of the fabric.

Furthermore, the electrical and morphological properties of polyaniline (PANI)-coated ultra-high-molecular-weight polyethylene yarns were investigated by Devaux *et al.* [95]. Also, Niu suggested that the EMSE of the PANI nanofibers coatings was in the range of 38–63 dB at the frequency range of 100 kHz -10 GHz. However, the content of applied PANI was relatively high (35%) [96].

To conclude, the high percolation threshold, as well as lower aspect ratios of ICPs compared to metals and carbon nanofillers, remained a challenging issue applying ICPs in a composite for electrical conductivity enhancement intended for EMSE applications [18], [25]. Moreover, the difficult processability as well as low-temperature stability, swelling, cracking, or softening of these polymers which have effects on the mechanical and electrical properties are the key complications of using ICPs for shielding applications.

1.2.3 **Electromagnetic shielding textiles using conductive polymer composites**

1.2.3.1 Conductive polymer composites

Conductive polymer composites (CPCs) are made of non-conductive polymer matrices with conductive fillers [97]. The utilized fillers can be zero-dimensional (e.g. fullerene), one-dimensional (e.g. carbon nanotube) or two-dimensional (e.g. graphene) as shown in Figure 1-10(a, b, and c).

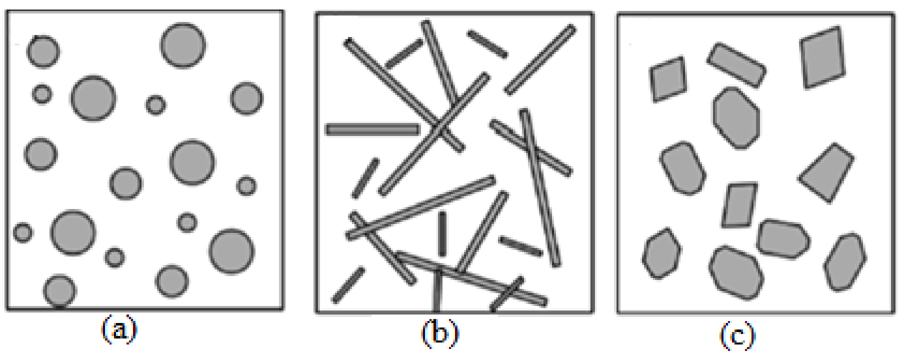

Figure 1-10- Schematic of (a) Zero-dimensional, (b) One-dimensional, and (c) Two-dimensional fillers in the polymer matrix [97]

1.2.3.2 Melt mixing method

Melt mixing method is one of the valued techniques for the fabrication of conductive filler-based composites since thermoplastic polymers soften when heating temperature exceeding their melting point. Additionally, this method is an appropriate technique for polymers that cannot be processed with solution techniques as a result of the insolubility of those polymers in solvents as well as time and cost efficiency of the melt mixing method [98], [99]. Thus, melt mixing method has been considered by many studies to develop CPCs for countless functions [99]–[105].

Moreover, the percolation threshold shows a critical amount of conductive filler which is required to build up a continuous conductive network throughout a polymer to alter an isolating polymer into a conductive polymer composite. In fact, the lowest amount of filler when an insulating is transformed into conductive material is known as the percolation threshold [53], [106], [107]. Theoretical percolation threshold can be defined using equation (9) which is so-called as power-law function where σ_o is scaling factor, ρ_c is the percolation threshold, σ is the conductivity of the conductive composite and ρ is the nanofiller content. The percolation threshold is generally determined by plotting the electrical conductivity of the composite when the graphical results of equation (9) allow to find the percolation point that the conductivity begins to level out [107]–[109].

$$\sigma = \sigma_o(\rho - \rho_C)^t, \text{ for } \rho > \rho c \quad (9)$$

The electrical conductivity of CPC as a function of filler volume fraction is shown in Figure 1-11. As can be seen, the conductivity of the CPC increases exponentially after the percolation threshold with increasing the amount of filler to the point that the saturation of the electrical conductivity occurs.

It should be taken into consideration that the percolation threshold of CPCs is influenced by different parameters including process method, polymer matrix and nanofillers properties [109]. Therefore, in the following, a number of studies have been reviewed on the subject of CPCs development with different nanofillers using the melt mixing method.

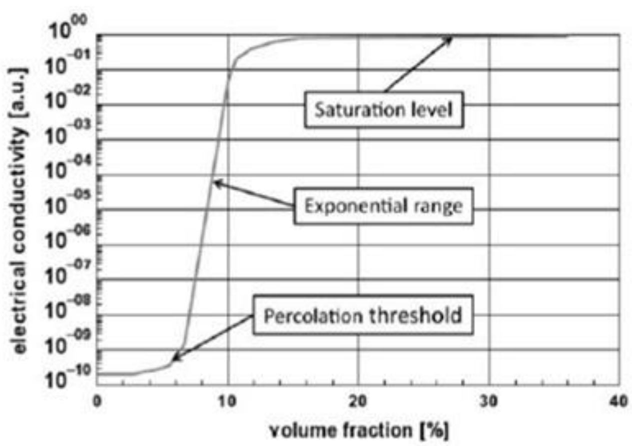

Figure 1-11- The classic graph of electrical conductivity of conductive polymer composites as a function of the nanofiller volume fraction [97]

For example, dispersion of nanofibers in different polymer matrices by melt processing was studied by Andrews et *al.* [100]. They suggested that the dispersion of low concentrations of MWCNT in polypropylene, polystyrene, and high impact polystyrene resulted in a reduction in the electrical surface resistivity of the produced composites. However, the reduction rate with increasing nanofiller concentration altered by changing the host polymer. They also suggested that an increase in Young's modulus and a decrease in tensile strength by the addition of MWCNTs into the polymer matrices for all the produced composites.

Furthermore, Chanklin investigated the electrical properties of the composites produced by addition of carbon nanofillers in several polymers in his dissertation [101]. He used polyamide 6 (PA6) as a thermoplastic polymer matrix while carbon nanotube (CNT) or carbon black (CB) was added to the polymer matrix.

He studied the electrical and mechanical properties of PA6-based composites with CNT and CB. He published the electrical resistance of the produced composites as presented in Figure 1-12. He also perceived a low electrical percolation threshold for CNT-PA6 composite (3.0 wt.% of CNT). He suggested that the reason was correlated to the high aspect ratio and high surface area as well as the uniform dispersion of CNT particles in the polymer matrix which led to the formation of conducting network as it was also reported by other studies [102].

Moreover, the tensile and electrical properties of carbon-filled polyamide (PA6,6) conductive composites were studied by Clingerman *et al.* [103]. They investigated the influences of carbon black and carbon fiber concentration on the electrical and mechanical properties of the PA6,6-based composites plates. They applied relatively high CB content to achieve a reasonable electrical conductivity for the developed composite plate (40 wt.% of CB).

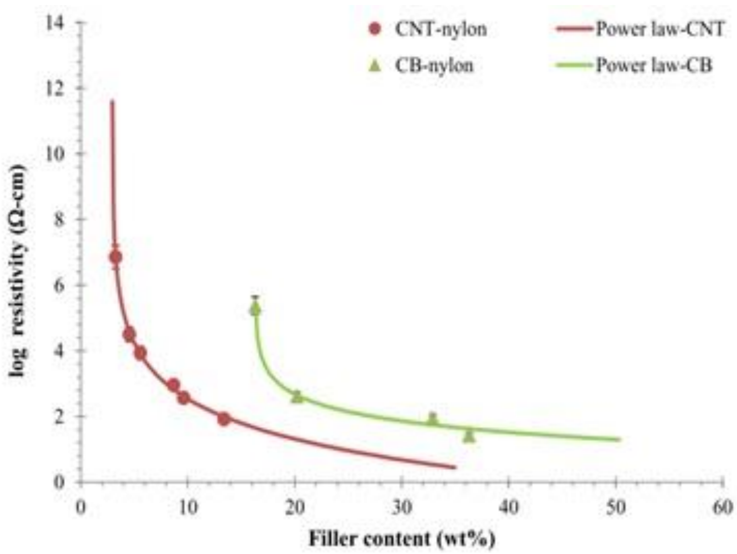

Figure 1-12- Electrical resistivity of CNT/PA6(nylon) and CB/PA6(nylon) composites [101]

Also, the percolation threshold of electrical conductivity as a function of alignment of single-wall carbon nanotubes (SWCNTs), varied in a controlled manner from isotropic to highly aligned SWCNTs was investigated by Du *et al.* [104]. They applied extensional forces to attain different degrees of nanofiller alignment in poly (methyl methacrylate) (PMMA) matrix and stated that the electrical conductivity followed by the SWCNTs alignment as well as SWCNTs concentration. In other words, the lowest percolation threshold observed when the distribution of SWCNTs orientations was slightly anisotropic at a fixed SWCNT concentration and aspect ratio. Moreover, the percolation threshold of the CNT-based composites using different methods, different polymers and CNT properties were reviewed by Spitalskya *et al.* [105].

1.2.3.3 Electrical conductivity and electromagnetic shielding effectiveness

As specified earlier, electrically conductive materials produce and transport free charges which initiate the shielding characteristics. Therefore, it has been attempted to define an experimental relationship between electrical conductivity (or electrical resistivity) and electromagnetic shielding effectiveness of CPCs [26], [110]–[113].

For instance, the electrical resistivity and the EMSE of MWCNT/PP composite plates developed by Al-Saleh and Sundararaj as a function of MWCNT content are shown in Figure 1-13 [26]. They suggested that the experimental relationship between the resistivity and the EMSE was in agreement with the theoretical relationship given in equations (3) and (4) [26].

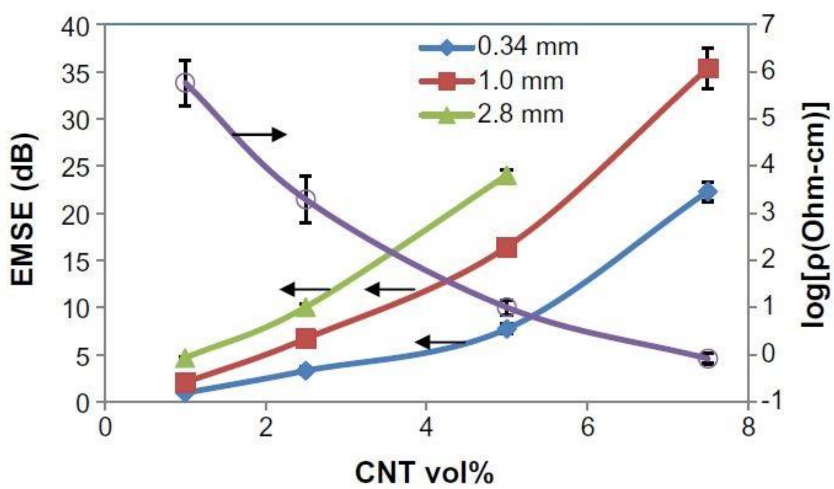

Figure 1-13- Electrical resistivity and EMSE of MWCNT/PP composites as a function of MWCNT content and the composite plate thickness (0.34, 1 and 2.8 mm) [26]

Moreover, MWCNT loading within polypropylene random copolymer was prepared by melt recirculation equipped twin-screw extruder and both electrical conductivity and shielding effectiveness were characterized by Verma *et al.* [110]. They indicated that the electrical conductivity, as well as shielding effectiveness, was improved by increasing the quantity of carbon nanofiller. Also, they suggested that the conductivity was not changed meaningfully after percolation threshold despite the fact that the shielding kept on growing with increasing the nanofiller quantity. It should be taken into consideration that the presence of iron catalysts inside MWCNT internal cavity led to better EMSE performance as a result of the ferromagnetic properties of iron. Hence, they achieved high EMSE by adding iron particles to the MWCNT-based composites due to the high electrical conductivity of iron.

In another study, an equation between electrical conductivity and electromagnetic shielding effectiveness was defined by Han *et al.* [111]. They suggested that the EMSE increases when the electrical conductivity of material increases, based on EMSE theory using equation (10).

$$\mathrm{EMSE} = 20\mathrm{Log}\left(1 + \frac{1}{2}\sigma\, \mathrm{d}Z_0\right) \tag{10}$$

where σ showed the electrical conductivity, d was the sample thickness, and Z_0 was the free space impedance (377 Ohm). They made a set of MWCNT/polyethylene (PE) and MWCNT/ polyphenylene sulfide (PPS) composites by melt mixing method when the quantity of MWCNT was in a range of 1-15 wt.% (1,3,5,10, and 15 wt.%). The EMSE of the developed composites was measured at two different frequencies (0.5 GHz and 1GHz) and the results were compared to the estimated values of EMSE. They declared that the shielding effectiveness (EMSE) results obtained from equation (10) were in good agreement with experimental results for both sets of the composites.

1.2.3.4 Synergism between conductive nanofillers

It should be taken into consideration that although increasing quantity of the conductive nanofillers increases the electrical conductivity of the final nanocomposite, a high quantity of nanofiller causes difficulties in the manufacturing process (especially for filament form). Thus, the addition of nanofillers results in deviation during the composite making process as a result of high viscosity. In addition, the cost of produced CPC is increased using high amount of carbon nanofillers.

Mechanism of conducting network formation in polymer-based composites having conductive nanofillers with different geometries (MWCNT, CB, hybrid conductive nanofillers of MWCNT and CB) is represented in Figure 1-14. The nanofiller particles with an identified geometry (e.g. CB) linked the nanofiller particles with another geometry shape (e.g. MWCNT) as shown in Figure 1-14(c).

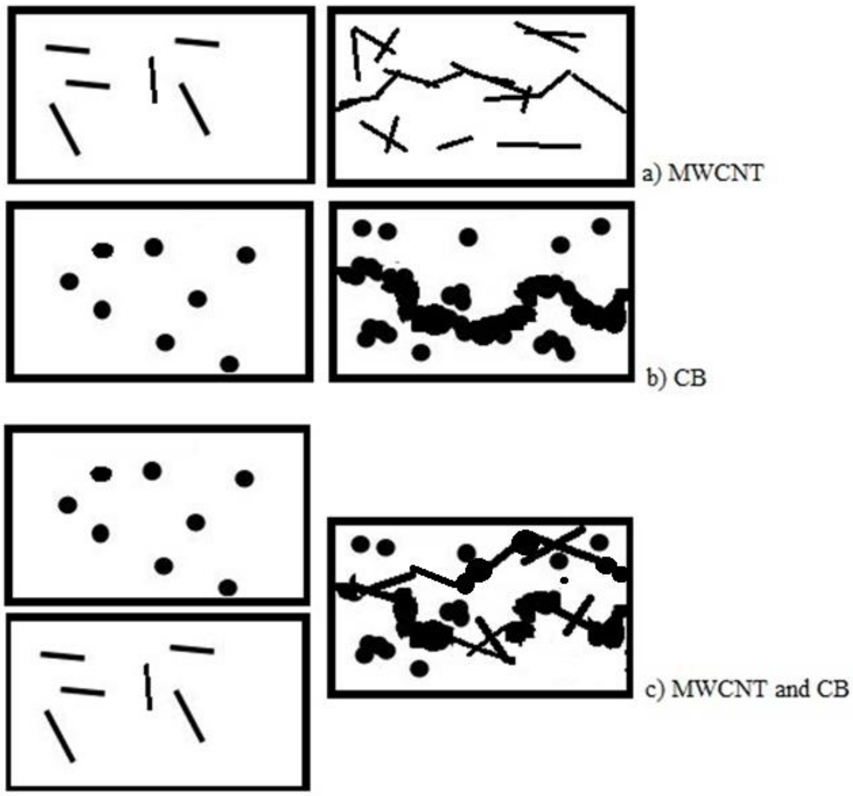

Figure 1-14- Mechanism of conducting network development in a polymer-based conductive composite containing (a) MWCNT, (b) CB, and (c) MWCNT and CB

As a result, a percolation threshold of electrical conductivity is detected with a lower quantity of nanofillers in a ternary composite having hybrid nanofillers in its composition. As a matter of fact, a conductive network developed throughout the polymer matrix by increasing the quantity of MWCNTs or CBs. Alternatively, applying synergism between MWCNT and CB nanofillers leads to higher electrical conductivity owing to a wider network growth through the matrix.

Therefore, it has been tried by a number of researchers to apply the synergy effects of carbon nanofillers to decline the complications of inclusion a high quantity of nanofillers to the polymer-based [114]–[122]

For instance, MWCNT and CB were introduced as electroconductive nanofillers in polypropylene copolymer using melt mixing method and the behavior of the percolation threshold was investigated by Zhang *et al.* [114]. They stated that the lowest percolation threshold was observed while the weight ratio of the nanofillers was 1:1 (MWCNT: CB) between three ratios of 1:1, 1:4 and 4:1. In brief, they stated that the percolation threshold of hybrid nanofillers filled CPC was significantly lower than the percolation threshold of either CB or MWCNT filled CPCs.

Furthermore, polybutylene terephthalate (PBT)-based composites with CB or CNT (SWCNT) were produced by melt compounding method with a nanofiller content of 1-15 wt.% by Dorigato *et al.* [115]. Besides, the composites containing hybrid nanofillers were produced with a total nanofiller amount of 4, 6, and 10 wt.% in order to investigate the synergism of CNT and CB. They stated that the PBT-based composite with a total nanofiller amount of 6 wt.% and a CNT: CB ratio of 2:1 showed the best electrical resistivity among all the produced composites.

Also, the electrical conductivity of polystyrene composite filled with carbon fiber (CF) and carbon black (CB) was studied by Motaghi *et al.* [116]. They observed that the combination of fillers resulted in higher electrical conductivity compared to the composite having only CF.

Similarly, the electrical conductivity of epoxy-based composite plates containing hybrid nanofillers of CNT and CB was studied by Peng Cheng *et al.* [123]. They suggested poor performance for electrical conductivity of the composite contained CB compared to the one contained CNT. They believed that the poor electrical conductivity was correlated to the spherical shape of CB as the spherical shape of CB provided lower aspect ratio compared to CNT and therefore, forming conducting networks in the polymer with CB was problematic.

They also applied CB to the composites having CNT before and after percolation and witnessed that adding CB to the composite with CNT (after percolation threshold) slightly improved the electrical conductivity. They stated that addition of mixed nanofillers of CB and CNT triggered higher electrical conductivity while CB improved the ductility of the composites.

Furthermore, the synergism of the other kinds of conductive nanofillers on CPCs characteristics such as electrical conductivity and shielding properties has been considered by several studies [124]–[127].

For example, a polypropylene (PP)-based composite having graphene nanosheets (GNSs) and carbon fibers (CFs) was made by melt mixing method and the synergism effects of the conductive fillers were studied on the electrical and electromagnetic shielding properties of the composites by Li *et al.* [124]. They suggested that the CPC with the equal quantity of CF and GNS generated a wider continuous conductive network which led to the higher electrical conductivity among all the produced composites. They also stated that the EMSE of the composite was around 20 dB at the frequency range of 1.28–2.00 GHz. Even though the electrical conductivity and the EMSE of the developed CPC were in the acceptable range, the high quantity of conductive fillers (20 wt.%) along with the high thickness of the composite (five layers of 0.6 mm) was necessary to obtain the required shielding.

Also, the synergism of polyaniline (PANI) and MWCNT in polymethyl methacrylate (PMMA) matrix was investigated by Makeiff and Huber [125]. They detected higher electrical conductivity due to the incorporating of a high quantity of MWCNT in the composite where hybrid nanofillers were applied. However, the electrical conductivity of the composite having 9 wt.% MWCNT was relatively great compared to all the other composites having different ratios of conductive fillers.

Furthermore, synergism of ICPs and carbon nanofillers and its influences on electrical conductivity and shielding properties of composites has been investigated in several studies [53], [125], [135], [136], [126], [128]–[134]. It has been said that the presence of ICPs has negative effects on the effectiveness of carbon nanofillers [53], [125]. Also, a high quantity of carbon nanofillers and expensive techniques are needed to obtain a good level of EMSE applying synergism between ICPs and carbon nanofillers [137], [129]. However, it is believed that the productive synergetic effect of nanofillers can be witnessed if the presence of ICPs does not alter the dispersion of the carbon nanofillers in the polymer matrix [53]. It should be also taken into account that the above-mentioned conductive composites have been used for specific applications as a form of films or plates [138], [139].

To conclude, the achievement of the mentioned studies is attractive for the specific applications in industry or military while the final cost and customization are not of great importance and fabric manufacturing for general protection has not been seeking out of that.

1.2.3.5 A mathematical model for percolation threshold of composites with hybrid nanofillers

Calculation of the percolation threshold of hybrid nanofillers has been directed in consequence of the productive effects of synergy between conductive nanofillers. Hence, a mathematical model was proposed to estimate the percolation threshold of hybrid carbon nanofillers in polymer composites (CPCs) by Sun *et al*. [140]. They proposed a model based on the fact that two carbon nanofillers make co-supporting conductive networks by extending the excluded volume theory. The excluded volume theory was primarily proposed by Balberg *et al.* [141], [142]. The volume around the object when the center point of an identical object is banned if the two are not to overlap is known as excluded volume.

According to the proposed model, percolation ensued when all the small volumes were occupied with MWCNTs or CBs or mixed of MWCNTs and CBs as given in Figure 1-15(a, b, c, d).

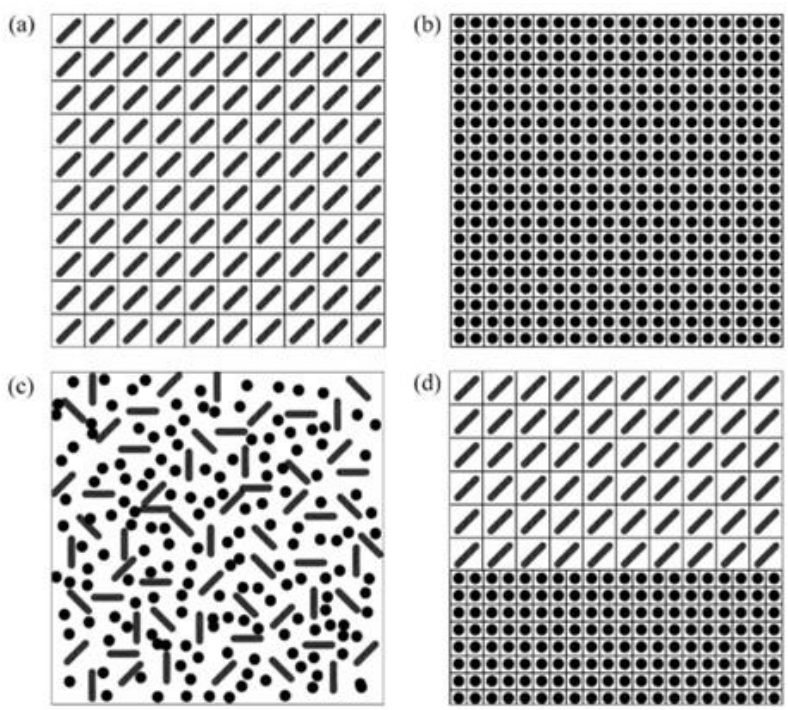

Figure 1-15- Schematic of the excluded volume theory for single nanofiller system (a) MWCNT and (b) CB, (c) hybrid nanofiller system (MWCNT and CB) in the real state and (d) hybrid nanofiller system (MWCNT and CB) in the extreme state [140].

A formula (equation (11)) was obtained for the systems containing two types of conductive nanofillers (A and B) where m_A is the weight fractions of nanofiller A and m_B is the weight fraction of nanofiller B in the composition. $\rho_{C,A}$ (or $\rho_{C,B}$) is the corresponding percolation concentration when A (or B) is the only type of nanofiller applied in the composite. It means that the composite is at percolation threshold state when the value of equation (11) is equal to 1.

$$\frac{m_A}{\rho_{C,A}} + \frac{m_B}{\rho_{C,B}} = 1 \qquad (11)$$

Moreover, they produced polymer composites by melt mixing method using polypropylene (PP) and polyoxymethylene (POM) as matrices and CB and MWCNT as nanofillers. The MWCNT quantity was fixed at 1 wt.% for PP-based composite and 0.5 wt.% for POM-based composite for mixed nanofiller systems (hybrid composites).

In addition, they applied the proposed model to calculate the quantity of nanofillers at percolation threshold in the extreme state using hybrid nanofillers in the composites although the real situation of hybrid nanofillers (MWCNT and CB) was not exactly similar to the model. Finally, the results of the mathematic model and experiment results were compared and they declared that the developed model was in agreement with the experimental results.

Therefore, the proposed model can be applied to approximate the percolation threshold of composites with mixed nanofillers in order to estimate the electrical properties of polymer-based composites.

1.2.3.6 Application of conductive composites for electromagnetic shielding textiles

Smart textiles (e-textiles) have been developed with new technologies that provide specific added values to the final products. In recent decades, the development of smart textiles has been growing intending to apply in the industry (e.g. sensors for force and pressure, heating applications, or electromagnetic shielding applications) [143].

The engineering of innovative materials that are capable to respond to external or internal stimuli is the main objective of smart textile growth. For instance, electrically conductive polymer composites (CPCs) which contain conductive fillers dispersed in a polymer matrix have attracted attention in numerous study fields like electromagnetic shielding applications [144], [145].

Moreover, as indicated previously, a lot of EMSE products are made of metallic yarns with high electrical conductivity like copper, silver, nickel and stainless steel [146]. However, poor washability and uncomfortability (e.g. high weight and skin allergy) can be mentioned as the main drawbacks of these products [64], [147]–[149].

As a result, electrically conductive polymer composites (CPCs) have been suggested to be applied for electrical conductivity enhancement with the aim of using for EMSE purposes in order to avoid the drawbacks of previous electrical conductive textiles. Textile-based composites have been highlighted to be replaced with EMSE traditional metal-based textiles thanks to the light weight, flexibility, thermal expansion matching, and low-cost production process of polymer-based composites.

The CPCs development by different studies is presented in the following in order to have a comprehensive understanding of the advantages and disadvantages of using CPCs in textile industry.

CPCs have been used as coating on textile surfaces to enhance electrical conductivity as applying conductive coating on textiles is a common way to enhance the electrical conductivity of textiles [150]–[153].

For example, a nonwoven nanofiber mat made of nylon 6 (PA6) was produced using the force spinning technology while carbon nanotube particles (CNTs) were bonded by covalent bonds to the surface of the PA6 mat by Weng *et al*. [150]. They suggested that the nylon mat coated with a larger content of CNT (10 wt.%) showed higher electromagnetic attenuation compared to the mat with 6 wt.% CNT and the mat without CNT.

In another study, a thin layer was coated on the surface of a set of nonwoven and knitted fabrics by Bonaldi *et al.* when a knife carried the coating paste on the fabrics for a specified thickness of the coated layer [151]. They suggested that MWCNT was the most influential synergistic material when the synergy between MWCNT and metals led to higher electrical conductivity and accordingly to the higher EMSE values.

As a final point, although coating is an economical technique to increase the electrical conductivity of textiles, coating wears away after a short period of use.

In recent years, inclusion of conductive nanofillers to the polymer matrix has been developed to enhance the electrical conductivity of textiles [2], [154]–[161]. Several structures of CPCs such as single-phase CPCs, segregated structures, double percolation structures, layer-by-layer assembly, multilayer structures, and foam structures have been developed in order to improve the electrical conductivity or shielding properties of the non-conductive polymers [162]–[169].

For example, single-phase CPCs consist of conductive fillers (one or more types of conductive fillers) dispersed in a single polymer matrix [162]. Thus, the conductive fillers should be well-dispersed in the matrix substrate so as to obtain the required electrical conductivity and electromagnetic shielding characteristics.

On the other hand, the segregated structure and double percolation structure are two main approaches with the selective localization potential for the conductive fillers.

In a segregated structure, the conducting filler is found at the polymer interfaces and formed a conductive network mostly by applying secondary filler in a segregated structure. In a double percolation method, the conductive fillers are selectively sited in one of the two immiscible polymer blends to form a percolated conductive network in one of the blended polymers. Double percolation method is commonly used for CPC generating with a low percolation threshold although the weak adhesive interaction between two polymers is the main drawback of this technique which limits the mechanical properties of the developed CPCs [163].

In the following, a number of previous studies exclusively on single-phase CPCs were reviewed due to the fact that the focus of the present thesis was on single-phase CPC development for fabric manufacturing which would be discussed in the next chapters.

Jagatheesan *et al.* reviewed the theory of electromagnetic shielding together with the electrical conductivity of fabrics and composites [2]. For example, they stated that applying 5 wt.% of mixed Ag and MWCNT in polystyrene-based composite resulted in the shielding effectiveness of 22 dB in the frequency range of 12.4-18 GHz. They suggested that the higher amount of nanofillers led to the higher electrical conductivity on one hand and increased the viscosity of the developed CPC on the other hand.

Jiang *et al.* reviewed the electromagnetic shielding characteristics of the conductive polymers and nanocomposites including CPCs [18]. They investigated the electrical conductivity and EMSE characteristics of a number of CPCs developed by several studies using various polymer matrices and conductive nanofillers. They observed that the electrical conductivity and shielding properties of the CPCs were influenced by nanofiller types and loadings, nanofillers synergism, polymer matrices and thickness of the composite films. They stated that the composites with carbon nanofillers are lightweight, economical, easy processable composites with reasonable mechanical properties that make them suitable for EMSE applications in textile industry.

Moreover, mass production of carbon nanotube (CNT) reinforced polymethyl methacrylate (PMMA) nonwoven nanofiber mats were developed by Weng *et al.* [170]. They declared that the electrical properties enhanced in comparison with PMMA nanofibers. Also, they stated that the developed conductive composite showed reasonable electromagnetic shielding effectiveness where the higher content of CNT led to higher EMSE. Also, they indicated that the embedding of aligned CNTs into the one-dimensional polymer nanofiber matrix resulted in mechanical improvements (better tensile strength). The only drawback of the above-mentioned study was that they examined the EMSE in a low-frequency range (0-1200 MHz) while they applied a very high concentration of CNTs to get a reasonable level of EMSE.

Furthermore, monofilament manufacturing of conductive composites for textile applications has been deliberated by a few numbers of studies [171]–[173]. For instance, monofilament producing PLA/CNT for sensor applications was investigated by Ferreira *et al.* [171]. It is also noted that the polymer properties together with the volume fraction of nanofillers play a major role in the filament manufacturing process.

1.2.3.7 Conductive polymer composites as printing materials

3D printing technology is the technology applied for the rapid production of 3D objects directly from digital computer-aided design (CAD) files [174], [175]. Fused deposition modeling (FDM) is the most inexpensive and common 3D printing method where a thermoplastic monofilament is pushed through a heated extrusion nozzle in this method to be printed on the 3D printer plate [175].

In recent years, 3D printing on textile fabric surfaces has been investigated by a number of studies in order to add desired properties to fabrics for different applications [176]–[180]. For example, 3D printing of several polymers on a group of textile materials was investigated by Pei *et al.* [179]. They suggested that the printed PLA (polylactic acid) showed the best adhesion, followed by nylon and ABS (acrylonitrile butadiene styrene) when the polymer filament was printed on the various types of fabrics. In another study, the morphological and electrical characterization of PLA-based composite before and after 3D printing was studied by Sanatgar *et al.* [180].

Therefore, 3D printing of the CPC monofilaments on the surface of fabrics remains reasonable for electrical conductivity enhancement of the non-conductive fabrics for different applications. In point of fact, it seems interesting to consider the 3D printing of conductive monofilaments on textile fabric surfaces for EMSE applications since this method is clean, easy to use, inexpensive, accessible, and no supporting material is required.

1.3 Complications and solutions of garment design

The ultimate goal of the present thesis was to virtually design a protective garment for pregnant women. Therefore, the complications and possibilities of the garment design especially for maternity length are discussed in this section.

Two-dimensional (2D) patterns have been used by apparel industries to manufacture fitted garments on three-dimensional (3D) mannequins for decades when the process of design was usually time-consuming and ineffective [181].

In recent years, significant improvement in the garment design industry has been obtained thanks to 3D design softwares advancement to overcome the limitations of the traditional 2D design methods. In fact, the time of garment design, final cost, comfort and fit of the final garment can be optimized using 3D design softwares [182]–[188].

A global diagram of generating a garment with a virtual 3D model of adaptive morph types (as shown in Figure 1-16) was presented by Cichocka *et al.* [183]. This global diagram consists of three internal switching parts: the human body model, the model of ease and style of clothing when modeling of the human body can be achieved through the development of morphology data collection and analysis. In addition, the ease model allows validating the concept of comfort and correcting garment draping by controlling the ease while the virtual garment validates the dynamic aspect of the fitting of garments.

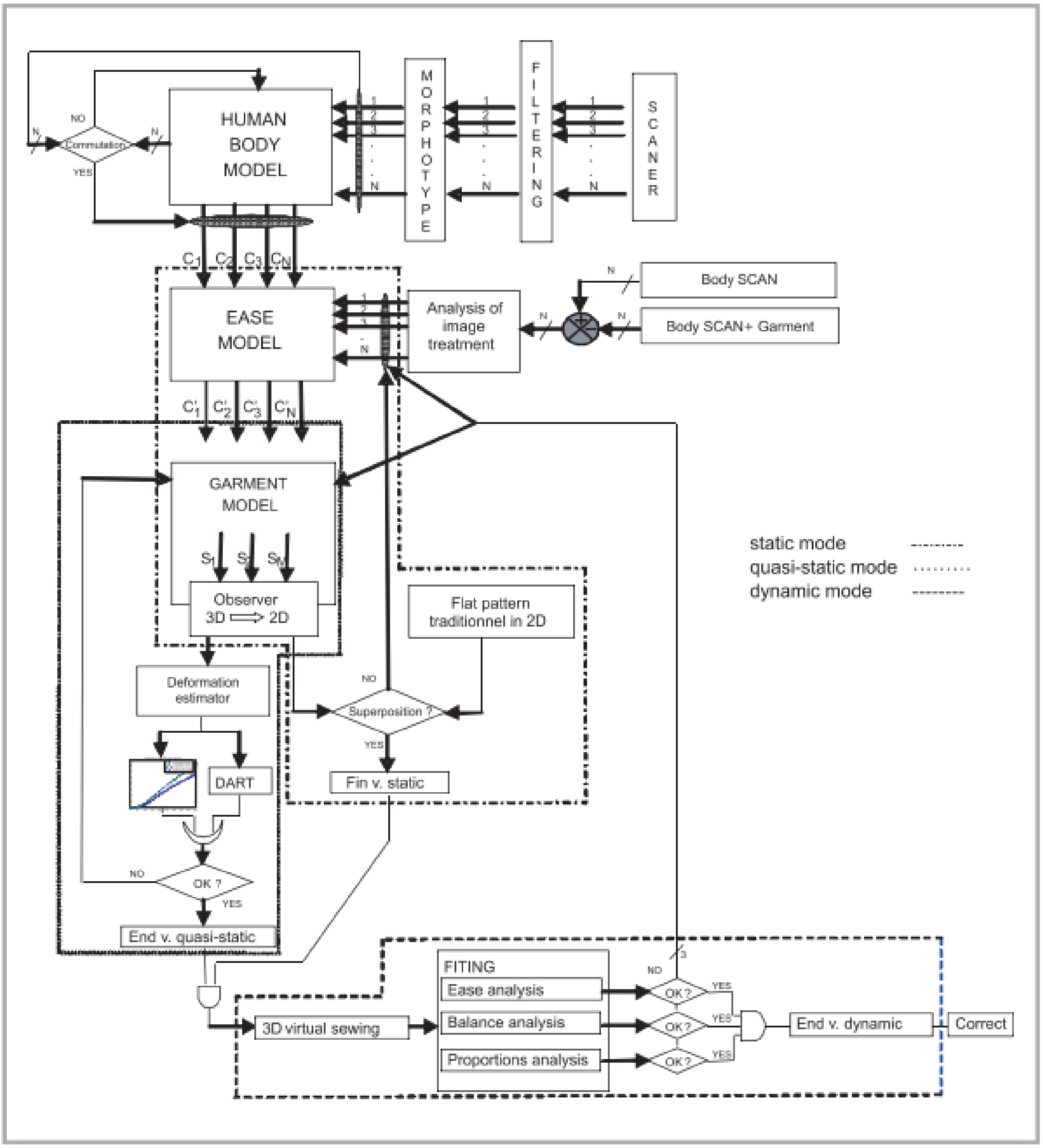

Figure 1-16- Global model of the garment making process [183]

1.3.1 Morphology analysis and garment design development

Body morphology data is essential for fitted garment design adapted to the human body. Therefore, the body morphology data has been collected and analyzed by several studies [182]–[188]. For instance, body morphology data was collected and applied to generate a virtual mannequin of the human body by Wang and Yuen [182]. They modeled the segments of torso, legs, and arms to make a 3D symmetric adaptive mannequin. They suggested that the developed mannequin was able to be adjusted according to the beauty and height of each subject.

Also, mathematical interpolation functions of input dimensions have been used to make parametric mannequins [189]–[193]. In one study, a skeleton model of a body was made based on extracted anatomical feature points (shown in Figure 1-17) by Li and Wang [189]. They generated wireframe of each part of the body (head, torso, arms, and legs), and combined these parts. They finally projected a model of human body with a sweep surface with a controllable wireframe structure of the body.

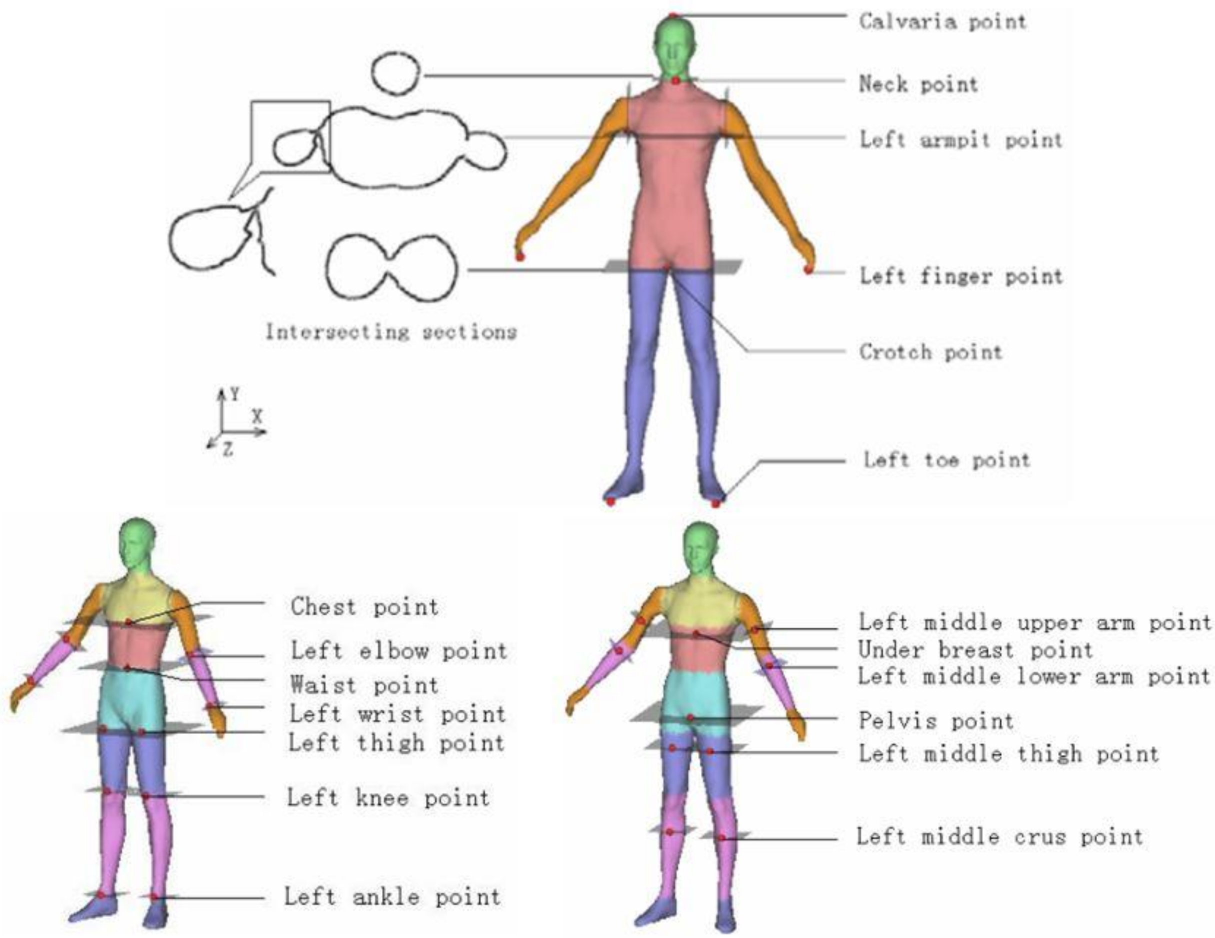

Figure 1-17- Anatomical feature points proposed by Li and Wang [189]

In another study, a framework for making feature-based human bodies in relation to the measurement dimensions was suggested by Wang although the input of the human structure was example-based and it was limited to the sizing dimensions [190].

Furthermore, the body morphology of disabled people has been investigated by several studies in order to provide the possibility of designing a fashioned and comfortable garment for this group of people [194]–[196].

Actual body morphology has been practically applied in garment design owing to the possibility of collecting and analyzing the detailed morphology of human body as specified [194]–[199].

In one study, the advantage of using advanced virtual tools and methods for the garment pattern design adapted to the 3D body model of people with scoliosis was discussed by Jepanovic *et al.* [196]. They stated that the designed garment for people with scoliosis showed a better appearance of the seams on the back and a good fit in the area of shoulder blades.

In another study, a web application was introduced that facilitated garment design, pattern derivation, and sizing using a new set of variables regarding stature, crotch and leg length of body measurements by Cordier *et al.* [197]. They developed a database using the measurements to apply in shopping via the internet and declared that the garments were fitted on the deformed body for tight, loose and freely float clothes around the body according to the measurements.

1.3.2 Garment design for pregnancy length

The physical appearance of a woman's body considerably changes during nine months of maternity period. Therefore, pregnancy mannequins have commercially been manufactured by several companies. These mannequins are practical in the pregnancy garment design industry although they are unable to show the actual body evolution of pregnant women, as well as these mannequins, are not applicable to every single pregnant woman. The reason is correlated to the fact that the available pregnancy mannequins are manufactured based on standard sizes. It should be also noted that the choice of changing the height or abdomen lines of pregnancy mannequins is reflected in some manufactured pregnancy mannequin products although these choices are limited. Thus, it is hardly possible to find a connection between the actual morphology of pregnant women and the available commercial mannequins in stock.

Consequently, characterization of body changes during pregnancy has been investigated by several studies concerning the fact that a woman's body undergoes apparent changes during pregnancy [200]–[206].

For example, the lower body shape of late pregnant women was studied by Wu *et al.* [203]. They classified the morphology data of a group of pregnant women with different body changes and suggested the collected data for applying in the garment pattern design for maternity.

Moreover, a new clothing design was suggested for pregnant women by Georgeta *et al.* [204]. They introduced several garment patterns in accordance with physical comfort for a pregnant woman when they considered four types of changes including shape, dimensions, weight, and body posture for garment pattern design. However, they have not investigated the body evolution during pregnancy period as they only focused on the last month of pregnancy.

In addition, the key design aspects of pregnancy support garments were studied by Rodriguez *et al.* [205]. They believed that the pregnancy garments for the modern plus-size patterns have to be advanced as a result of growing obesity along with beauty standards.

Furthermore, an adaptive garment model using actual data of a group of pregnant women was made by Sohn and Bye [206]. They virtually tailored a pattern on a pregnant body and suggested that the patterns changed with the body changes although not consistently. They showed fit of the final produced pattern for two different women (A and B) in the 8th month of pregnancy as represented in Figure 1-18. However, the sleeveless sheath designed dress was not correctly fitted in the abdomen to the hip area.

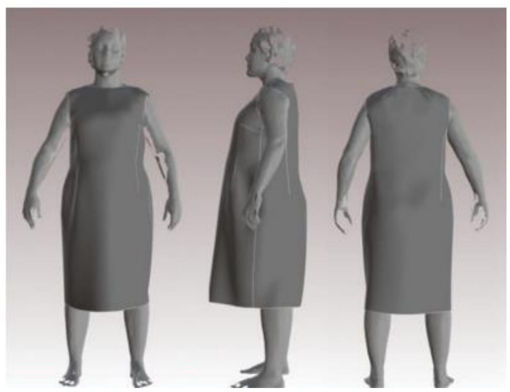

(a)

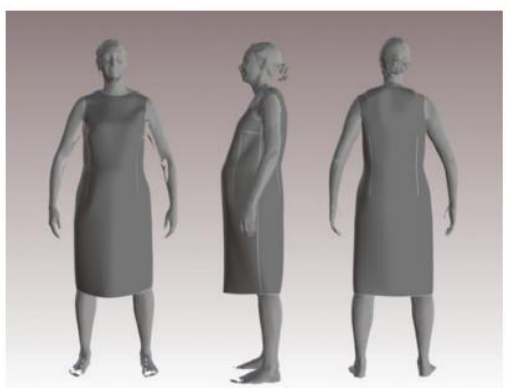

(b)

Figure 1-18- Fit of the final produced pattern for (a) subject A and (b) subject B in month 8 of pregnancy [206]

1.4 Research strategy

Electromagnetic shielding effectiveness definition and theory, as well as characteristics and measurements, were described in detail in this chapter. Also, the main techniques and materials for electrical conductivity enhancement in textiles for electromagnetic shielding applications reviewed in detail.

As explained in this chapter, metal yarns and fibers are highly effective for electrical conductivity enhancement and electromagnetic shielding effectiveness improvement in textiles. However, poor washability, uncomfortability (e.g. high weight and skin allergy) and mechanical abrasion are the limitations of using metals in textiles. Also, intrinsic conductive polymers suffer from weak mechanical properties which make them incompatible to be applied in the traditional textile process.

Thus, the research moved in the direction of thermoplastic polymer-based nanocomposite development for electromagnetic shielding effectiveness application. It was found that polymer-based nanocomposite seemed to be an effective and reliable substance for electrical conductivity development intended for electromagnetic shielding effectiveness expansion in textiles. A polymer-based nanocomposite was suggested to be replaced with metal-based electromagnetic shielding effectiveness textiles due to the light weight, flexibility, durability, and thermal expansion matching of the polymer-based nanocomposites.

A research strategy is presented in order to accomplish the objective of the study:

I. A set of 2D and 3D woven fabrics were manufactured using metals as electrical conductive yarns in order to investigate the effects of woven fabric characteristics on electromagnetic shielding effectiveness behavior. First, the effects of electrically conductive yarn density, two different metal materials, and 2D simple woven weave structures were investigated on electromagnetic shielding effectiveness (measured in an anechoic chamber). Then, the effects of structural parameters of a set of 3D woven fabrics with metal-based yarns on electromagnetic shielding behavior were analyzed while the quantity of the electrically conductive material was increased through the thickness of the 3D woven structures. The idea was to overcome the limits of the 2D manufactured fabrics for electromagnetic shielding purposes.

II. A textile-based nanocomposite monofilament was suggested to be replaced with metal-based textiles for electromagnetic shielding effectiveness due to the properties of the polymer-based nanocomposites like light weight and well-established manufacturing processes. Therefore, A set of CPC monofilaments was developed so as to boost the electrical conductivity of PA6,6-based nanocomposites which is a popular polymer in textiles. Therefore, two different nanofillers including multiwall carbon nanotube (MWCNT) and carbon black (CB) in PA6,6 matrix were used to develop the electrical conductive nanocomposites and the electrical and morphological properties of the developed nanocomposites was investigated.

III. In the next step, the synergism between nanofillers was applied to increase the electrical conductivity and decline the complications caused by the inclusion of nanofillers in the melt mixing method. In addition, a high-structured carbon black (KB) was mixed with MWCNT added to the polymer matrix in order to study the effects of adding KB (high-surface-area nanofiller) on electrical properties.

IV. Two candidate monofilaments were chosen regarding the electrical and morphological properties for woven fabric making intended for EMSE personal protection clothing. The mechanical properties of the candidates were also analyzed. Woven structures were designed applying the monofilaments candidates and cotton yarns and the EMSE was evaluated in a mode-stirred chamber were applied since the measurement completed in a mode-stirrer chamber seem to be more accurate as such apparatus allows evaluating the shielding effectiveness of fabrics in a realistic electromagnetic environment where the wave polarization cannot be controlled. It should be noted that the final application of the produced fabrics is for personal protective clothing in a living environment where the wave polarization cannot be controlled.

V. The final goal of this thesis was to protect both mother and fetus against the existing radiation in human living environment. So, first, a parametric graphical method was utilized to develop a 3D virtual mannequin for the pregnancy period based on women's weight by analyzing body morphology evolution during pregnancy. After that, a customized protective garment block pattern was virtually designed which was well-fitted on the 3D virtual mannequin of the pregnant subject.

Chapter 2: The effects of structural parameters of woven fabrics with metal yarns on electromagnetic shielding behavior

This chapter discusses the effects of structural parameters of a set of two-dimensional (2D) and three-dimensional (3D) woven fabrics using metal yarns as electrically conductive materials for electromagnetic shielding effectiveness (EMSE).

Firstly, a set of 2D woven fabrics was weaved and the EMSE of the woven fabrics was measured and analyzed. Then, due to the fact that changing the properties of the 2D woven fabrics have not established a considerable growth in the level of EMSE, a set of 3D warp interlock woven fabrics with metal yarns was introduced for the EMSE applications in the frequency range of 1-6 GHz. It is also noted that there are more potentials in the design of 3D warp interlock woven fabric structures compared to 2D woven fabrics.

2.1 Characterization

2.1.1 Waviness degree of the yarns

Waviness degree or crimp is determined by the relation of the length of yarn in the fabric to the length of the fabric in the warp direction or weft direction [207], [208]. So, crimp percentage is measured by the ratio between the length of the fabric sample and the corresponding length of the straightened yarn when it is being removed from the fabric as represented in Figure 2-1.

In this chapter, the crimp percentage of the yarns (waviness degree) was determined for all the woven samples in both warp direction(y) and weft direction(x) based on ASTM D3883-04 standard [208]. 10 yarn samples, each 10 cm in length, were used for the measurement and the mean value of crimp percentage for each variant was calculated according to the standard.

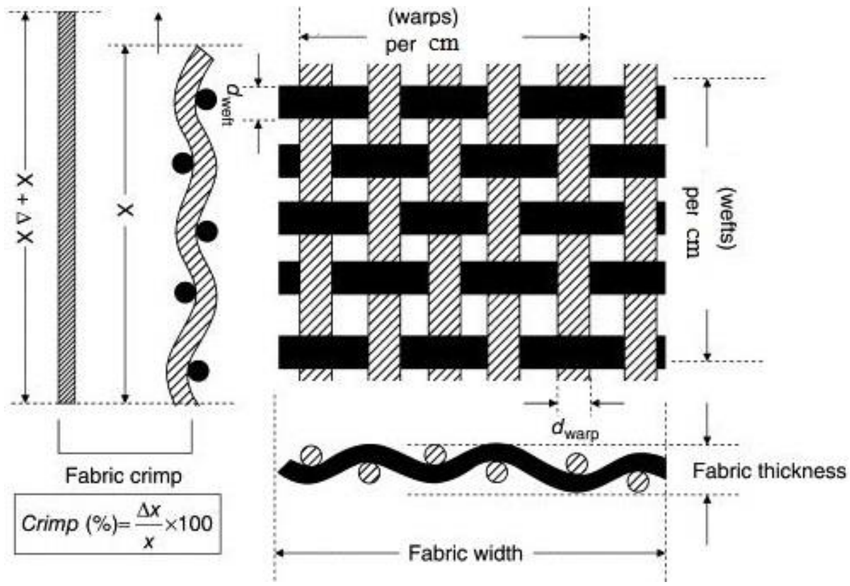

Figure 2-1- Waviness degree (crimp) definition of the yarns in a woven fabric [207]

Also, the amount of yarns in warp direction(y) and weft direction(x) per square meter can be calculated for woven fabrics using equation (12) and (13) while m shows the weight of the yarn (g), P is the symbol of yarn density (yarns/cm), N_m shows the metric number of the yarn and W_D is the waviness degree of the yarn (%). The total quantity of the yarns in a woven fabric can be defined using equation (14).

$$m_{warp} = \frac{P_{warp}}{N_{m(warp)}}(W_{Dwarp} + 100)\ (g/m^2) \tag{12}$$

$$m_{weft} = \frac{P_{weft}}{N_{m(weft)}}(W_{Dweft} + 100)\ (g/m^2) \tag{13}$$

$$m_T = m_{warp} + m_{weft}\ (g/m^2) \tag{14}$$

2.1.2 Fabric porosity

The porosity of woven fabrics can be estimated using equation (15) where cover factor (CF) is a measure of the area of the fabric occupied by yarn systems (g/cm^3) and ρ_{fiber} is the fiber density (g/cm^3). Hence, the porosity of all the manufactured woven fabrics was estimated using equation (15). It should be taken into account that the total fiber density was determined using equation (16) since different materials were used for all the fabrics [207], [209], [210].

$$\text{Porosity} = \left(1 - \frac{CF}{\rho_{fiber}}\right) \times 100 \tag{15}$$

$$\rho_{fiber} = \frac{\text{quantity of fiber1 } (\%) \times \rho_{fiber1} + \text{quantity of fiber2 } (\%) \times \rho_{fiber2}}{100} \tag{16}$$

2.1.3 The electrical conductivity of fabrics

The electrical properties of fabric samples can be measured using 4-wire ohms measurement (4w). The principle of this method is shown in Figure 2-2(a) [211]. The electrical resistance of the 2D woven fabrics was measured using Keithley SMU 2461 source meter by applying a given DC voltage and measuring the current passing through the sample. The voltage varied from -0.5 to 5 V with an automatic increment of 0.5 V and the (I/V) curve was plotted for each fabric sample. The electrical resistance (R) was concluded as the inverse slope of the curve. The electrometer was connected with a Keithley resistance chamber given in Figure 2-2(b) where the fabric sample was located between the two electrodes in the resistance chamber.

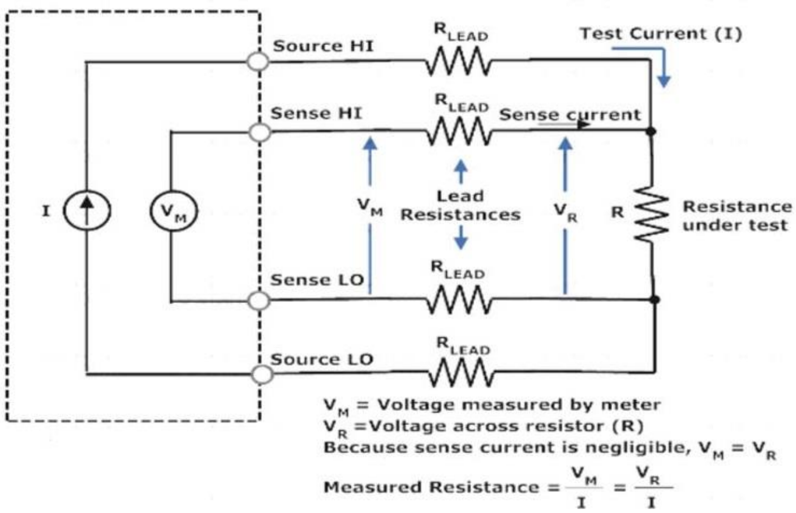

(a)

(b)

Figure 2-2- (a) The schematic of the resistance measurement principle, (b) Keithley resistance chamber

All fabric samples had to be prepared with a dimension of $10 \times 10\ cm^2$. Then, the resistance of the sample was measured, and σ or the volume electrical conductivity (S/m) was calculated using equation (17) where R represents the measured electrical resistance (Ω) and t indicates the thickness of the fabric sample (m).

$$\sigma = \frac{22.9}{t} \times \frac{1}{R} \quad (17)$$

2.1.4 Electromagnetic shielding effectiveness measurements using an anechoic chamber

As explained in Chapter 1, there are several approaches to measure the EMSE of planar materials like woven fabrics. For example, an anechoic chamber has been employed to measure the EMSE of the fabrics by numerous related studies [30], [32], [34], [35], [41], [212], [213].

In this chapter, a measurement setup was set in an anechoic chamber to measure the EMSE of the woven fabrics. A schematic of the measurement setup in an anechoic chamber is represented in Figure 2-3. In this setup, two horn antennas were used as emitting and receiving antennas. The receiving antenna was surrounded by absorbent pyramids with the purpose of determining accurate EMSE of the fabric samples.

The EMSE measurement of the woven fabrics was carried out at the frequency range of 1-6 GHz (intermittently every 100 MHz) for the woven fabric samples (2D and 3D) while the dimension of each specimen was 16×16 cm^2. It is noted that the measurements were completed at the frequency range of 1-6 GHz where this frequency range is in accordance with the utilized frequencies for commonly use electronic devices such as handsets [214].

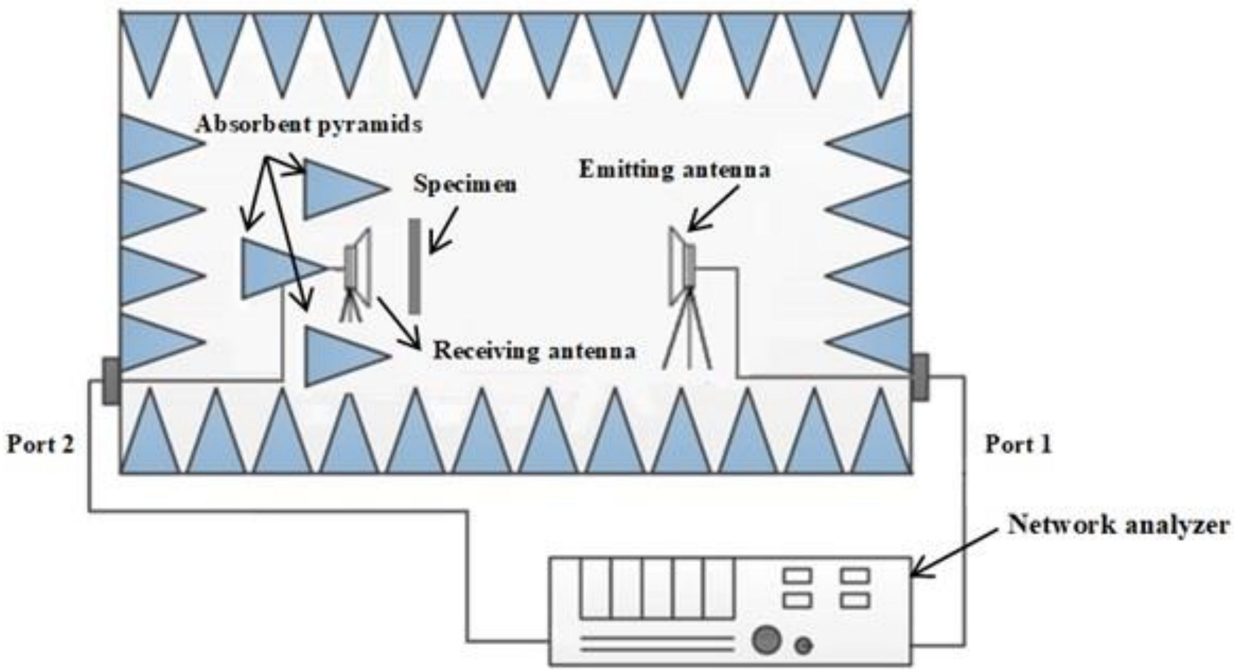

Figure 2-3- Schematic demonstration of the proposed setup for EMSE measurement in an anechoic chamber [215]

A reference test was performed without any fabric samples to consider the losses in the cables, the antennas, and free space. It should be noted that this measure was recorded before running the experiments and the measured value was considered the reference value for all the woven fabrics ($S21_{reference}$).

After that, the measurement was accomplished when the fabric specimen was located in the required place in the measurement setup ($S21_{with\ sample}$). The transmission measurement had to be normalized for all the woven fabrics using the reference value using equation (18) where S21 is a measure of the electric field (E), which transfers from port 1 to port 2, by a vector network analyzer.

$$\mathrm{EMSE(dB)} = \mathrm{S21}_{\text{with sample}}\mathrm{(dB)} - \mathrm{S21}_{\text{reference}}\ \mathrm{(dB)} \qquad (18)$$

2.2 Two-dimensional (2D) woven fabrics for electromagnetic shielding effectiveness

As discussed in Chapter 1, the properties of woven fabrics have diverse effects on the electromagnetic shielding behavior of woven fabrics. In the following section, a set of 2D woven fabrics was manufactured and the effects of the fabric properties were investigated on the EMSE behavior.

2.2.1 Materials for 2D woven fabrics

- Polyamide 12 (PA12) staple yarn coated with silver (N_m 40/2), (17% silver, 83% polyamide 12) supplied by Queen in China, (with a conductivity of 62.1×10^6 S/m) for weft.
- Inox staple yarn (N_m 5/2) supplied by Tibtech in France, (with a conductivity of 1.32×10^6 S/m) for weft.
- Wool/Polyethylene terephthalate (PET) staple yarn (N_m 20/2) with the ratio of (40%Wool: 60% PET) for warp.

2.2.2 Conception and weaving of 2D woven fabrics

Three simple weave structures (plain, 2/2 Z-twill, and 4 end irregular satin) were used for 2D woven fabrics making in this chapter. The schematics of the three weave structures are shown in Figure 2-4.

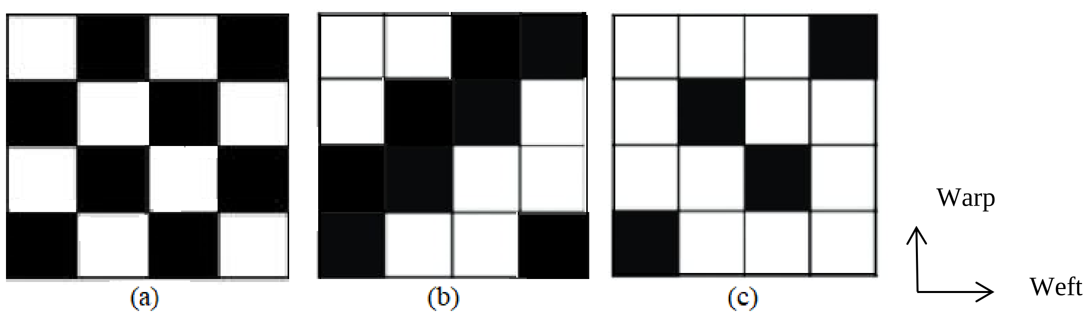

Figure 2-4- The weave structures used for 2D woven fabrics making, (a) Plain, (b) 2/2 Z-twill and (c) 4 end irregular satin

For the first set of the 2D woven fabrics, wool/PET staple yarns were inserted in warp direction and polyamide 12 staple yarns coated with silver (PA12 coated with silver) were inserted in weft direction. On the other hand, Inox staple yarns were inserted in weft direction for the second set of the 2D woven fabrics keeping the same warp yarns material and threading. The objective was to apply two different electrical conductive yarns in two different sets of proposed woven fabrics. Also, two weft yarn densities 8 (yarns/cm) and 16 (yarns/cm) were used for the electrically conductive weft yarns (PA12 coated with silver) in the first set of the 2D woven fabrics while the conductive weft density was only 8 (yarns/cm) for the second set of the 2D woven fabrics. The structural characteristics of all the 2D woven fabrics (S1-S7) are listed in Table 2-1. It should be noted that all the woven samples were weaved using ARM AG CH-3507 Biglen weaving loom manufactured in Switzerland.

Table 2-1- Structural characteristics of 2D woven fabrics

			Variant						
No.	Characteristics		S1	S2	S3	S4	S5	S6	S7
1.	Weave structure		Plain	Plain	Twill	Twill	Plain	Twill	Satin
2.	Raw material	warp	Wool-PET						
		weft	PA 12 coated with silver				Inox		
3.	Yarn fineness	warp	20/2				20/2		
	(N_m)	weft	40/2				5/2		
4.	Yarn density	warp	18	18	18	18	18	18	18
	(yarns/cm)	weft	16	8	16	8	8	8	8
5.	Crimp percentage	warp	3.3	2.3	3.2	2.2	4.2	3.9	3.6
	or waviness degree (%)	weft	2.7	2	1.3	1.2	3.6	3.1	1.5

Furthermore, graphical representation of the 2D woven fabrics with three different weave structures containing electrical conductive yarns (PA12 coated with silver or Inox) in weft direction sketched by Wisetex software (virtual textile software) are shown in Figure 2-5.

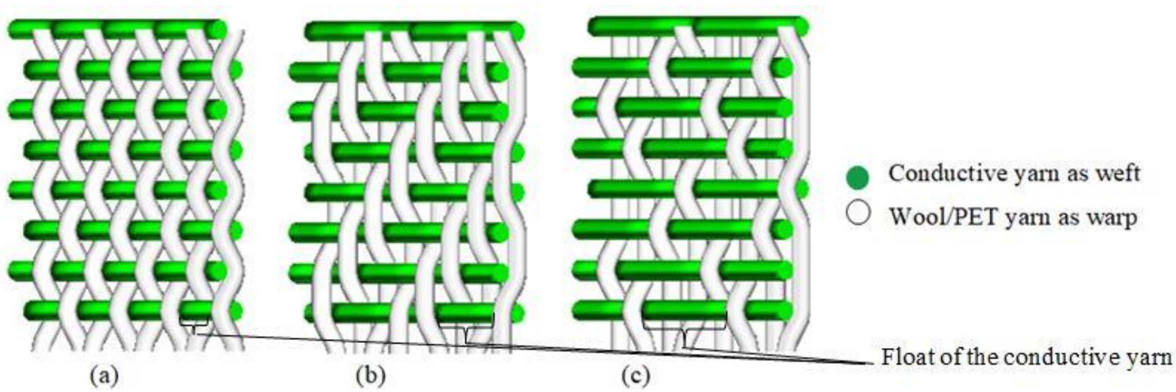

Figure 2-5- Graphical representation of the 2D woven fabrics, (a) Plain weave structure, (b) 2/2 Z-Twill weave structure, (c) 4 end irregular Satin weave structure (sketched by Wisetex software)

Also, the float of the conductive wefts for three weave structures is indicated in Figure 2-5. The float of the yarn (e.g. wefts) is the length of the yarn between two consecutive intersections with the yarns at right angles to it (e.g. warps). The float of the wefts is increased from plain weave structure to 2/2 Z-twill weave structure, followed by 4 end irregular satin weave structure.

Moreover, areal density, width, thickness, and volume density of all the manufactured 2D woven fabrics are listed in Table 2-2. Also, the porosity and the volume electrical conductivity of all the 2D woven fabrics which were determined using the explained methods in section 2.1.3 are represented in Table 2-2.

Table 2-2- Areal density, width, thickness, fabric density, porosity and the volume electrical conductivity of the manufactured 2D woven fabrics

			Variant						
No.	Property	Unit	S1	S2	S3	S4	S5	S6	S7
1.	Areal density	g/m^2	137	127	152	128	202	208	217
2.	Fabric width	cm	25	25	25	25	25	25	25
3.	Fabric thickness	mm	0.46	0.58	0.54	0.68	0.7	0.80	0.95
4.	Fabric density	g/cm^3	0.298	0.220	0.281	0.188	0.341	0.323	0.256
5.	Fabric porosity	%	83	86	84	88	94	95	96
6.	Electrical conductivity	S/m	250	180	428	290	120	146	121

2.2.3 Investigation of the electromagnetic shielding effectiveness of 2D woven fabrics

The EMSE of all the manufactured woven fabrics using two different metal yarns (S1-S4) and (S5-S7) was measured in weft direction(x) at the frequency range of 1-6 GHz and represented in Figure 2-6.

As explained earlier, directive horn antennas were applied as emitting and receiving antennas and the test was performed when the fabric width was parallel to the vertical antenna polarization. It means that the EMSE of the samples was measured in weft direction(x) since the conductive yarns were inserted in the weft direction of the woven fabrics during weaving.

Moreover, the average curve of the EMSE values of each 2D woven fabric (S1-S7) is shown in Figure 2-7. Five consecutive EMSE values (intermittently every 100 MHz) at the frequency band of 1-6 GHz were used to calculate the mean value of the EMSE at every 500MHz. The average of EMSE values was calculated and presented in order to address the results clearly by reducing the scattering of data where the EMSE at different frequencies for each woven sample could be distinguished.

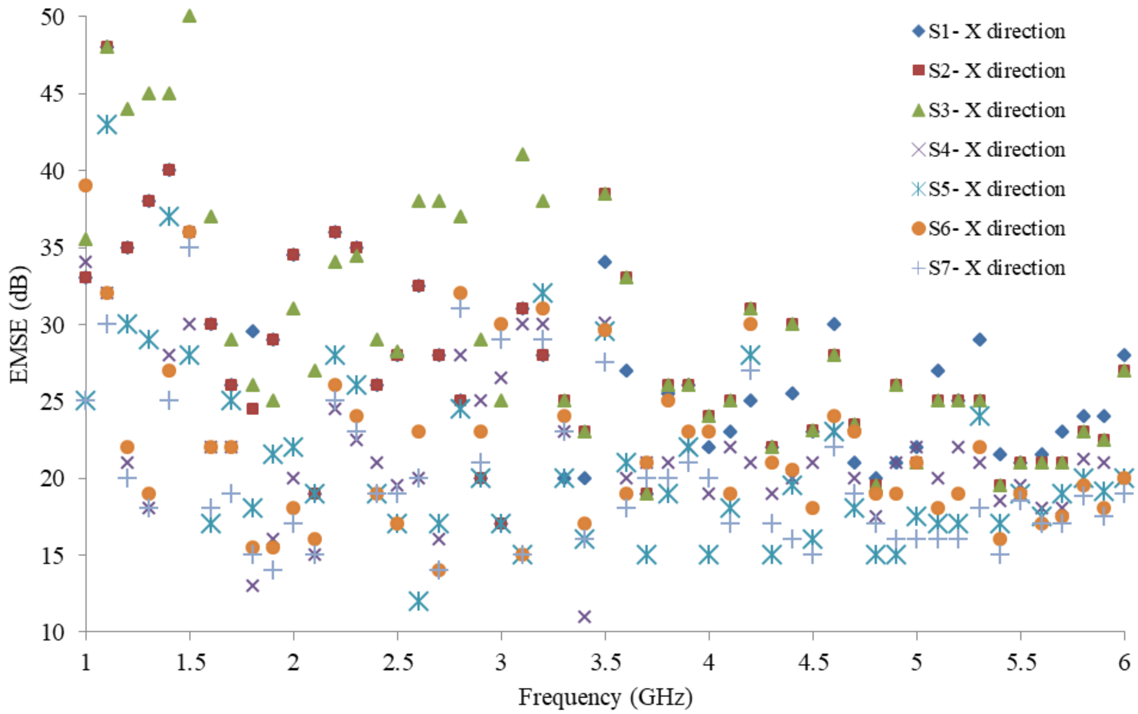

Figure 2-6- The EMSE of the 2D woven fabrics (S1, S2, S3, S4, S5, S6, and S7) measured in weft direction(x)

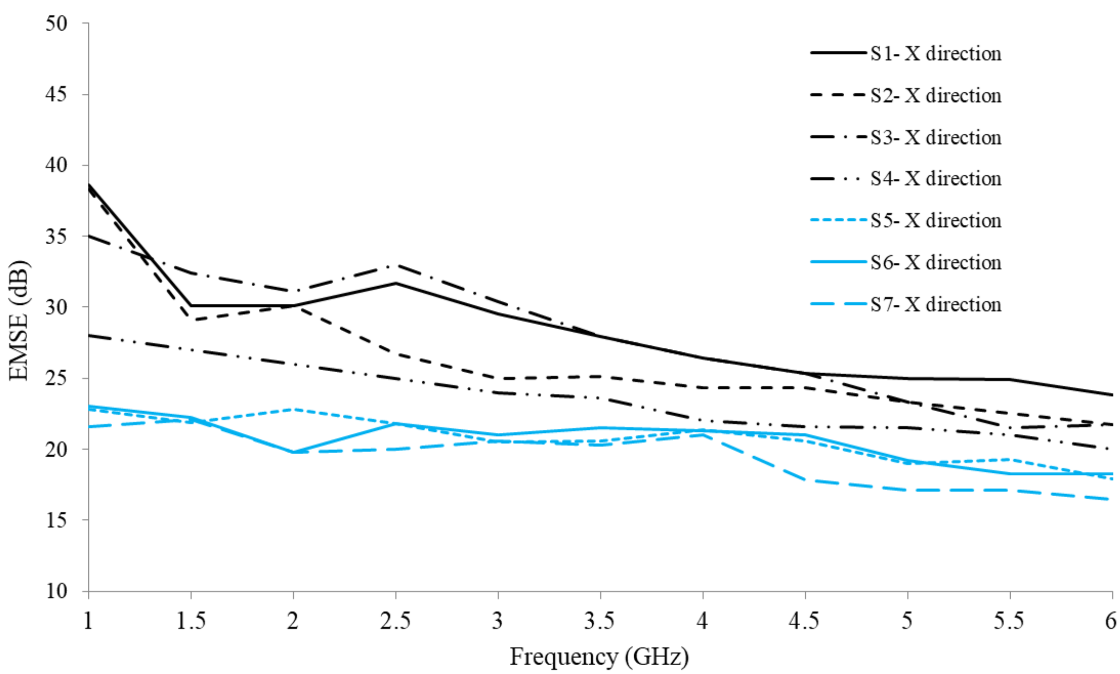

Figure 2-7- The average curves of the EMSE for the 2D woven fabrics (S1-S7) measured in weft direction(x)

The main idea of producing a set of 2D woven fabrics using metallic yarns with different weave structures, metal types and density of the conductive yarns was to study the effects of these characteristics on the level of the EMSE.

First of all, four different woven fabrics were produced using PA 12 coated with silver as the conductive material in weft direction of the woven fabrics (S1-S4). Two different simple woven structures were applied to manufacture the woven fabrics samples of S1-S4 while the density of the conductive yarns was 16 (yarns/cm) for S1 and S3 and it was 8 (yarns/cm) for S2 and S4. It should be noted that the warp yarns were non-conductive (wool/PET yarns) and the warp density was set at 18 (yarns/cm) for all the fabrics. The strategy was to investigate the effects of two weave structures (as given in Table 2-1) together with changing the yarn density on the EMSE behavior of the first set of 2D woven fabrics.

As can be seen in Figure 2-7, the EMSE values of samples S1 and S3 were nearly the same (23-39 dB for S1 and 21-35 dB for S3) while the density of the conductive yarns was equal for S1 and S3. However, the weave structure was different for S1 and S3. In the higher frequency (6 GHz), the difference between the EMSE values of S1 and S3 was bigger (39 dB vs 35 dB).

Also, the EMSE of S2 and S4 was lower than the EMSE of S1 and S3 (5% lower EMSE for S2 compared to that of S1 and 12% lower EMSE for S4 compared to the EMSE of S3) due to the lower density of the conductive yarns for S2 and S4 (8 yarns/cm) in comparison with S1 and S3 (16 yarns/cm). It is attributed to the bigger number of the conductive yarns occupied per unit area applying larger yarn density of the conductive yarns.

Secondly, another set of 2D woven fabrics with Inox yarns as wefts were produced with three different weave structures (S5, S6, and S7). The main purpose was to define the best weave structure among three suggested simple weave structures for electromagnetic waves attenuation while the yarn density and the conductive material was the same for S5, S6, and S7.

The results showed that the EMSE level was approximately the same for S5, S6, and S7 despite the fact that the weave structures were dissimilar for these three woven fabrics as presented in Table 2-1. However, the EMSE values of S7 were a little lower (5%) than those of S5 and S6 which can be correlated to the weave structure of S7. It should be mentioned that the weave structure of S7 was 4 end irregular satin (Figure 2-4(c)).

The woven fabrics weaved with plain weave structure (S1 or S2 or S5) showed slightly higher EMSE values compared to the ones weaved with twill weave structure (S3 or S4 or S6) followed by the one weaved with satin weave structure (S7). The reason was correlated to the effects of floats of the conductive yarns on the EMSE which was also previously declared by Liu and Wang [84]. In fact, the plain weave fabric showed better shielding than that of the twill weave fabric followed by the satin weave fabric while the yarn density and conductive material remained unchanged.

Generally speaking, the interlace points between warps and wefts were the least for the woven fabric weaved with satin weave structure, and the floats were more so that the fabric was looser and the EMSE was lower. Moreover, the interlace points of the twill weave structure were fewer than that of the plain weave structure and more than that of the satin weave structure and consequently, the EMSE of the fabric weaved with twill weave structure was between the EMSE of the woven fabrics with plain and satin weave structures.

On the other hand, the similarity of the EMSE results of the woven fabrics with plain or twill weave structures having the same quantity of the same conductive materials ((S1 and S3), (S2 and S4) and (S5 and S6)) can be correlated to the diagonally arranged of the conductive yarns floats in the woven fabrics. It should be noted that this phenomenon has been previously acknowledged by Ozdemir *et al.* [85].

Comparing the EMSE results of the manufactured 2D woven fabrics with two different conductive yarns (PA 12 coated with silver or Inox), higher EMSE values were revealed for the woven fabrics with PA 12 coated with silver yarns as wefts (S2 and S4) keeping the same weave structures (plain for S2 and S5 and twill for S4 and S6) as well as the same yarn density 8 (yarns/cm).

The EMSE of S2 was in the range of 21-38 dB while the EMSE was in the range of 17-23 dB for S5. Also, the EMSE of S4 was varied in the range of 20-28 dB by changing the frequency between 1 and 6 GHz while it was 18-23 dB for S6. The reason was associated with the higher electrical conductivity of silver in comparison with Inox where the electrical conductivity of silver is nearly fifty-fold as big as Inox (the conductivity of silver is 62.1×10^6 S/m and the conductivity of Inox is 1.32×10^6 S/m). However, the quantity of electrically conductive material was greater in S5 and S6 due to the bigger diameter of Inox yarns (yarn fineness: Nm 5/2) in comparison with PA 12 coated with silver yarns (yarn fineness: Nm 40/2).

It should be also noted that no correlation was detected between the EMSE and the electrical conductivity of the 2D woven fabrics given in Table 2-2. For example, the EMSE of S3 and S1 were nearly the same while the electrical conductivity was relatively higher for S3 (428 S/m) in comparison with the electrical conductivity of S1 (250 S/m).

However, the weaved woven fabrics with PA 12 coated silver yarns as conductive weft revealed both the higher volume electrical conductivity and the EMSE values (e.g. the electrical conductivity of S2 weaved with PA 12 coated with silver as weft yarns was 180 S/m and its EMSE was in the range of 21-38 dB while the electrical conductivity was 120 S/m and the EMSE was in the range of 17-23 dB for S5 having Inox as conductive wefts).

2.3 Three-dimensional (3D) warp interlock woven fabrics for electromagnetic shielding effectiveness

The effects of structural parameters on the EMSE properties of 2D woven fabrics were investigated in section 2.2. As explained, changing the metal yarns density, weave structures and conductivity of the yarns have slightly changed the EMSE of the manufactured 2D woven fabrics. In the following section, a set of five variants of 3D warp interlock woven fabrics containing silver multifilament yarns arranged in 3D orthogonal grids were produced. The ultimate goal was to examine the increase in the EMSE as a factor of increasing the quantity of the conductive material per unit area through the thickness of the compound woven fabrics when the yarn density and yarn fineness of the conductive yarns were fixed. The effects of structural parameters of 3D warp interlock woven fabrics on the EMSE was studied due to the fact that there were more possibilities in structures design and properties alterations of 3D woven fabrics compared to 2D woven fabrics which have not been considered by previous studies in the field of shielding textiles.

The amount of the conductive material per unit area in a woven fabric can be increased by two following methodologies while the unit cell size of the woven fabric kept constant:

a. Increasing the yarn undulation, for both simple and compound woven fabrics
b. Increasing the number of conductive yarn systems in compound woven fabrics

Undulation of the yarns (Figure 2-8) in a woven fabric is changed by changing the weave structure. A weave structure with higher interlacing frequency can be employed to increase the undulation of the yarns in a simple 2D woven fabric (for instance, plain weave structure instead of satin weave structure). It should be taken into account that the higher interacting frequency between the yarns in a woven fabric results in lower floats of the yarns as discussed in the previous section.

On the other hand, the amplitude of undulation can be increased together with increasing the interlacing frequency of the yarns in a compound woven fabric. As a result, increasing the binding depth (BD) in a compound woven fabric leads to the larger amplitude of the yarns' undulation.

Here, it was essential to explain the explanation of undulation; amplitude and frequency and binding depth in woven fabrics as these parameters were applied to change the quantity of conductive material in the proposed 3D warp interlock woven structures.

Undulation characterizes as displacement of the yarn axis from its linear position caused by the incorporation of the yarn in the woven structure. The structural parameters of compound woven fabrics such as warp and weft yarn properties (raw material, fineness, and density), weave structure, weaving and finishing process can alter the displacement of the yarn axis. Yarn undulation is expressed by either amplitude or frequency while amplitude (h) denotes the distance between projections of two consecutive yarns centres of the same yarns system on a vertical plane as given in Figure 2-8. Also, the number of crossing wefts (or warps) by a warp (or a weft) in a regular repeated manner is indicated as undulation frequency. Yarn undulation degree or waviness degree which is also called crimp in practice is commonly shown in percentage. Moreover, binding depth (BD) is the number of weft layers crossed by a warp yarn in a weave repeat while the binding depth modification can alter the amplitude of the warp yarns in 3D warp interlocks woven fabrics.

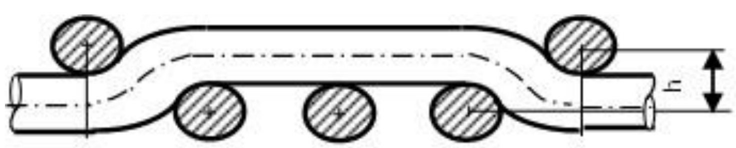

Figure 2-8- The yarn undulation in a woven fabric (h) [215]

The compound woven structures were designed in order to integrate the conductive yarns so that they were not apparent on the fabric faces thanks to the 3D interlock woven structures. This parameter was of great importance since the final application of the manufactured woven fabrics was for wearable EMSE devices. Also, the continuity of the conductive network at all the binding points was apprehended in the design of the structures.

2.3.1 Materials for 3D warp interlock woven fabrics

- Silver multifilament yarn (N_m 9.26, 10×0.04mm) supplied by Elektrisola in Germany. This multifilament yarn is low electrical resistance and high corrosion resistance (with a conductivity of 62.5 S/m², tensile strength 220 MPa, maximum elongation 40%) for both warp and weft.

- Pure cotton staple yarn (N_m 20/2) for warp.
- Pure cotton staple yarn (N_m 16/2) for weft.

It should be taken into account that non-conductive yarns do not have any direct contribution to the EMSE behavior of fabrics. As a result, the non-conductive yarns were substituted with cotton yarns for 3D warp interlock woven fabrics. The reason was associated with the breathability and comfortability of the pure cotton yarns. However, any common textile yarn could be used as a non-conductive yarn in the manufactured woven structures.

2.3.2 Conception and weaving of 3D warp interlock woven fabrics

Silver multifilament yarns were integrated as conductive warp and weft yarns in the structures of 3D warp interlock woven fabrics. The silver multifilament yarns were strengthened by doubling with cotton yarns (N_m 20/2 cotton yarns in warp direction and N_m 16/2 cotton yarns in weft direction) to reinforce the silver multifilament yarns.

In other words, the utilized silver multifilament yarn was fine (diameter: 0.12 mm) with a low friction resistance. So, the silver multifilament was reinforced with cotton yarns for warp and weft insertion in order to protect silver against the mechanical forces (e.g. mechanical abrasion) during weaving and use. Hence, the developed hybrid conductive yarns (cotton/silver) were applied in both warp direction(y) and weft direction(x) of the 3D woven interlock woven structures.

Four 3D warp interlock woven fabrics structures were designed employing hybrid conductive yarns in both warp direction and weft direction. The conductive yarns integrated into the middle ply for the first four variants (V1, V2, V3, and V4) as specified in Table 2-3. These variants (V1-V4) were designed with three weft yarn systems where the hybrid conductive yarns were engaged in between of the two other cotton weft yarn systems. Also, the density of the conductive weft yarns was 7 (yarns/cm) for all the four designed variants (V1-V4).

Moreover, to have the same density of the conductive warps 11 (yarns/cm) for all the four variants (V1-V4), the distribution of warps in the Reed was finished by using 3 yarns/dent (1: cotton yarn, 1: conductive yarn, 1: cotton yarn).

An additional variant (denoted by DL), was also designed with two weft yarn systems where hybrid conductive yarns were engaged in both weft systems. The other structural properties of the variant DL e.g. yarn fineness, yarn density of each layer, warp systems number and the ratio between conductive and nonconductive yarns in warp direction were comparable to the other four variants (V1-V4). Structural characteristics of all the 3D warp interlock woven fabrics (V1-V4 and DL) are shown in Table 2-3.

Table 2-3- Structural characteristics of the 3D warp interlock woven fabrics [215]

No.	Characteristics			Variant V1	V2	V3	V4	DL*
1.	Number of yarn systems	warp		3	3	3	3	3
		weft		3	3	3	3	2
2.	Raw material	warp		Wp_1: Cotton Wp_2: Cotton + Silver Wp_3: Cotton				
		weft		Wf_1: Cotton Wf_2: Cotton + Silver Wf_3: Cotton				Wf_1: Cotton + Silver Wf_2: Cotton + Silver
3.	Yarn fineness (m/g or N_m)	Cotton warps		N_m 20/2				
		Cotton wefts		N_m 16/2				
		Silver		N_m 9.26				
4.	The ratio of yarn systems	warp		$1Wp_1{:}1Wp_2{:}1Wp_3$				
		weft		$1Wf_1{:}1Wf_2{:}1Wf_3$				$1Wf_1{:}1Wf_2$
5.	Yarn density (yarns/cm)	Per layer	warp	11	11	11	11	11
			weft	7	7	7	7	7
		total	warp	33	33	33	33	33
			weft	21	21	21	21	14

* DL is the abbreviation for double-layer.

Also, graphic representations of longitudinal sections of the 3D warp interlock woven fabrics with hybrid yarns are demonstrated in Figure 2-9. It should be taken into account that the metal exposure to the air was avoided by binding the warps with three layers of the wefts in a way that the conductive warps were not apparent on the exterior faces of the designed woven fabrics in the structures of V1, V2, V3, and V4. The reason was to protect the metal yarns from oxidation as well as preventing metal touch with the skin of the wearer. As specified in Chapter 1, metals can largely cause skin allergic for the wearer although silver caused fewer issues of allergic, oxidation and corrosion in comparison with other metals.

Least possible binding depth was suggested for the first variant (V1) as represented in Figure 2-9(a), followed by V2 (Figure 2-9(b)), V3, and V4 (Figure 2-9(c and d)). Accordingly, the hybrid conductive yarns covered a larger depth of the thickness of the manufactured 3D warp interlock woven fabrics by increasing the binding depth (BD) from V1 to V4. It should be noted that the binding depth of V3 and V4 were identical at the maximum possible layers for the designed compound woven fabrics (BD=2 layers) as indicated in Figure 2-9(c and d).

Similarly, the waviness degree of the silver multifilament warp yarns was enlarged through increasing the binding depth (BD) of the conductive warps in the designed fabrics which would be discussed further in this chapter. Hence, binding depth of the conductive warps was set at BD = 0 layer for V1, was enlarged to BD = 1 layer for V2 and BD = 2 layers for V3 and V4.

Furthermore, additional woven fabric (DL) produced with two hybrid conductive yarns as symbolized in Figure 2-9(e) when the binding depth (BD=2 layers) was the same as two other manufactured variants (V3 and V4). Two separated conductive weft yarn systems were integrated into the structure of DL which caused the discontinuity in the conductive warps alignments through the thickness of the fabric (DL). It should be also noted that unit cell length and width (unit cell size) were the same for all the designed structures (V1, V2, V3, V4, and DL).

Longitudinal cross-sections, weave structures and 3D renderings of the five compound woven variants (sketched by Wisetex software) are represented in Table 2-4 to reveal the position of the conductive yarns in the designed structures.

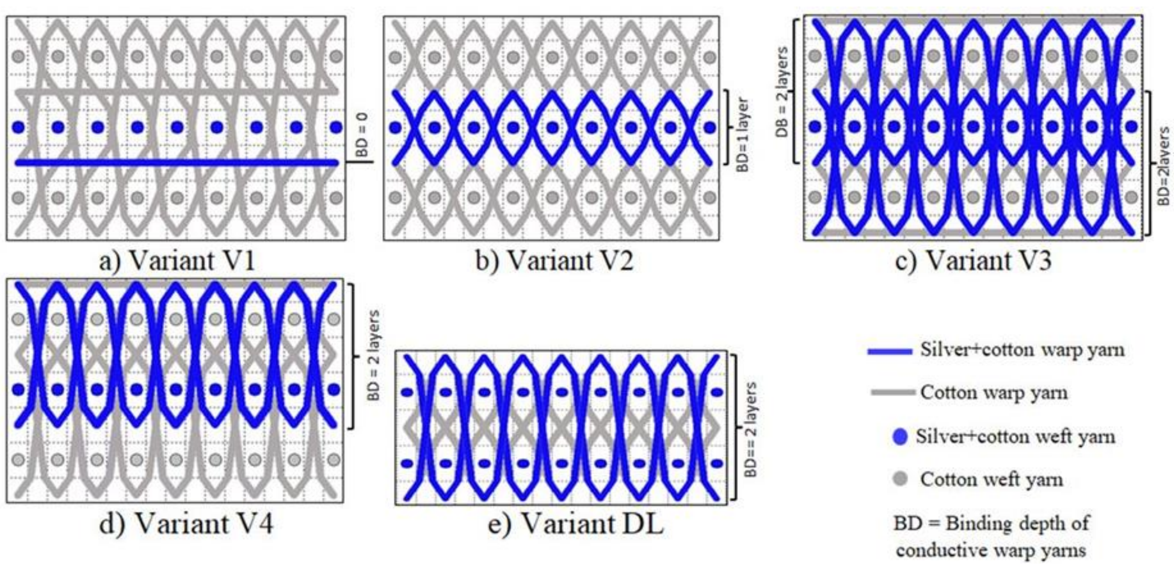

Figure 2-9- Graphic representations of longitudinal sections of five 3D warp interlock woven fabrics containing silver multifilament yarns in both warp direction and weft direction (sketched by Wisetex software) [215]

Table 2-4- Longitudinal section, weave structure and 3D rendering for the designed 3D warp interlock woven fabrics with an embedded conductive network [215]

Var.	Longitudinal section of the designed fabric containing conductive yarns*	Weave structure (1 repeat)	3D rendering of the designed fabric
V1	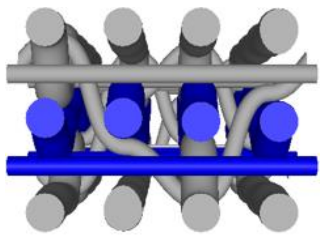	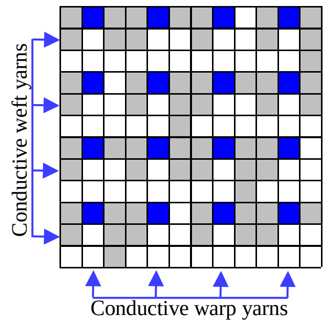	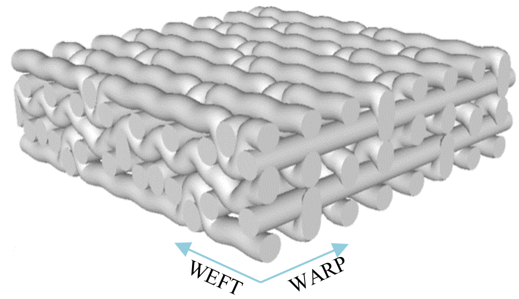
V2	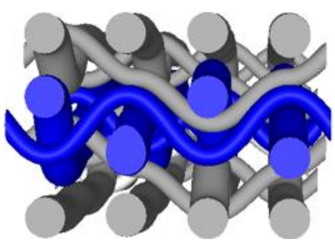	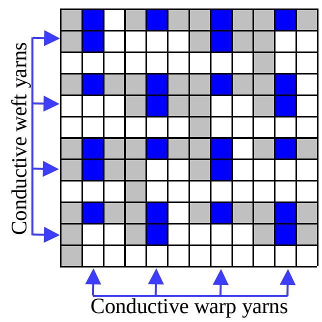	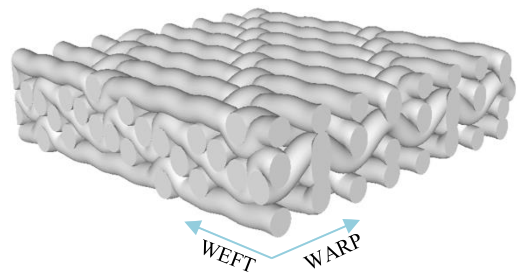
V3	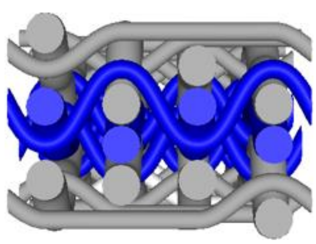	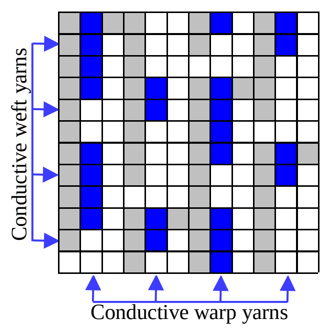	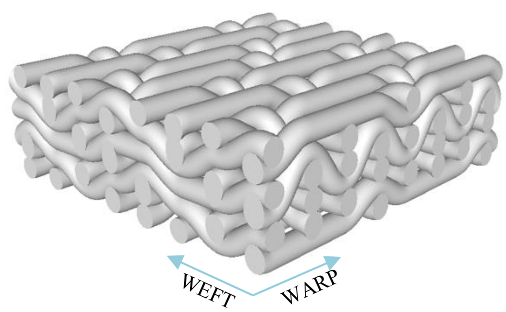
V4	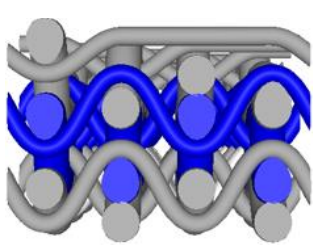	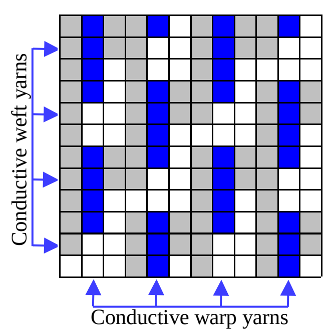	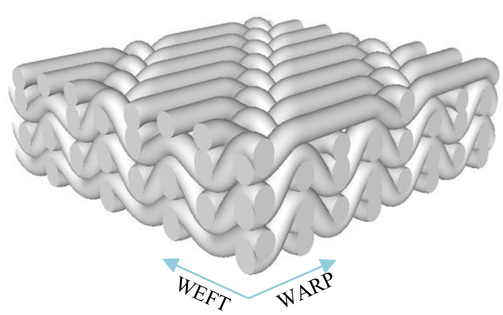

DL 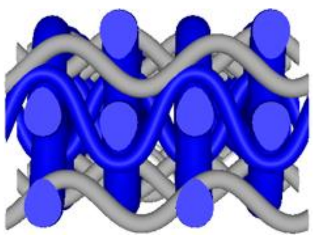 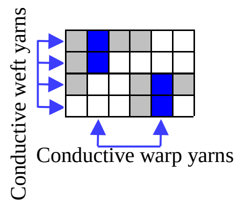

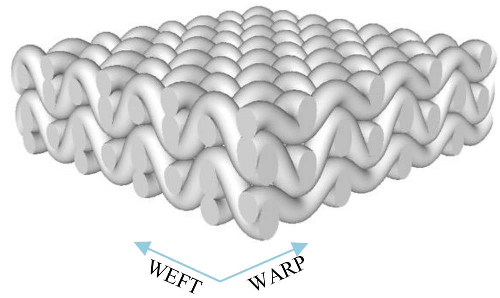

*Legend: Silver/cotton warp yarn; Cotton warp yarn; Silver/cotton weft yarn; Cotton weft yarn

In the next step, all the variants were weaved using ARM AG CH-3507 Biglen weaving loom. Straight threading on 12 shafts, Reed fineness of 10 dents/cm and 3 warp yarns/dent were deliberated as warp settings while the settings kept the same for weaving the variants (V1-V4 and DL). The face and back of all the compound woven variants are demonstrated in Figure 2-10.

As the final application of the manufactured compound woven variants was for personal protective clothing against radiation, different weave structures were selected for the face layer of the compound woven structures. It has to be considered that changing the weave structure of the face layer could not change the shielding behavior of the compound woven fabrics since this ply was composed of pure cotton yarns which were non-conductive. However, changing the weave structure of the face layer can change the shielding characteristics of the compound woven fabrics by altering the quantity or arranging of the conductive yarns through the thickness of the compound woven fabrics.

As can be seen in Figure 2-10, weave structures of the face and back ply of the compound woven fabrics were the same for V1 (4 ends irregular satin weave), V2 (1/3 twill weave), V3 (4 ends irregular satin weave), and DL (plain weave). On the other hand, the weave structures of the face and back ply were not matching for V4 (3/1 twill weave for the face ply and plain weave for the back ply).

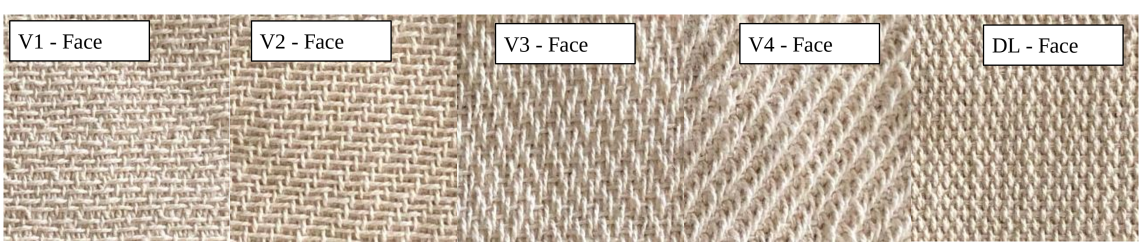

a) The face of the manufactured compound woven fabrics

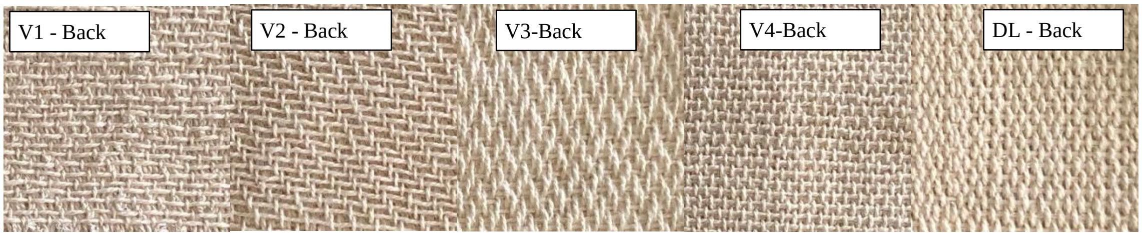

b) The back of the manufactured compound woven fabrics

Figure 2-10- The face and back of the 3D warp interlock woven fabrics (V1, V2, V3, V4, and DL) [215]

Furthermore, the images of the weaving loom and one of the manufactured variants (DL) are shown in Figure 2-11(a and b).

(a)

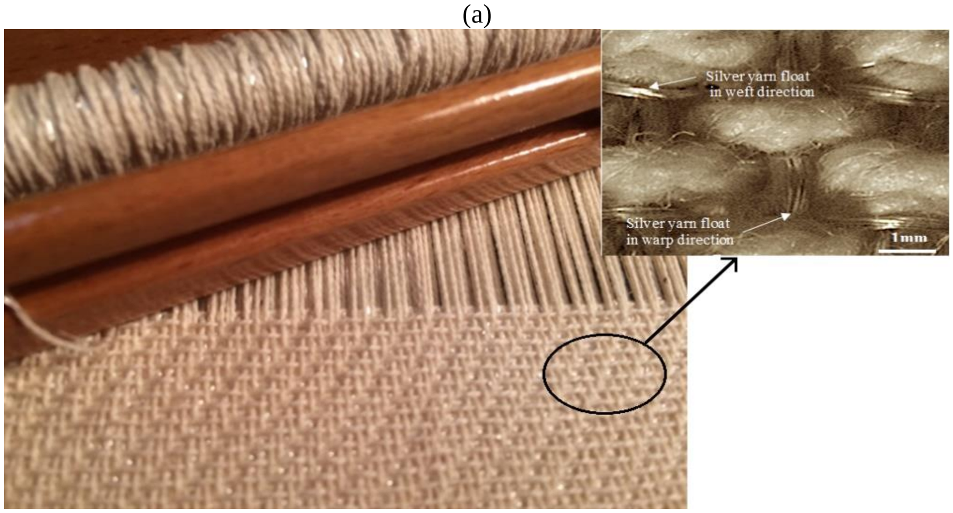

(b)

Figure 2-11- The images of (a) ARM weaving loom during weaving the variants and (b) The woven variant (DL)

The measured fabric density, width, thickness, and porosity of all the manufactured 3D warp interlock woven fabrics are listed in Table 2-5. The dissimilarity in the thickness of different variants was due to the movement of the yarns through the thickness in the relaxed state of the 3D warp interlock woven fabrics. As a matter of fact, the yarns moved through the thickness of each variant to find the minimum state of energy.

As can be understood from Table 2-5, the yarns remained in the preliminary position in V2 and V3 as the movement of the yarns was insignificant. Conversely, the lower fabric thicknesses were observed for V1 and V4 because the yarns relocated to find the position with the minimum state of the energy.

The fabric thickness of DL was smaller in comparison with the thicknesses of the other weaved variants (V1-V4) for the reason that there were only two weft yarn systems in the structure of this particular variant (DL).

Table 2-5- Fabric density, width, thickness, and porosity of the variants (V1-V4 and DL) [215]

			Variant				
No.	Property	Unit	V1	V2	V3	V4	DL
1.	Fabric density	g/cm^3	0.359	0.330	0.366	0.361	0.395
2.	Fabric width	cm	23	23	23	23	23
3.	Fabric thickness	mm	2.2	2.5	2.4	2.3	1.9
4.	Porosity	%	90	91	90	91	92

It should be taken into consideration that determining the electrical conductivity of the manufactured 3D warp interlock woven fabrics seemed irrelevant because the hybrid conductive yarns were integrated into the middle of the woven structures and the outer layers were made of pure cotton yarns.

Here, it was suggested in this thesis (Chapter 2 and Chapter 3) to correlate the EMSE of the woven fabrics with different structures and the properties of the conductive yarns (e.g. conductivity, quantity, etc.) which remained reasonable for all the manufactured woven fabrics.

2.3.3 **Structural characteristics of the 3D conductive networks**

The four manufactured 3D warp interlock woven variants (V1, V2, V3, and V4) had three warp yarn systems and three weft yarn systems in their structures. Two exterior layers of the woven fabrics consist of cotton warp and weft yarn systems with different simple woven structures while the conductive grid was suggested in the middle of each variant.

The effects of increasing the waviness degree of the conductive yarns were studied on the EMSE in the present thesis as the conductive yarns covered larger amplitude of the thickness of the 3D warp interlock woven fabrics by increasing the waviness degree of the conductive warps. It should be noted that the waviness degree was increased while the unit cell size kept constant.

On the other hand, the fifth variant (DL) composed of only two weft yarn systems while hybrid conductive yarns were introduced as wefts in the structure of this particular variant. Therefore, the conductive weft yarn density was doubled in DL compared to the other variants to study the effects of the density together with waviness degree of the conductive yarns on shielding properties of the compound woven fabrics. The performance of this factor on the EMSE will be further discussed in the next section.

The graphical representations of the conductive grids for all the five variants (front-left perspective view, longitudinal section, and cross-section) sketched by Wisetex software are displayed in Table 2-6.

As described earlier, only conductive component contributes to the EMSE behavior of textile products. So, the 3D conductive grid of each variant was the only operational part in EMSE behavior of the manufactured woven fabrics. Therefore, the structural characteristics of the conductive networks of all the variants were analyzed.

First, the waviness degree of the silver multifilament yarns was determined based on ASTM D3883-04 standard explained in section 2.1.1. Waviness degree (crimp percentage) of the conductive warp and weft yarns were measured by pulling out the silver multifilament yarns in both warp direction(y) and weft direction(x) of the compound woven variants. The mean values of the waviness degree for the silver multifilament warps and wefts of each variant was calculated using the measurements of 10 yarn samples, each 10 cm in length.

The properties of 3D conductive grids of all the variants are listed in Table 2-7. As can be seen in Table 2-7, waviness degree of the conductive warp yarns was gradually increased from V1 to V4. The waviness degree of the conductive warps was increased among four different variants (V1-V4) to increase the quantity of the conductive material through the thickness of the variants. The effects of the conductive material growing through the thickness of the variants by changing the yarn placement were investigated on shielding behavior of the manufactured variants. It should be taken into account that the calculated mass of the conductive material in warp direction(y) was enlarged from V1 to V4 (up to 13.5%) due to increasing the waviness degree of the conductive warps (20%).

Table 2-6- Wisetex based 3D geometrical illustration of the 3D conductive networks [215]

Variant	Front-left perspective view	Longitudinal section	Cross-section
V1	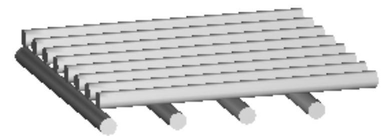		
V2	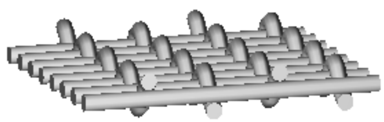		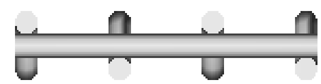
V3	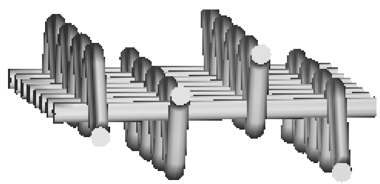	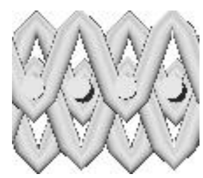	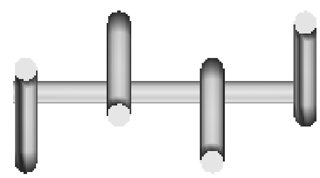
V4	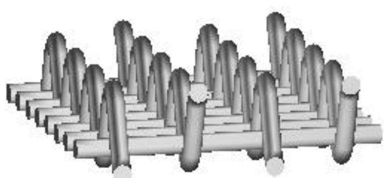		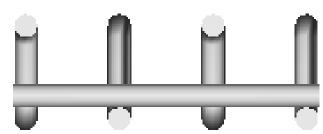
DL	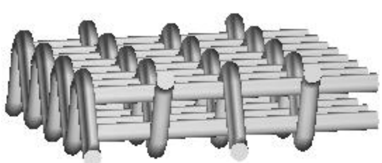	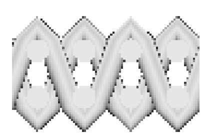	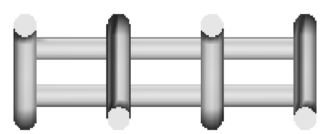

Similarly, the waviness degree of silver wefts was increased from V1 to V3 with the amount of 4.4%. However, the waviness degree of the conductive wefts was nearly the same for V3 and V4 as given in Table 2-7 (7.1 % for V3 vs 6.5 % for V4).

Furthermore, the calculated weight of the silver wefts and accordingly, the total mass of silver was greater for DL among all the variants since all the wefts (two weft yarn systems) were hybrid conductive yarns (cotton/silver) in the fifth manufactured variant (DL).

Table 2-7- Properties of the 3D conductive networks [215]

No.	Property	Unit	Variant V1	V2	V3	V4	DL
1.	Silver yarn diameter	mm	0.12	0.12	0.12	0.12	0.12
2.	Fabric unit cell width	mm	1.43	1.43	1.43	1.43	1.43
3.	Fabric unit cell length	mm	0.91	0.91	0.91	0.91	0.91
4.	Waviness degree of warp	%	4.4	11.4	17	24.8	16.8
5.	Waviness degree of weft	%	2.7	3.8	7.1	6.5	4.7
6.	Calculated mass of warp	g/m^2	124.0	132.3	139.0	148.3	138.7
7.	Calculated mass of weft	g/m^2	77.6	78.5	81.0	80.5	158.3
8.	Calculated mass of the conductive grid	g/m^2	201.6	210.8	220.0	228.8	297.1
9.	Vertical magnitude of the 3D conductive grid	mm	0.68	0.74	2.4	1.9	1.9

2.3.4 **Investigation of the electromagnetic shielding effectiveness of the compound woven fabrics**

The setup in an anechoic chamber which was represented in Figure 2-3 was employed to measure the EMSE of the manufactured 3D warp interlock woven fabrics (V1-V4 and DL) at the frequency range of 1-6 GHz.

The effects of growing the waviness degree of the conductive yarns was deliberated due to the fact that the conductive yarns covered larger amplitude of the thickness of the variants where the unit cell size kept unchanged and the EMSE was evaluated in the directions at right angles to the thickness of the variants (warp direction(y) and weft direction(x)).

It is noted that the binding depth (BD) of the conductive warps was BD =0 layer for V1, increased to BD=1 layer for V2 and BD=2 layer for V3 which led to increasing the waviness degree of silver multifilament warps from V1 to V3.

In addition, the waviness degree of the conductive warps was larger for V4 in comparison with the waviness degree of the conductive warps of V3 even though the binding depth of V3 and V4 were equal (BD=2 layers). The waviness degree of the warps for V4 was increased by changing the interlacing frequency of the cotton yarns which formed the outer layers of the compound woven variant (3/1 twill weave on the face and plain weave on the reverse side of the fabric).

Also, the discontinuity in arranging the conductive warps through the thickness of DL was due to the two conductive weft systems.

2.3.4.1 Investigation of the EMSE of the 3D warp interlock woven variants

The EMSE of all the five variants (V1-V4 and DL) in warp direction(y) and weft direction(x) is publicized in Figure 2-12(a and b) at the frequency range of 1-6 GHz.

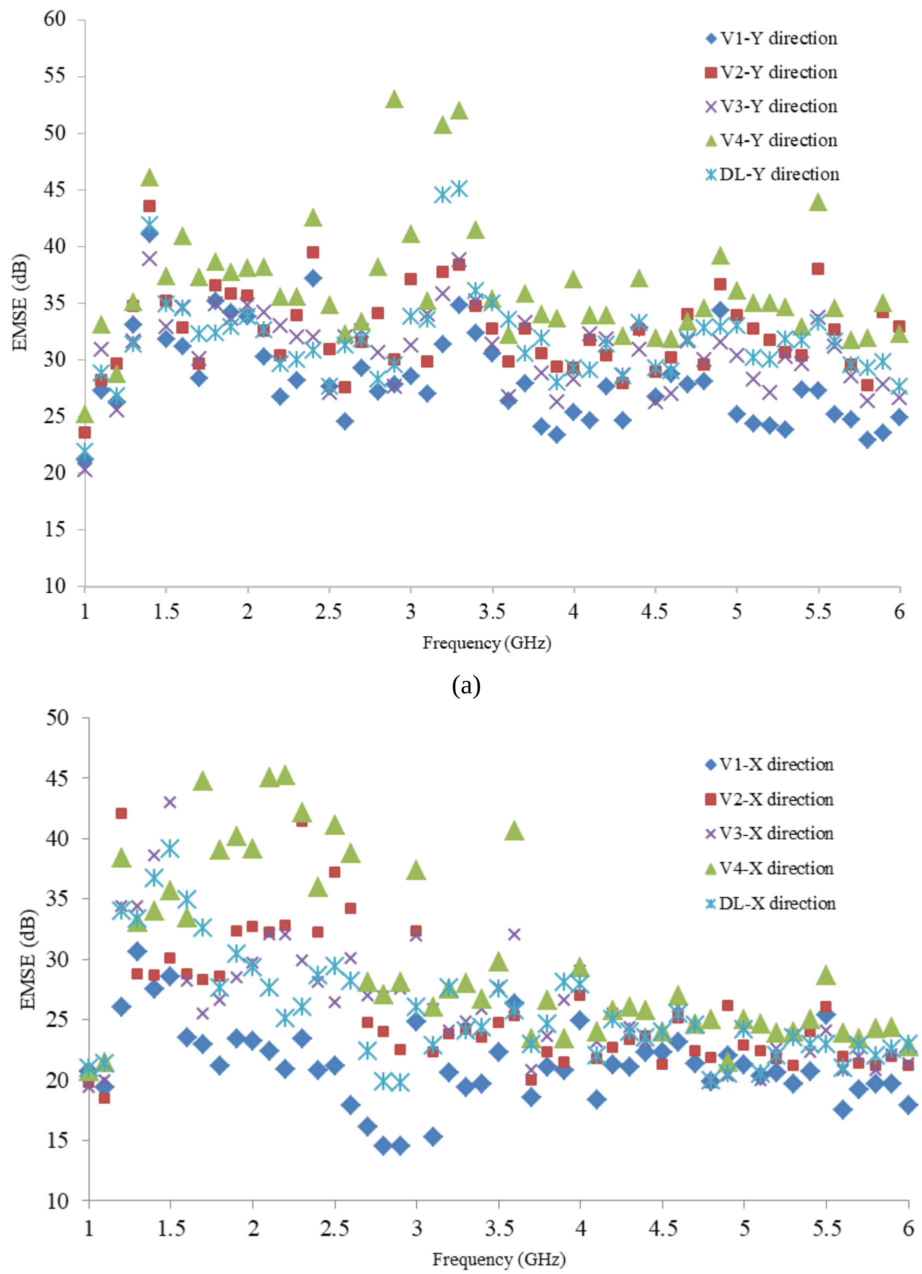

(a)

(b)

Figure 2-12- The EMSE of V1, V2, V3, V4, and DL measured in (a) Warp direction(y) and (b) Weft direction(x) [215]

The average curves of the EMSE values in both warp direction(y) and weft direction(x) are displayed in Figure 2-13(a and b), respectively. Five consecutive EMSE values (intermittently every 100 MHz) using all the data of five repeated EMSE measurements were used to calculate the mean values of the EMSE for each 3D warp interlock woven variant. The average curves of the EMSE were presented in order to compare the EMSE results of the variants by reducing data scattering where changes of the EMSE can be straightforwardly tracked.

The EMSE results displayed in Figure 2-13(a and b) specified that V1 ensured the minimum EMSE values while V4 showed the highest shielding values in both warp direction(y) and weft direction(x).

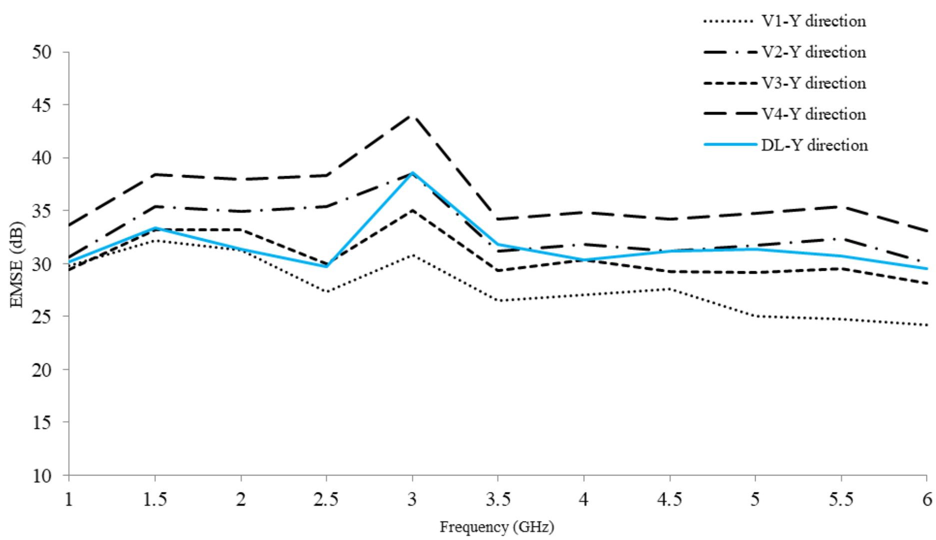

(a)

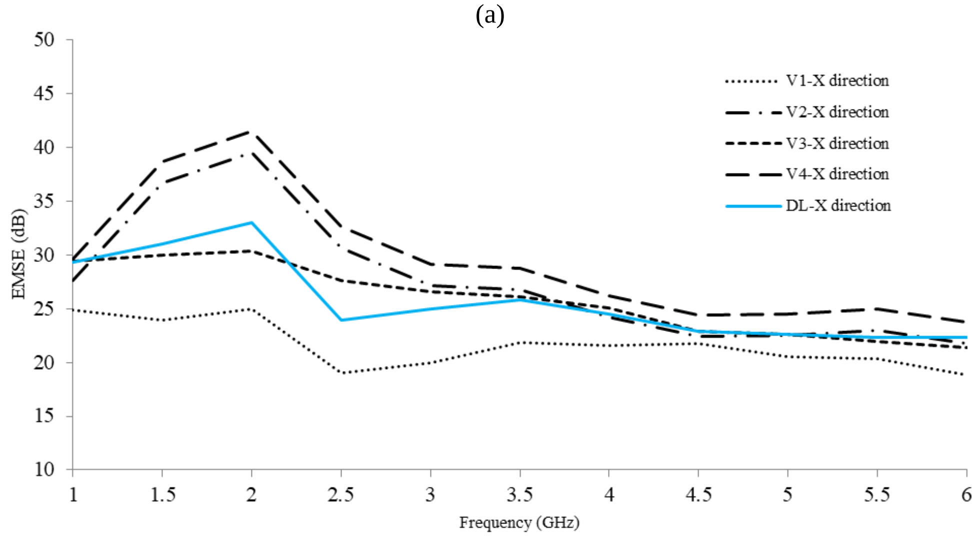

(b)

Figure 2-13- The average curve of EMSE for V1, V2, V3, V4 and DL in (a) warp direction(y) and (b) weft direction(x) [215]

As mentioned earlier, an increase in the undulation of the conductive yarns through the thickness of the variants ensued altering in the waviness degree of the silver multifilament yarns in warp direction(y). Besides, the alteration in waviness degree of warps caused changes in waviness degree of wefts as a result of the bond of the warp and weft yarn systems in the 3D warp interlock woven fabrics. In other words, the way that different warp and weft yarn systems interlaced in association with the binding depth (BD) layers led to waviness degree variations of the yarns.

The EMSE range (minimum-maximum) in warp direction(y) and weft direction(x), binding depth(BD), vertical magnitude of 3D conductive grids, waviness degree of the conductive warps and, mass of conductive grids are shown in Table 2-8 in the direction of investigating the effects of the conductive yarn arranging and undulation on the EMSE behavior of the variants.

It is noted that vertical or warp direction(y) showed that the fabric length was parallel to the vertical antenna polarization when the EMSE was measured. On the other hand, horizontal or weft direction(x) specified that the fabric width was parallel to the vertical antenna polarization during EMSE measurement tests.

Table 2-8- The EMSE values measured in warp direction(y) and weft direction(x), binding depths, the vertical magnitude of conductive grids, waviness degree of the conductive warps and, calculated mass of conductive grids of the manufactured 3D warp interlock woven variants [215]

			Variant				
No.	Property	Unit	V1	V2	V3	V4	DL
1.	EMSE values in warp direction(y)*	dB	24-31	30-38.5	28-37	33-44	29-37.5
2.	EMSE values in weft direction(x)*	dB	19-25	22-39.5	21.5-33	24-41.5	22-33
3.	The depth of binding (BD)	-	0	1	2	2	2
4.	Vertical magnitude of the 3D conductive grid	mm	0.68	0.74	2.4	1.9	1.9
5.	Waviness degree of conductive warp	%	4.4	11.4	17	24.8	16.8
6.	Calculated mass of the conductive grid	g/m^2	201.6	210.8	220.0	228.8	297.1

* The minimum and maximum values of the measured EMSE at the frequency range of 1-6 GHz

Figure 2-14 represents the maximum EMSE values measured in warp direction(y) and weft direction(x) versus different parameters of the 3D conductive grid (binding depth, the magnitude of the 3D conductive grid, waviness degree of the conductive warps, and mass of the conductive grid).

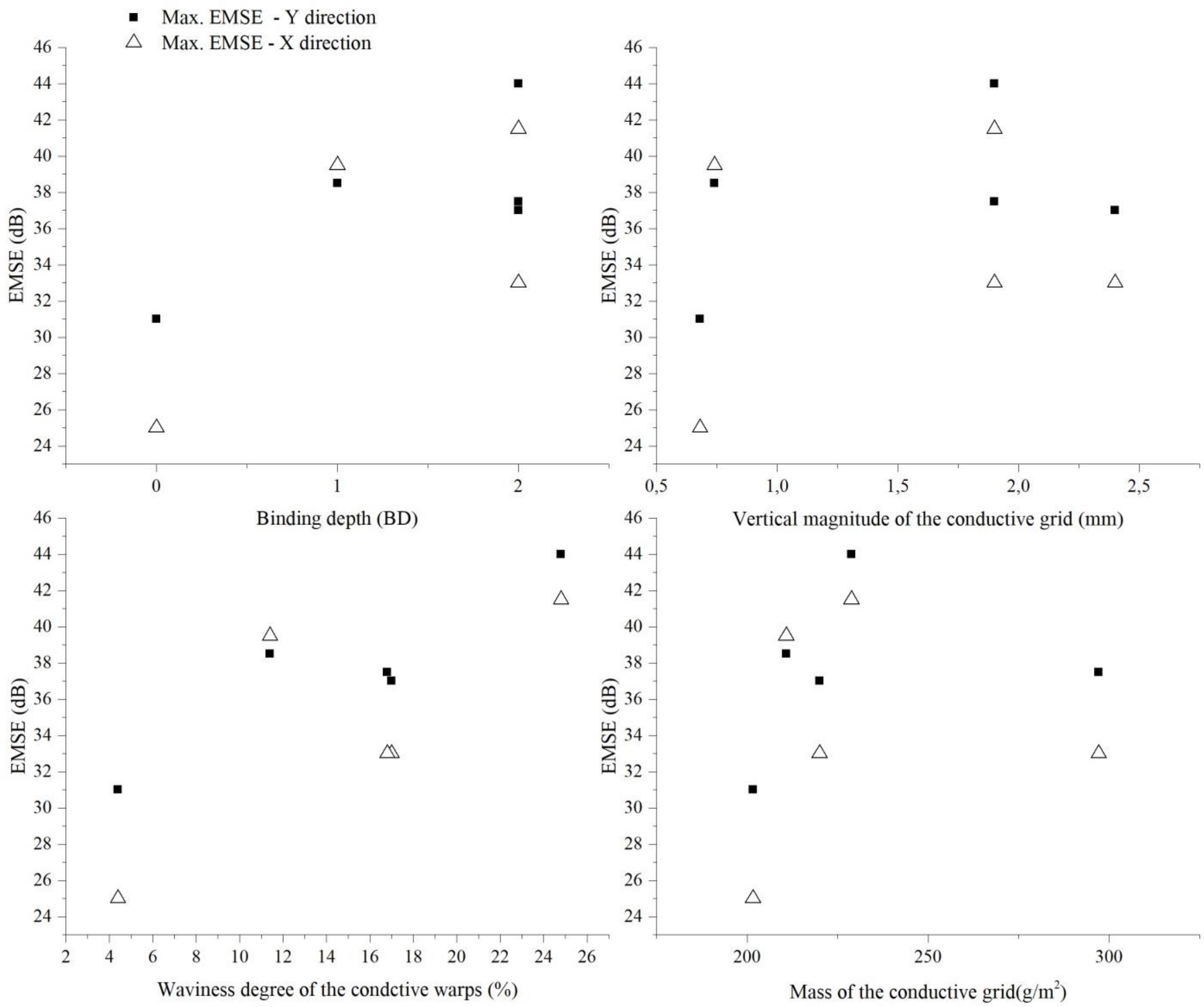

Figure 2-14- The Maximum EMSE values measured in warp direction(y) and weft direction(x) versus different parameters of the 3D conductive network

The EMSE results of all the compound variants (Figure 2-14) showed that the EMSE values of V2 were bigger in comparison with the EMSE values of V1 in both warp direction(y) and weft direction(x) while BD was increased from 0 to 1 layer for V2 compared to V1. Similarly, the greater EMSE values were detected for V4 in comparison with the EMSE values of V2 because of the larger BD of V4 (BD=2 layers for V4). In point of fact, the higher BD, namely the higher amplitude of the conductive yarns through the thickness of the variants led to the superior attenuation where the EMSE measurement was accomplished in perpendicular directions (warp direction or weft direction) to the direction of the fabric thickness. However, the EMSE values of

V3 were smaller than those of V4 and V2 regardless of the fact that the binding depth of V3 and V4 were comparable (BD=2 layers).

Moreover, no correlation was realized between the shielding level of the compound variants and the vertical magnitude of 3D conductive networks. For example, the vertical magnitude of the 3D conductive grid of V3 was 2.4 mm although the EMSE of V3 was approximately the same as the EMSE of DL (vertical magnitude of the 3D conductive grid of DL=1.9 mm) as indicated in Figure 2-14.

The conductive warps were alternatively arranged through the thickness of V3 which was the reason for the larger vertical magnitude of the 3D conductive grid of V3 compared to the other variants with the same binding depth. The inconsistency in the orientation of the conductive warps through the variant thickness was correlated to the placement of the conductive warps although the bigger thickness of the variant was covered by conductive warps in V3.

Furthermore, V4 showed the maximum shielding among all the five variants due to the greatest waviness degree of the conductive warps in the variant V4. Also, the maximum EMSE values of V3 and DL were approximately equal where the waviness degrees of the conductive warps were the same for these two variants. Therefore, a correlation between the waviness degree of the conductive warps and the EMSE results can be acknowledged. However, the EMSE of V2 with a lower waviness degree of the conductive warps was marginally larger to the EMSE level of V3 and DL.

Overall, the results indicated an increase of 40% in the EMSE measured in warp direction(y) and an increase of 25% in the EMSE measured in weft direction(x) for V4 in comparison with V1 while the difference of total consumed silver for weaving these two woven variants was around 14%. Increasing of 14% attenuation measured in warp direction(y) was observed for V4 compared to V2 by increasing 9% of the total silver amount. Also, comparing the maximum values of EMSE measured in weft direction(x) of V2 and V1, 17% higher attenuation was observed for V2 than that of V1 while the mass difference of silver as the only conductive component of the manufactured structures was 5%.

Considering the EMSE results, larger binding depth and uniform distribution of silver multifilament yarns initiated a growth in waviness degree of the conductive yarns in warp direction(y) which led to an enlargement in the EMSE values of V4 in both warp direction(y) and weft direction(x). In other words, a stronger shield against the electromagnetic waves emitted parallel to the warps or wefts of the variant (warp direction or weft direction) was generated using a larger magnitude of the conductive component through the thickness (z-direction) of V4.

In contrast, the first variant (V1) was designed and weaved ensuring the least possible waviness degree owing to the BD=0 layer (4.4 % waviness degree for silver multifilament warps and 2.7 % waviness degree for silver multifilament wefts in practice). Therefore, the minimum values of the EMSE were detected for V1 among all the manufactured variants (V1-V4 and DL) as revealed in Table 2-8.

Additionally, the lower waviness degree of silver warps for V3 was perceived in comparison with silver warps' waviness degree of V4 as a result of the changes in the distribution of the conductive yarns for V3. As a result, lower EMSE values of V3 were witnessed compared to the EMSE values of V4 with equal binding depth (BD=2) layers.

Also, the distribution of the conductive yarns was not uniform through the thickness of DL because of doubling the conductive weft yarn systems. Accordingly, lower EMSE values for DL were measured in comparison with EMSE results of V4 due to the inconsistency of the conductive yarns through the thickness of DL where the binding depth of these two variants was comparable (BD=2) layers.

In addition, the bigger EMSE values of V2 compared to EMSE values of DL were correlated to the distribution of the conductive yarns which was uniform through the thickness of V2. The uniform distribution of the conductive yarns in V2 made a better shield in warp direction and weft direction. However, BD and waviness degrees of silver multifilament warps were lower for V2 than those of V3 and DL as presented in Table 2-8.

Moreover, the EMSE values of DL and V3 were approximately equal where the similarity can be inferred to the equal waviness degree of silver multifilament yarns in warp direction(y), equal binding depth (BD) and the yarn distribution of the yarns through the thickness of these two variants (DL and V3). In point of fact, the binding depth was the same for these two variants (BD=2) layers and the waviness degree of the conductive warps was closely the same (16.8 % for DL vs 17% for V3). Therefore, the same attenuation level was perceived for V3 and DL in both warp direction(y) and weft direction(x) although the mass of silver was considerably lower (~35% lower) for V3.

In summary, the larger undulation of silver multifilament yarns through the thickness of the manufactured compound woven variants and consequently, greater waviness degree of the conductive yarns initiated better attenuation (higher EMSE) although arranging of the conductive warps through the thickness of the compound variants played an important role in the level of EMSE of the woven variants that cannot be ignored.

Accordingly, the results (Figure 2-14) revealed that increasing of the waviness degree of the conductive yarns (silver multifilament yarns) from V1 to V4 led to better protection against electromagnetic waves in the frequency between 1 and 6 GHz while the other parameters (e.g. the yarn density, yarn fineness and ratio between cotton/silver and silver yarns) remained unchanged.

2.3.4.2 Analysis of the EMSE measured in warp direction(y) and weft direction(x)

The EMSE values (minimum-maximum) measured at the frequency band of 1-6 GHz along with with the characteristics of the conductive grids of all the manufactured variants (V1-V4 and DL) for instance waviness degree of the silver multifilament yarns in warp direction(y) and weft direction(x) is revealed in Table 2-9.

Table 2-9- The EMSE values and the characteristics of the conductive grids [215]

				Variant				
No.	Property		Unit	V1	V2	V3	V4	DL
1.	EMSE values in warp direction(y)		dB	24-31	30-38.5	28-37	33-44	29-37.5
2.	EMSE values in weft direction(x)		dB	19-25	22-39.5	21.5-33	24-41.5	22-33
3.	Density of conductive yarns	warp	Yarns/cm	11	11	11	11	11
		weft		7	7	7	7	14
4.	Waviness degree of conductive warp		%	4.4	11.4	17	24.8	16.8
5.	Waviness degree of conductive weft		%	2.7	3.8	7.1	6.5	4.7
6.	Cell size length		mm	0.91	0.91	0.91	0.91	0.91
7.	Cell size width		mm	1.43	1.43	1.43	1.43	1.43

The results suggested that the EMSE values measured in warp direction(y) were greater in comparison with the EMSE values measured in weft direction(x) for all the five variants (Figure 2-14). Both yarn density and waviness degree of the silver multifilament yarns were bigger in warp direction(y) in comparison with the yarn density and waviness degree of the conductive yarns in weft direction(x) for the first four variants (V1, V2, V3, and V4). So, the higher level of the EMSE in warp direction(y) can be because of the higher yarn density or the greater waviness degree of the conductive yarns or both in warp direction(y) of the first four variants (V1-V4).

The EMSE results of the manufactured 2D woven fabrics in section 2.2.3 showed that increasing the yarn density resulted in the higher EMSE values of 2D woven fabrics although the attenuation enlargement was not significant. Also, some former studies have stated that the effects of the conductive yarn density on the EMSE of the woven fabrics as an individual parameter cannot be verified [86], [87], [216]. The previous studies suggested that the theory of the shielding behavior with altering the conductive yarn density of a woven structure could not be established as a result of alteration in the shape of apertures by changing the yarn density and size of apertures. In other words, they specified that the effects of the placing of the conductive yarns were significant on the EMSE behavior of the woven fabrics.

It is known that the structures of 3D warp interlock woven fabrics are more complex in comparison with simple 2D woven structures as the conductive yarns are arranged through the thickness of the 3D woven fabrics irrespective of the yarn density. Consequently, the waviness degree increase of the conductive component caused by generated changes in the alignment of the conductive yarns had a big impact on the level of the EMSE.

The dissimilarity of the EMSE measured in warp direction(y) and weft direction(x) was in agreement with the difference between the waviness degree of the conductive warps and conductive wefts (Table 2-9). So, it was suggested that the difference in the EMSE values measured in warp direction(y) and weft direction(x) for each variant initiated by dissimilarity in waviness degree of the silver multifilament yarns in warp direction(y) and weft direction(x). Increasing the waviness degree of the conductive yarns in warp direction(y) as a result of the presence of the conductive warps in the transverse direction was the reason for the higher EMSE values due to the fact that the EMSE was measured in the parallel direction to the warps.

Also, the EMSE values of DL in warp direction(y) were greater than the EMSE values in weft direction(x) while warp density of the conductive yarns was 11 (yarns/cm) and weft density of total conductive yarns was 14 (yarns/cm) for DL. Therefore, the higher EMSE values measured in warp direction(y) of DL were correlated to the almost fourfold larger waviness degree of the silver multifilament warps in comparison with the waviness degree of the silver multifilament wefts.

The maximum EMSE values were suggested at 3 GHz for all the variants inspecting the EMSE curve of each variant in warp direction(y). In the same way, the maximum EMSE value was suggested at 2 GHz for each variant as illustrated in Figure 2-13(a and b) when the EMSE measurement was done in weft direction(x).

It is noted that waviness degree of the conductive warps and wefts, and mass of the conductive grids were different for different variants on one hand and the unit cell length and width were the same for all the variants on the other hand as shown in Table 2-9. The cell length was 0.91 mm and the cell width was 1.43 mm for all the five compound woven variants (V1, V2, V3, V4, and DL).

It was suggested that the increase of the EMSE level in a particular frequency happened as a result of the correlation between the unit cell size (length or width) of the 3D warp interlock woven fabrics and the wavelength of the electromagnetic waves at that specific frequency. Accordingly, the maximum EMSE beheld at 3 GHz (wavelength =100 mm) in warp direction(y) where the warp spacing was roughly 1 mm and it was perceived at 2 GHz (wavelength =150 mm) in weft direction(x) where the weft spacing was approximately 1.5 mm for all the compound variants (V1, V2, V3, V4, and DL). It is noted that the maximum attenuation was perceived at 3 GHz in warp direction(y) and 2 GHz in weft direction(x) irrespective of the quantity of the conductive component, waviness degree and the number of the conductive yarns systems.

Hence, any modifications in yarn spacing (unit cell size) of the 3D warp interlock woven fabrics have effects on the EMSE values at a specified frequency range. Therefore, the unit cell size of a woven structure should be considered during the design phase of compound woven fabrics regarding the targeted frequency for EMSE applications.

The EMSE results in the frequency between 1 and 6 GHz for all the compound woven variants in both warp direction(y) and weft direction(x) suggested that these manufactured variants were excellent to be applied as electromagnetic shield fabrics in the frequency band of 2-3 GHz due to the possible correlation between the wavelength and the unit cell size of the manufactured compound woven variants. For instance, the value of the EMSE was around 28 dB for V1 and 39 dB for V4 at 1.8 GHz and 2.4 GHz while 1.8 GHz corresponds to the frequency for mobile applications and 2.4 GHz corresponds to ISM bands (the radio spectrum of industrial, scientific and medical) in Europe [214].

2.4 Summary

Two sets of 2D woven fabrics (seven different woven fabrics) and a set of five 3D warp interlock woven fabrics were designed and manufactured using metal-based yarns as the conductive component for electromagnetic shielding effectiveness development. The EMSE of all the manufactured woven fabrics was evaluated using a measurement setup in an anechoic chamber for the frequency band of 1-6 GHz. The main objective of this chapter was to define the effects of the properties of the fabrics on the EMSE of the woven fabrics. The following conclusions were accomplished of the structural analysis of the manufactured 2D and 3D woven fabrics along with the EMSE examination.

2.4.1 The EMSE of 2D woven fabrics

Seven samples of 2D woven fabrics were produced using two conductive yarns with different conductivity. The main idea was to determine the optimized weave structure among three basic weave structures (plain, twill, and satin) with the intention of the electromagnetic shielding effectiveness applications. Also, two different densities of the conductive yarns (8 (yarns/cm) and 16 (yarns/cm)) were applied to weave the woven fabrics to study the effects of the conductive yarn density on the EMSE.

The EMSE results of the manufactured 2D woven fabrics showed that doubling the conductive yarn density led to a slightly higher EMSE level (~10%). S1 and S3 exposed higher EMSE values in comparison with the EMSE values of S2 and S4 due to the higher density of the conductive yarns ensuring the same weave structure and the same conductive material for S1 and S2 or S3 and S4.

In addition, 2D woven fabrics with plain weave structure (S5 (or S1 or S2)) showed marginally better EMSE, followed by the woven fabrics with twill weave structure (S6 (or S3 or S4)), and the woven fabric with satin weave structure (S7). The effects of weave structures on the EMSE were correlated to the difference between the floats of the conductive yarns for different weave structures where all the other parameters like yarn density and fineness stayed unchanged.

On the other hand, the EMSE results of S1 (23-39 dB) and S3 (21-35 dB) were approximately equal at most frequencies in the frequency range of 1-6 GHz. Also, the similar EMSE values were observed for S2 and S4 or S5 and S6 at some frequencies. This similarity can be inferred to the diagonally arranged of the conductive yarn floats in these woven fabrics although the weave structures were not identical.

Moreover, the results revealed higher EMSE values (in the range of 20-30 %) for the woven fabrics using PA 12 coated with silver yarns as conductive wefts due to the higher electrical conductivity of silver in comparison with Inox (electrical conductivity of silver is almost fifty-fold as big as Inox).

To sum up, the effects of the conductive yarn density along with the weave structure were not of great importance on the EMSE level of the 2D woven fabrics. To clarify, the EMSE was slightly increased even though the conductive yarn density was doubled for some woven samples. Also, metal yarns were exposed to the air and could not be easily protected from oxidation, corrosion and mechanical abrasion in the manufactured 2D woven fabrics. Also, skin touch with the wearer could not be controlled where the metallic yarns appeared on the outer layer of the fabrics.

2.4.2 The EMSE of 3D warp interlock woven fabrics

Four 3D warp interlock woven fabrics were designed and produced for the EMSE applications encompassing three warp yarn systems and three weft yarn systems (V1, V2, V3, and V4). The hybrid conductive yarns made of cotton staple yarns and silver multifilament yarns were used in the middle yarn systems for both warp direction(y) weft direction(x). Undulation of the conductive yarns (binding depth) was enlarged among four manufactured compound woven variants with the same setup of the weaving loom.

The compound woven structures were designed to integrate the conductive yarns inside the variants. The idea was to keep the metal yarns hidden inside the variants to avoid the skin touch with the wearer and to ensure the continuity of the conductive network at all the binding points.

On contrary, the fifth compound woven structure (DL) was designed and manufactured with only two weft yarn systems (all the weft were hybrid conductive yarns) acquiring the same yarn fineness and warp density as all the other compound variants.

The EMSE results of 3D warp interlock woven fabrics showed that larger binding depth (BD) of the conductive yarns led to greater coverage of the thickness of the 3D woven fabrics by conductive warps. As a result, the woven variants with larger BD showed higher attenuation. In other words, undulation of the conductive yarns through the thickness of the manufactured 3D warp interlock woven variants promised a higher level of electromagnetic attenuation (EMSE

(V4) > EMSE (V2) >EMSE (V1)). For example, an increase of 40% in the attenuation level was observed for V4 with BD=2 layers in comparison with V1 with BD=0 layers (warp waviness difference between V1 and V4 was nearly 20 %).

Moreover, positioning of the conductive warps was not uniform through the thickness of V3 and DL which led to lower EMSE values in comparison with the EMSE values of V4 while the variants V3, V4, and DL were weaved having the same binding depth (BD=2) layers.

Also, the EMSE values of DL and V3 were comparable (29-37.5 dB for DL and 28-37 dB for V3). This similarity was correlated to the equivalent floats of the conductive yarns through the thickness of these variants which led to similar waviness degrees of the silver multifilament yarns in warp direction(y) for V3 and DL (17% for V3 vs 16.8 % for DL). However, total mass of the conductive component was comparatively larger in DL.

Studying the EMSE graphs of the compound woven fabrics in warp direction(y) and weft direction(x), the difference between the EMSE measured in warp direction(y) and weft direction(x) was witnessed. The dissimilarity occurred because of the higher waviness degree of the conductive yarns in warp direction(y) than the waviness degree of the conductive yarns in weft direction(x) for all the variants (V1-V4 and DL). In a few words, increasing of the waviness degree of the conductive yarns generated by changing the displacement of the conductive component had a major influence on the level of the EMSE.

The results of the EMSE measurements showed that the 3D warp interlock woven variants were excellent for electromagnetic shielding applications in the frequency band of 2-3 GHz due to the possible correlation between the wavelength of the electromagnetic waves and the unit cell size of the woven variants.

The EMSE results of all the manufactured variants were in satisfactory range (19-44 dB) for personal wearable shielding applications. These compound woven fabrics can be applied for shielding the household appliances, FM/AM radio broadcast sets, cellular phones, computers, buildings, etc, too.

To conclude, changing the positioning of the conductive yarns by changing the parameters such as waviness degree played a key role in the EMSE level of the compound woven variants.

Chapter 2 discussed the influences of the characteristics of 2D and 3D woven fabrics on the EMSE of the manufactured woven fabrics using commercial metallic yarns. It was suggested to apply metal yarns in mid-play of the compound woven fabrics in order to avoid the difficulties caused by metal exposure to the air or the skin touch with the wearer as the ultimate goal of the present thesis was to design and manufacture a shielding fabric for personal wearable protection against the existence electromagnetic waves in the human living environment.

However, as identified in Chapter 1, the shielding fabrics made of metal yarns suffer from poor washability and uncomfortability (e.g. heavyweight and skin allergy) where the production process of the metal yarns is also complicated and expensive.

In the next chapter, a polymer-based monofilament development would be suggested to be replaced with metal yarns in the woven fabric making process for personal protection against radiation to reduce the limitations of the shielding fabrics containing metal yarns.

Chapter 3: Conductive monofilament development for EMSE fabric manufacturing

As discussed in Chapter 2, the EMSE fabrics made of metal yarns suffer from poor washability and uncomfortability such as high density as well as skin allergy causes for the wearer. Also, the production process of metallic yarns is complicated and expensive.

To decline the limitations of the EMSE fabrics containing metal yarns, a polymer-based monofilament was suggested in Chapter 3 for the woven fabric making process intended for personal protection against radiation.

Chapter 3 presents conductive polymer-based monofilament generating by melt mixing method using extrusion. The development of a new conductive monofilament yarn was investigated in this chapter since conductive polymer nanocomposites (CPCs) can be lightweight, inexpensive (using a low quantity of nanofillers), and corrosion-resistant. Also, melt mixing method is an adaptable technique for thermoplastic polymers since this method is environmentally friendly, cost-effective, and suitable for mass production.

The above-mentioned properties made the developed CPC monofilament yarn using melt mixing method an appropriate alternative for garment making process for personal protection against electromagnetic waves. Thus, monofilament yarns were produced considering the desired electrical conductivity for weft insertion in the woven fabric structures. Finally, the electromagnetic shielding effectiveness of the manufactured woven fabrics with the CPC monofilaments was measured in the frequency range of 1-10 GHz.

3.1 Conductive monofilament manufacturing

3.1.1 Materials

The following materials were applied for monofilament manufacturing in the present chapter:

- Polyamide 6,6 (PA6,6) - Torzen™ U4803 NC01 PA6.6 resin (density: 1.14 g/cm^3) was used as thermoplastic polymer matrix of the nanocomposites.
- Multiwall Carbon Nanotube (MWCNT) - Nanocyl NC7000 series (surface area: 250 - 300 m^2/g; density: 1.30–2.00 g/cm^3 with an average diameter of 9.5 nm and length: 1.5 μm) was purchased from Nanocyl S.A., (Belgium).

- Carbon Black (CB) - Printex L6 powder series (surface area: 200 m^2/g; density: 1.7–1.9 g/cm^3 and particle size: 18 nm) which has a spherical cross-section, was purchased from Orion Engineered Carbons Company, (Germany).
- Carbon Black (KB) - Ketjenblack EC-300J series (surface area: 800 m^2/g; density: 2.1 g/cm^3 and particle size: 39.5 nm) was supplied by Akzo Nobel in Netherlands. Ketjenblack EC-300J has a high effective surface area due to the contribution of internal voids.

It should be noted that the main objective of this chapter was to replace the common conductive yarns (metallic yarns) with the developed monofilaments for shielding textiles production. It is also noted that the presence of nanofillers could cause a reduction in the elasticity of the matrix polymer. The strategy to avoid this problem was to use a polymer with appropriate mechanical properties as the matrix of the nanocomposites to decline the probable complications caused by low mechanical properties. As a result, PA6,6 was chosen as the matrix of the nanocomposites since it is a commercial polymer suitable for the desired application and it has been mainly used for textile applications, especially in the garment industry. PA6,6 is also durable and weather-resistant which makes it a suitable candidate to manufacture a wearable textile device for personal protection.

In addition, MWCNT, CB, and KB were selected among conductive nanofillers in order to increase the conductivity of the polymer-based nanocomposites. Transmission electron microscopy (TEM) images of three nanofillers are illustrated in Figure 3-1(a, b, c). These nanofillers provide different surface areas that lead to dissimilarity in nanofiller dispersion and percolation threshold of the electrical conductivity in conductive polymer nanocomposites (CPCs). For example, the pore structure of KB allows it to perform as highly conductive carbon nanofiller in comparison with CB having a spherical cross-section.

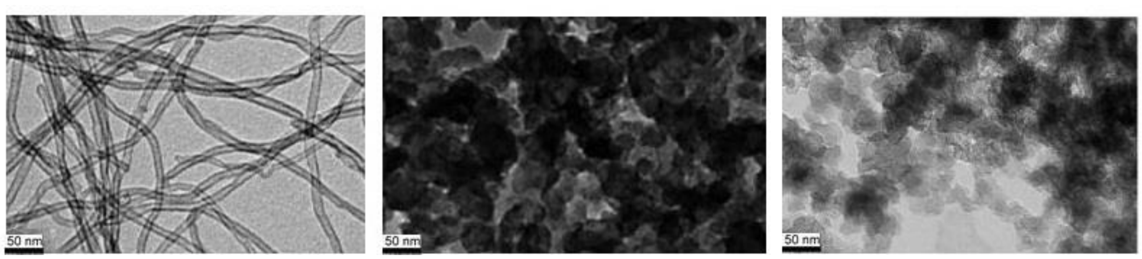

(a) (b) (c)

Figure 3-1- Transmission electron microscopy images of (a) MWCNT, (b) CB and (c) KB [59]

3.1.2 Nanocomposites development

Two sets of conductive polymer nanocomposites (CPCs) were suggested in the present chapter. First, MWCNT particles were added to the polymer matrix (PA6,6) by melt mixing process using extrusion in order to determine the experimental percolation threshold of electrical conductivity of the PA6,6-based nanocomposite contained MWCNTs. Consequently, the quantity of MWCNT was ranged from 0.5 to 5 wt.% in the PA6,6-based nanocomposite.

Another set of PA6,6-based nanocomposites was developed using CB particles with the quantity of nanofiller (CB) ranged from 5 to 30 wt.%.

It should be noted that all the pellets mixed with MWCNTs or CBs were dried at 80°C for 12 hours before extrusion. The pellets should be well dried before introducing to the extruder as PA6,6 pellets promptly absorb water molecules in the air of the room and it causes complications in extrusion process of the CPCs which may result in a poor quality of the produced CPCs. The formulations of all the developed CPCs are listed in Table 3-1.

The nanocomposites with MWCNT or CB were blended by melt mixing method using co-rotating twin-screw extruder ThermoHaake (screw diameter: 16 mm and L/D: 25) while the rotation speed was fixed to 100 rpm and the temperatures of the extruder were set at 270°C in feeding zone and 280°C, 280°C, 279°C and 278°C in barrels zones, respectively.

The schematic diagram of the twin-screw extruder and an image of the applied extruder device in this chapter are shown in Figure 3-2(a and b). It should be taken into consideration that PA6,6 is a thermoplastic polymer and as a result, the melt mixing method was applicable for development of the nanocomposites.

A cooling bath (Yvroud, France) with closed circulation of water in room temperature was applied in order to cool down the manufactured monofilaments efficiently. Consequently, the produced monofilaments were collected when the speed was fixed at 1 m/min.

Table 3-1- Formulation of the conductive polymer nanocomposites (CPCs) [59]

Sample Code	PA66 wt. %	MWCNT wt. %	CB (Printex) wt. %	KB (Ketjenblack) wt. %
PA	100	-	-	-
PA-MWCNT0.5	99.5	0.5	-	-
PA-MWCNT1	99	1	-	-
PA-MWCNT1.5	98.5	1.5	-	-
PA-MWCNT2	98	2	-	-
PA-MWCNT3	97	3	-	-
PA-MWCNT5	95	5	-	-
PA-CB5	95	-	5	-
PA-CB7.5	92.5	-	7.5	-
PA-CB10	90	-	10	-
PA-CB15	85	-	15	-
PA-CB20	80	-	20	-
PA-CB30	70	-	30	-
PA-MWCNT1.8-CB1.8	96.4	1.8	1.8	-
PA-MWCNT1.7-CB3.3	95	1.7	3.3	-
PA-MWCNT1.3-CB5.2	93.5	1.3	5.2	-
PA-MWCNT2.6-CB2.6	94.8	2.6	2.6	-
PA-MWCNT2.5-CB5	92.5	2.5	5	-
PA-MWCNT2-CB7.8	90.2	2	7.8	-
PA-MWCNT2.6-KB*2.6	94.8	2.6	-	2.6
PA-MWCNT2.5–KB*5	92.5	2.5	-	5
PA-MWCNT2–KB*7.8	90.2	2	-	7.8

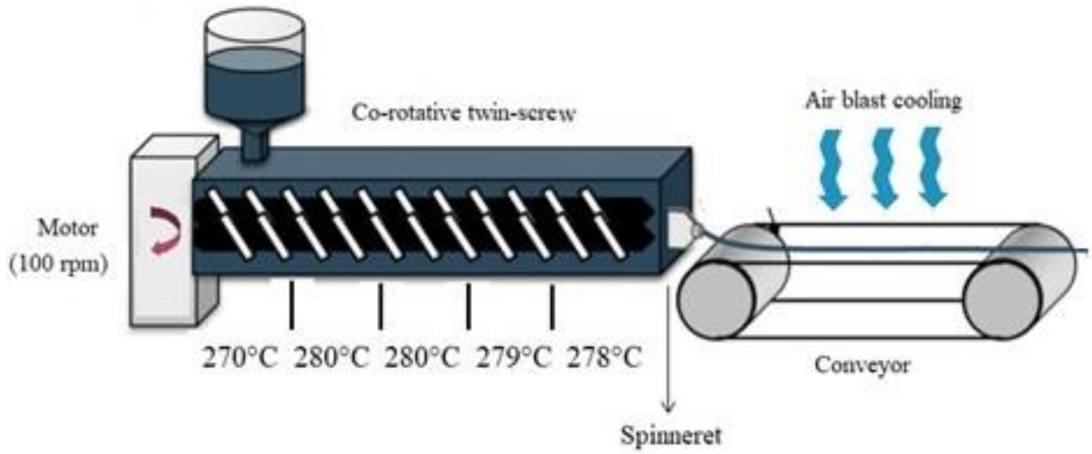

(a)

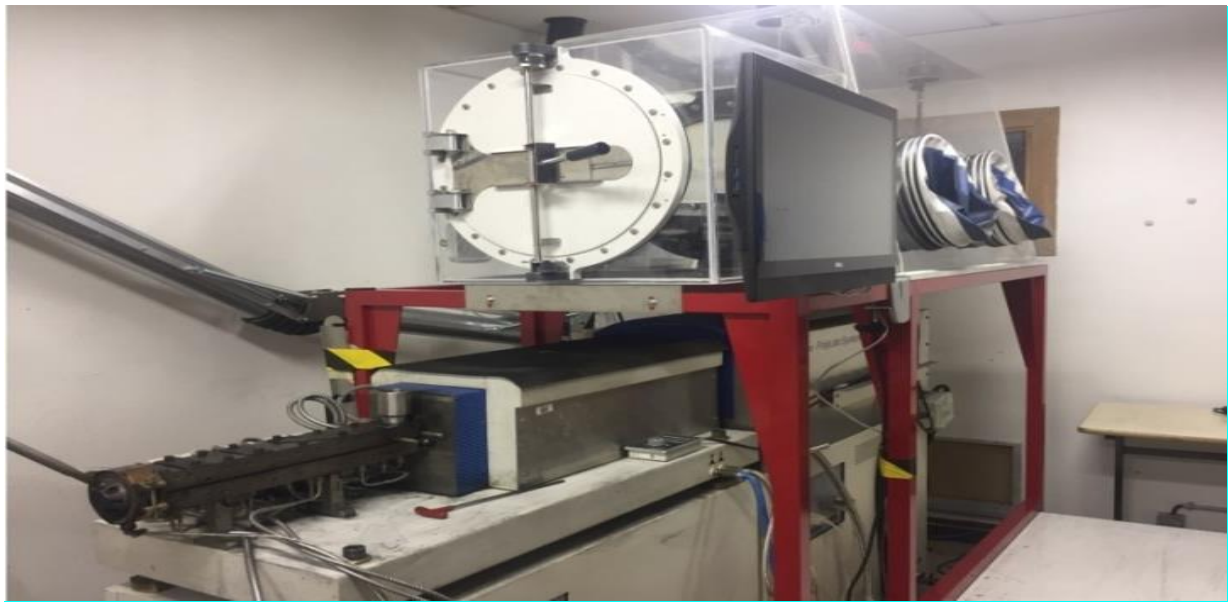

(b)

Figure 3-2- (a) Schematic and (b) Image of the co-rotating twin-screw extruder ThermoHaake

3.2 Characterization

3.2.1 Electrical conductivity measurement

As explained in Chapter 1, the electrically conductive materials produce and conduct free charges which lead to electromagnetic shielding effectiveness. So, the electrical properties of the developed nanocomposites had to be investigated. Consequently, electrical properties of the monofilaments were measured using 2-wire ohms measurement (2w). The principle of this method is shown in Figure 3-3.

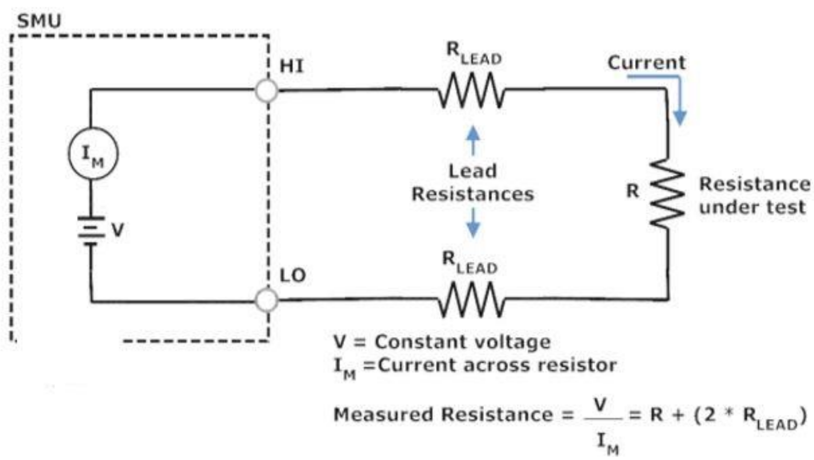

Figure 3-3- The schematic of the resistance measurement principle [180]

The electrical resistance of all the produced monofilaments was measured by means of Keithley SMU 2461 source meter given in Figure 3-4(a) by applying a given DC voltage and measuring the current passing through the monofilament. The voltage applied between two points spaced by L = 1 cm was varied from -0.5 to 5 V with an automatic increment of 0.5 V and the (I/V) curve was plotted for each nanocomposite sample. The electrical resistance (R) was concluded as the inverse slope of the curve.

The electrometer was connected with the clips (Figure 3-4(b)) to the monofilaments with the measurement length of 1 cm. 10 measurements for each conductive polymer nanocomposite specimen was carried out. It should be noted that no significant difference between the resistance of rods in different measurement lengths of 1, 2 and 5 cm was observed which confirmed that the rods conductivity was homogeneous.

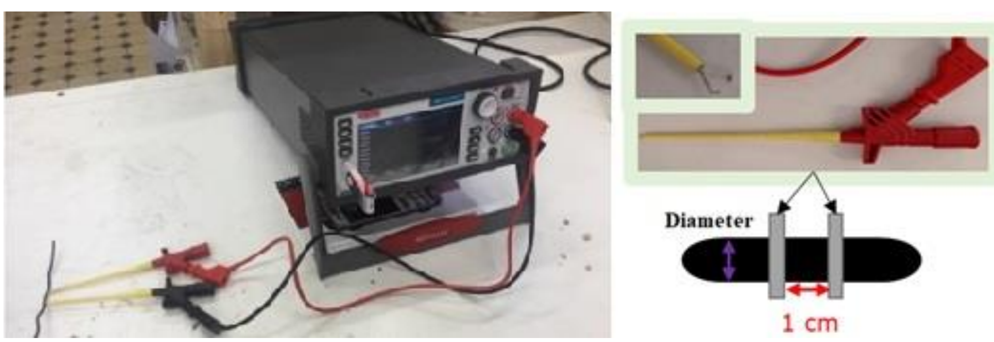

Figure 3-4- (a) The resistance measurement method and (b) The clips used for the measurement

Equation (22) was applied to calculate the electrical conductivity of the produced nanocomposites where R shows the electrical resistance of the material (Ω), V is the voltage (V), I is the current (A), ρ is the resistivity (Ω.m), L is the length between two points (m), σ represents the electrical conductivity ($(\Omega.m)^{-1}$ or Siemens per meter (S/m)) and S is the cross-section of the monofilament (m^2). It should be noted that the cross-section of the monofilament was calculated using the mean value of the rod diameter (circular diameter).

$$R = \frac{V}{I} \tag{19}$$

$$R = \frac{\rho L}{S} \tag{20}$$

$$\sigma = \frac{1}{\rho} \tag{21}$$

$$\sigma = \frac{L}{S \times R} \tag{22}$$

Afterward, the percolation threshold was determined by plotting the electrical conductivity of the produced nanocomposites having MWCNTs or CBs versus reduced nanofiller mass concentration and fitting with a power-law function as shown in equation (23) where σ_o is scaling factor, ρ_c is the percolation threshold, σ is the conductivity of the produced CPC and ρ is the nanofiller content of the CPC.

$$\sigma = \sigma_o(\rho - \rho_C)^t \text{ , for } \rho > \rho_c \tag{23}$$

3.2.2 **Transmission electron microscopy (TEM)**

The samples were embedded into epoxy resin and ultramicrotome along the longitudinal direction using a diamond knife on a Leica ultra-cut UCT microtome, at Cryo temperature (-120°C) to give a section with a nominal thickness of 70 nm. Then, sections were transferred to Cu grids of 400 meshes. Bright-field TEM images of the nanocomposites were obtained at 200kV under low dose condition with FEI TECNAI G2 20 electron microscope, using a Gatan CCD camera and Gatan digital micrograph software when both low magnification and high magnification images were taken of the nanocomposite samples in order to ensure the representative analysis.

3.2.3 **Melt flow index (MFI)**

Melt flow index (MFI) is defined as the measure of the viscosity (flowability) of thermoplastic polymers in grams over 10 minutes at a given temperature. The melt flow tester from ThermoHaake was applied for MFI measurements to analyze the spinning feasibility by defining the viscosity of the molten nanocomposites. A schematic of the MFI indexer is sketched in Figure 3-5.

The tests were performed at 280°C with 2.16 kg load complies with ISO 1133-1 when all the nanocomposite pellets were dried at 80°C for 12 hours before the measurements. It should be noted that the MFI test was repeated three times for each nanocomposite sample and the results were averaged.

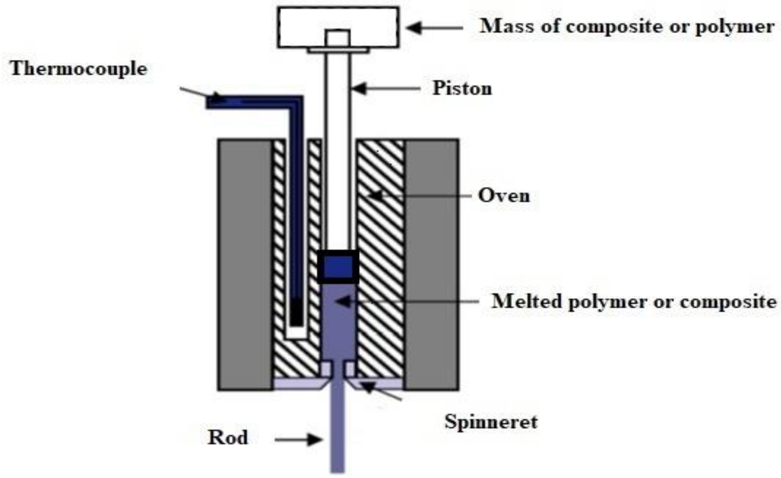

Figure 3-5- A schematic of Melt Flow Indexer

3.3 Investigation of the electrical and morphological properties

The electrical conductivity of all the monofilaments contained MWCNT (0.5-5 wt.%) and CB (5-30 wt.%) was calculated using equation (22). The electrical conductivity of the PA6,6-based nanocomposites containing MWCNT(blue curve) and CB (red curve) as a function of the nanofiller mass concentration are plotted in Figure 3-6.

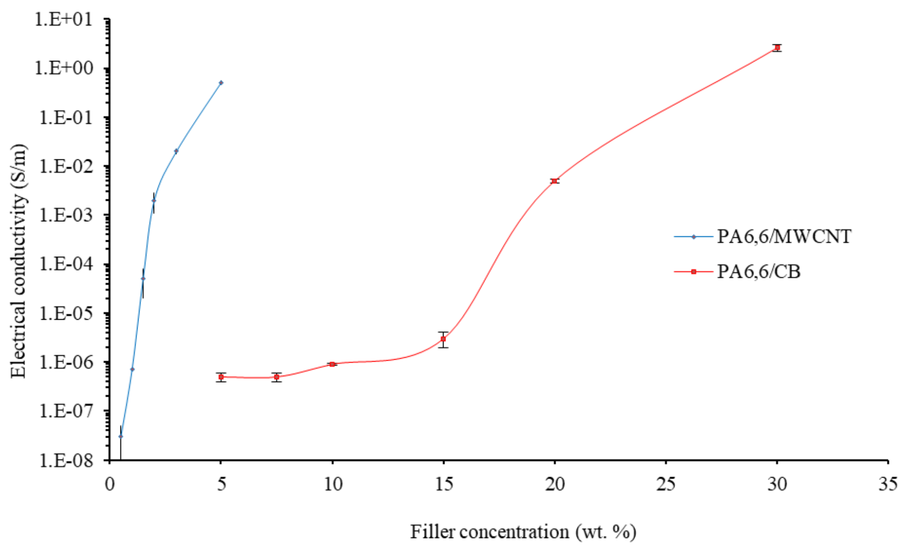

Figure 3-6- Electrical conductivity as a function of the nanofiller mass concentration for PA6,6-based nanocomposites containing MWCNT(Blue curve) and CB (Red curve) [59]

The quantity of the conductive nanofillers should be higher than its amount at percolation threshold for network construction by nanofillers through the nanocomposite. Hence, the percolation threshold of the electrical conductivity (σ_{th}) of PA6,6-based nanocomposites filled with MWCNTs or CBs was determined on the curves of the electrical conductivity versus nanofiller mass concentration using power-law function given in equation (23).

The conductive network was developed by increasing the content of MWCNTs or CBs in the developed CPCs. As shown in Figure 3-7(a), the critical component was 0.8 when the percolation threshold was 2 wt.% (MWCNT) for the nanocomposite filled with MWCNT. Also, the critical component was 0.4 and the percolation threshold was 15 wt.% of the nanofillers for the nanocomposite filled with CB as displayed in Figure 3-7(b).

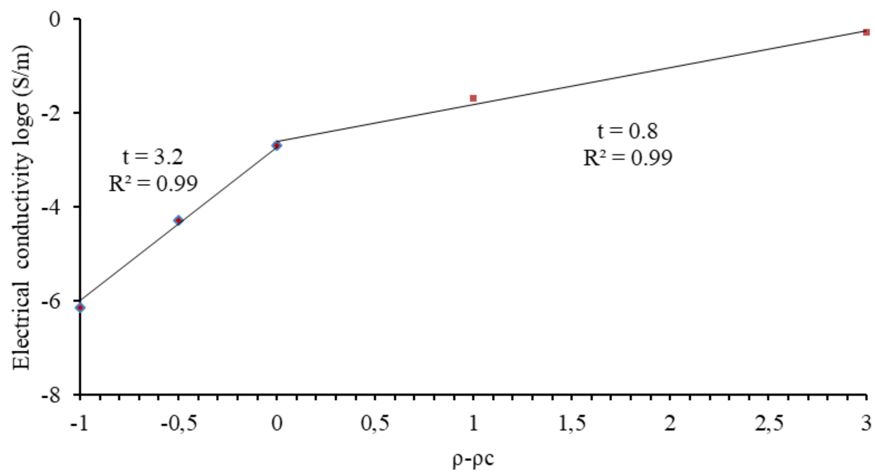

(a)

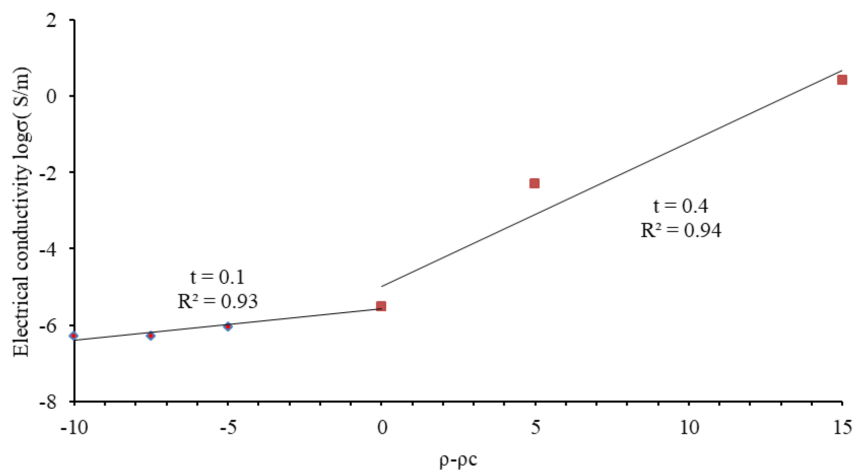

(b)

Figure 3-7- Calculation of the percolation threshold by application of power law ($\sigma = \sigma_o(\rho - \rho_C)^t$, for $\rho > \rho_c$) to experimental data for nanocomposites containing (a) MWCNT and (b) CB [59]

Moreover, the dispersion of MWCNTs was perceived using TEM images for two samples before (PA-MWCNT1.5) and after (PA-MWCNT5) percolation threshold in Figure 3-8(a and b).

MWCNT nanofillers were not well-dispersed in PA-MWCNT1.5 due to the agglomeration of the nanofillers in some zones as well as insufficient mass concentration of MWCNTs. As a result, the conductive network of nanofillers was not formed through the PA6,6 matrix as shown in Figure 3-8(a).

On the other hand, the conductive network construction can be easily detected in Figure 3-8(b) which established the electrical conductivity in the nanocomposite (PA-MWCNT5). The dispersion of MWCNTs was comparatively improved in PA-MWCNT5 containing 5 wt.% of the nanofiller even though some agglomeration regions can be observed in Figure 3-8(b). It was believed that the dispersion of the MWCNTs was developed due to the compatibility of MWCNTs with PA6,6 as the matrix by inclusion of a higher quantity (5 wt.%) of the nanofiller (MWCNT) in PA-MWCNT5 in comparison with PA-MWCNT1.5 containing only 1.5 wt.% of MWCNTs.

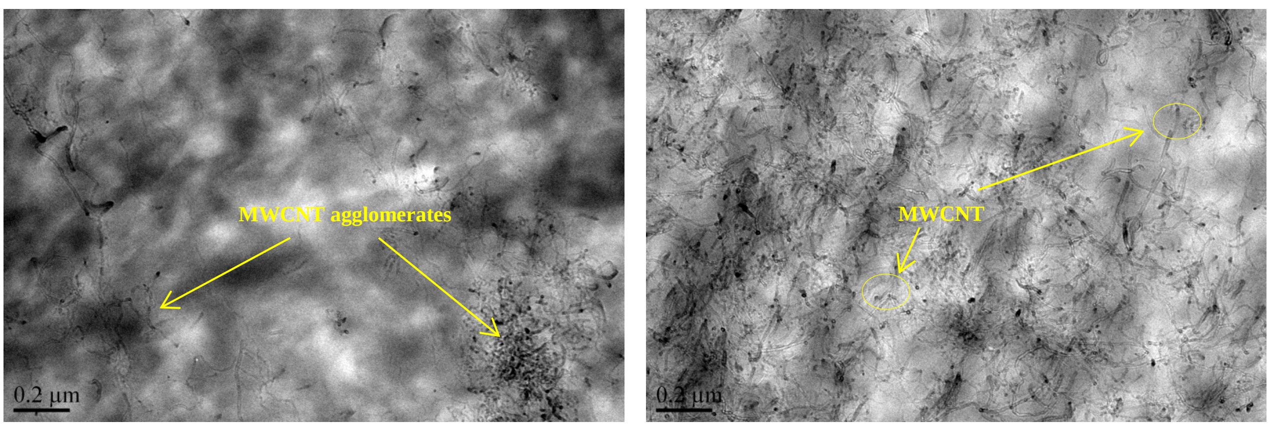

(a) (b)

Figure 3-8- Transmission electron microscopy images of (a) PA-MWCNT1.5 and (b) PA-MWCNT5 [59]

In addition, the TEM images of PA-CB10 and PA-CB20 are revealed in Figure 3-9(a and b) to investigate the performance of CB nanofillers at two different concentrations before and after percolation. It was suggested that CBs were agglomerated in more regions in PA-CB10 in comparison with PA-CB20 while CB particles were better dispersed in PA-CB20 and the conductive pathways were formed throughout the nanocomposite (PA-CB20) which made it an electrically conductive nanocomposite.

The nanocomposite having MWCNT had a quite low percolation threshold compared to the CPC with CB as the conductive nanofiller. This was correlated to the higher surface area of MWCNT compared to CB which cooperated in better dispersion of nanofillers in polymer matrix and electrical conductivity enhancement. In other words, the MWCNT dispersion was satisfactory in the polymer matrix and the electrical conductivity was recognized in the polymer (PA6,6) using less amount of MWCNT compared to CB.

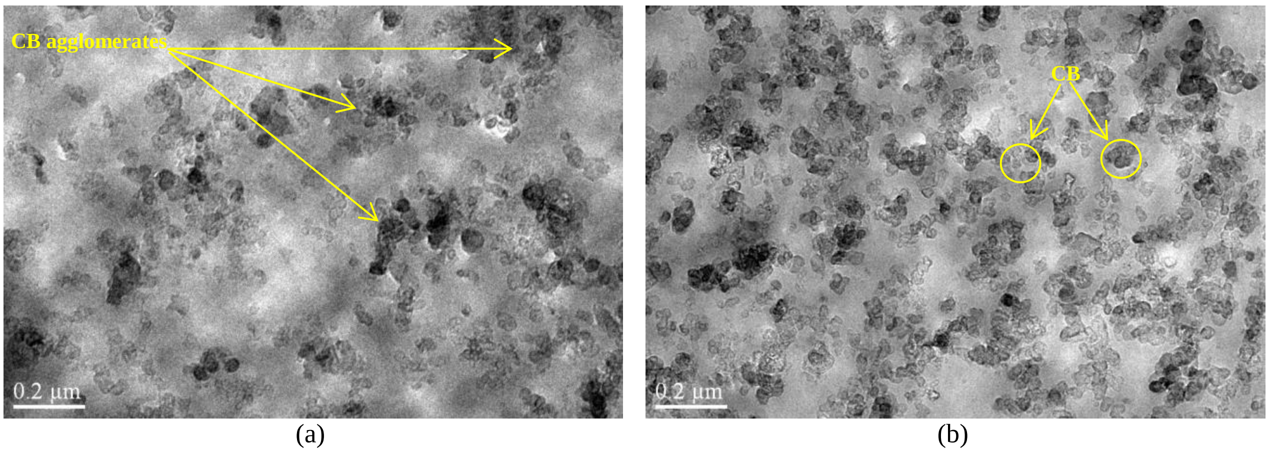

Figure 3-9- Transmission electron microscopy images of (a) PA-CB10 and (b) PA-CB20 [59]

It should be taken into account that the monofilament making process using extrusion is strongly influenced by the viscosity of the nanocomposite. Therefore, the melt flow index (MFI) value of the nanocomposite should be in the standard range for melt mixing process by means of extrusion. Adding carbon nanofillers inside the conductive polymer nanocomposites (CPCs) is the main cause of difficulties in the monofilament making process as a result of high viscosity.

The viscosity of the polymer matrix could intensely increase by nanofiller addition, mainly at high loading of the nanofillers which has adverse effects on polymer processability during extrusion. The evaluation of the MFI is of great importance to evaluate the possibility to prepare the electrically conductive materials that could be heated through the Joule effect (the production heat as the result of a current flowing through a conductive medium is known as Joule effect) [115].

In fact, viscosity had a major impact on determining spinnability conditions and the possibility of melt spinning of the nanocomposites. Hence, having low values of MFI admit that the extrusion process of thermoplastic polymers meets complications.

Therefore, the MFI values of all the nanocomposites were determined by the MFI test. The curves of measured MFI values of PA6,6-based nanocomposites containing MWCNT(blue curve) and CB (red curve) are indicated in Figure 3-10.

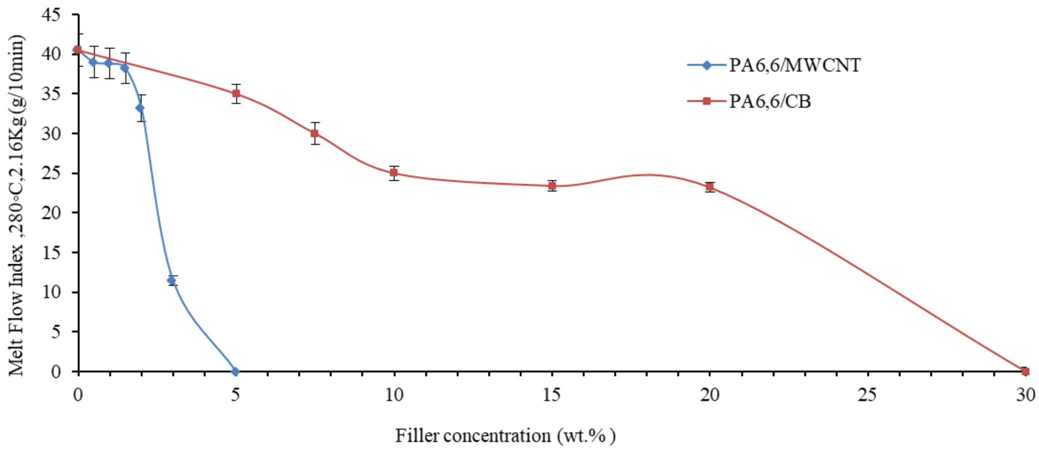

Figure 3-10- Melt flow index values for PA6,6/MWCNT and PA6,6/CB nanocomposites [59]

As can be perceived in Figure 3-10, the MFI value was decreased by increasing the quantity of nanofillers (MWCNT or CB). The same trend was observed for MFI values of both PA6,6/MWCNT and PA6,6/CB nanocomposites although the viscosity was meaningfully increased using the smaller amount of MWCNTs compared to CBs.

The drop in MFI value by adding nanofillers confirmed that the nanofillers particles caused viscosity complications in extrusion process although the electrical conductivity was increased. For instance, PA-MWCNT5 and PA-CB30 cannot be applied in the traditional monofilament yarn making process by melt mixing method due to the high viscosity. In addition, MFI value reduction using a fewer amount of MWCNT compared to CB was owing to the higher surface area of MWCNT particles. To sum up, the composition of the produced CPCs should be optimized in terms of both electrical conductivity and viscosity.

3.4 Synergism of conductive nanofillers (MWCNT:CB or KB)

As discussed earlier, the synergy effects between CB and MWCNT significantly increase the electrical conductivity of the nanocomposites [114]. The aim of using a mixture of nanofillers was to obtain higher electrical conductivity having a lower quantity of carbon nanofillers. The main purpose was to increase the electrical conductivity on one hand and to decrease the viscosity complications in the extrusion process on the other hand.

The mechanism of the conductive pathway construction with one nanofiller (MWCNT) and the ternary mechanism by adding CB to the nanocomposite is shown in Figure 3-11. As shown in Figure 3-11, new active conductive pathways were formed thanks to the presence of the second nanofiller particles (CB) due to the synergism between CB and MWCNT which led to the higher [217].

A mathematic model was applied in the present chapter to estimate the percolation threshold of hybrid carbon nanofillers in the polymer matrix. The proposed model was suggested by Sun *et al.* where the amount of nanofillers at percolation threshold in the extreme state using hybrid nanofillers in nanocomposites can be calculated [140]. However, the real state of hybrid nanofillers (MWCNT and CB) was not exactly similar to the state of the nanofillers in the model.

Equation (23) was used for the nanocomposites containing two types of conductive nanofillers (A (e.g. MWCNT) and B (e.g. CB)) where m_A is the weight fraction of nanofiller A (e.g. MWCNT) and m_B is the weight fraction of nanofiller B (e.g. CB). The nanocomposite is at its percolation threshold state when the value of the equation (24) is equal to 1.

$$\frac{m_A}{\rho_{C,A}} + \frac{m_B}{\rho_{C,B}} = 1 \tag{24}$$

Thus, a set of conductive nanocomposites was produced having various ratios of MWCNT and CB. In addition, three conductive polymer nanocomposites were produced applying a greater extent of MWCNT and CB compared to percolation state to study the electrical conductivity performance of the nanocomposites after percolation threshold.

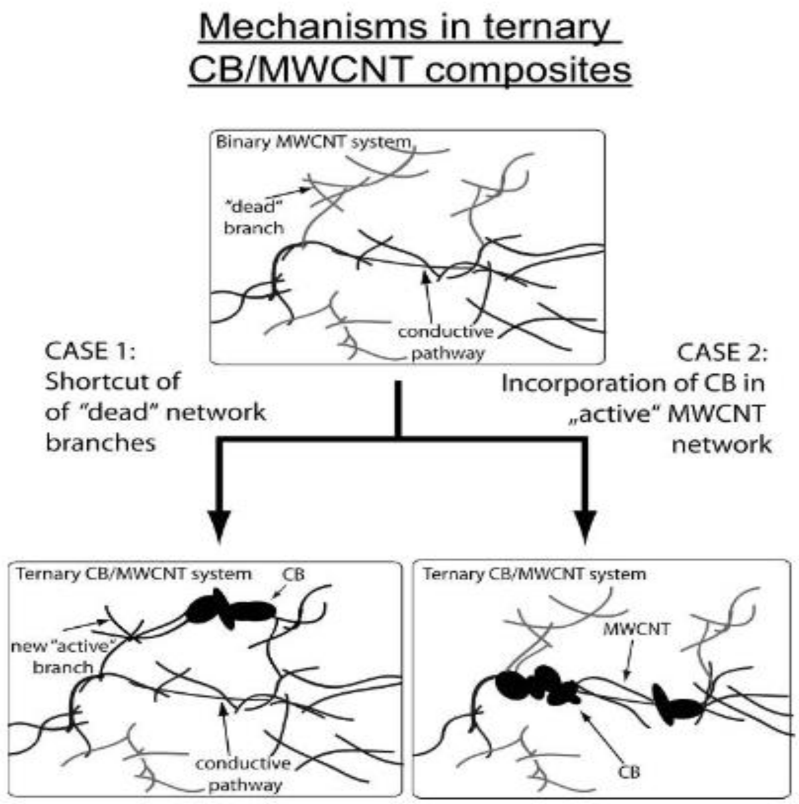

Figure 3-11- Mechanism of synergy effects between MWCNT and CB [217]

Moreover, three nanocomposites were produced while the CB was replaced by KB keeping the same amount of nanofillers and the same nanofillers ratio. The compositions of all the ternary nanocomposites are presented in Table 3-1.

3.4.1 Electrical and morphological properties of the ternary nanocomposites

Thermoplastic polymers are not generally electrically conductive while using conductive nanofillers is a well-known technique to enhance the electrical conductivity of the non-conductive polymers. On the other hand, adding the high quantity of conductive nanofillers increased both the viscosity and the cost of the developed nanocomposites.

The best available alternative was to use the constructive effects of synergy between MWCNT and CB in order to increase the electrical conductivity of the nanocomposite polymers while the amount of carbon nanofillers kept reasonably low.

Therefore, different nanocomposites were produced using three weight ratios of MWCNT and CB (1MWCNT:1CB, 1MWCNT: 2CB and 1MWCNT: 4CB) in the present study. Three CPCs were generated at percolation threshold and three nanocomposites were produced while more amount of carbon nanofillers (50% greater) compared to the quantity of nanofillers at percolation threshold was added to the polymer matrix (Table 3-1).

The percolation threshold of the electrical conductivity of the nanocomposites having mixed nanofillers was calculated using equation (23) [140]. The electrical conductivity of all the six nanocomposites was calculated and represented in Figure 3-12 and the evident growth of the electrical conductivity was observed due to the positive effects of synergism between MWCNTs and CBs.

In addition, the dispersion of nanofillers in PA6,6 was observed for two samples (PA-MWCNT1.7-CB3.3) and (PA-MWCNT2.5-CB5) using TEM images represented in Figure 3-13(a and b).

It should be noted that the dispersion of nanofillers was perceived for these two monofilament samples due to the fact that the higher electrical conductivity was observed for the samples with the ratio of 1MWCNT:2CB at the percolation threshold (MWCNT1.7-CB3.3) as well as after percolation threshold (PA-MWCNT2.5-CB5) among all the produced nanocomposite samples with different ratios (1MWCNT:1CB, 1MWCNT: 2CB and 1MWCNT: 4CB).

The dispersion of carbon nanofillers was satisfying for sample PA-MWCNT2.5-CB5 given in Figure 3-13(b) and the connection network was well-formed by nanofillers in the polymer matrix. Also, the connection path was detected in the image of PA-MWCNT1.7-CB3.3 (Figure 3-13(b)) although the nanofillers were not well dispersed as in PA-MWCNT2.5-CB5.

Furthermore, carbon nanofillers in PA-MWCNT2.5-CB5 were very well dispersed compared to the nanofillers in the nanocomposites contained only MWCNTs or CBs due to the fact that one of the nanofiller particles (e.g. CB) played a connection role in the middle of the other nanofiller particles (e.g. MWCNT) which led to the uniform dispersion of nanofillers inside the nanocomposite. Concisely, the nanofillers were adequately dispersed in PA-MWCNT2.5-CB5 and so that, PA-MWCNT2.5-CB5 revealed the highest electrical conductivity amongst all the manufactured nanocomposites filled with CBs, MWCNTs or combination of MWCNTs and CBs.

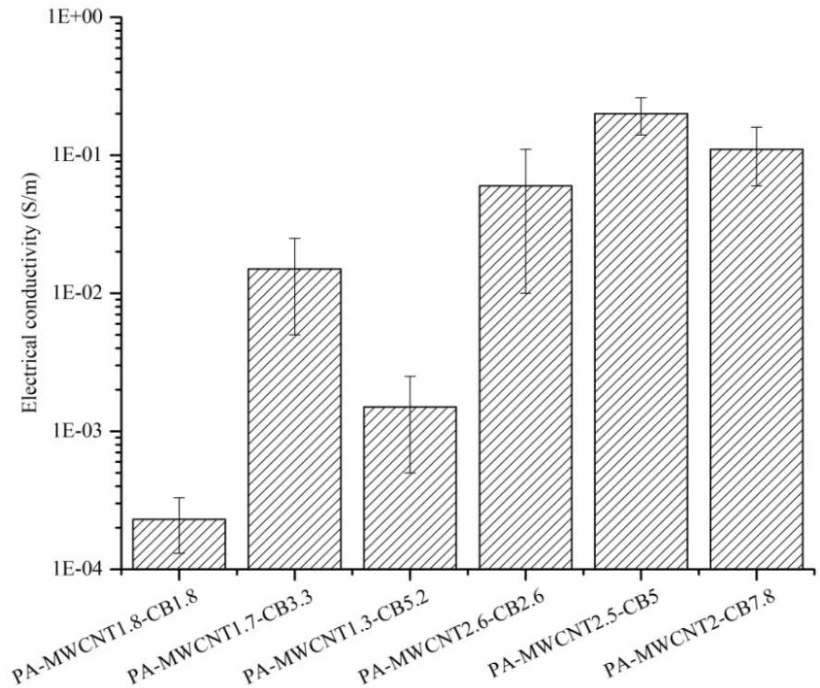

Figure 3-12- Electrical conductivity of the nanocomposites versus nanofillers mass concentration (MWCNT:CB) [59]

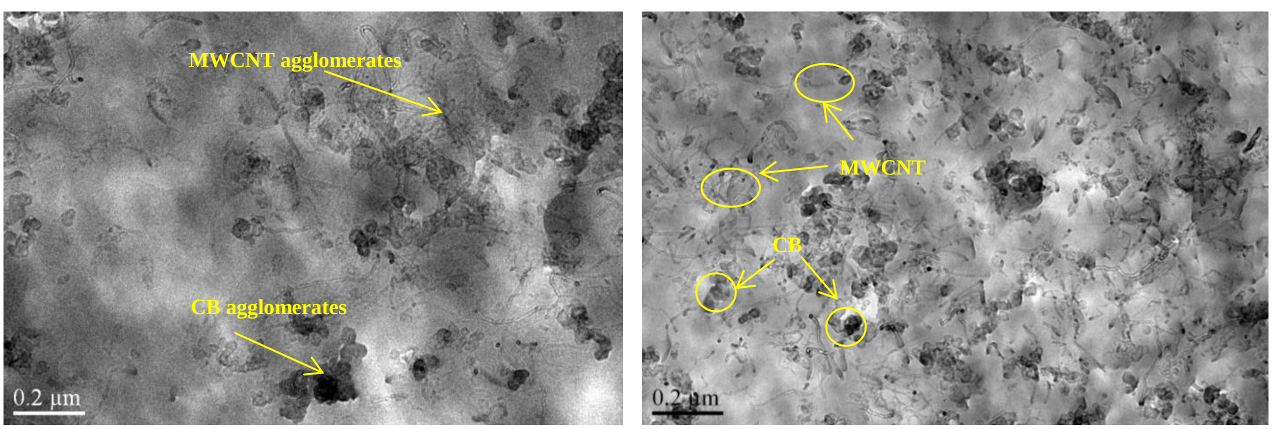

Figure 3-13- TEM images of (a) PA-MWCNT1.7-CB3.3 and (b) PA-MWCNT2.5-CB5 [59]

Moreover, the MFI values of all the six produced nanocomposites having MWCNT:CB is demonstrated in Figure 3-14. The higher quantity of the mixed nanofillers led to the lower MFI values. Also, the MFI results were compared to the MFI values of the nanocomposites contained only one kind of nanofillers (MWCNT or CB) in their compositions and it was suggested that badly performed viscosity was diminished as a result of the synergy effects between carbon nanofillers.

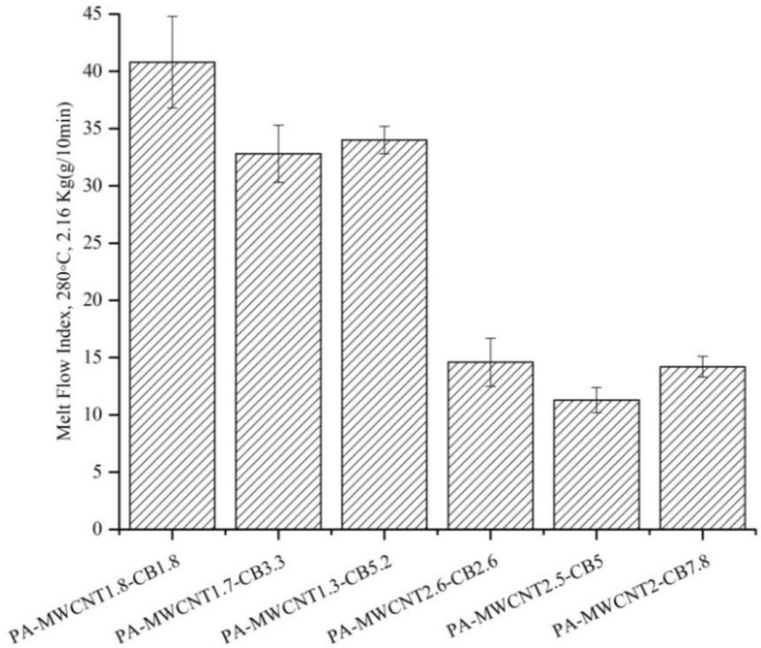

Figure 3-14- Melt flow index values of the PA6,6-based nanocomposites with MWCNT:CB [59]

In the following, CB was substituted with KB using the same mass concentration of three most conductive nanocomposites. Consequently, a set of three nanocomposites was prepared with MWCNT and KB (PA-MWCNT2.6-KB*2.6, PA-MWCNT2.5–KB*5 and PA-MWCNT2–KB* 7.8) as given in Table 3-1.

The idea of replacing CB with KB in the nanocomposites was to investigate the influence of the surface area of the conductive additive on the electrical conductivity due to the fact that the surface area of KB* is four times greater than the surface area of CB.

The electrical conductivity of six nanocomposites contained MWCNT:KB or MWCNT:CB is illustrated in Figure 3-15. The higher electrical conductivity was witnessed for the nanocomposites with MWCNT and KB compared to the ones with MWCNT and CB while all other parameters kept constant (unchanged). This increase was correlated to the higher surface area of KB in comparison with the surface area of CB and therefore, PA-MWCNT2–KB*7.8 showed the highest electrical conductivity followed by PA-MWCNT2.5–KB*5 among the nanocomposites samples.

Moreover, the MFI values of the six manufactured nanocomposites with MWCNT:CB and MWCNT:KB are represented in Figure 3-16.

As discussed earlier, the viscosity of CPCs plays a major role in the extrusion process. Hence, PA-MWCNT2-KB*7.8 cannot be considered for the monofilament making process with melt mixing method because the MFI value of this nanocomposite was zero.

In other words, the high viscosity of the nanocomposite with a high content of KB (PA-MWCNT2-KB*7.8) made it incompatible with melt mixing process despite the fact that the electrical conductivity was comparatively high compared to the one contained the same quantity of CB and MWCNT.

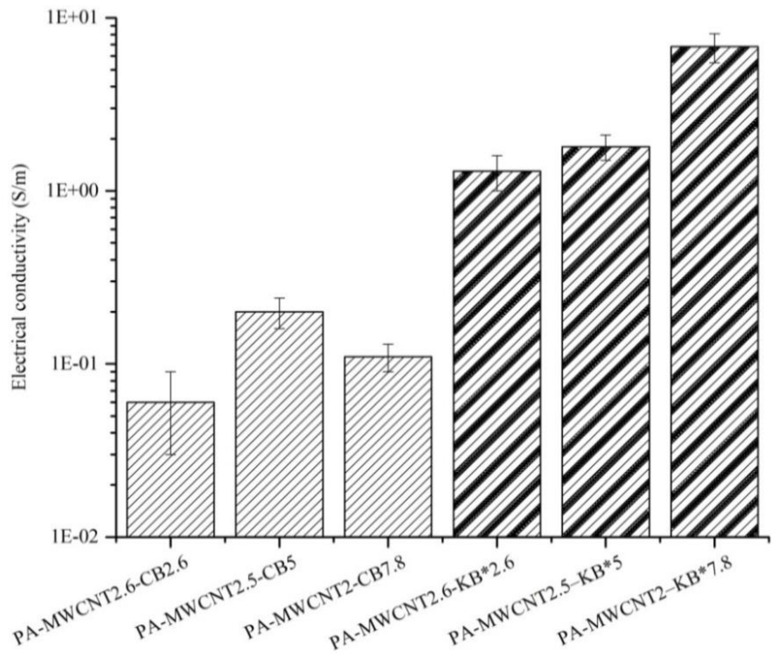

Figure 3-15- Electrical conductivity versus nanofillers concentration (MWCNT:CB and MWCNT:KB) [59]

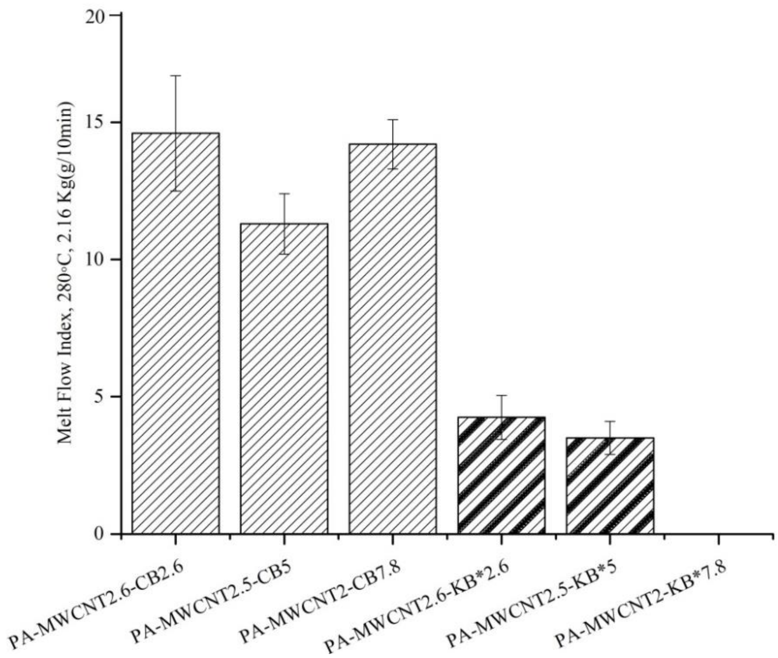

Figure 3-16- Melt flow index values of the PA6,6/MWCNT:CB and PA6,6/MWCNT:KB nanocomposites [59]

3.4.2 Mechanical properties of the monofilaments for fabric manufacturing

- Measurement method

Tensile test of two candidate monofilaments for fabric manufacturing was implemented using Tinius Olsen H5KT Benchtop tensile tester (ISO 2062) at 20-25◦C, 65 RH%. The sample length for the tensile test was fixed at 100 mm and the speed of traction was 50 mm/min. It should be mentioned that the tensile test was carried out for 5 specimens of each monofilament and the mean value was calculated. The device during tensile test of one of the monofilament samples is represented in Figure 3-17.

Figure 3-17- Tinius Olsen H5KT Benchtop tensile tester

- The mechanical properties

Two candidates were preferred among all the produced conductive polymer nanocomposites for monofilament producing with the aim of applying in woven fabric manufacturing regarding the electrical conductivity and MFI values. PA-MWCNT2.5-CB5 showed the highest electrical conductivity (0.2 S/m) among all the produced CPCs containing MWCNT and CB. In addition, the viscosity (MFI value) of PA-MWCNT2.5-CB5 was acceptable for melt mixing method. As a result, this nanocomposite (PA-MWCNT2.5-CB5) was selected to be applied as weft conductive yarn for woven fabric manufacturing.

Moreover, one of the nanocomposite samples having MWCNT and KB was nominated for woven fabric manufacturing (PA-MWCNT2.5–KB*5) to study the electromagnetic shielding effectiveness of the two developed monofilaments with the same quantity of nanofillers.

It should be taken into consideration that the electrical conductivity of PA-MWCNT2.5–KB*5 was (2 S/m) which was tenfold greater than the measured electrical conductivity for PA-MWCNT2.5-CB. However, the MFI value of PA-MWCNT2.5–KB*5 was relatively low compared to PA-MWCNT2.5-CB5.

Then, the tensile test was performed for these two developed monofilaments while the tensile test was implemented for 5 specimens of each monofilament and the mean values were calculated. The force-extension graph for two developed samples (PA-MWCNT2.5-CB5) and (PA-

MWCNT2.5–KB*5) is shown in Figure 3-18. Also, the mechanical properties of (PA-MWCNT2.5-CB5) and (PA-MWCNT2.5–KB*5) are publicized in Table 3-2.

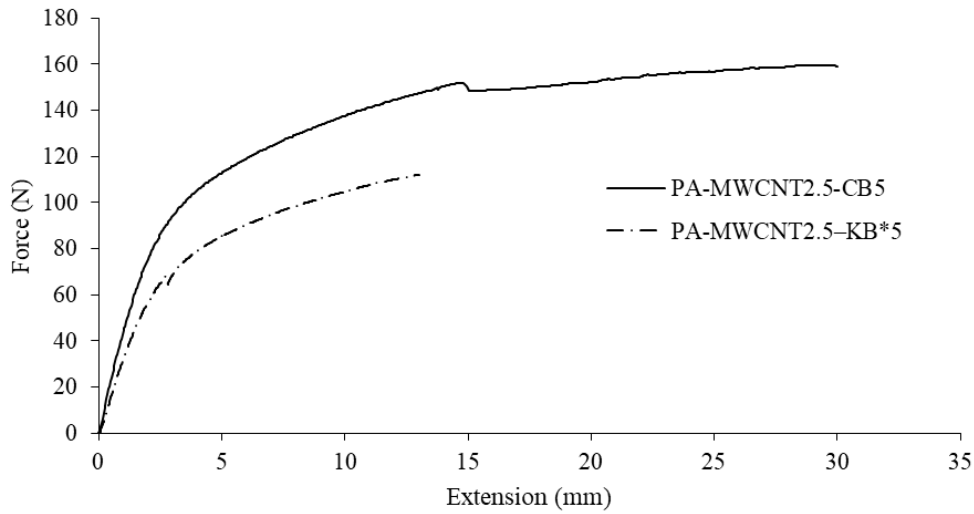

Figure 3-18- Force (N) vs extension (mm) graphs of the selected monofilaments for fabric manufacturing

Table 3-2- Mechanical properties of the monofilaments for weaving [59]

			Monofilament	
No.	Property	Unit	PA-MWCNT2.5–CB5	PA-MWCNT2.5–KB*5
1.	Initial diameter	mm	1.40	1.40
2.	Maximum Force	N	159.6	112.1
3.	Elongation at Maximum Force	delta l, mm	29.9	13
4.	Stress at Maximum Force	MPa	103.5	72.8
5.	Strain at Maximum Force	delta l/l_0	0.3	0.13
6.	Elastic Modulus (E)	GPa	2.78	2.08
7.	Modulus of Rigidity(G)	GPa	1.39	1.04
8.	Tenacity	cN/Tex	8	5.6

As stated by previous studies, the incorporation of MWCNT nanofillers in polyamide matrices considerably increases both the tensile strength and modulus of the polymer and makes it tougher and more resistant to deformation [101], [105], [218]. Also, it is been said that the incorporation of CB particles into the nanocomposites with MWCNTs may enhance the ductility of the nanocomposites [219].

Here, the results showed that the tenacity of PA-MWCNT2.5–CB5 was bigger (8 cN/Tex) in comparison with the tenacity of PA-MWCNT2.5–KB*5 (5.6 cN/Tex). Also, it was suggested that replacing CB with KB in the composition of the proposed nanocomposite monofilament resulted in a reduction in the elastic modulus from 2.78 to 2.08 GPa. Moreover, the elongation at break moderately was lower for PA-MWCNT2.5–KB*5 (13 mm) in comparison with MWCNT2.5–CB5 (~30 mm) indicating that the nanocomposite monofilament became brittle using KB in the nanocomposite structure. Therefore, it was concluded that using KB in the CPC monofilament composition (PA-MWCNT2.5–KB*5) caused poorer mechanical properties in comparison with the nanocomposite containing PA6,6, MWCNT, and CB (PA-MWCNT2.5–CB5).

3.5 Fabric manufacturing using developed monofilaments

3.5.1 Materials

The following yarns were applied for woven fabric manufacturing in this chapter:

- PA-MWCNT2.5–CB5 monofilament
- PA-MWCNT2.5–KB*5 monofilament
- Cotton yarns (N_m 20/2), two-ply cotton yarn is composed of two single strands and metric number (N_m) specifies the number of one thousand meters of yarn per kilogram.
- Silver multifilament (N_m 9.26, 10×0.04mm) supplied by Elektrisola company in Germany. This multifilament yarn is low electrical resistance and high corrosion resistance (the conductivity 62.5×10^6 S/m, tensile strength 220 MPa, maximum elongation 40%).

An image of the developed conductive monofilament (PA-MWCNT2.5–CB5) is shown in Figure 3-19.

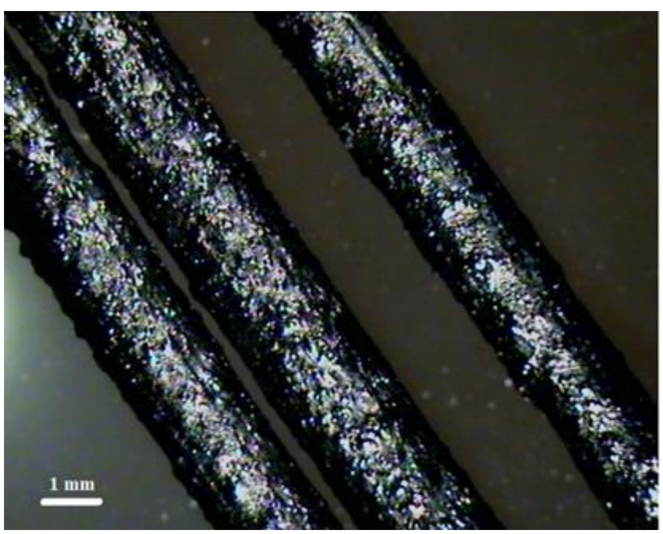

Figure 3-19- The produced conductive monofilament for weft insertion in weaving process [59]

3.5.2 Woven fabric design and manufacturing

A compound woven structure was designed (compact two-ply weave structure with stuffer weft) when the developed monofilaments were introduced as stuffer wefts in the middle of the designed woven structure. The designed structure consists of two warp yarn systems and three weft yarn systems as depicted in Figure 3-20.

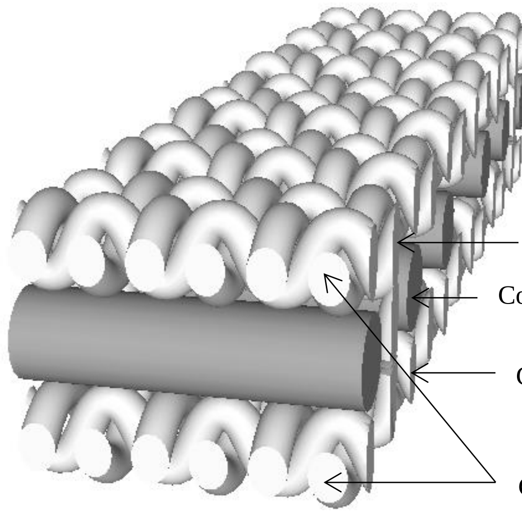

Figure 3-20- Designed structure of compact two-ply woven fabric with conductive monofilament as stuffer weft [59]

ARM AG CH-3507 Biglen weaving loom manufactured in Switzerland was applied for weaving all the woven samples in Chapter 3 where conductive monofilaments (PA-MWCNT2.5–CB5 or PA-MWCNT2.5–KB*5) were applied as stuffer wefts in the middle of the woven structure as specified in Figure 3-20.

Two weft and two warp yarn systems made the outer layers with plain weave structure (face and back) of the woven fabric. The conductive monofilaments were introduced in the middle of the structure as stuffer wefts in weft direction.

It is noted that stuffer yarns are straight yarns inserted in the middle of compound woven fabrics. The reason for inserting conductive monofilaments as stuffer yarns was to provide the possibility of introducing common textile yarns on the exterior faces of the manufactured woven fabric. Thus, a variety of textile yarns and colours can be used for the outer faces of the woven structure since the ultimate application of the produced fabric is for personal protective clothing and the design and colour would be of great importance for the wearer.

The structural characteristics of the two manufactured woven samples (Sample 1 and Sample 2) are described in Table 3-3. Also, an image of the manufactured woven sample using conductive monofilaments is shown in Figure 3-21.

Table 3-3- Structural characteristics of compact two-ply woven samples (Sample 1 and Sample 2) with monofilaments as stuffer wefts

					Sample code	
No.	Fabric characteristics			Unit	Sample 1	Sample 2
1.	Thickness			mm	3.37	3.66
2.	Arial density			g/cm^2	0.136	0.155
3.	Porosity			%	72.5	71
4.	Material	Warp	Face		Cotton	Cotton
			Back		Cotton	Cotton
		Weft	Face		Cotton	Cotton
			Stuffer		PA-MWCNT2.5-CB5	PA-MWCNT2.5-KB*5
			Back		Cotton	Cotton
5.	Yarn diameter	Warp	Face	mm	0.42	0.42
			Back		0.42	0.42
		Weft	Face		0.42	0.42
			Stuffer		1.40	1.40
			Back		0.42	0.42
6.	Yarn density	Warp	Face	yarns/cm	15	15
			Back		15	15
		Weft	Face		8	8
			Stuffer		4	4
			Back		8	8

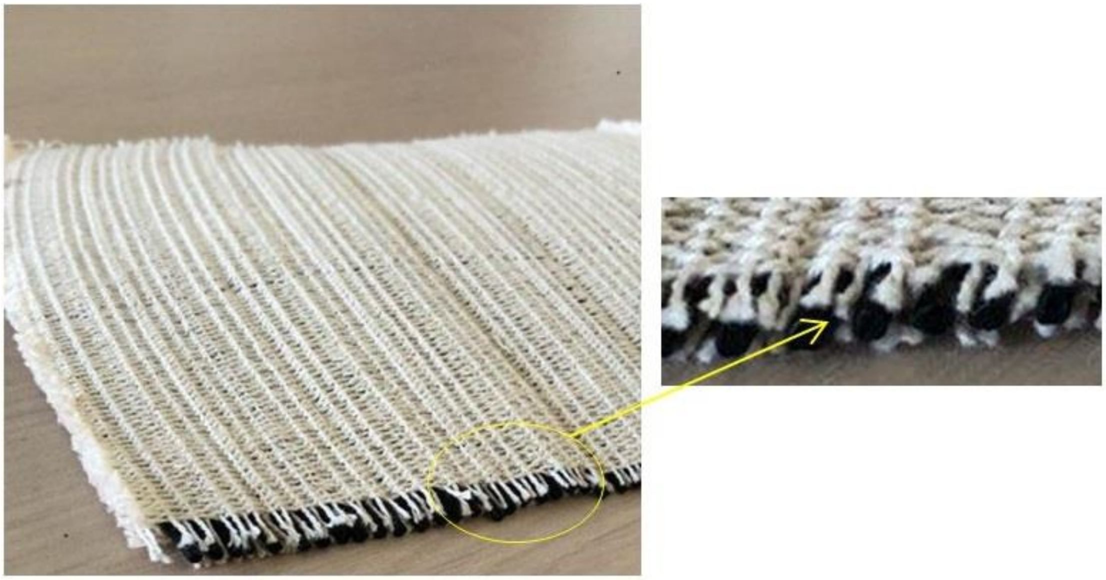

Figure 3-21- Image of Sample 1 (Cotton woven fabric with embedded conductive monofilaments) [59]

Additionally, another woven sample (Sample 3) was designed and weaved using PA-MWCNT2.5–CB5 monofilaments as conductive wefts and cotton yarns as warps. This sample was introduced as a 24-shaft satin mixed with plain with the weft ratio of 4:2 (4PA-MWCNT2.5–CB5 monofilaments: 2 cotton yarns). A graphic representation of Sample 3 is shown in Figure 3-22. Also, the structural characteristics of Sample 3 are revealed in Table 3-4.

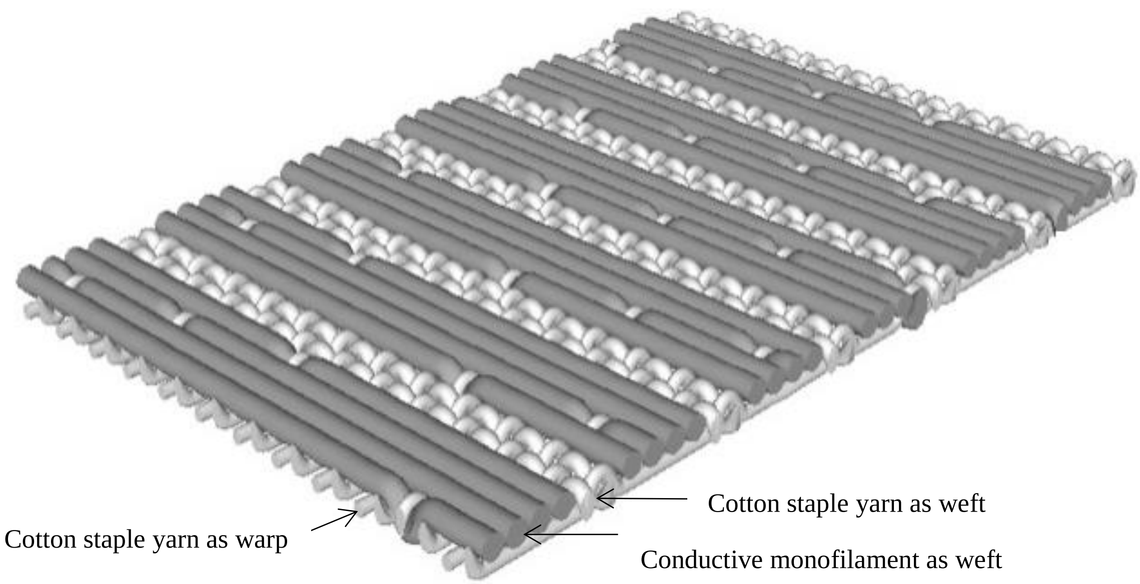

Figure 3-22- Graphic representation of Sample 3 with PA-MWCNT2.5-CB5 as conductive weft

Table 3-4- Structural characteristics of Sample 3

					Sample code
No.	Fabric characteristics			Unit	Sample 3
1.	Thickness			mm	3.54
2.	Arial density			g/cm^2	0.189
3.	Porosity			%	64.7
4.	Material	Warp			Cotton
		Weft	Satin		PA-MWCNT2.5-CB5
			Plain		Cotton
5.	Yarn diameter	Warp		mm	0.42
		Weft	Satin		1.40
			Plain		0.42
6.	Yarn density	Warp		yarns/cm	15
		Weft	Satin		5
			Plain		4

Sample 3 was designed and weaved in order to increase the yarn density of the conductive monofilament in weft direction compared to Sample 1 using the same monofilament (PA-MWCNT2.5-CB5). Also, the contact between the monofilament yarns was ensured using satin weave structure for conductive wefts in Sample 3.

A repeat of plain weave structure with cotton yarns was mixed with satin weave structure using PA-MWCNT2.5-CB5 as conductive wefts (weft ratio of 4 monofilaments: 2 cotton yarns) to increase the stability of Sample 3. In point of fact, the inclusion of cotton yarns in weft direction using plain weave structure resulted in fixing the monofilaments in the structure of Sample 3.

An image of the produced sample (Sample 3) is represented in Figure 3-23.

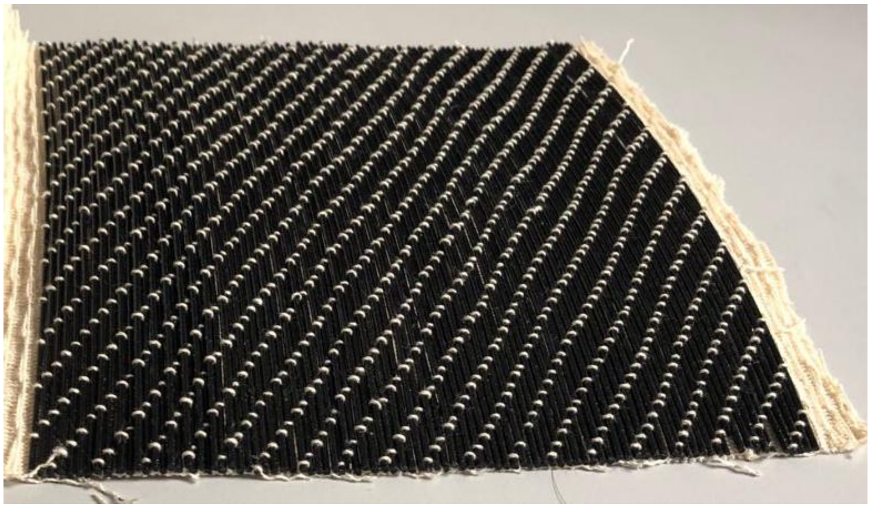

Figure 3-23- Sample 3 with PA-MWCNT2.5–CB5 as conductive weft

3.5.3 Supplementary woven fabrics

First, an adaptive head was installed on the extrusion device to add silver multifilament as core to the extruded PA6,6. A schematic of the adaptive head on co-rotating twin-screw extruder ThermoHaake for addition of the silver multifilament to the extruded PA6,6 is shown in Figure 3-24. It should be noted that the same silver multifilament was applied in Chapter 2 and Chapter 3 of this thesis for different EMSE fabric manufacturing.

The idea of making a core-sheath yarn was to use silver multifilament for shielding properties while the conductive multifilament was protected using PA6,6 as cover. The main reason was to avoid metal exposure to the air to preserve the metal from oxidation. Also, metal touching with the skin of the wearer during use would be prevented, as metals potentially cause skin allergies for the wearer. Furthermore, it should be taken into account that the electrical conductivity of the employed polymer (PA6,6) as the sheath of the yarn is nearly 3.4×10^{-14} S/m [220] indicating that the PA6,6 has no contribution to the EMSE behaviour of the manufactured fabrics.

The diameter of the silver multifilament was 0.12 mm and the diameter of the adaptive head was 1 mm. So that, the diameter of the final silver multifilament coated with PA6,6 was 1 mm.

Then, the developed core-sheath yarn was applied as stuffer wefts in Sample 4 weaved with compact two-ply woven structure shown in Figure 3-20. Also, both silver multifilament coated with PA6,6 and PA-MWCNT2.5–CB5 were applied parallel to each other in the woven fabric as stuffer wefts (Sample 5).

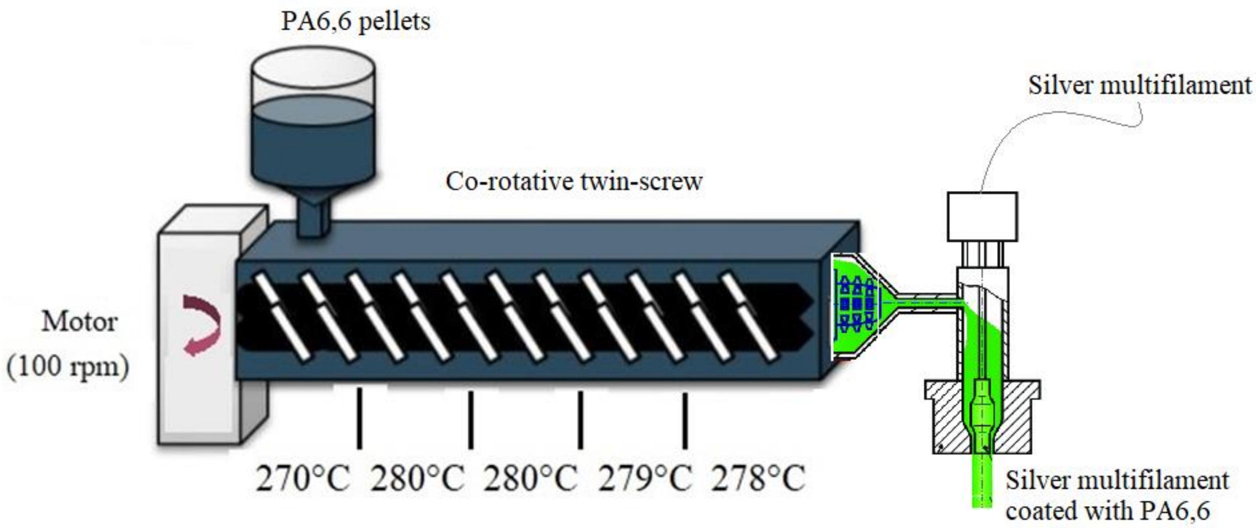

Figure 3-24- Schematic of adaptive head on the co-rotating twin-screw extruder ThermoHaake for addition of silver multifilament as core to extruded PA6,6

Moreover, the images of the core-sheath yarn of silver multifilament coated with PA6,6, Sample 4 with core-sheath yarn as conductive stuffer weft, and Sample 5 using both core-sheath yarn and PA-MWCNT2.5–CB5 monofilament as conductive stuffer wefts are shown in Figure 3-25(a, b and c), respectively. Also, the structural characteristics of Sample 4 and Sample 5 are listed in Table 3-5.

(a) (b) (c)

Figure 3-25- (a) Silver multifilament coated with PA6,6, (b) Sample 4 with silver multifilament coated with PA6,6 as conductive yarn and (c) Sample 5 with both silver multifilament coated with PA6,6 and PA-MWCNT2.5–CB5 as conductive yarns

Table 3-5- Structural characteristics of Sample 4 and Sample 5

No.	Fabric characteristics			Unit	Sample Code: Sample 4	Sample Code: Sample 5
1.	Thickness			mm	2.8	3.65
2.	Arial density			g/cm^2	0.153	0.197
3.	Porosity			%	74.1	73.8
4.	Material	Warp	Face		Cotton	Cotton
			Back		Cotton	Cotton
		Weft	Face		Cotton	Cotton
			Stuffer		Silver multifilament coated with PA6,6	PA-MWCNT2.5-CB5 Silver multifilament coated with PA6,6
			Back		Cotton	Cotton
5.	Yarn diameter	Warp	Face	mm	0.42	0.42
			Back		0.42	0.42
		Weft	Face		0.42	0.42
			Stuffer		1.00	1.40 1.00
			Back		0.42	0.42
6.	Yarn density	Warp	Face	(yarns/cm)	15	15
			Back		15	15
		Weft	Face		8	8
			Stuffer		4	4 4
			Back		8	8

3.6 3D printing of the developed monofilament on textiles

3.6.1 Materials

- PA-MWCNT2.5–CB5 monofilament
- Pure cotton woven fabric with plain weave structure (with the areal density of 0.03 g/cm^2 and the fabric thickness of 0.38 mm)

3.6.2 3D printing on fabrics

Electrical conductive materials are attached to textiles using different methods such as the incorporation of conductive yarns into the fabric or mounting electronic components (e.g.

sensors) on the surface of the fabric in order to develop smart textiles. However, the functional material in modified textiles may influence the flexibility and drapability of the fabric.

3D printing method using fused deposition modeling (FDM) is one of the popular methods which makes it possible to deposit thermoplastic functional polymers or nanocomposites on the surface of fabric to develop functional and smart textiles [180]. The 3D printing method is clean, easy to use, inexpensive, accessible, and no liquid resin or supporting material is required. Consequently, this method has been applied for deposition of polymers on textiles [221].

Therefore, in the present chapter, this method was applied for the deposition of the developed conductive monofilament directly on woven fabrics in order to gain the advantages of the 3D printing method.

So, firstly, several CAD designs were drawn and transferred to a 3D printable format using Simplify3D software. Three grid structures and one solid structure were designed (Figure 3-26) when the dimension of all the structures was fixed to 160×160 mm^2.

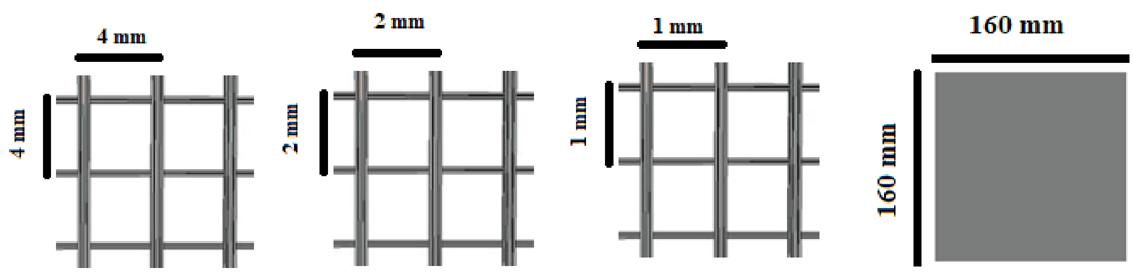

Figure 3-26- Web structures with various grid sizes and the solid structure for 3D printing

Two-head Volumic Stream 3D printer supplied in France was applied while the maximum printing size of the printer was 300×210×300 mm^3 with the nozzle diameter of 0.4 mm. The developed conductive monofilament (PA-MWCNT2.5-CB5) was printed on the surface of the pure cotton woven fabric with plain weave structure. For this purpose, plain woven fabric made of cotton was longitudinally positioned on the 3D printer platform in warp direction.

This conductive monofilament (PA-MWCNT2.5-CB5) was chosen for 3D printing layers on the surface of the fabric due to its high electrical conductivity amongst all the produced CPCs with PA6,6, MWCNT, and CB. Also, the monofilaments having the combination of KB and MWCNT in the polymer matrix were not appropriate for 3D printing layers on the surface of the fabric due to the lamination of each printed layer of the nanocomposite on the surface of the fabric during printing as well as the unevenness of the CPCs through the length of the monofilaments.

Then, PA-MWCNT2.5–CB5 monofilament was 3D printed on the surface of the fabric using four different design structures. The parameters of the 3D printing parameters are listed in Table 3-6. Also, images of the positioned fabric on the platform of the 3D printer and the FDM printing of PA-MWCNT2.5–CB5 monofilament on the fabric are represented in Figure 3-27.

In addition, the electrical conductivity of the solid structure printed layer with a thickness of 0.5 mm was determined using 4-wire ohms and the conductivity was 1×10^{-4} S/m suggesting that the conductivity of the CPC was decreased up to several orders of magnitude in comparison with the loaded monofilament (0.2 S/m). It should be also noted that the applied 4-wire ohms method for electrical conductivity measurement explained in detail in Chapter 2.

Table 3-6- Printing parameters for 3D printing of PA-MWCNT2.5-CB5 on cotton fabric

Printing parameters	Layer thickness	Nozzle temperature	Bed temperature	Printing velocity	Polymer flow	Filament diameter	Extrusion width
Unit	mm	◦C	◦C	mm/s	%	mm	mm
Quantity	0.1- 0.2-0.4-0.5	265-280	40	30	100	1.75	0.4

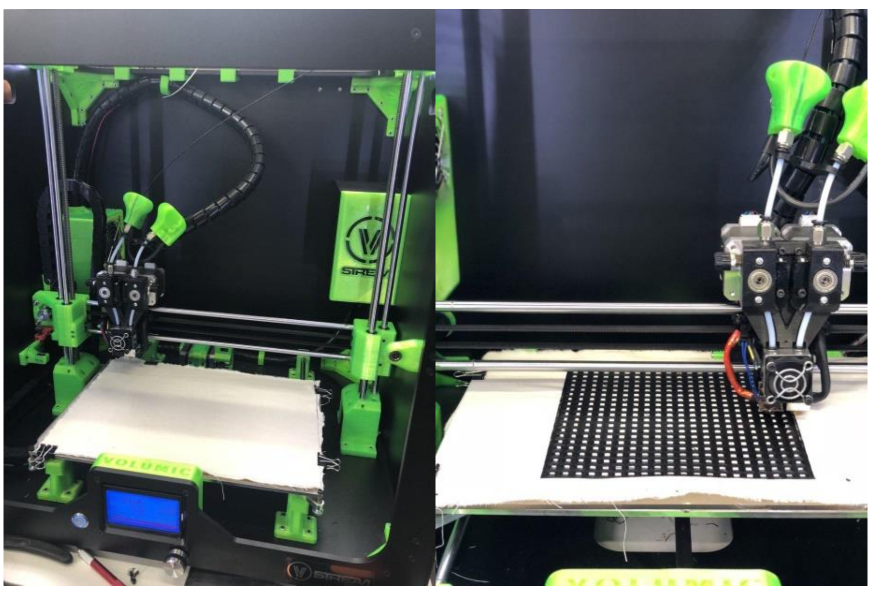

Figure 3-27- FDM printing of PA-MWCNT2.5-CB5 monofilament on cotton fabric

3.7 Electromagnetic shielding effectiveness of the manufactured woven fabrics

To this point, the objective of Chapter 3 was to generate conductive monofilaments of the best choices of the manufactured CPCs with reference to the electrical conductivity and viscosity. In addition, the selected monofilament yarns were applied in weaving process in order to make wearable electromagnetic shielding clothing for personal protection against radiation.

Accordingly, two developed monofilaments (PA-MWCNT2.5–CB5 and PA-MWCNT2.5–KB*5) were selected owing to their electrical conductivity (~0.2 S/m for PA-MWCNT2.5–CB5 and ~ 2 S/m for PA-MWCNT2.5–KB*5) and viscosity in order to manufacture electromagnetic shielding woven samples (Sample 1, Sample 2, Sample 3, and Sample 5). It should be also noted the MFI value of the most conductive monofilament contained PA6,6, MWCNT, and CB (PA-MWCNT2.5–CB5) was 11.5 g/10min (at 280^{o}C, 2.16 Kg load) which is in the acceptable range for melt mixing method (10-35 g/10min).

On the other hand, Sample 4 was weaved using silver multifilament coated with PA6,6 as stuffer conductive weft yarn using the compact two-ply weave structure.

Moreover, PA-MWCNT2.5–CB5 was printed on the surface of the cotton woven fabric using four different designed structures in an attempt to advance the EMSE of the common woven fabric made of cotton.

Therefore, the EMSE of all the developed fabrics had to be measured to find out the suitable choices for personal protection against radiation.

3.7.1 Mode-stirrer chamber setup for the EMSE measurements

As discussed in Chapter 1, an anechoic chamber with a cut-out portion has been used by many studies for EMSE measurements of fabrics. Also, the EMSE of the produced woven fabrics in Chapter 2 was evaluated in an anechoic chamber at the frequency range of 1-6 GHz.

However, such EMSE measurements were dependent on the wave polarization and were unable to evaluate the shielding effectiveness of the fabrics in a realistic electromagnetic environment. As a result, in this chapter, an electromagnetic reverberation chamber (mode-stirred chamber) was hired to measure the EMSE of the developed woven samples. This apparatus allows assessing the EMSE of the fabrics in a realistic electromagnetic environment where the wave polarization cannot be controlled.

A simple schematic of the mode-stirred chamber for EMSE measurements based on IEC61000-4-21 standard used in this chapter is displayed in Figure 3-28 [222].

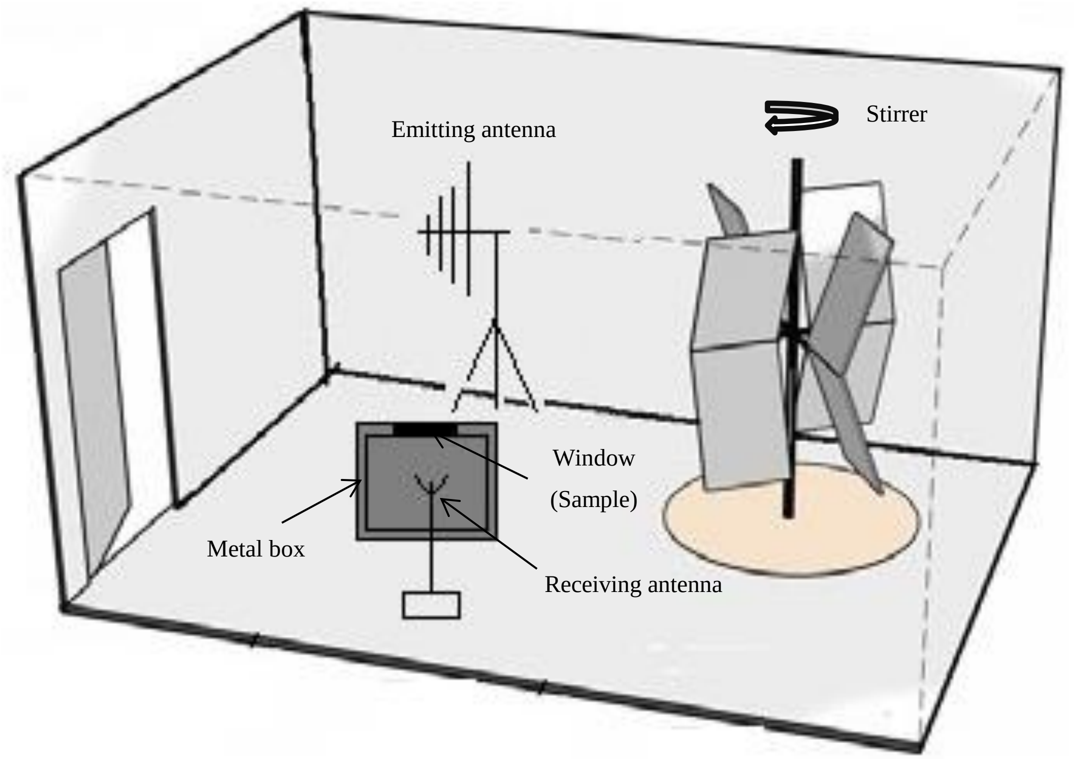

Figure 3-28- Schematic of the mode-stirred chamber for shielding effectiveness measurement [59]

It is noted that all the wave polarizations were deliberated for the measurement owing to the stirrer. In fact, the stirrer was rotated from θ = 0 to θ = 360 degrees (one complete turn) by steps of 4 degrees where P_S (θ) and P_{REF} (θ) were recognized by receiving antenna. The average values of P_S and P_{REF} incorporated over all the measurements were measured to compute the EMSE using equation (25).

$$\mathrm{EMSE(dB)} = 10\log_{10}\left(\frac{P_{REF}}{P_S}\right) \tag{25}$$

The mode stirred chamber including the stirrer, emitting antenna and metallic closed box with and without fabric sample used in the present chapter is demonstrated in Figure 3-29.

Figure 3-29- The utilized mode-stirred chamber for EMSE measurement

A two-layered sample was presented in front of the window of the metallic box for the measurement. Two pieces of each woven sample were placed at right angles to each other in an attempt to have conductive monofilaments in both vertical and horizontal directions and the EMSE was measured at the frequency range of 1-10 GHz.

As a matter of fact, the application of the produced woven fabrics was to shield the human body against the electromagnetic waves existing in the living environment. So, the manufactured fabrics were classified as EMSE fabrics for general use as specified in Table 3-7 [223].

It should be also mentioned that the electromagnetic wave polarizations cannot be controlled in the human living environment. Therefore, the mode-stirrer chamber was chosen for EMSE measurements in Chapter 3 for the reason that the EMSE measurement in a reverberation chamber (mode-stirred chamber) gives a realistic shielding of the manufactured fabrics in comparison with other EMSE measurement methods.

Table 3-7- Performance specifications of electromagnetic shielding textiles [223]

Grade	5 Excellent	4 Very good	3 Good	2 Moderate	1 Fair
Percentage of electromagnetic shielding	SE>99.9%	99.9%≥SE>99%	99%≥SE>90%	90%≥SE>80%	80%≥SE>70%
Shielding effectiveness (SE*) in general use	SE>30dB	30dB≥SE>20dB	20dB≥SE>10dB	10dB≥SE>7dB	7dB≥SE>5dB

*SE is the abbreviation for shielding effectiveness with the same meaning of electromagnetic shielding effectiveness (EMSE) used in the text

3.7.2 The EMSE results and discussion

3.7.2.1 The EMSE results of Sample 1 and Sample 2

The EMSE of two compound woven samples with conductive monofilaments as stuffer weft yarns (PA-MWCNT2.5-CB5 for Sample 1 and PA-MWCNT2.5-KB*5 for Sample 2) was evaluated in the frequency range of 1-10 GHz in a mode-stirred chamber.

The EMSE of Sample 1 and Sample 2 together with the average curves of the EMSE are illustrated in Figure 3-30. It should be noted that the results of these two woven samples are presented in Figure 3-30 to compare the effects of the formulation of nanocomposites (PA-MWCNT2.5-CB5 for Sample 1 and PA-MWCNT2.5-KB*5 Sample 2) on the EMSE.

As specified earlier in Chapter 3, two monofilaments were selected for fabric manufacturing as a result of the higher electrical conductivity and reasonable viscosity among all the developed CPCs. These two factors made the aforesaid monofilaments applicable for yarn making process by melt mixing method.

The scattered EMSE data can be described by determinate numbers of measurements where the stirrer was rotated by steps of 4 degrees and the EMSE was computed by the average of 90 measurements. Therefore, the intervals had to be narrowed for data scattering reduction which resulted in additional numbers of measurements. Nonetheless, the average value of the EMSE at each frequency was reflected as the EMSE level of each sample at that frequency.

It should be taken into consideration that the average values were not meaningfully affected by increasing the number of measurements and so, the number of measurements retained 90 for all the samples. Also, the close-fitting curve was drawn for the EMSE results of each woven sample to simplify tracing the results over the frequency range of 1-10 GHz.

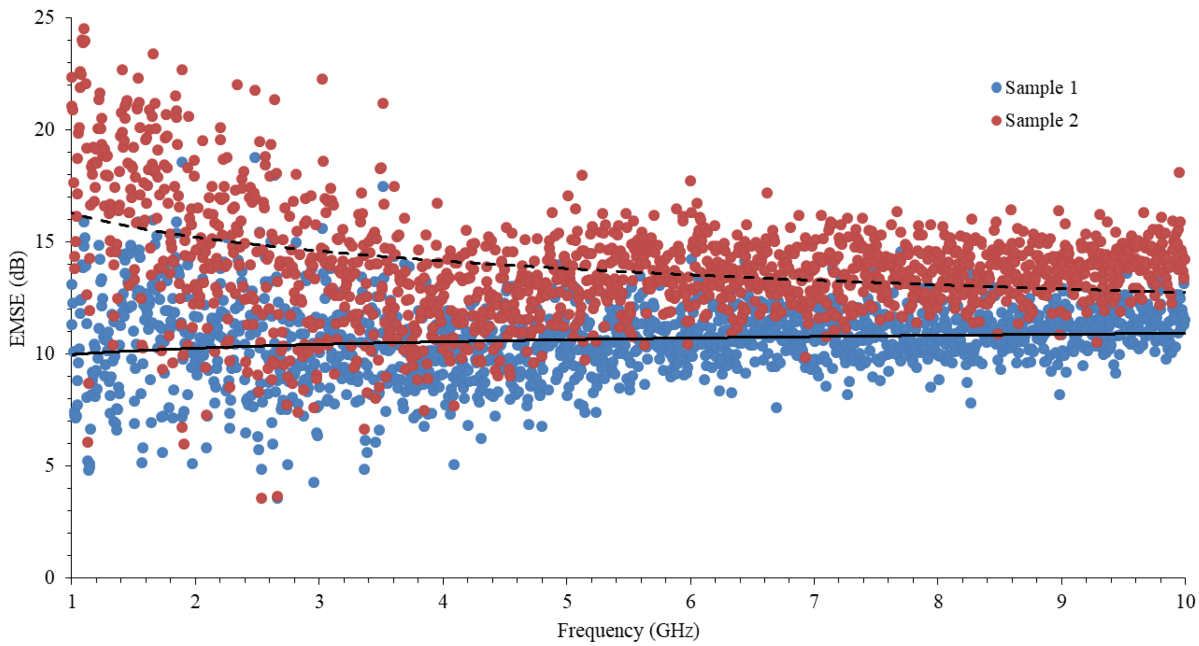

Figure 3-30- The EMSE of Sample 1 and Sample 2 with conductive monofilaments as stuffer wefts in the frequency band of 1-10 GHz [59]

The EMSE of Sample 2 was 16 dB at the frequency of 1 GHz while the EMSE was marginally reduced to 13 dB at the frequency of 10 GHz. The results showed the EMSE value of 15.5 dB for sample 2 in the frequency between 1.8 GHz and 2.4 GHz while the EMSE value of sample 2 was 14 dB at the frequency of 5.8 GHz. It is noted that the frequency of 1.8 GHz corresponds to the frequency for mobile applications and 2.4 GHz and 5.8 GHz correspond to the ISM bands in Europe [214]. Moreover, the average value of the EMSE of Sample 1 was greater than 10 dB in the frequency range of 1-10 GHz.

Comparing the EMSE results of Sample 1 and Sample 2, Sample 2 with PA-MWCNT2.5-KB*5 monofilament as conductive stuffer weft showed higher EMSE in comparison with sample 1 with PA-MWCNT2.5-CB5 monofilament as conductive stuffer weft. The EMSE difference between Sample 2 and Sample 1 was correlated to the tenfold bigger electrical conductivity of PA-MWCNT2.5-KB*5 compared to the electrical conductivity of PA-MWCNT2.5-CB5.

Furthermore, it was suggested that these two compact woven samples using the selected monofilaments were suitable for personal protection clothing against existing radiation in the human living environments based on the EMSE grades for general use as given in Table 3-7.

3.7.2.2 The EMSE results of Sample 3

The EMSE results of Sample 1 and Sample 3 are presented in Figure 3-31 for the frequency band of 1-10 GHz measured in the mode-stirred chamber with the intention of comparing the EMSE results of two samples weaved with PA-MWCNT2.5-CB5 as conductive wefts.

As shown in Figure 3-31, the EMSE of Sample 3 was higher than the EMSE of Sample1 in the frequency range of 1-10 GHz although the same conductive monofilament (PA-MWCNT2.5-CB5) was employed to weave both Sample 1 and Sample 3.

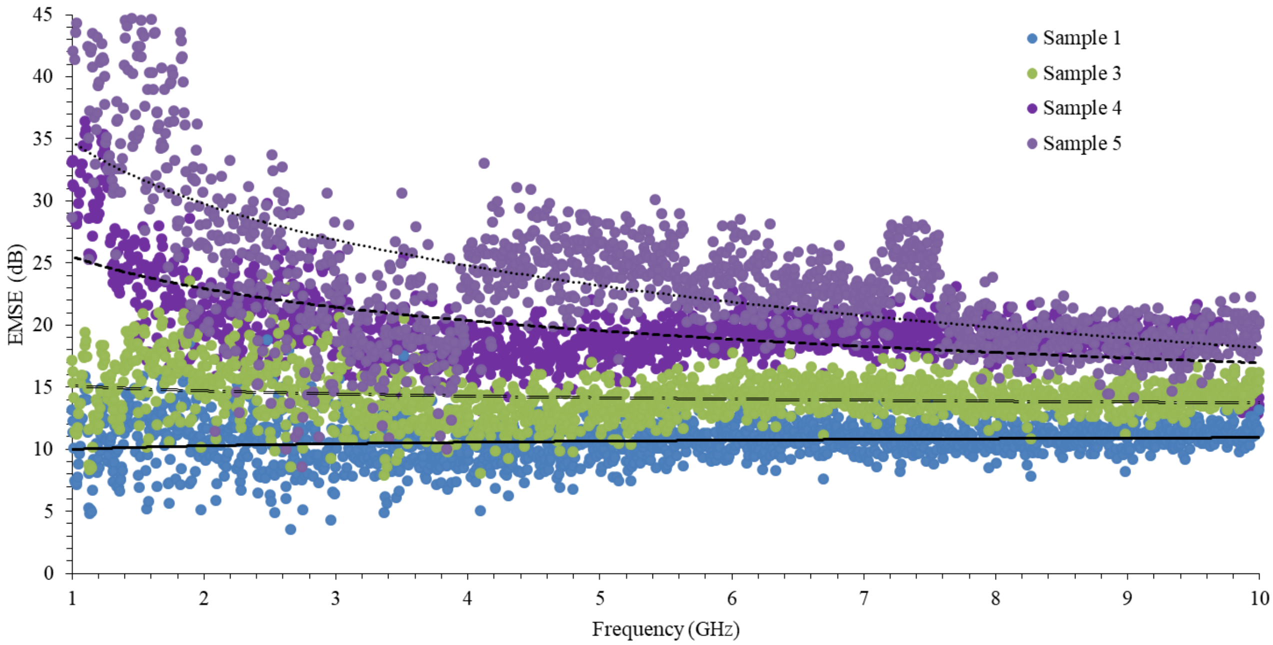

Figure 3-31- The EMSE of Sample 1, Sample 3, Sample 4, and Sample 5 in the frequency band of 1-10 GHz

Sample 3 was weaved using a simple 2D weave structure in order to ensure the continuity between the conductive monofilaments in the woven structure. Also, the conductive monofilament yarns density was increased in Sample 3 (5 yarns/cm) in comparison with Sample 1 (4 yarns/density) thanks to employing a simple woven structure for Sample 3.

Consequently, the EMSE of Sample 3 was nearly 15 dB in the frequency band of 1-10 GHz while the EMSE of Sample 1 weaved with the same conductive monofilament was around 11 dB. In other words, the EMSE of Sample 3 was approximately 40% higher than the EMSE of Sample 1 by only changing the weave structure which led to greater yarn density of the conductive monofilaments together with added contact points between the conductive yarns.

Also, the EMSE results of Sample 2 and Sample 3 were closely comparable. Thus, it was suggested that the EMSE of Sample 3 was improved by changing the weave structure using a more approachable monofilament for melt mixing method (PA-MWCNT2.5-CB5) as opposed to using a monofilament with higher conductivity and lower MFI value (PA-MWCNT2.5-KB*5).

3.7.2.3 The EMSE results of Sample 4 and Sample 5

As explained in section 3.5.3, Sample 4 was manufactured using silver multifilament coated with PA6,6 as stuffer wefts using the compound woven structure given in Figure 3-20. Also, Sample 5 was produced using both silver multifilament coated with PA6,6 and PA-MWCNT2.5-CB5 as stuffer wefts where these two conductive yarns were inserted next to each other in the compact two-ply woven fabric structure.

In other words, Sample 4 was produced with silver multifilament yarns where the metal was protected from potential oxidation and skin touch with the wearer using PA6,6 on the outer sheath of the yarn. Also, Sample 5 was produced with two different conductive yarns having metal and CPC monofilament as conductive components in order to study the effects of the synergy between metal and developed conductive monofilament yarns with MWCNT and CB on the EMSE.

Hence, the EMSE of Sample 4 and Sample 5 were evaluated in the mode-stirred chamber at the frequency range of 1-10 GHz. The results showed that the EMSE of Sample 4 was in the range of (17-25 dB) while the EMSE of Sample 5 was between 19 and 35 dB as displayed in Figure 3-31.

The EMSE results of Sample 5 revealed that using both conductive yarns in one direction as conductive wefts led to higher EMSE level in comparison with the EMSE of Sample 4 with only metal monofilament coated with PA6,6 in its structure (35 dB vs 25 dB). The reason was correlated to the higher quantity of the conductive materials of Sample 5 compared to Sample 4.

In other words, supplementary PA-MWCNT2.5–CB5 monofilaments in Sample 5 (4 yarns/cm) compared to Sample 4 led to 10 dB greater attenuation of Sample 5 where the EMSE difference of Sample 4 and Sample 5 was comparable to the EMSE of Sample 1 with PA-MWCNT2.5–CB5 (Figure 3-31).

In few words, adding another conductive yarn (PA-MWCNT2.5–CB5) to the woven structure played a significant role in increasing the EMSE of Sample 5 while the fabric structure was kept the same for Sample 4 and Sample 5. Also, it should be noted that both Sample 4 and Sample 5 were protective enough to be applied for EMSE applications for personal protection against radiation.

3.7.2.4 The EMSE results of cotton fabrics with the conductive printed layers

As specified in section 3.6, PA-MWCNT2.5-CB5 monofilament was used as the conductive material to be printed on the surface of cotton woven fabric with four different structures (three grid structures and one solid structure) given in Figure 3-26.

The EMSE of the cotton woven fabric with printed layers of PA-MWCNT2.5-CB5 on its surface was measured in the mode-stirred chamber at the frequency range of 1-10 GHz. The EMSE results showed that printing the PA-MWCNT2.5-CB5 monofilament as the conductive component on the surface of the cotton fabric did not lead to shielding behavior of the cotton fabric. In addition, no EMSE upward was perceived for the printed fabrics with PA-MWCNT2.5-CB5 although the thickness of the conductive layer was increased from 0.1 mm to 0.5 mm.

The reason can be correlated to the dilution of the conductive monofilament during 3D printing on the surface of fabrics which leads to a reduction in the electrical conductivity of the printed layer. This phenomenon was firstly identified in former studies [180]. It has been said that the electrical conductivity decreased because of the changes in the pathways of the conductive network (nanofiller network) during 3D printing process as a result of the diameter difference of the loaded monofilament and the extruded monofilaments from the 3D printer.

Also, the measured electrical conductivity of the printed layers in Chapter 3 was relatively low (1×10^{-4} S/m) which confirmed the results of the former studies. Moreover, as discussed earlier, a level of electrical conductivity is required to enhance the EMSE properties in the textile fabrics using conductive nanocomposites CPCs.

In brief, it was suggested that the 3D printing of the developed conductive monofilament with MWCNT and CB was impracticable for the EMSE enhancement of the fabric for personal protection.

3.8 Summary

This chapter ensured two objectives; the first purpose was to enhance the electrical conductivity in a polymer matrix by the inclusion of carbon conductive nanofillers by melt mixing method and the second purpose was to make a shielding fabric using the developed polymer-based conductive nanocomposite to decline the drawbacks of the traditional electromagnetic shielding textile products.

First, a mix of multiwall carbon nanotube and carbon black were added to the polymer matrix in order to study the synergy effects of carbon nanofillers on the electrical conductivity. The electrical conductivity was increased thanks to the synergism of carbon nanofillers while the difficulties caused by high viscosity were weakened. Accordingly, 1.7 wt.% of MWCNT and 3.3 wt.% of CB (1MWCNT:2CB) were used to make a PA6,6-based nanocomposite at electrical percolation threshold. It should be noted that the electrical conductivity of the nanocomposites with 1.7 wt.% of MWCNT and 3.3 wt.% of CB was higher than the PA6,6-based nanocomposite having 20 wt.% of CB and the same as the nanocomposite with 3 wt.% of MWCNT.

In brief, the synergy effects between multiwall carbon nanotube and carbon black had a positive influence on conductive network development in the nanocomposite which resulted in improved electrical conductivity as well as acceptable viscosity for extrusion. Also, it should be noted that the developed polymer-based monofilament was lightweight, corrosion-resistant and the manufacturing process was very well established and these characteristics made it a suitable candidate for EMSE clothing with the aim of personal protection.

In the second phase, the nominated conductive monofilaments ((PA-MWCNT2.5–CB5 and PA-MWCNT2.5–KB*5) were applied in the weaving process so as to manufacture shield fabrics for wearable personal protection. The results showed that the EMSE of the woven samples (Sample 1 and Sample 2) using the conductive monofilaments as stuffer wefts in the middle of the structure was promising (EMSE≥10 dB).

Furthermore, Sample 3 was weaved using PA-MWCNT2.5-CB5 monofilaments in a simple woven structure to increase the quantity of the conductive component in cooperation with ensuring the continuity between the monofilaments compared to Sample 1 and Sample 2. The EMSE of Sample 3 increased compared to Sample 1 weaved with the same conductive monofilament while the EMSE of Sample 2 and Sample 3 were nearly the same. So, it was suggested that the EMSE of the woven fabrics can be improved by changing the weave structure.

Also, Sample 4 was weaved with silver multifilament coated with PA6,6 and Sample 5 was weaved with both silver multifilament coated with PA6,6 and PA-MWCNT2.5–CB5 as stuffer wefts and the higher EMSE of Sample 5 was perceived because of the presence of PA-MWCNT2.5–CB5 monofilaments where the EMSE difference of Sample 4 and Sample 5 was equivalent to the EMSE of Sample 1. It is attributed to the fact that the only difference between Sample 4 and Sample 5 was using PA-MWCNT2.5–CB5 monofilament (with the same quantity applied in Sample 1) in cooperation with core-sheath conductive weft in Sample 5 while Sample 1 was weaved with only PA-MWCNT2.5–CB5 monofilaments as conductive wefts.

It should be mentioned that Sample 1, Sample 2, and Sample 3 weaved using the developed nanocomposite monofilaments were suggested in Chapter 3 for the wearable personal protection devices against the electromagnetic waves (EMSE values of 10-16 dB) existing in the human living environment. Moreover, the two other woven samples (Sample 4 and Sample 5) were developed with the potential of the wearable application where the higher attenuation is required.

Furthermore, no shielding was detected for cotton fabric with 3D printed layers of PA-MWCNT2.5–CB5 in the frequency range of 1-10 GHz despite the fact that the thickness of the printed conductive layer was increased to 0.5 mm. Hence, it was suggested that the 3D printing of the conductive monofilament was not capable for shielding application. However, it is recommended to increase the quantity of the conductive nanofillers in nanocomposites together with improving the structural design and the continuity of the conductive layer in order to enhance the EMSE of textiles using the 3D printing method in the future studies.

In conclusion, the electrical conductivity was enhanced using the synergism between carbon nanofillers where the viscosity was in the standard range for monofilament making process by extrusion. In addition, the EMSE of the woven fabrics made of the developed conductive nanocomposite was promising for personal protective clothing. In Chapter 4, one of the prepared shield fabrics would be considered for comfortable protective pregnancy garment design for personal protection against radiation.

Chapter 4: Virtual mannequin simulation for electromagnetic shielding maternity garment design

This chapter discusses the development of a 3D virtual mannequin for pregnancy period using a parametric graphical method for protective garment design against radiation. First, the body evolution of a pregnant woman was investigated and 3D adaptive mannequin model was made based on weight changes during pregnancy while the developed model was validated by investigating the body changes of another pregnant woman.

In the second phase, a garment block pattern was virtually designed using the developed mannequin. The garment block pattern was designed in a way to have a suitable fit on the virtual adaptive mannequin by allocating darts and seams to the 3D designed pattern. It should be taken into account that the designed garment block pattern is applicable for protective garment manufacturing using the EMSE woven fabric produced in Chapter 3.

4.1 The 3D virtual mannequin design process

Although pregnancy mannequins are mass-produced by different companies, those mannequins are usually incapable to indicate detailed body evolution of pregnant women. In fact, available commercial pregnancy mannequins are unfitting for every individual pregnant woman due to the fact that those mannequins are manufactured using standard sizes. Additionally, the choices of changing the height or abdomen line of the mannequin were integrated by several companies although these possibilities are limited.

To sum up, satisfactory mannequins of pregnant women are not supplied for close-fitting garments design of the pregnancy period. Thus, it is necessary to make an applicable mannequin to design a well-fitted shielding garment for maternity period.

A methodology framework was suggested in this chapter for garment block pattern making for pregnant women with the purpose of resolving the complications of pregnant morphology analysis for garment design. This methodology framework is illustrated in Figure 4-1. As can be seen, the first step was to develop a 3D virtual mannequin for pregnancy length which would be discussed in the following.

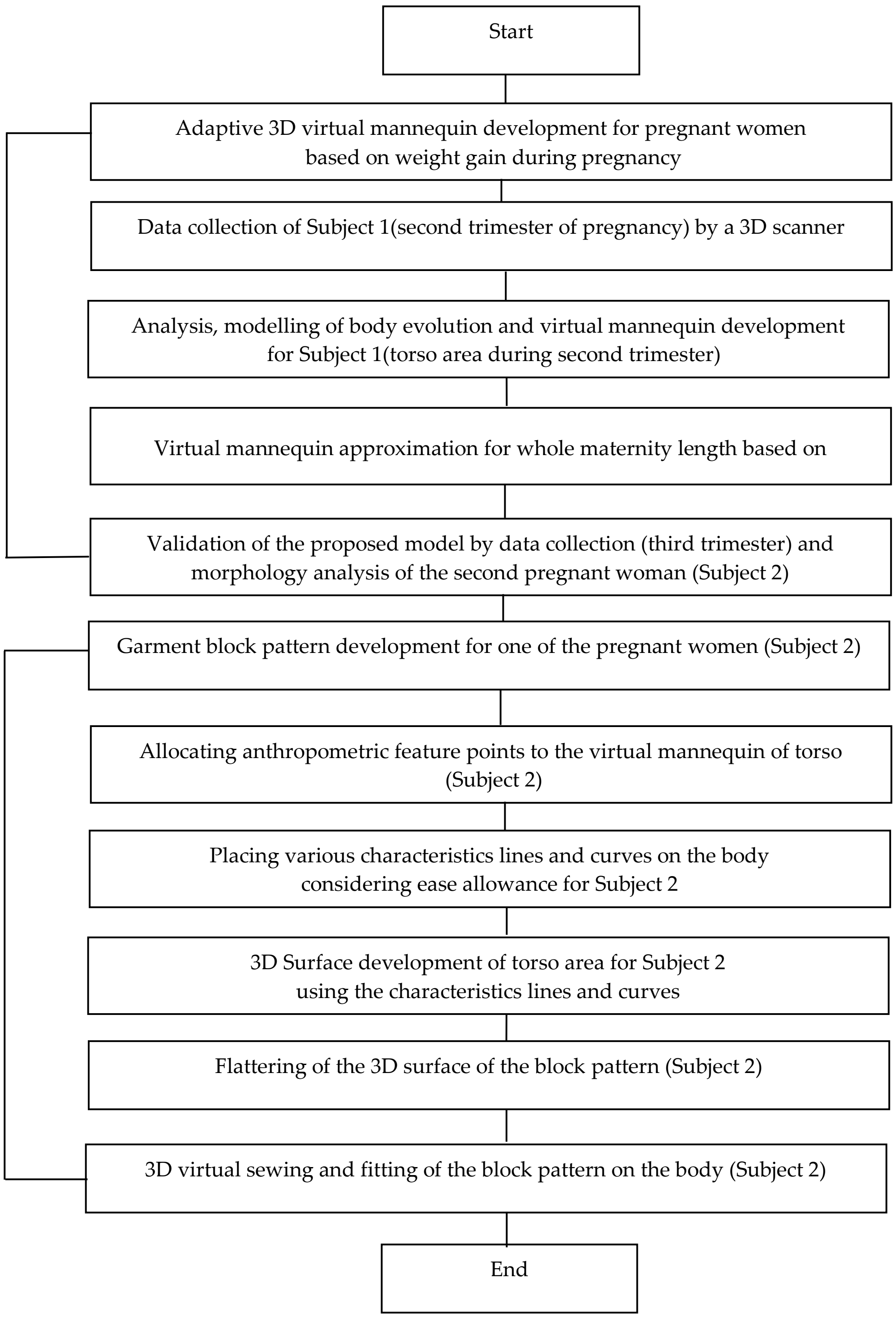

Figure 4-1- The general schemes of garment block pattern design process [224]

4.1.1 Computer-aided design tools

The general scheme of the garment block pattern design process is shown in Figure 4-2. The following software programs were used in this chapter with the intention of 3D virtual garment design for pregnancy period.

- ScanWorX^{TM}: This software has been established by Human Solution and it is used to control and record the data of body scanning. It should be mentioned that the attained body scan data from the 3D scanner is a set of points which is called as a point cloud and simulates the shape of the scanned body.
- Geomagic Design X: This software has been industrialized by INUS Technology in the direction of 3D objects control and edit. The point clouds of the scanned data can be simulated using the meshing tool in the software environment so as to get a smooth surface of the body. In addition, the error holes shaped during scanning can be revised and filled to ensure an unbroken 3D form of the surface.
- Design Concept: This software has been developed by Lectra to facilitate different geometric shapes sketching and representing in a 3D environment where this software provides the options of 3D garment prototyping and flattening corresponding 2D patterns.
- Modaris: This software has been developed by Lectra which is practical for 2D garment patterns making and corrections. Also, the 3D virtual try-on process is provided in this software where the characteristics of the fabrics for the required design can be modeled in the try-on process.

4.1.2 Data collection

Every three sequential months of pregnancy period are termed as a trimester and accordingly, three trimesters of pregnancy period are listed in Table 4-1.

The whole body of the first pregnant woman (Subject 1) was scanned between 16th and 26th weeks of pregnancy length. Hence, the body morphology data of each week was collected and saved during the second trimester of her pregnancy.

It should be noted that the pregnant woman has been scanned using 3D Scan Tecmath supplied by Human Solution while she was dressed in her underwear. She had to stand in a predefined position in the area of the accessibility of the lasers during scanning. After that, the scanner data was transferred to ScanworX^{TM} software supplied by Human Solution while the data was digitized by this software.

Next, the body changes of Subject 1 were studied week by week to analyze the body evolution of Subject 1 throughout the second trimester of her pregnancy. It should be taken into account that morphology analysis was limited to the second trimester due to the fact that Subject 1 has been uniquely available for body scanning between the 16^{th} and 26^{th} weeks of her pregnancy.

In addition, it is noted that the final application of the designed garment was to protect both mother and fetus against the harmful effects of electromagnetic waves and accordingly, this chapter was focused on the morphology study and garment making for torso area of the pregnant women [1], [3], [4].

The attained scanned data had to be transformed in a format so as to make a surface of the pregnant body that was readable by most CAD (computer-aided design) systems. So, the scanned data of Subject 1 was introduced into Geomagic Design X software in order to reconstruct the modified parts at the time of scanning and to smooth the surface of the scanned body.

All the meshes were merged, repositioned and cleaned in Geomagic Design X software. For example, the scanned body of the 24^{th} week of pregnancy is displayed before and after mesh modifications in the Geomagic Design X environment in Figure 4-3 (a and b). The reformed surfaces were transferred into Design Concept to be applied for morphology investigation.

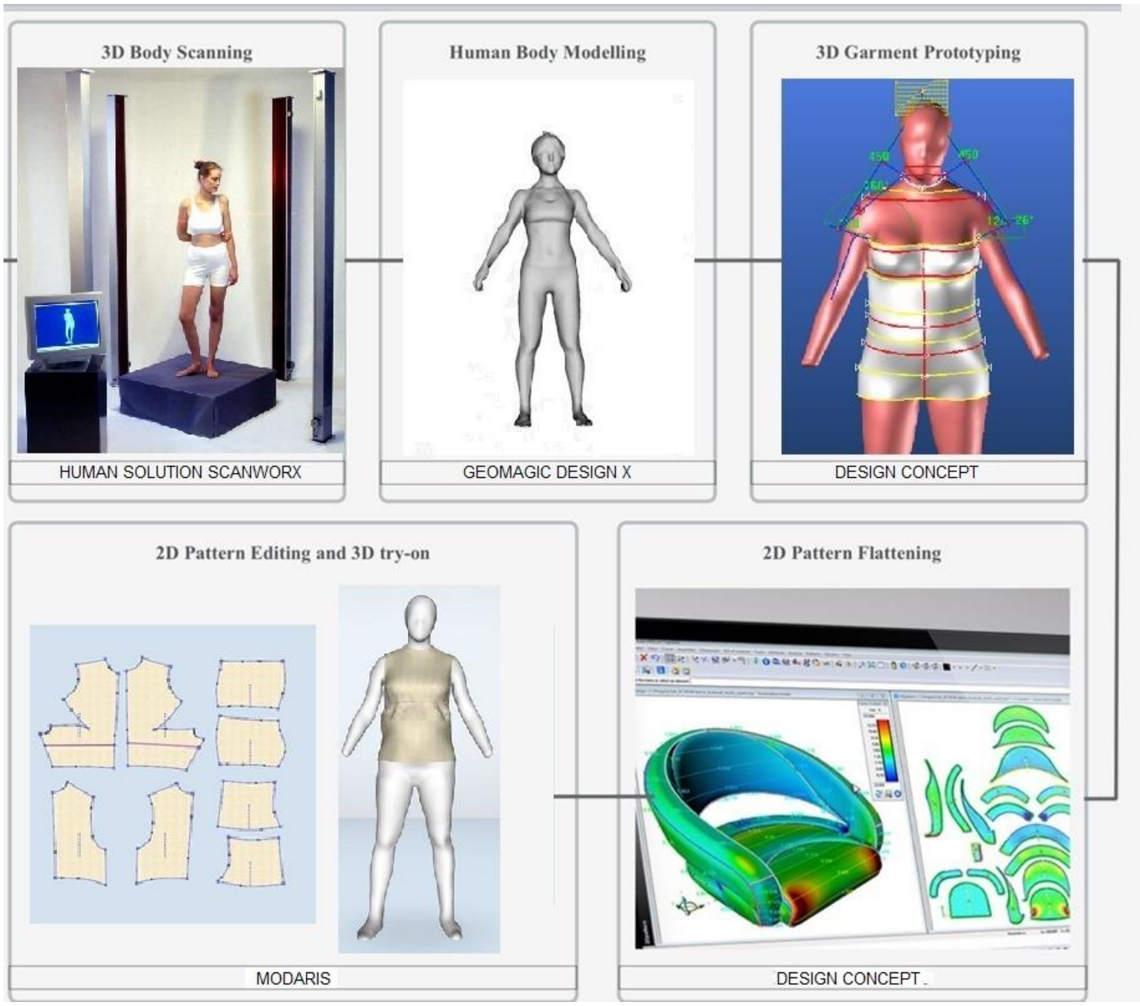

Figure 4-2- The CAD pieces of software

Table 4-1- Pregnancy trimester chart [224]

Trimester	Month	Week
1	1	1-4
	2	5-8
	3	9-13
2	4	14-17
	5	18-21
	6	22-26
3	7	27-30
	8	31-35
	9	36-40

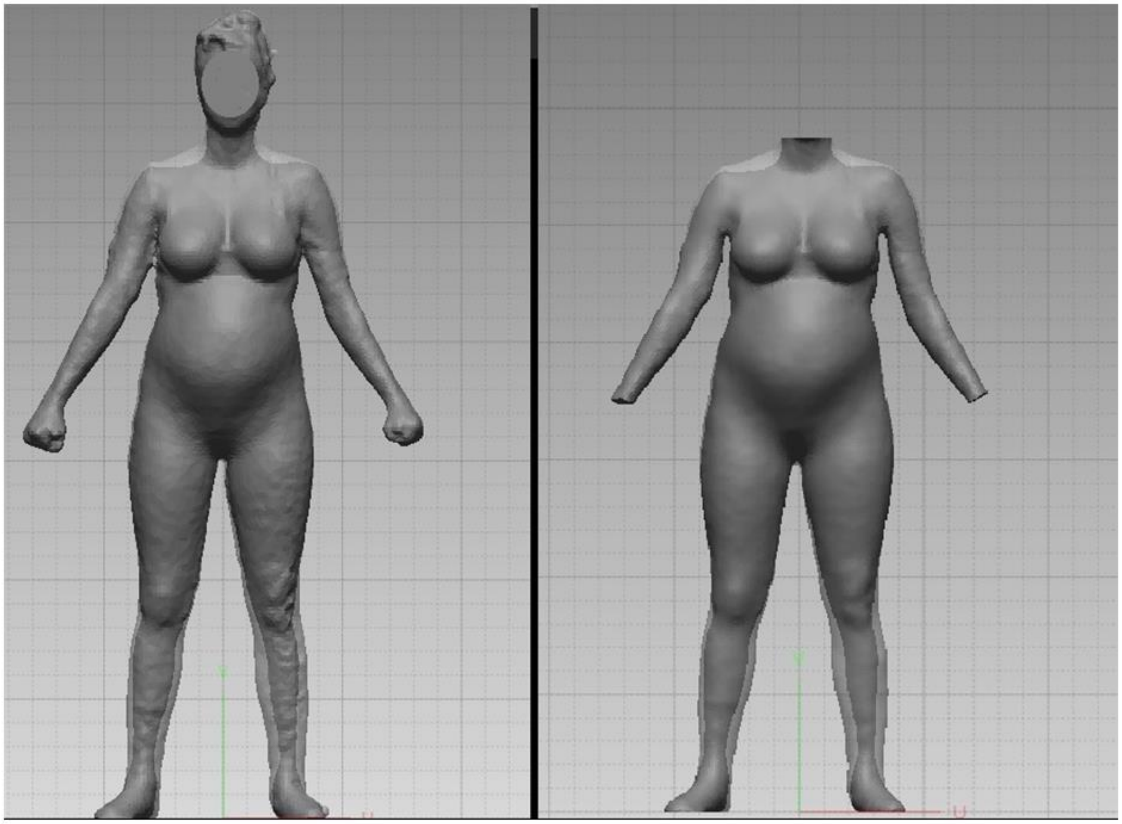

(a) (b)

Figure 4-3- The scanned body of Subject 1 (a) Before and (b) After improvement of meshes in Geomagic Design X

4.1.3 Investigation of body evolution

All body surfaces of Subject 1 were introduced into the 3D Design Concept software environment for body examination. For this purpose, the body surfaces of all the weeks between the 16th and 26th weeks of pregnancy were individually imported into the Design Concept environment and the surfaces were cleaned.

Next, the bodies were placed at a joint reference point to facilitate the body evolution investigation. It should be noted that all the shapes have to be in a joint reference position to acquire a precise visualization of body evolution. The scanned body of the 16th week of pregnancy was considered as the reference body. Consequently, the legs of all the weeks were located in the same position of the reference body. The primary and the adjusted positions of another scanned body (e.g. 20th week) on the reference body (16th week) are shown in Figure 4-4(a and b). As can be seen in Figure 4-4(b), the position of legs was correct for the second scanned body.

On the other hand, the position of the spine line for the body of the 20th week was incorrect (Figure 4-4(c and d)). This was correlated to the fact that the posture of the pregnant woman was changed for each scan in comparison to the previous and the next ones. Consequently, positions of the spine lines were corrected for all weeks according to the reference body in an attempt to have the same spine position for all the bodies.

(a) (b) (c) (d)

Figure 4-4- (a) The initial position of the pregnant body of 16th (magenta colour) and 20th (silver colour) weeks of pregnancy, (b) The body position based on the appropriate position of the legs, (c) and (d) The position of spine lines (Subject 1) [224]

Then, each scanned body was equally separated into the left part and right part using the spine line as the reference axis and all the spine lines were extracted to be compared. For this purpose, the positions of spine lines were revised according to the first scanned body (16th week) in order to improve the analysis of body evolution.

All the spine lines were repositioned in view of the pivot point on the crotch curve and the positions of under bust, belly and waist points. The positions of spine lines are illustrated in Figure 4-5 (a and b) before and after adjustment while the body evolution was clearly visible after adjustment.

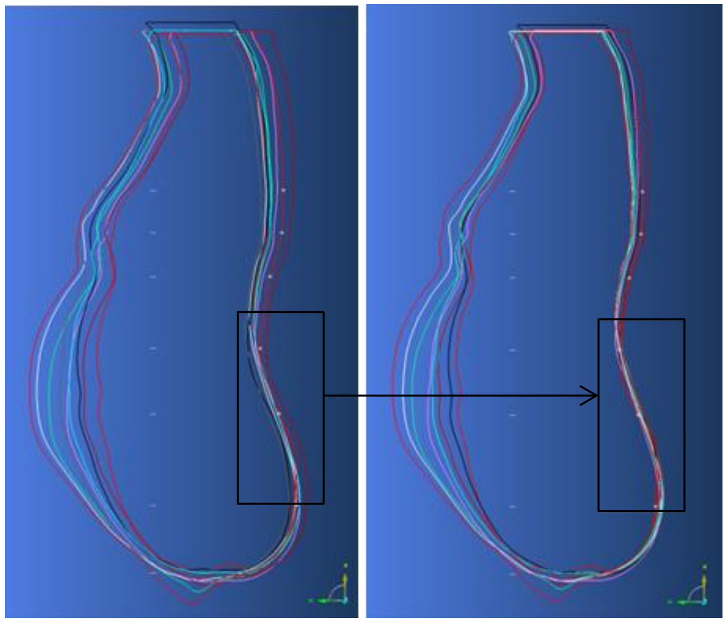

(a) (b)

Figure 4-5- All the spine lines (a) Before and (b) After spines corrections (Subject 1) [224]

Afterward, the reference subject was cut toward its height direction. The formula to define the position of each cross-section is indicated in Table 4-2. Henceforth, the scanned body of each week was cut according to its particular spine line for the weeks between 16th and 20th weeks.

As specified earlier, the morphology study was completed for torso area of the pregnant women for the reason that the final application of the designed garment was to protect both mother and fetus against the harmful effects of electromagnetic waves.

Table 4-2- Cutting parameters [224]

Parameter	Formula
Height	H
Armpit	0.751×H
Breast	0.7186×H
Underbust	0.685×H
Waist	0.63×H
Belly	0.58×H
Hip	0.51×H
Crotch	0.458×H

The cutting curves for all weeks of the second trimester were pulled out to examine the body evolution from 16th to 26th weeks of pregnancy. In addition, the sketched curves were required for outlining the image of clothing which would be discussed later in this chapter. The perspective view of all the extracted curves is shown in Figure 4-6.

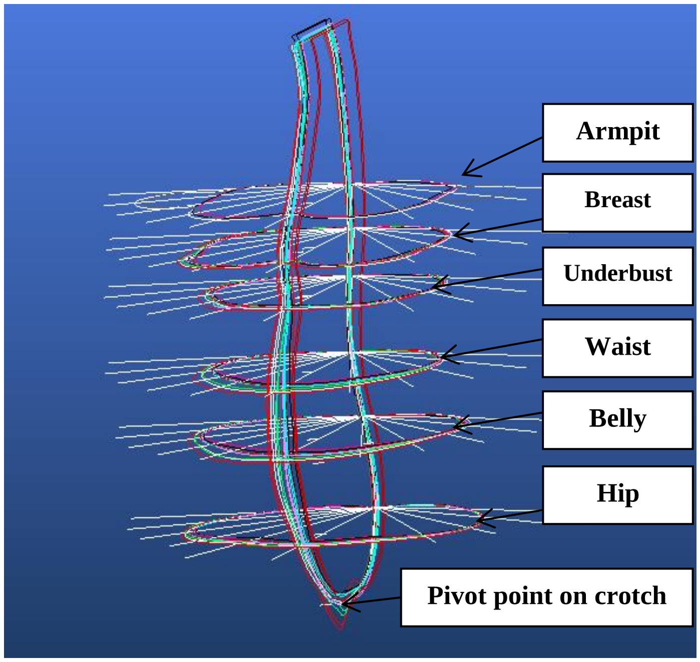

Figure 4-6- Cross-section curves for the 16th–26th weeks of pregnancy (Subject 1) [224]

The linear growth of different points at different angles with constant intervals (15◦) on the curves was measured to have a comprehensive visualization of body evolution. For example, the curves of different weeks and angular lines for waist and belly are shown in Figure 4-7. In point of fact, the growth of all the curves was measured at different angles considering the spine point on the cross-section curve as the reference point. The objective was to precisely outline the evolution of the body during the pregnancy period. The lengths of angular lines for waist between the 16th and 26th weeks of pregnancy are represented in Figure 4-8.

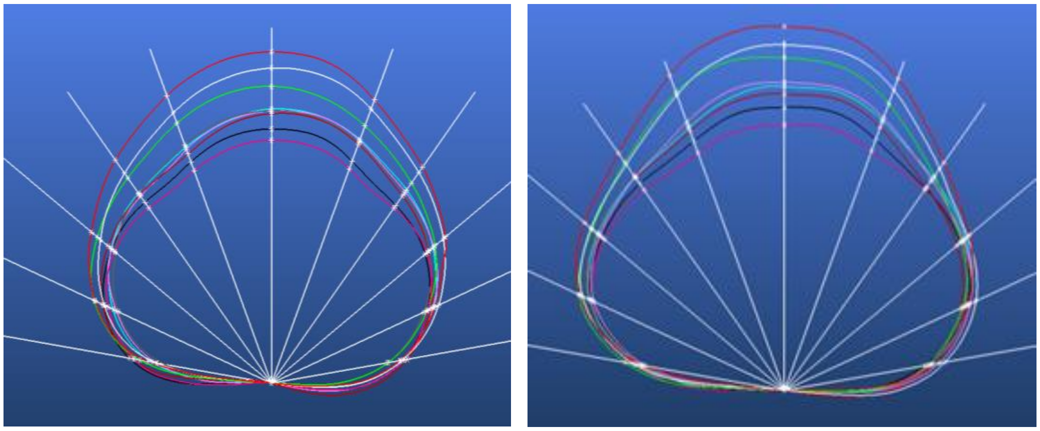

(a) (b)

Figure 4-7- Cross-section curves and angular lines with 15◦ intervals for (a) Waist and (b) Belly of Subject 1

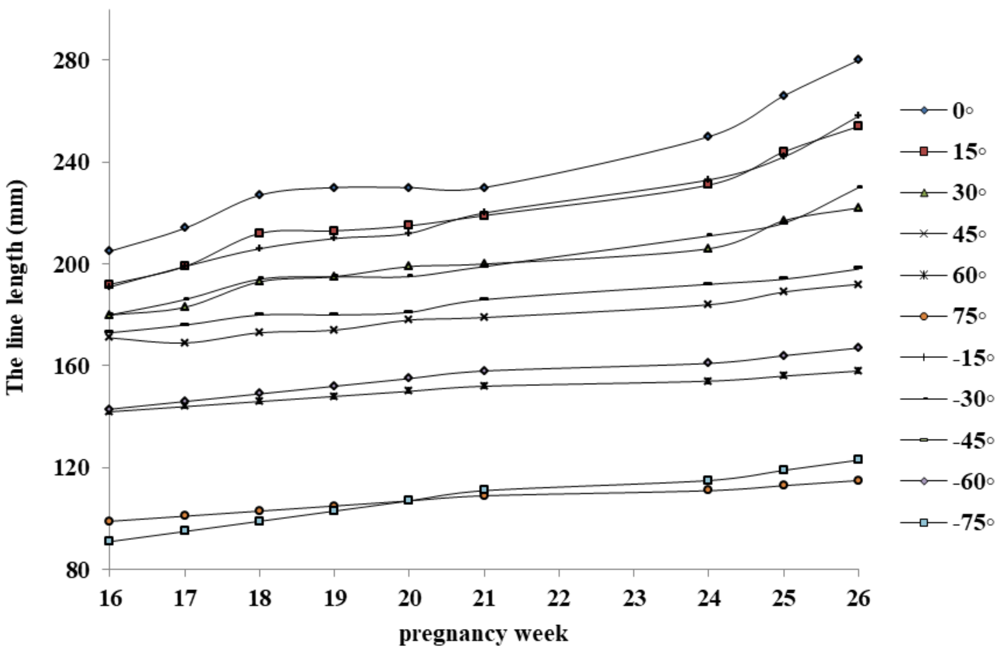

Figure 4-8- Waist linear changes between 16th and 26th weeks at different angles for Subject 1

Moreover, the circumference growth of different cross-sections in torso area of Subject 1 between the 16th and 26th weeks of pregnancy is revealed in Figure 4-9. The growth of all the curves was nearly linear while the rising amounts for belly and waist were the highest among all the cross-section curves (28% growth of waist and 18% growth of belly circumferences between 16th and 26th weeks).

The lengths of angular lines for all the cross-sections in torso were prepared into an Excel file and the total increase (16th-26th weeks) was calculated for all the curves. The sorted data in the Exel file was used to develop an adaptive surface of torso using a linear model of line lengths from

16th to 26th weeks of pregnancy period. In point of fact, a linear model was used to estimate the increase of the lengths of the angular lines since the circumferences of each contour (cross-section) tended to follow a linear growth over the second period of pregnancy.

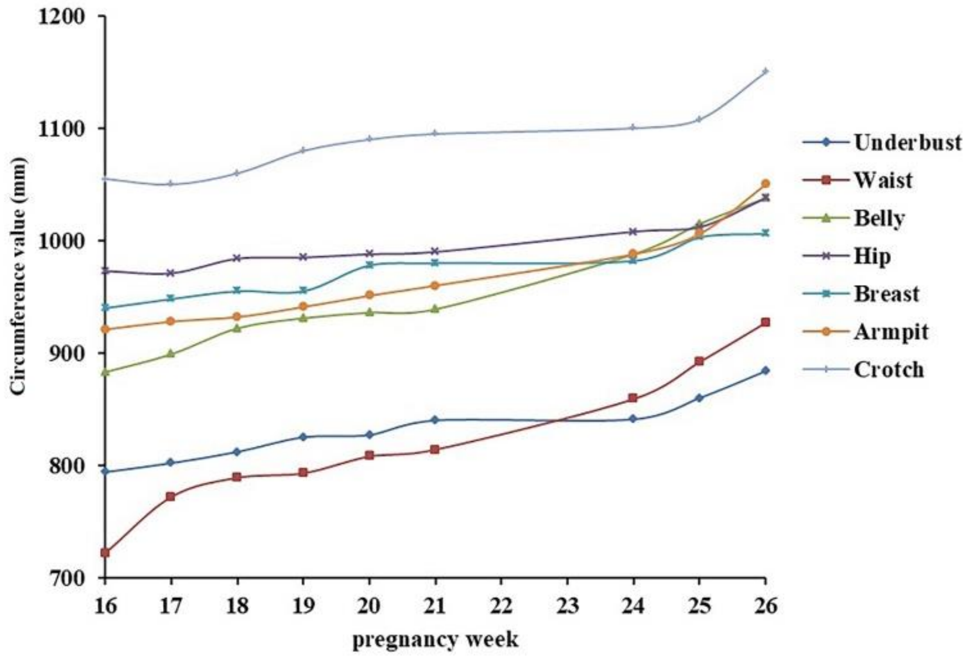

Figure 4-9- Circumference growth of different cross-sections in torso for the first pregnant woman (Subject 1) between the 16th and 26th weeks of pregnancy [224]

On the other hand, a different approach was employed to analyze changes in the crotch cross-section. For this purpose, the left leg curve (crotch) of Subject 1 was reconstructed for the 16th week of pregnancy in order to resolve the holes initiated during the body scanning process.

The barycentre point of the left leg was defined in the Design Concept software environment and it was considered as the local axis coordinate for the left leg. The primary cross-sections of the crotch are represented in Figure 4-10(a) and the barycentre point of the left leg (16th week) in crotch is shown in Figure 4-10(b). Then, the leg was duplicated regarding the spine line as the reference axis to generate identical curves for both the left and right legs. Finally, the adaptive crotch curve for Subject 1 was sketched as given in Figure 4-10(c).

At this point, all the data was exported from the Excel file to the Design Concept environment to make an adaptive mannequin for torso area of Subject 1. The completed adaptive surfaces for the 16th and 26th weeks of pregnancy are demonstrated in Figure 4-11(a and b).

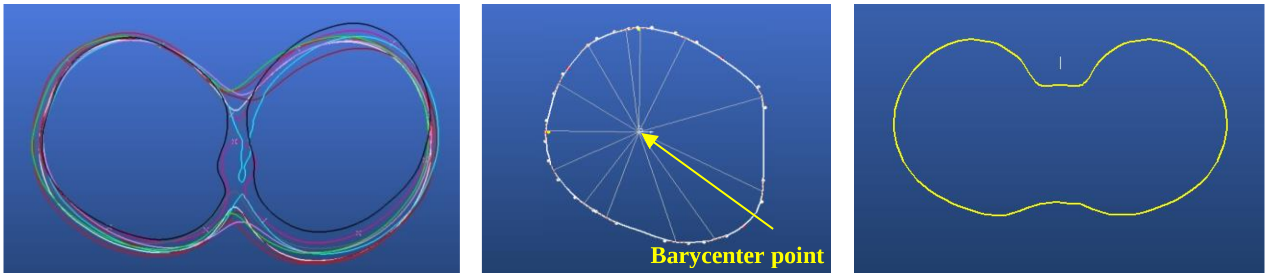

(a) Primary cross-sections (b) Reconstructed left leg (16^{th} week) (c) Adaptive cross-section curve

Figure 4-10- The process of adaptive crotch reconstruction for Subject 1

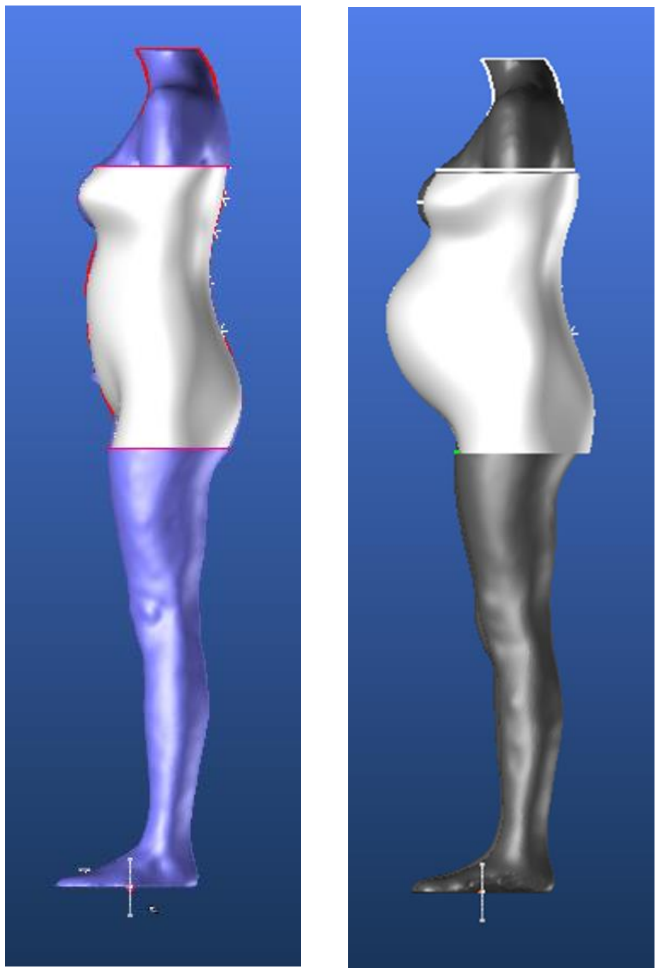

(a) (b)

Figure 4-11- Surface mannequin modeling for (a)16^{th} and (b) 26^{th} weeks of pregnancy for Subject1

4.1.4 **Virtual mannequin estimation based on weight gain**

The virtual mannequin was developed and verified by real data of the scanned body (Subject 1) in section 4.1.3 for the pregnancy weeks of 16-26 while the ultimate purpose of the present study was to develop a virtual mannequin for the whole period of maternity to facilitate garment design for pregnant women.

Therefore, in the following, two techniques were proposed for virtual mannequin development for the whole pregnancy period based on weight gain during pregnancy and the available scanned data.

- Method 1

It was suggested to evolve the virtual mannequin for the weeks before 16th and after 26th weeks of pregnancy based on weight gain during the period of pregnancy. As a result, the trend of weight gain of the pregnant woman (Subject 1) was delineated throughout her pregnancy in order to define the correlation between the trends of weight gain and body evolution.

It should be taken into account that the weight of Subject 1 was 58 kg before pregnancy and 73 kg on her delivery day. Also, as specified earlier, the evident changes of the body happen in torso area during pregnancy. For that reason, relating the weight gain and torso evolution during pregnancy instead of the evolution of the whole-body remains reasonable.

The trend of weight gain during pregnancy has been discussed by a number of studies [201], [202], [225]–[227]. The anticipated weight gain graph of Subject 1 based on the proposed trend in the above-mentioned studies (Method 1) is represented in Figure 4-12.

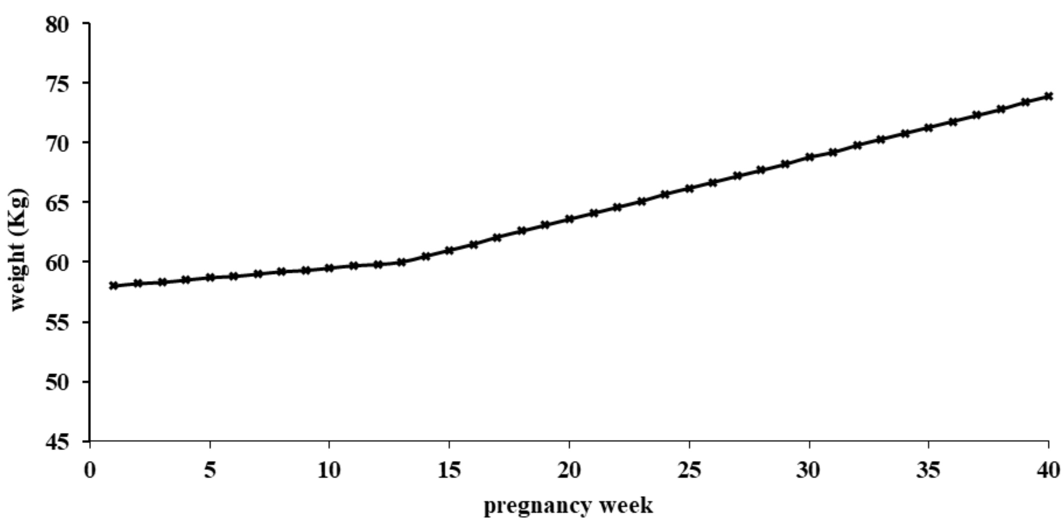

Figure 4-12- The weight gain graph of Subject 1 based on the proposed trend by Method 1 [224]

Subsequently, the changes of each contour were projected based on weight gain during pregnancy and the cross-section curves of torso area in the second trimester. First, the gradients of the weight gain curves were measured for the first, the second, and the third trimesters of pregnancy (Subject 1) and the ratio between these gradients was calculated.

Then, the body evolution of the first and third pregnancy trimester was projected and the surface of torso was generated for the whole maternity period. Figure 4-13(a, b, and c) represents the virtual mannequin for 10th, 20th and 30th weeks of pregnancy formed based on the weight gain profile (Method 1) for Subject 1, respectively.

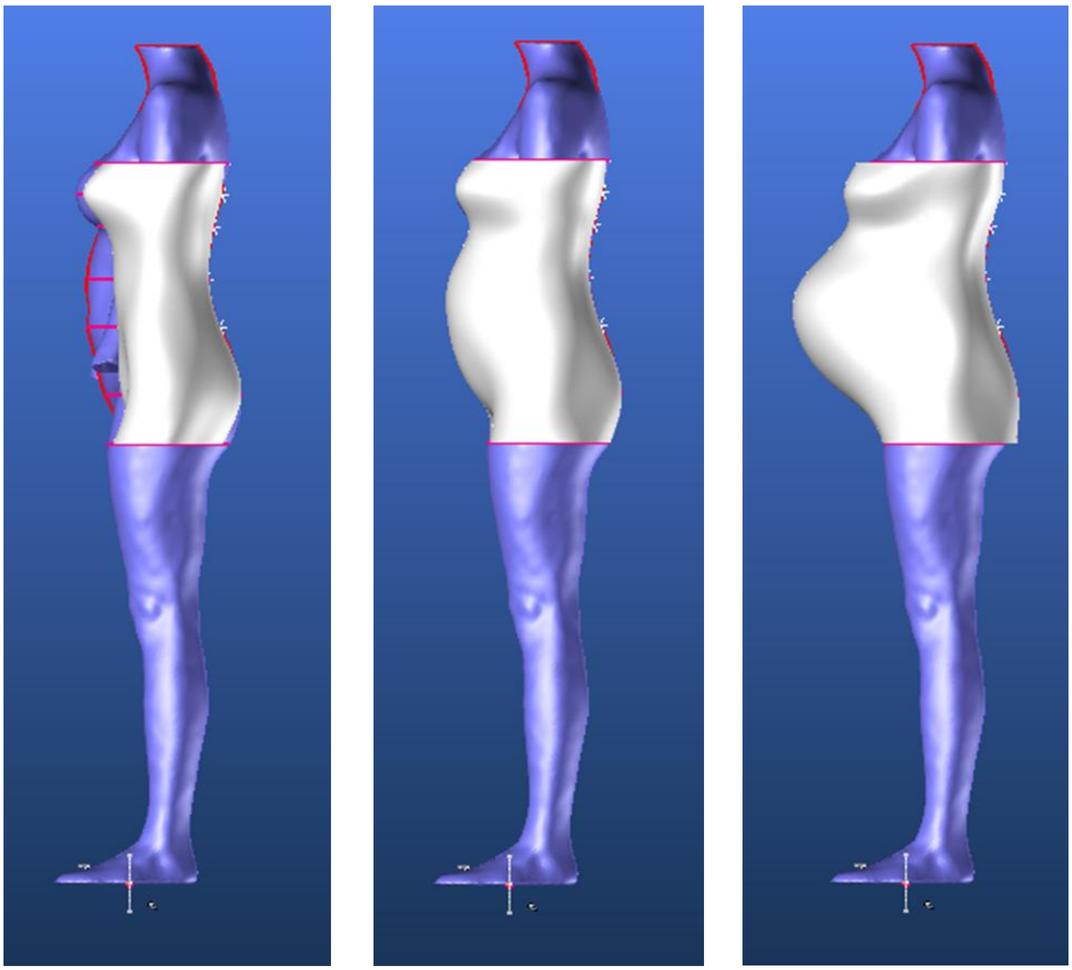

(a) (b) (c)

Figure 4-13- Virtual mannequins of (a) 10th, (b) 20th and (c) 30th weeks of pregnancy based on Method 1 on the reference body of Subject 1

However, the simulated deformation of Subject 1 based on the proposed weight gain by Method 1 was not coherent to the actual changes of the pregnant body (Subject 1) for both the first and the third trimester of pregnancy. In fact, the developed virtual mannequin has not shown the normal profile of torso as displayed in Figure 4-13(a and c).

- Method 2

Another weight gain trend during pregnancy (Method 2) was suggested in this chapter in order to resolve the problems of the developed virtual mannequin associated with the trend proposed by the former method [202], [228]. The weight gain graph based on the proposed weight gain trend by Method 2 for Subject 1 is shown in Figure 4-14(solid line).

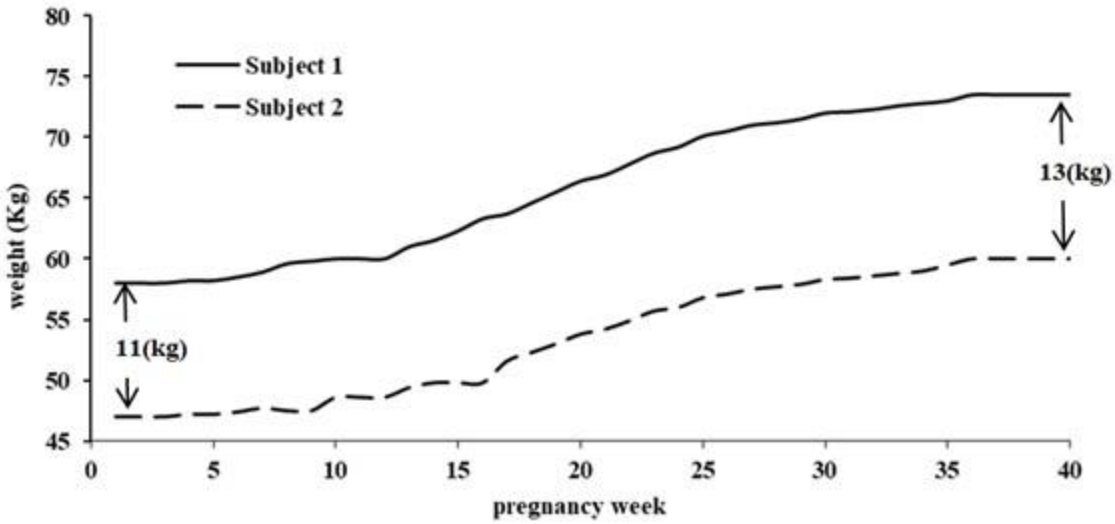

Figure 4-14- The weight gain graph of Subject 1 and Subject 2 based on the proposed trend by Method 2 [224]

Accordingly, the virtual mannequin for the first and third trimesters of Subject 1 was completed based on the weight gain suggested by Method 2 and existing data of the body evolution between the 16th and 26th weeks of pregnancy. It should be also taken into consideration that the weight of Subject 1 was regularly measured during her entire pregnancy in order to have the actual weight gain profile of Subject 1 and the weight gain profile of Subject 1 was nearly in accordance with the proposed weight gain trend by Method 2.

Thus, the virtual mannequin of Subject 1 was made for all the maternity period as shown in Figure 4-15. It shows that the made virtual mannequin of Subject 1 applying the weight gain trend (Method 2) seemed reasonable for the whole maternity length.

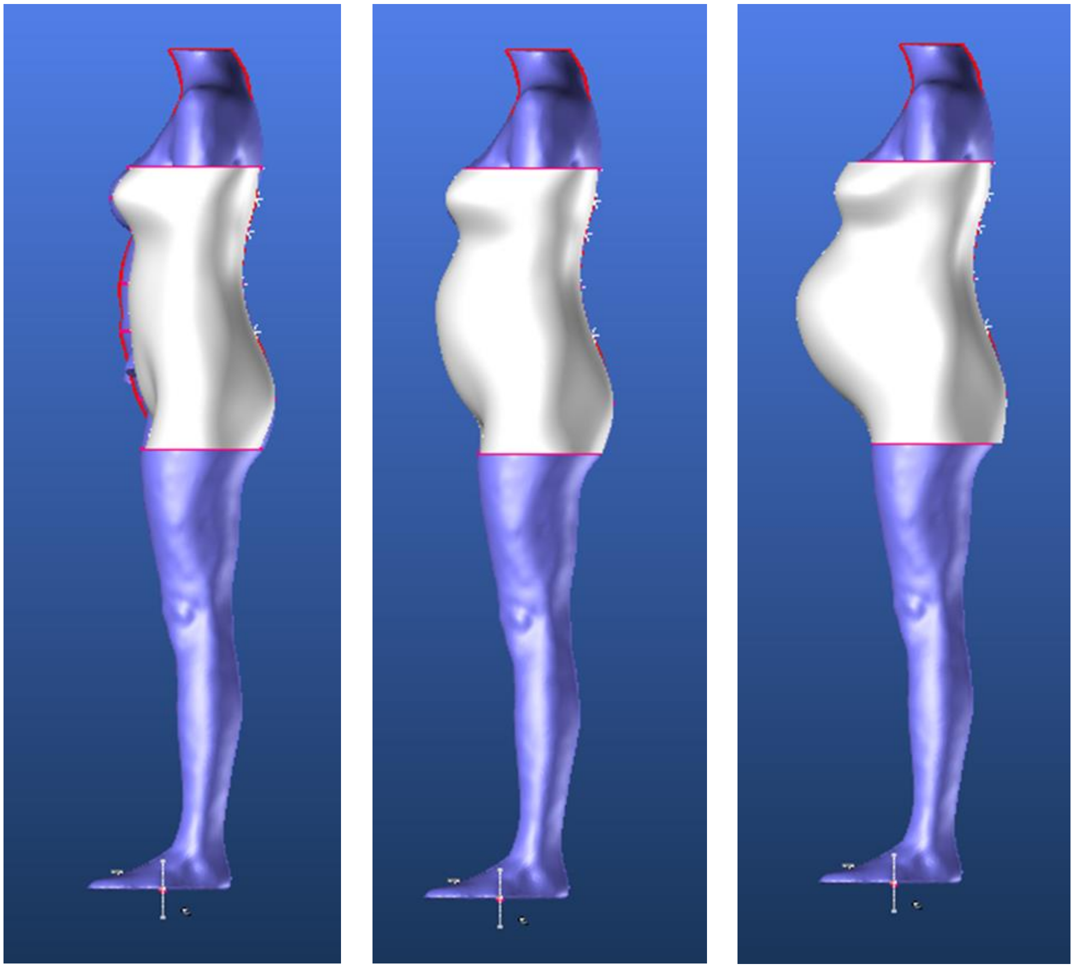

(a) (b) (c)

Figure 4-15- Developed virtual mannequins of (a) 10th, (b) 20th and (c) 30th weeks of pregnancy based on weight gain proposed in Method 2 on the reference body of Subject 1 [224]

4.1.5 Validation of the proposed model

Due to the fact that the trend of weight gain (Method 2) was in agreement with the actual weight profile of Subject 1 during her pregnancy period, Method 2 was applied to estimate the weight gain of Subject 2 during her pregnancy period.

The weight gain graph based on the proposed trend by Method 2 is displayed for Subject 2 in Figure 4-14 (dashed line) where her weight was 47 kg before pregnancy and 60 kg on her delivery day. It should be noted that the actual weight profile of Subject 2 was in good agreement with the projected weight gain graph using the proposed trend by Method 2.

It is also noted that the body scanning data of Subject 2 was only collected for the weeks between the 30th and 35th weeks of pregnancy (the third trimester) since the pregnant woman (Subject 2) was only presented for scanning during this period of time.

Consequently, first of all, the body morphology of the second pregnant woman (Subject 2) was analyzed between the 30th and 35th weeks of pregnancy. For this purpose, the attained data through the body scanner was transformed into Geomagic Design X software to improve the body surface and reconstruct the modified parts during scanning. Then, the surfaces were exported into the 3D Design Concept software environment for morphology analysis.

The positions of all the scanned bodies of Subject 2 were adjusted in respect of the legs and spine lines using the same process described for Subject 1. However, the scanned body of the 30th week of pregnancy was chosen as the reference body for Subject 2.

All the scanned body of Subject 2 (30th-35th weeks of pregnancy) was cut toward the height direction of Subject 2 with the same formula signified in Table 4-2. It should be noted all the bodies were cut according to their individual spine lines. Figure 4-16 shows the perspective view of the cross-section curves of torso area for Subject 2.

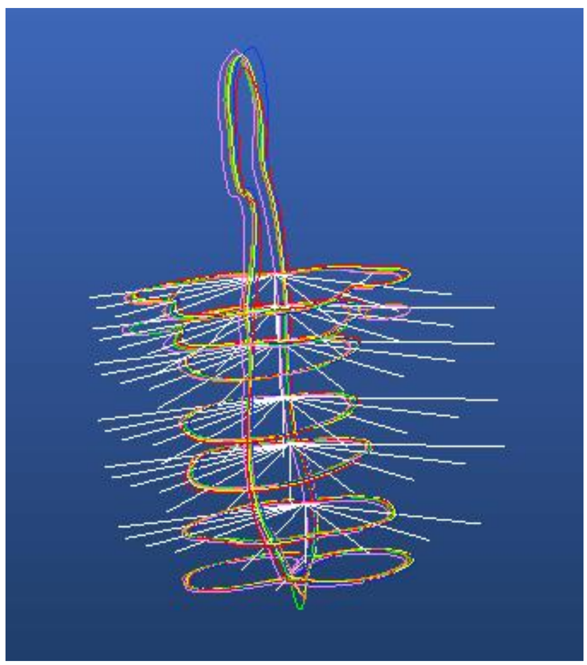

Figure 4-16- Cross-section curves for 30th-35th weeks of pregnancy (Subject 2)

Moreover, the evolution of the circumference of the cross-section was measured at different angles considering the spine line as the reference. The circumference growth of different cross-sections for torso area of Subject 2 is depicted in Figure 4-17 while an increasing can be detected for the curves during this specific span of time. Nonetheless, the increasing rate was lower than the increasing rate of the same cross-section circumference for Subject 1 during her second trimester (8% growth of belly and waist circumferences between 30th and 35th weeks of pregnancy). The rising trend of cross-section circumferences was in good agreement with the trend of weight gain given by Method 2.

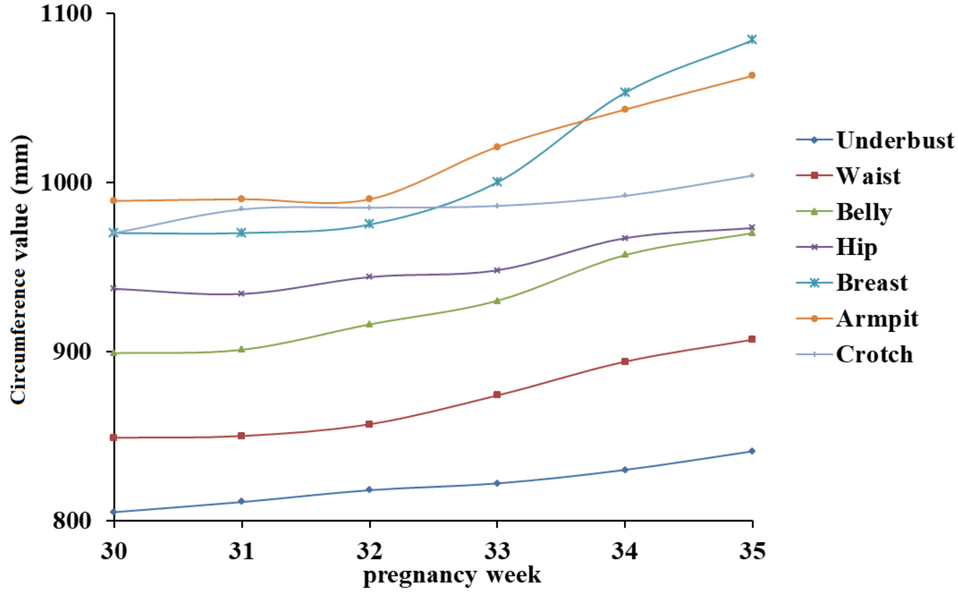

Figure 4-17- Circumference growth of different cross-sections in torso area for Subject 2 between 30th and 35th weeks of pregnancy

Next, an adaptive surface for the whole pregnancy period was created based on the weight gain for the entire pregnancy period (Method 2) and available scanned data of the third trimester. The developed virtual mannequin of Subject 2 is shown in Figure 4-18 that appeared correct to be applied for computer-generated garment design.

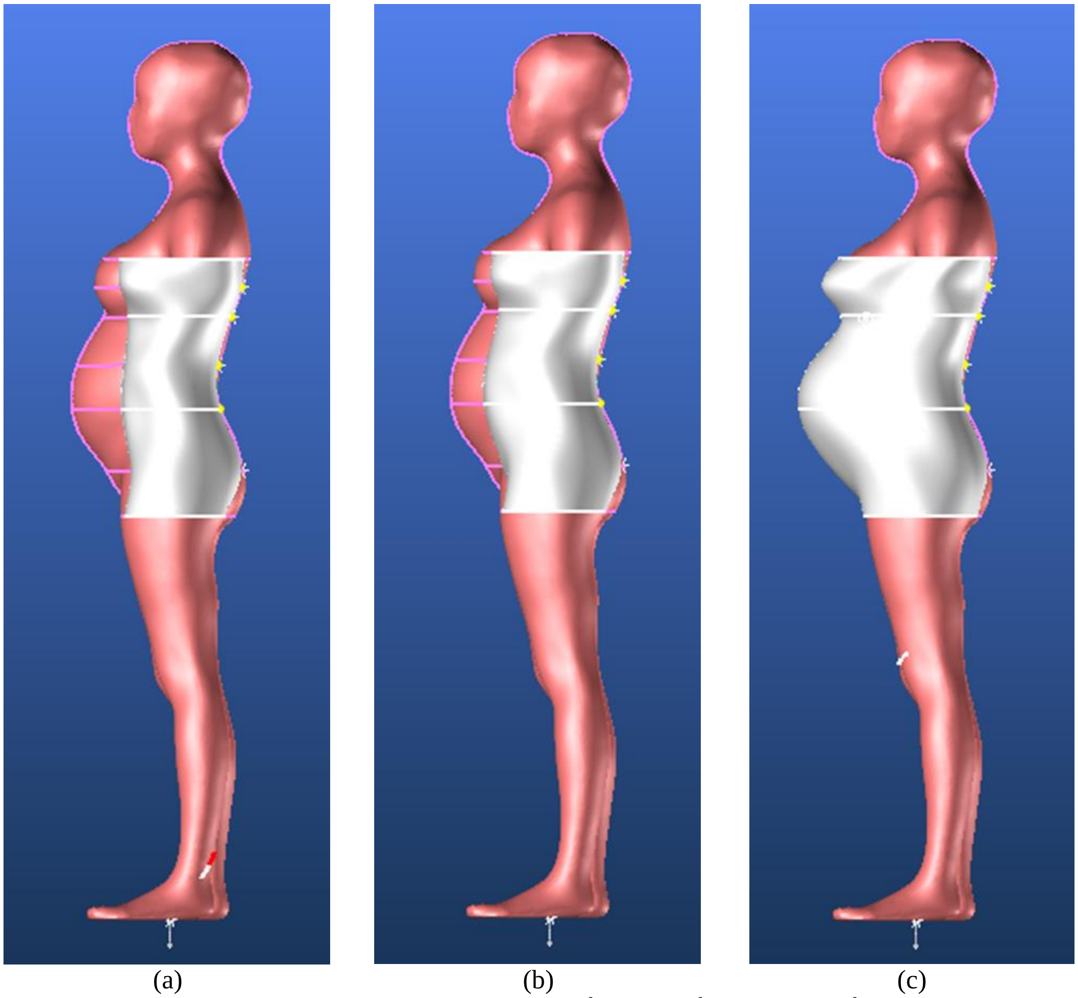

Figure 4-18- Developed virtual mannequin of (a) 10th, (b) 20th and (c) 30th weeks of pregnancy on the reference body (30th weeks) of the second pregnant woman (Subject 2)

4.2 Garment block pattern development

A garment block pattern was suggested using the developed adaptive mannequin for one of the studied pregnant women (Subject 2). Hence, the virtual mannequin completed for torso was merged with non-evolving parts of the scanned body of the 35th weeks of pregnancy of Subject 2 in the Geomagic Design X software environment. It is taken into account that the pregnant women experienced considerable changes around torso during pregnancy although the evolution of the other parts of the body was slight.

Next, the basic anthropometric feature points (e.g. shoulder tips, front neck, and side hip) were determined on the virtual mannequin for Subject 2 using the proposed method by Hamad *et al.* [229]. The anthropometric feature points for Subject 2 are shown in Figure 4-19. It should be noted that defining the anthropometric feature points was essential to identify the boundaries of the pattern for the design of the garment block pattern.

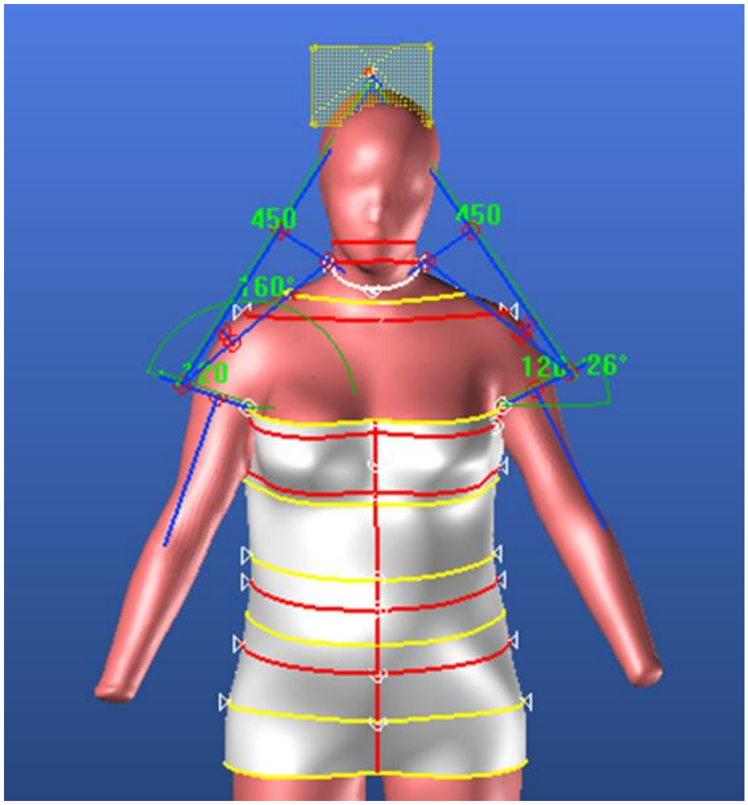

Figure 4-19- The anthropometric feature points [224]

The General principle of the garment block pattern design process established by Efrat [230] is shown in Figure 4-20(a). The 3D shape of the garment block pattern was controlled by feature points of the breast and scapula denoted in Figure 4-20(b).

The triangular surfaces for the front and back of torso were created using the feature points of breast and scapula connected with necklines, shoulder lines, armhole lines, the sidelines of the body and the middle lines of the back and front. Each triangle surface was molded by connecting two adjacent limit points and the corresponding breast points for the front and scapular points for the back of the block pattern (red curves in Figure 4-20(c)). Also, the connection between the tangent curves near the breast Figure 4-20(d) and straight lines distant from the breast determined the volume form of the breast.

Moreover, angular lines (Figure 4-21) were used to develop the correct design curve of armhole. The armhole design curve was made by connecting the extremities points (underarm point, shoulder point, front pitch and back pitch points (denoted in Figure 4-22) close to the body shape.

It should be noted that all the design curves were outlined considering the 3D ease allowance lengths [231], [232].

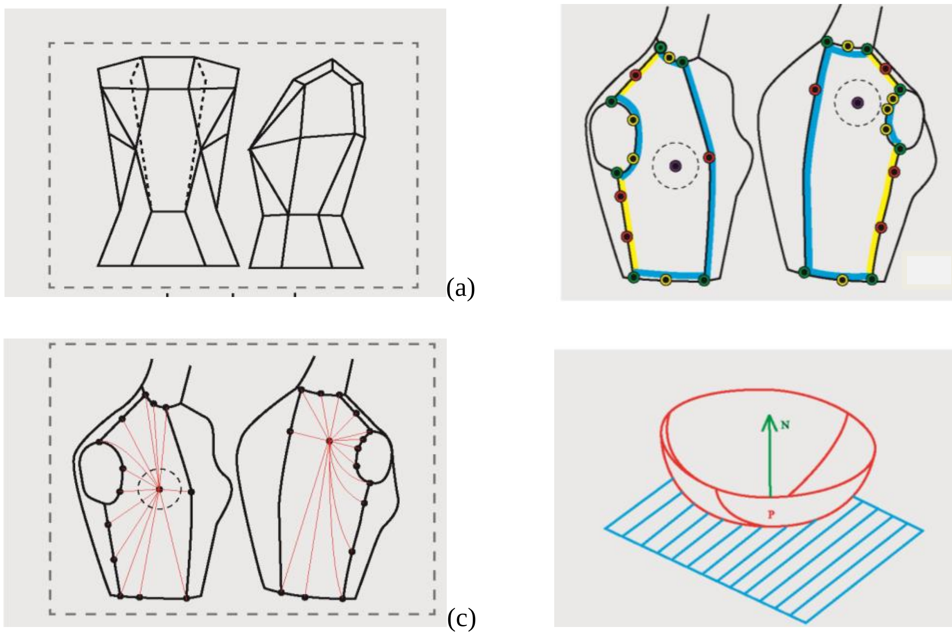

Figure 4-20- (a) General principle of the garment block pattern design, (b) Characterization of shape controlling points for breast and scapular, lines (yellow) and curves (blue) for garment framework defining, (c) Triangular surfaces generation and (d) Outlining the normal line of a curve (red color shows the formed curve, blue color illustrates the tangent and green color shows the normal line to the tangent line [230]

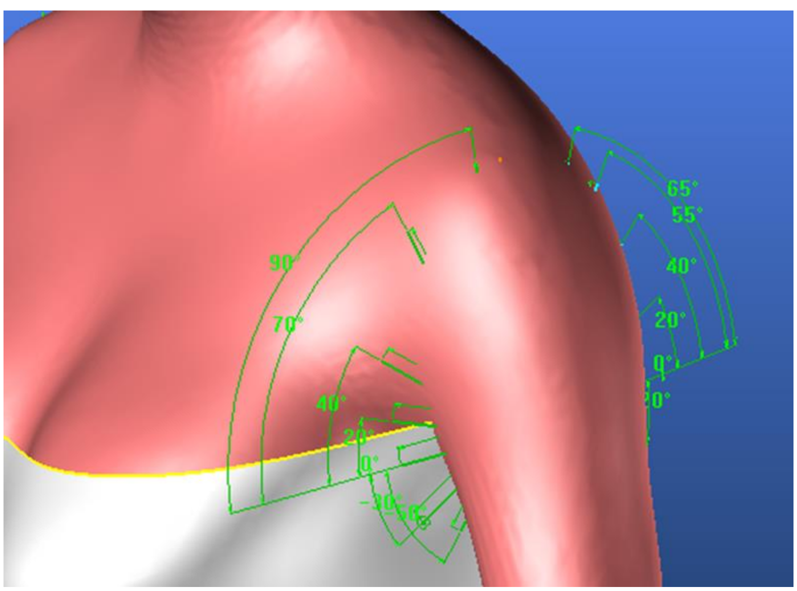

Figure 4-21- The angular lines for armhole design curve development [224]

Finally, 3D graphical model of garment block pattern considering the 3D ease allowances was obtained (pattern outline in Figure 4-22 (orange network)). Also, several surfaces were allocated to the waist, belly, hip, and breast for garment design on the outlines of the 3D graphical model of the garment.

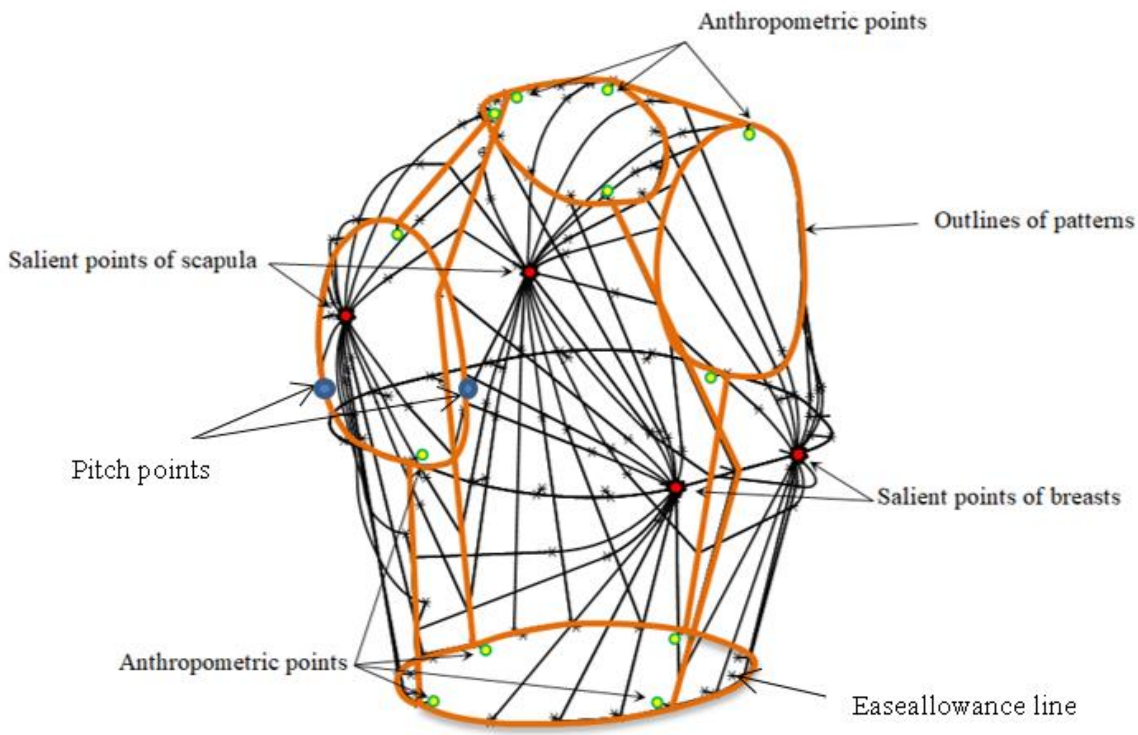

Figure 4-22- 3D graphic model of garment with 3D ease allowances [233]

The garment block pattern was modeled by triangulating the surfaces of different parts from the front and back of the pattern. The front and back of the garment block pattern are demonstrated for Subject 2 in the 3D Design Concept environment in Figure 4-23(a and b). It is noted that no requirement was necessary for the number and size of triangular meshes since the fabric properties can be provided during the virtual try-on simulation.

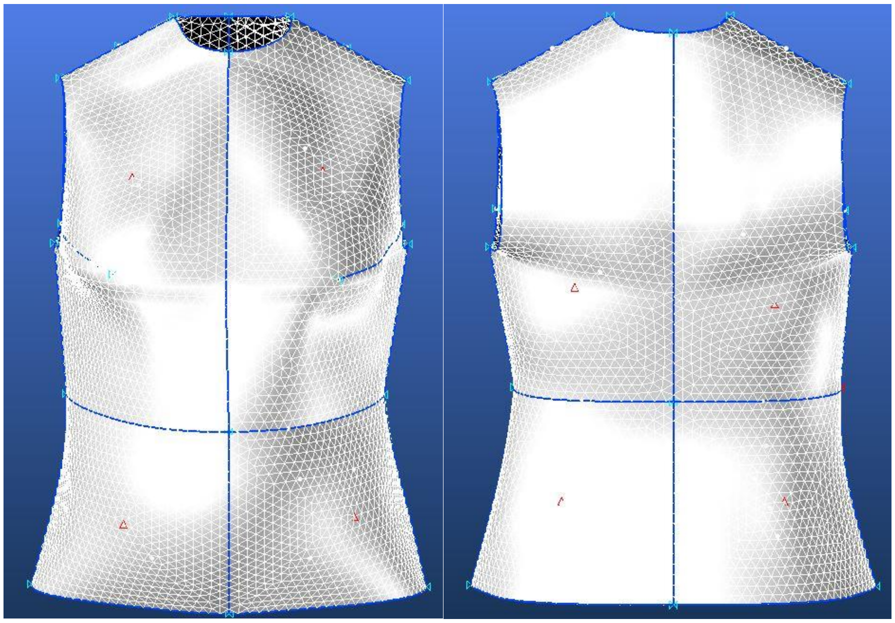
(a) (b)

Figure 4-23- (a) Front and (b) Back of the garment block pattern for Subject 2 in the Design Concept

Then, the flattening process was applied to achieve the corresponding 2D pattern of the designed garment in the 3D Design Concept. Therefore, eight 2D pieces were created including four pieces for the front and four pieces for the back of the garment.

All the pattern pieces were imported into the Modaris software for adjustment after the flattened 2D block pattern was made. All eight pieces were sewn together in the Modaris software environment.

As specified earlier, a pregnant woman's body endures considerable changes in torso while other parts do not experience noticeable changes. Therefore, the formed virtual mannequin of torso was combined with non-evolving parts of the 35th week scanned body of the pregnant woman (Subject 2) on the way to try-on the virtual garment block pattern on the entire virtual mannequin.

In the next step, the garment block pattern was virtually tried on the completed mannequin of Subject 2. However, the drape of the garment block pattern was not suitable since the garment block pattern was not well-tailored on the body of the pregnant woman (Subject 2).

To improve the fitting of the designed pattern, several darts were allocated to different pieces of the block pattern in the 3D Design Concept software environment and the garment drape was simulated in dynamic mode. Hence, two chest clip darts were employed for two upper front pieces of the pattern intended for the improved garment fitting on the body. The chest clip darts for two upper front pieces of the pattern can be found in Figure 4-24(a).

Also, two elastic seams were allocated to the designed block pattern with the intention of garment fitting improvement on the body in the Modaris software environment. The most important characteristic of a well-constructed sewn seam is strength, elasticity, durability, security, and appearance while seams provide special effects for the garments. Therefore, the elastic seams were hired to assist the pattern to follow the form of the body in the presence of the forces during the course of dynamic drape simulation.

It should be noted that the commercial maternity garments were firstly analyzed to get a rough estimation for the right position of the seams intended for the best form and fit of the pregnancy garment. Next, the good position of the elastic seams was fixed using trial and error method (different positions were distributed while the place of the seams was intended to be between the armpit and underbust points of the pregnant woman).

The garment block pattern was simulated using two darts and two elastic seams (Figure 4-24(a)). It should be taken into account that the pieces were edited in the Modaris software environment before assigning them to the 3D environment for virtual try-on with the aim of getting a well-fitted pregnancy garment.

Briefly, design–display–evaluation correction was continually implemented to attain an adequate design. The front and side view of the virtual try-on of the garment block pattern on the developed mannequin is displayed in Figure 4-24(b and c). As can be seen, the block pattern with two chest clip darts and two elastic seams proposed a suitable fit on the pregnant virtual mannequin of Subject 2.

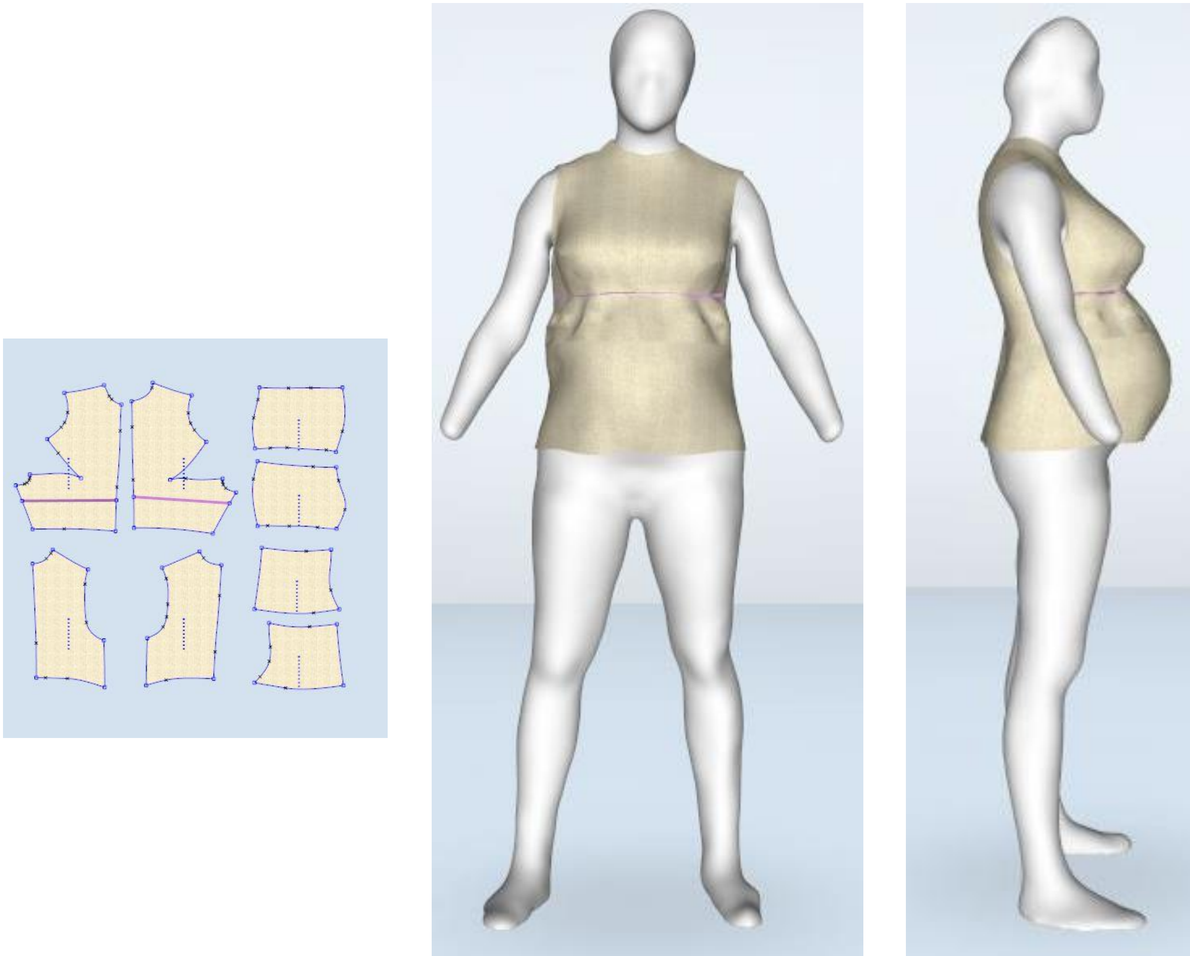

(a) (b) (c)

Figure 4-24- (a) The garment block pattern, (b) Front and (c) Side view of the corresponding virtual try-on [224]

It should be noted that the characteristic of one of the predefined fabrics was assigned to all the eight pieces of the garment block pattern for dynamic drape simulation. The characteristics of the selected woven fabric for drape simulation were in agreement with the characteristic of Sample 1 (the manufactured EMSE woven fabric with conductive monofilament as stuffer weft (Table 3-3).

4.3 Results and discussion

As explained earlier, the main objective of the present thesis was to develop a garment with electromagnetic shielding effectiveness properties for pregnant women to protect both mother and fetus against radiation.

Also, insufficient numbers of mannequins with accurate sizes are supplied for pregnant women in the apparel and design industry. However, 3D design and body measurement systems have been developed in recent years and accordingly, the 3D virtual mannequin has been technologically advanced for different body figures and styles spending less time and cost.

Therefore, in this chapter, a 3D virtual mannequin was suggested for pregnancy period. In the following, the results of the proposed model for pregnancy mannequin making and corresponding garment design were discussed.

4.3.1 Pregnancy mannequin

To begin with, a pregnant woman was scanned at regular intervals (every week) and the data was stored. Then, the body changes of torso (between the crotch and underbust) were analyzed for the specific duration of pregnancy (16^{th}-26^{th} weeks).

In the next step, a 3D adaptive virtual mannequin was made using the linear model for the pregnant woman (Subject 1) and the produced surface for torso was fitted on the scanned body for the second trimester.

In a few words, the body modification of torso was analyzed and the collected data was applied to generate a 3D adaptive virtual mannequin using the linear model for Subject 1. The produced surface of torso was in good agreement with the scanned body of the pregnant woman for all the weeks during the second trimester.

It is noted that the necessity of virtual mannequin development for the pregnancy period to be applied in the garment design sector was remained unreturned since the virtual mannequin was produced only for the second trimester of the pregnancy period.

In addition, it appears unmanageable to scan a pregnant body every week without any break or gap in between. The gaps occur because of several problems e.g. each pregnant woman experiences enormous changes in her physical and mental statuses during pregnancy due to the hormone changes and fetal growth. As a result, one pregnant woman may be cautioned to take an absolute rest for a definite period of her pregnancy or another is not sure the week's number of her pregnancy especially during the course of the first weeks of pregnancy. For a similar reason, the body scanned data was not accessible for all the weeks of pregnancy for Subject 1.

Therefore, the possibility of mannequin development for whole pregnancy length was considered with existing body scan data for a definite duration of pregnancy. So, it was suggested to outline the possible correlation between the weight gain and body morphology growth during the period of maternity.

Thus, the body growth of the pregnant woman was estimated based on the existing body scanning data in combination with weight gain during pregnancy to create a virtual mannequin for whole maternity period.

For this purpose, a proposed trend of weight gain (Method 1) was employed to produce a virtual mannequin for the whole pregnancy length. However, the results of the predicted mannequin were not promising as the body has not indicated normal changes for the studied case (Subject 1).

Alternatively, another proposed weight gain trend (Method 2) was applied and the mannequin was generated for the entire pregnancy period based on the weight gain trend proposed by Method 2. The results showed that the formed mannequin of Subject 1 was well-accorded to the actual evolution of the body over the pregnancy period. It means that the generated mannequin using weight gain trend (Method 2) in cooperation with accessible body scan data was in good agreement with the actual body profile during pregnancy.

4.3.2 Model validation

Body scan data of another pregnant woman (Subject 2) was collected and the body evolution was examined for a different period of pregnancy (the third trimester of her pregnancy). The purpose was to verify the suggested model of the 3D virtual mannequin based on weight gain during pregnancy deliberated in the previous section.

It should be taken into consideration that the weight of pregnant women before pregnancy and total weight gain during nine months of pregnancy is approximately available for every single pregnant woman. It is correlated to the fact that the visible body changes during pregnancy such as weight are frequently recorded by doctors or in hospitals.

Consequently, the suggested model for mannequin making based on weight gain had to be verified for further studies of garment design. So, the 3D virtual mannequin of Subject 2 was developed based on the information provided by the body scanner and the weight increase of the pregnant woman during her pregnancy.

First, the mannequin of Subject 2 was made for certain pregnancy duration based on the available body scanning data (the third trimester). Next, the adaptive mannequin was advanced for the whole pregnancy period based on the trend of weight gain. The results showed that the formed adaptive mannequin based on the weight gain is in accordance with the actual figure of the pregnant woman.

It has to be taken into account the scanned bodies of Subject 2 were acquired during the third trimester of her pregnancy although the data of the scanned bodies of Subject 1 were collected during the second trimester of her pregnancy. The reason was correlated to the fact that these two women (Subject 1 and Subject 2) were presented for body scanning at different time spans with regard to their health conditions and their personal preferences.

To conclude, it was suggested that the proposed model to create a 3D virtual mannequin based on weight gain of mothers during pregnancy was valid for two studied pregnant women (Subject 1 and Subject 2). Therefore, it is suggested that the 3D virtual mannequins can be produced using the weight gain forecast of each pregnant woman and this model is applicable in the ready-to-wear sector. Also, the proposed model can be practical to make customized pregnancy mannequin while further mannequin making for a bigger group of pregnant women based on the proposed model is recommended.

4.3.3 Garment block pattern

In this section, a basic garment block pattern was proposed relating to the developed virtual mannequin for Subject 2. It should be noted that the final objective of the present thesis was to make a well-fitted protective garment for pregnant women with the intention of protecting both mother and fetus against radiation. So, it was suggested to virtually design a block pattern for torso area of the pregnant women.

Therefore, a block pattern was completed in the Design Concept environment using the anthropometric feature points, characteristic lines and curves determined on the developed virtual mannequin of Subject 2. Then, all the pieces of the garment block pattern were flattened and the developed garment block pattern was virtually tried on the virtual mannequin of the pregnant woman.

The result revealed that the developed block pattern was well-fitted on the adaptive mannequin of Subject 2. Hence, it was suggested that the proposed method of 3D virtual mannequin making was applicable for creating a fitted pregnancy garment block pattern with electromagnetic shielding properties for personal protective application as it was the ultimate goal of this research.

4.4 Summary

A well-fitted garment block pattern was developed for a pregnant woman with the potential of applying in protective garment manufacturing against electromagnetic waves. It should be noted that this work concentrated on adaptive mannequin making and garment design for torso since most protection would be applied on torso to protect both mother and fetus against the negative effects of radiation.

First, the body morphology during pregnancy was investigated and the adaptive mannequin surface was produced for the indicated period of pregnancy and the virtual mannequin surface was verified by available body scanned data. Afterward, the virtual mannequin was established for the entire pregnancy period based on the weight gain throughout pregnancy for a pregnant woman (Subject 1).

In the next step, a virtual mannequin surface for another pregnant woman (Subject 2) was made with a similar process. The objective of making a virtual mannequin for Subject 2 was to validate the proposed model for mannequin development based on weight gain during the period of maternity. The results showed that the developed adaptive mannequin was accurate for the entire maternity period of Subject 2.

To clarify, the made mannequins for two different pregnant women (Subject 1 and Subject 2) using weight gain during pregnancy confirmed the precision of the proposed method of mannequin estimation for whole pregnancy period.

So, it was suggested that the established mannequin based on the weight gain approximation during maternity period was necessary in order to make a personalized protective garment for pregnant women in view of the actual body evolution during pregnancy.

To finish, the adaptive mannequin was applied to make a virtual garment block pattern for Subject 2. Chest clip darts and elastic seams were allocated to the two-upper front pieces of the pattern and the result of virtual try-on suggested that the garment block pattern was well-fitted on the 3D virtual mannequin of the pregnant woman during the course of dynamic drape simulation.

Conclusions and future works

Textiles have been massively utilized for electromagnetic shielding effectiveness (EMSE) applications due to the increasing concern of health issues caused by human exposure to radiation. Fetuses are potentially at higher risk due to the rapid growth of the neurological system and body organs in early life stages. Hence, protecting the fetuses against the detrimental effects of the electromagnetic waves is essential during pregnancy period in consequence of the extensive presence of electromagnetic waves in the human living environment.

A lot of electromagnetic shielding textiles are made of metallic yarns and composites since metals are highly electroconductive materials. However, using metallic yarns and composites is restricted because of their poor washability, uncomfortability, and corrosiveness.

Therefore, it was necessary to introduce more practical materials in the textile industry avoiding the weaknesses of traditional materials for electromagnetic shielding applications. For this purpose, conductive polymer nanocomposites (CPCs) have been proposed for electrical conductivity enhancement in textiles.

This Ph.D. work aimed the utilization of carbon nanofillers as the conductive additive in a thermoplastic polymer matrix (PA6,6), commonly used in the garment industry, for developing CPC monofilaments intended for shielding textile manufacturing for personal protection. The main objective of this thesis was to generate a durable electroconductive nanocomposite monofilament with acceptable viscosity for applying in melt mixing method using extrusion.

This thesis consists of three main parts in an attempt to accomplish all the requirements for electromagnetic shielding garment development using electroconductive yarns for pregnancy period.

In the first part of the thesis, the influences of woven fabric characteristics were investigated on the EMSE behavior of the woven fabrics. Towards that end, different 2D simple woven fabrics and 3D warp interlock woven fabrics were designed and manufactured using metal-based yarns as conductive materials. The concentration of this part was to identify the effects of structural parameters (e.g. yarn density and weave structure) on the EMSE improvement of the woven fabrics.

Simple 2D woven structures are widely used in the garment industry and as a result, firstly, a set of simple woven fabrics was produced for shielding purposes in this research. Then, the influences of structural characteristics were studied on the EMSE behavior of the woven fabrics.

The shielding of the woven fabrics was evaluated using an anechoic chamber in the frequency range of 1-6 GHz. This frequency range (1-6 GHz) is in accordance with the utilized frequencies for commonly use electronic devices such as handsets.

The EMSE results of 2D woven fabrics showed that doubling the conductive yarn density resulted in a slightly higher EMSE (~ 5% higher) keeping the same fabric characteristics such as weave structure and conductive yarn (PA coated with silver).

Also, the fabrics with plain weave structure revealed better EMSE values compared to the fabrics with the twill weave structure, followed by the satin weave structure. The more the floats of the conductive yarns are, the looser the simple woven fabric is, and the lower the EMSE is. However, the diagonally arranged of the conductive yarn floats could result in similar EMSE despite the different amounts of the floats of the conductive yarns.

In addition, usage of the yarn with higher conductivity (PA coated with silver) in the woven fabric structure led to higher EMSE in comparison with using the yarn with lower electrical conductivity (Inox) in the simple woven structures. Moreover, the EMSE of all the 2D woven fabrics was in the acceptable range for personal wearable shielding applications (17–39 dB).

In a few words, the EMSE results of the manufactured simple woven fabrics showed that the effects of the conductive yarn density together with the weave structure were not significant on the EMSE behavior of the woven fabrics. Also, metal yarns applied in simple woven fabrics could not be retained from oxidation, corrosion, mechanical abrasion, and skin touch with the wearer due to the limitations of the structures of the simple woven fabrics.

Consequently, a set of 3D warp interlock woven fabrics was designed where metal yarns were integrated into the middle (mid-ply) of the compound woven structures to avoid the difficulties caused by metal exposure to the air or the skin touch with the wearer.

The increase of the EMSE was examined as a factor of increasing the quantity of the conductive material per unit area in the frequency range of 1-6 GHz. The quantity of the conductive material per unit area in the 3D woven fabrics was enlarged by increasing the yarn undulation of the conductive warps, while the yarn density and yarn fineness were fixed for all the manufactured woven variants.

Moreover, the binding of the warps with layers of wefts was set in a way that metal yarns were not apparent on the exterior faces of the woven fabrics. The main reason was to avoid metal exposure to the air to preserve the metal from oxidation as well as the metal touch with the skin of the wearer. It is attributed to the fact that the compound woven fabrics were designed for wearable applications.

The EMSE results showed that increasing the undulation of the conductive yarns (waviness degree) through the thickness of the manufactured 3D warp interlock woven variants resulted in higher EMSE attenuation. Changing the position of the conductive yarns by changing the fabric parameters e.g. the waviness degree, played a significant role in the EMSE of the 3D warp interlock woven variants. For example, an increase of 40% in the level of the EMSE was detected by 14% increasing the amount of the conductive yarn (silver multifilament yarn) as a result of increasing the waviness degree of the conductive warps from 4.4 % to 24.8 %.

To conclude, the EMSE of the 3D woven variants was in acceptable range (19–44 dB) for personal wearable protective applications in the frequency range of 1-6 GHz. These woven variants are excellent for EMSE applications in the frequency band 2–3 GHz owing to the possible correlation between the wavelength of the electromagnetic waves and the unit cell size of the compound woven structures. Also, these fabrics can be used for shielding the household appliances, FM/AM radio broadcast sets, cellular phones, computers, etc.

In the second part of the thesis, an alternative polymer-based monofilament yarn was produced for applying in the weaving process to develop an electromagnetic shield fabric for personal protection. The development of conductive polymer nanocomposite (CPC) monofilaments was investigated in order to replace the traditional shielding yarns (metallic yarns) with a polymer-based yarn.

In order to achieve that objective, a set of conductive nanocomposites were prepared using the combination of multiwall carbon nanotube (MWCNT) and carbon black (CB) in a thermoplastic polymer matrix (PA6,6) by melt mixing method using extrusion. The electrical conductivity results indicated that the percolation threshold of the developed nanocomposite using the synergism between MWCNT and CB (1MWCNT:2CB) was at 1.7 wt.% of MWCNT and 3.3 wt.% of CB where the conductivity of this nanocomposite was higher than the conductivity of the nanocomposite contained only 20 wt.% of CB and the same as the nanocomposite contained 3 wt.% of MWCNT.

It should be taken into account that the mass concentration of the nanofillers had to be optimized in terms of the electrical conductivity and viscosity to develop an applicable nanocomposite in the melt mixing method (extrusion). Therefore, the MFI values of the developed CPCs were determined and the results showed that the MFI value of the most conductive monofilament with PA6,6, MWCNT, and CB was 11.5 g/10 min (at 280 °C, 2.16 Kg load) which was in the acceptable range for extrusion process (10-35 g/10 min).

Moreover, a set of CPCs with the same ratio of carbon nanofillers was produced while CB (Printex) was replaced with high-structured KB (Ketjenblack). The electrical conductivity of the nanocomposites with 2.5 wt.% of MWCNT and 5 wt.% KB (PA-MWCNT2.5–KB*5) was tenfold greater than the nanocomposite with 2.5 wt.% of MWCNT and 5 wt.% of CB (PA-MWCNT2.5–CB5). This is correlated to the fact that KB ensures a high effective surface area due to the contribution of the internal voids.

Furthermore, two conductive monofilaments (PA-MWCNT2.5–CB5 and PA-MWCNT2.5–KB*5) were applied in weaving process to make woven fabrics for wearable personal protection against the electromagnetic waves.

The EMSE of the manufactured fabrics was evaluated in the mode-stirred chamber in the frequency range 1–10 GHz. The mode-stirred chamber was employed for the EMSE measurements due to the fact that such an apparatus allows the measurements in a realistic electromagnetic environment where the wave polarization cannot be controlled such as the human living environment.

It should be noted that the EMSE measurements were completed in an anechoic chamber in the frequency range of 1-6 GHz for all the manufactured fabrics in this research. Conversely, the EMSE measurements were accomplished in a mode-stirred chamber only for the target fabrics of the thesis (woven fabrics with conductive monofilament yarns). It was believed that introducing the results of EMSE measured in an anechoic chamber for the woven samples having monofilaments in their structures does not improve the readability of the manuscript since the more accurate results were presented (measured in the mode-stirred chamber) where it was also possible to increase the frequency range (1-10 GHz) for the measurements.

The EMSE of all the woven samples using the CPC monofilaments was promising for personal protective clothing. In addition, the EMSE results revealed that the electrical conductivity of the nanocomposites, the yarn density of the conductive monofilaments, and the weave structures of the woven fabrics had significant effects on the level of the EMSE.

To clarify, increasing the density of the conductive weft monofilament (PA-MWCNT2.5–CB5) yarns from 4 to 5 (yarns/cm) led to the greater EMSE values for the frequency range of 1-10 GHz

(15 vs 11 dB). Also, the substitution of PA-MWCNT2.5–CB5 with PA-MWCNT2.5–KB*5 with tenfold electrical conductivity in the two-ply compact woven fabric structure resulted in a higher attenuation level (16 vs 11 dB).

Furthermore, due to the fact that the ultimate goal of this thesis was to protect both mother and fetus against the harmful effects of electromagnetic waves, it was suggested to employ a parametric graphical method to develop a 3D adaptive mannequin for protective pregnancy garment design. Thus, in the third part of the thesis, a new virtual model for mannequin estimation based on body scanned data of the pregnant women and weight gain during pregnancy was proposed to design an adapted protective garment block pattern for pregnancy period.

For this purpose, the body morphology of a pregnant woman was analyzed using her body scanned data. Then, a 3D adaptive mannequin model was developed based on the scanned data and her weight gain during pregnancy. The proposed model was validated by making a virtual mannequin for another pregnant woman using a similar process and comparing the results.

Next, the developed mannequin based on weight gain was applied to design a customized garment block pattern for pregnancy period. To end with, the fabric characteristics according to the characteristics of one of the developed shielding fabric were assigned to the block pattern pieces and the virtual try-on of the developed garment block pattern suggested that it was well-fitted on the 3D virtual mannequin of the pregnant woman. The proposed method is applicable for making a fitted pregnancy garment block pattern with electromagnetic shielding properties for personal protection against radiation in the human living environment.

The results of this thesis can motivate future research in some directions. Some suggestions are listed in the following.

- Proposing a model for estimating the correlation between the unit cell size of compound woven fabrics and the wavelength (or frequency) of the electromagnetic waves.
- Study of the effect of the water content of the developed CPC monofilaments on the electrical conductivity and the electromagnetic shielding behavior of the produced fabrics.
- Investigation of reducing the monofilament diameter to improve the flexibility of the monofilament and transform it into a multifilament strand.
- Applying other common thermoplastic polymers in the garment industry (e.g. polyester) as the matrix of the nanocomposite in order to investigate the possibility of achieving a lower percolation threshold of the mixed nanofillers or higher electrical conductivity.

- Examination of the quantity and ratio of MWCNT and CB to attain the sufficient electrical conductivity of the monofilament for 3D printing on textile fabrics aimed for the EMSE applications.

References

[1] A. Zamanian and C. Hardiman, "Electromagnetic radiation and human health: A review of sources and effects," *EMR Hum. Heal.*, vol. 16, no. July, pp. 16–26, 2005.

[2] K. Jagatheesan, A. Ramasamy, A. Das, and A. Basu, "Electromagnetic shielding behaviour of conductive filler composites and conductive fabrics ??? A review," *Indian Journal of Fibre and Textile Research*, vol. 39, no. 3. 2014.

[3] K. A. Hossmann and D. M. Hermann, "Effects of electromagnetic radiation of mobile phones on the central nervous system," *Bioelectromagnetics*, vol. 24, no. 1, pp. 49–62, 2003.

[4] O. Erogul *et al.*, "Effects of electromagnetic radiation from a cellular phone on human sperm motility: An in vitro study," *Arch. Med. Res.*, vol. 37, no. 7, pp. 840–843, 2006.

[5] V. Anderson and K. H. Joyner, "Specific Absorption Rate Levels Measured in a Phantom Head Exposed to Radio Frequency Transmissions From Analog Hand-Held Mobile Phones," vol. 69, pp. 60–69, 1995.

[6] V. Anderson and J. Rowley, "Brief Communication Measurements of Skin SurfaceTemperature During Mobile Phone Use," vol. 162, no. November 2005, pp. 159–162, 2007.

[7] P. P. Pathak and V. Kumar, "Harmful electromagnetic environment near transmission tower," *Indian J. Radio Sp. Phys.*, vol. 32, pp. 238–241, 2003.

[8] J. Y. Kim, H. T. Kim, K. H. Moon, and H. J. Shin, "Long-Term Exposure of Rats to a 2 . 45 GHz Electromagnetic Field : Effects on Reproductive Function," pp. 1308–1314, 2007.

[9] F. Teimori, A. A. Khaki, A. Rajabzadeh, and L. Roshangar, "The effects of 30 mT electromagnetic fields on hippocampus cells of rats," *surgucak Neurol. Int.*, pp. 1–14, 2016.

[10] K. Amac, H. Tayefi, M. Kiray, H. A. Bagriyanik, C. Pekcetin, and C. Ozogul, "The effects of exposure to electromagnetic field on rat myocardium," *Toxicol. Ind. Health*, vol. 29, no. 5, pp. 418–425, 2013.

[11] A. S. H. Alchalabi, E. Aklilu, A. R. Aziz, H. Rahim, S. H. Ronald, and F. Mohd, "Impact of electromagnetic radiation exposure during pregnancy on embryonic skeletal development in rats," *Asian Pacific J. Reprod.*, vol. 6, no. 3, pp. 104–111, 2017.

[12] E. K. Osei and K. Faulkner, "Radiation risks from exposure to diagnostic X-rays,"

Radiogr., vol. 6, pp. 131–144, 2000.

[13] L. Oncol, “Radiotherapy during pregnancy : fact and fiction,” vol. 6, no. May, pp. 328–333, 2005.

[14] C. H. Mccollough *et al.*, “Radiation Exposure and Pregnancy: When Should We Be Concerned?,” *radiographics*, vol. 27, no. 4, pp. 909–918, 2007.

[15] L. Birks *et al.*, “Maternal cell phone use during pregnancy and child behavioral problems in fi ve birth cohorts,” vol. 104, pp. 122–131, 2017.

[16] A. Wdowiak, P. A. Mazurek, A. Wdowiak, and I. Bojar, “Effect of electromagnetic waves on human reproduction,” *Ann. Agric. Environ. Med.*, vol. 24, no. 1, pp. 13–18, 2017.

[17] M. Mahram and M. Ghazavi, “The Effect of Extremely Low Frequency Electromagnetic Fields on Pregnancy and Fetal Growth, and Development,” *Arch. Iran. Med.*, vol. 16, no. 4, pp. 221–224, 2013.

[18] D. Jiang *et al.*, “Electromagnetic Interference Shielding Polymers and Nanocomposites - A Review,” *Polym. Rev.*, vol. 59, no. 2, pp. 280–337, 2019.

[19] S. J. Orfanidis, *Electromagnetic Waves and Antennas*. Rutgers University, 2016.

[20] “http://www.mpoweruk.com.” .

[21] s.a. Schelkunoff, *Electromagnetic waves*. D. Van Nostrand Company, inc; 1st Ed 11th prt edition (1943), 1943.

[22] K. Kaiser, *Electromagnetic shielding*, First Edit. NY: Taylor & Francis, 2005.

[23] S. Celozzi, R. Araneo, and G. Lovat, *Electromagnetic Shielding*. New Jersey: A JOHN WILEY & sons, inc., publication, 2008.

[24] S. Kuester, G. M. O. Barra, J. C. Ferreira, B. G. Soares, and N. R. Demarquette, “Electromagnetic interference shielding and electrical properties of nanocomposites based on poly (styrene-b-ethylene-ran-butylene-b-styrene) and carbon nanotubes,” *Eur. Polym. J.*, 2016.

[25] P. Saini and M. Arora, “Microwave Absorption and EMI Shielding Behavior of Nanocomposites Based on Intrinsically Conducting Polymers, Graphene and Carbon Nanotubes,” in *New Polymers for Special Applications*, First edit., Ailton De Souza Gomes, Ed. InTech Janeza Trdine 9, 51000 Rijeka, Croatia, 2012, pp. 71–112.

[26] M. H. Al-Saleh and U. Sundararaj, “Electromagnetic interference shielding mechanisms of CNT/polymer composites,” *Carbon N. Y.*, vol. 47, no. 7, pp. 1738–1746, 2009.

[27] S. Maiti, N. K. Shrivastava, S. Suin, and B. B. Khatua, "Polystyrene/MWCNT/graphite nanoplate nanocomposites: Efficient electromagnetic interference shielding material through graphite nanoplate-MWCNT-graphite nanoplate networking," *ACS Appl. Mater. Interfaces*, 2013.

[28] M. H. Al-Saleh, W. H. Saadeh, and U. Sundararaj, "EMI shielding effectiveness of carbon based nanostructured polymeric materials: A comparative study," *Carbon N. Y.*, vol. 60, pp. 146–156, 2013.

[29] "Designation: D4935 – 10 Standard Test Method for Measuring the Electromagnetic Shielding Effectiveness of Planar Materials 1."

[30] V. Šafářová and J. Militký, "Comparison of methods for evaluating the shielding effectiveness of textiles," in *Vlakna a Texti*, 2012.

[31] Tadeusz W.Więckowski and J. M. Janukiewicz, "Methods for Evaluating the Shielding Effectiveness of Textiles," *FIBRES Text. East. Eur.*, vol. 14, no. 5, pp. 18–22, 2006.

[32] T. Więckowski and J. Janukiewicz, "Methods for evaluating the shielding effectiveness of textiles," *IEE Colloq. Screen. Connect. Cables Enclosures*, vol. 14, no. 5, pp. 18–22, 1992.

[33] V. David, E. Vremera, A. Salceanu, I. Nica, and O. Baltag, "On the characterization of electromagnetic shielding effectiveness of materials," in *IASI-Imeko*, 2007, no. 4.

[34] A. Niembro-martin, E. Pistono, P. Lemaître-auger, T. Vuong, G. Eymin, and P. Tourtollet, "Efficient Setup for the Measurement of Transmission- Coefficients with a Single-Room Anechoic Chamber," *IEEE*, pp. 3–5, 2014.

[35] S. Geetha, K. K. S. Kumar, and 1 D. C. Trivedi Chepuri R. K. Rao, 1 M. Vijayan, "EMI Shielding: Methods and Materials—A Review," *J. Appl. Polym. Sci.*, vol. 112, pp. 2073–2086, 2009.

[36] I. Standard, "Electromagnetic compatibility (EMC) -- Part 4-21 : Testing and measurement techniques - Reverberation chamber test methods (IEC 61000-4-21 : 2011 (EQV))," vol. 2011, 2011.

[37] C. L. Holloway, D. A. Hill, J. Ladbury, G. Koepke, and R. Garzia, "Shielding Effectiveness Measurements of Materials Using Nested Reverberation Chambers," *IEEE Trans. Electromagn. Compat.*, vol. 45, no. 2, pp. 350–356, 2003.

[38] S. Lall´ech`ere, S. Girard, D. Roux, P. Bonnet, and F. Paladian, "Mode stirred reverberation chamber (msrc): a large and efficient tool to lead high fre- quency

bioelectromagnetic," *Prog. Electromagn. Res.*, vol. 26, no. June, pp. 257–290, 2010.

[39] X. C. Tong, *Advanced materials and design for electromagnetic interference shielding*. newyork: Taylor and Francis, 2009.

[40] V. Šafářová and J. Militký, "Electromagnetic shielding properties of woven fabrics made from high-performance fibers," *Text. Res. J.*, vol. 84, no. 12, pp. 1255–1267, 2014.

[41] C. Morari and I. Bălan, "Methods for determining shielding effectiveness of materials," *Electroteh. Electron. Autom.*, vol. 63, no. 2, pp. 126–136, 2015.

[42] E. Sano and E. Akiba, "Electromagnetic absorbing materials using nonwoven fabrics coated with multi-walled carbon nanotubes," *Carbon N. Y.*, vol. 78, pp. 463–468, 2014.

[43] C. Guo, L. Zhou, and J. Lv, "Effects of expandable graphite and modified ammonium polyphosphate on the flame-retardant and mechanical properties of wood flour-polypropylene composites," *Polym. Polym. Compos.*, vol. 21, no. 7, pp. 449–456, 2013.

[44] R. Erdem, "Evaluation of electromagnetic shielding effectiveness of multi-axial fabrics and their reinforced PES composites," *Bull. Mater. Sci.*, 2016.

[45] H. G. Örtlek, C. G. Ş. O. Ğ. Lu, G. Okyay, and Y. T. Ğ. Lu, "Investigation of electromagnetic shielding and comfort properties of single jersey fabrics knitted from hybrid yarns containing metal wire," *tekstil ve konfeksiyon*, pp. 90–101, 2012.

[46] F. Z. Engin and I. Usta, "Electromagnetic shielding effectiveness of polyester fabrics with polyaniline deposition," *Text. Res. J.*, vol. 84, no. 9, pp. 903–912, 2014.

[47] H. C. Chen, K. C. Lee, J. H. Lin, and M. Koch, "Fabrication of conductive woven fabric and analysis of electromagnetic shielding via measurement and empirical equation," *J. Mater. Process. Technol.*, 2007.

[48] U. Lundgren, "Characterization of Components and Materials for EMC Barriers materials for EMC barriers, PhD diss., Luleå tekniska universitet," 2004.

[49] "MIL-STD-285, Military standard: attenuation measurements for enclosures, electromagnetic shielding, for electronic test purposes, method of." 1956.

[50] F. Çeken, Ö. Kayacan, A. Özkurt, and Ş. S. Uğurlu, "The electromagnetic shielding properties of some conductive knitted fabrics produced on single or double needle bed of a flat knitting machine," *J. Text. Inst.*, vol. 103, no. 9, pp. 968–979, 2012.

[51] H. G. Ortlek, T. Alpyildiz, and G. Kilic, "Determination of electromagnetic shielding performance of hybrid yarn knitted fabrics with anechoic chamber method," *Text. Res. J.*,

vol. 83, no. 1, pp. 90–99, 2013.

[52] H. Spiegelaar and E. VanderHeyden, “The Mode Stirred Chamber -A Cost Effective EMC Testing Alternative,” *IEEE*, 1995.

[53] J. M. Thomassin, C. Jérôme, T. Pardoen, C. Bailly, I. Huynen, and C. Detrembleur, “Polymer/carbon based composites as electromagnetic interference (EMI) shielding materials.” Materials Science and Engineering R, pp. 211–232, 2013.

[54] C. L. Holloway and E. F. Kuester, “Corrections to ‘ Closed-Form Expressions for the Current Density on the Ground Plane of a Microstrip Line , With Application to Ground Plane Loss ,’” vol. 54, no. 11, pp. 4018–4019, 2006.

[55] C. L. Holloway *et al.*, “On the Use of Reverberation Chambers to Simulate a Rician Radio Environment for the Testing of Wireless Devices,” vol. 54, no. 11, pp. 3167–3177, 2006.

[56] S. Member, C. Samuelsson, and B. K. Vallhagen, “Shielding effectiveness and hpm vulnerability of energy-saving windows and window panes,” *IEEE Trans. Electromagn. Compat.*, pp. 1–8, 2018.

[57] D. Ingegneria *et al.*, “Applicability of Measurement Uncertainty Models in a Reverberation Chamber Including Frequency Stirring,” *2018 IEEE Symp. Electromagn. Compat. Signal Integr. Power Integr. (EMC, SI PI)*, no. 3, pp. 504–509, 2018.

[58] L. Bastianelli *et al.*, “Experimental analysis of the aging effects on shielding effectiveness of cementitious composites,” pp. 71–75, 2018.

[59] M. Javadi *et al.*, “Electrical conductivity enhancement of hybrid PA6 , 6 composite containing multiwall carbon nanotube and carbon black for shielding e ff ectiveness application in textiles,” *Synth. Met.*, vol. 251, no. March, pp. 75–84, 2019.

[60] M. Imai, K. Akiyama, T. Tanaka, and E. Sano, “Highly strong and conductive carbon nanotube/cellulose composite paper,” *Compos. Sci. Technol.*, 2010.

[61] C. R. Paul, *Introduction to electromagnetic compatibility*, Second edi. Lexington, Kentucky: John Wiley & Sons, Inc., 2006.

[62] 2017. Available: https://www.lessemf.com. , NY, USA, “““Online Warehouse for Gaussmeters, EMF Meters and Electromagnetic Field Shielding.””” .

[63] “www.solianiemc.com.” .

[64] S. Maity, K. Singha, P. Debnath, and M. Singha, “Textiles in Electromagnetic Radiation Protection,” *J. Saf. Eng.*, vol. 2, no. 2, pp. 11–19, 2013.

[65] “www.lairdtech.com.” .

[66] S. Liu, “Electrically Conductive Cotton Textile and Its Applications,” no. June, 2016.

[67] Y. Atwa, N. Maheshwari, and I. A. Goldthorpe, “conductive textiles,” *J. Mater. Chem. C*, vol. 3, no. March, pp. 3908–3912, 2015.

[68] E. Gasana *et al.*, “Electroconductive textile structures through electroless deposition of polypyrrole and copper at polyaramide surfaces,” *Surf. Coatings Technol.*, vol. 201, no. 6, pp. 3547–3551, 2006.

[69] Y. Lu, S. Jiang, and Y. Huang, “Ultrasonic-assisted electroless deposition of Ag on PET fabric with low silver content for EMI shielding,” *Surf. Coatings Technol.*, 2010.

[70] R. Perumalraj and B. S. Dasaradan, “Electromagnetic shielding effectiveness of copper core yarn knitted fabrics,” *Indian J. Fibre Text. Res.*, vol. 34, pp. 149–154, 2009.

[71] H. M. Mofarah and S. S. Najar, “Investigating the electromagnetic shielding effectiveness of copper / cotton full Milano and 1 × 1 rib weft-knitted fabrics,” *J. Text. Inst.*, vol. 0, no. 0, pp. 1–10, 2018.

[72] D. D. Soyaslan and İ. İ. SOYASLAn, “Milano rib knitted fabric and its composite for electromagnetic shielding applications in engineering,” in *Proceedings of 27th The IIER International Conference, St. Petersburg*, 2015, no. June, pp. 59–61.

[73] H. G. Turksoy and T. Alpyildiz, “Determination of electromagnetic shielding performance of hybrid yarn knitted fabrics with anechoic chamber method,” *Text. Res. J.*, no. February 2014, 2013.

[74] K. B. Cheng, S. Ramakrishna, and K. C. Lee, “Electromagnetic shielding effectiveness of copper/glass fiber knitted fabric reinforced polypropylene composites,” *Compos. Part A Appl. Sci. Manuf.*, 2000.

[75] Ayse Bedeloglu, “Electrical, electromagnetic shielding, and some physical properties of hybrid yarn-based knitted fabrics,” *J. Text. Inst.*, vol. 104, no. 11, pp. 1247–1257, 2013.

[76] M. Štefečka *et al.*, “Electromagnetic shielding efficiency of plasma treated and electroless metal plated polypropylene nonwoven fabrics,” *J. Mater. Sci.*, vol. 39, no. 6, pp. 2215–2217, 2004.

[77] M. Sonehara, T. Sato, K. Yamasawa, and Y. Miura, “Preparation and Characterization of a Nano-fiber Cloth for Electromagnetic Wave Shielding,” *J. Magn. Soc. Japan*, vol. 33, no. 3, pp. 293–297, 2009.

[78] F. Çeken, Ü. H. Erdoğan, O. Kayacan, and Ş. S. Uğurlu, "Electromagnetic shielding efficiency of nonwoven insulation panels designed with recycled textiles and copper wires," *J. Text. Inst.*, vol. 103, no. 6, pp. 669–675, 2012.

[79] Y. J. Tan, J. Li, Y. Gao, J. Li, S. Guo, and M. Wang, "A facile approach to fabricating silver-coated cotton fiber non-woven fabrics for ultrahigh electromagnetic interference shielding," *Appl. Surf. Sci.*, vol. 458, no. April, pp. 236–244, 2018.

[80] M. S. Ozen, E. Sancak, A. Beyit, I. Usta, and M. Akalin, "Investigation of electromagnetic shielding properties of needle-punched nonwoven fabrics with stainless steel and polyester fiber," *Text. Res. J.*, vol. 83, no. 8, pp. 849–858, 2013.

[81] G. Ababei, V. David, I. Nica, A. Pica, and H. Chiriac, "Omni-Directional Selective Shielding Multilayered Material for High Frequency Radiation," vol. 48, no. 11, pp. 4309–4312, 2012.

[82] H. Özdemir and A. Özkurt, "The effects of weave and conductive yarn density on the electromagnetic shielding effectiveness of cellular woven fabrics," *Tekst. ve Konfeksiyon*, vol. 23, no. 2, pp. 124–135, 2013.

[83] R. Perumalraj and B. S. Dasaradan, "Electromagnetic shielding effectiveness of doubled copper-cotton yarn woven materials," *Fibres Text. East. Eur.*, vol. 80, no. 3, pp. 74–80, 2010.

[84] Z. Liu and X. C. Wang, "Influence of fabric weave type on the effectiveness of electromagnetic shielding woven fabric," *J. Electromagn. Waves Appl.*, vol. 26, no. 14–15, pp. 1848–1856, 2012.

[85] H. Özdemir, Ş. S. Uğurlu, and A. Özkurt, "The electromagnetic shielding of textured steel yarn based woven fabrics used for clothing," *J. Ind. Text.*, vol. 45, no. 3, pp. 416–436, 2015.

[86] K. B. Cheng, M. L. Lee, S. Ramakrishna, and T. H. Ueng, "Electromagnetic Shielding Effectiveness of Stainless Steel/Polyester Woven Fabrics," *Text. Res. J.*, pp. 42–49, 2001.

[87] A. Das, V. K. Kothari, A. Kothari, A. Kumar, and S. Tuli, "Effect of various parameters on electromagnetic shielding effectiveness of textile fabrics," *Indian J. Fibre Text. Res.*, vol. 34, no. 2, pp. 144–148, 2009.

[88] K. Ş. Lar, "Electromagnetic shielding effectiveness of cellular woven the effects of weave and conductive yarn density on the electromagnetic shielding effectiveness of cellular

woven fabrics," no. June 2016, 2013.

[89] R. Perumalraj, B. S. Dasaradan, R. Anbarasu, P. Arokiaraj, and S. Leo Harish, "Electromagnetic shielding effectiveness of copper core-woven fabrics," *J. Text. Inst.*, vol. 100, no. 6, pp. 512–524, 2009.

[90] D. N. Pandey and A. Basu, "Electromagnetic shielding performance of three-dimensional woven fabrics with copper-based hybrid yarn in X-band frequency range," *J. Ind. Text.*, no. July, pp. 1–19, 2018.

[91] M. Neruda and L. Vojtech, "Electromagnetic shielding effectiveness of woven fabrics with high electrical conductivity : Complete derivation and verification of analytical model," *Materials (Basel).*, vol. 11, no. 1657, pp. 1–20, 2018.

[92] R. Liang, W. Cheng, H. Xiao, M. Shi, Z. Tang, and N. Wang, "A calculating method for the electromagnetic shielding effectiveness of metal fiber blended fabric," *Text. Res. J.*, vol. 88, no. 9, pp. 973–986, 2018.

[93] Alan J Heeger, "Semiconducting and Metallic Polymers: The Fourth Generation of Polymeric Materials," *Synth. Met.*, vol. 125, pp. 23–42, 2001.

[94] M. S. Kim *et al.*, "PET fabric/polypyrrole composite with high electrical conductivity for EMI shielding," *Synth. Met.*, 2002.

[95] E. Devaux *et al.*, "Processing and characterization of conductive yarns by coating or bulk treatment for smart textile applications," *Trans. Inst. Meas. Control Inst. Meas. Control*, vol. 29, no. 34, pp. 355–376, 2007.

[96] Y. Niu, "Electromagnetic Interference Shielding With Polyaniline Nanofibers Composite Coatings Yuhua," *Polym. Eng. Sci.*, pp. 355–359, 2008.

[97] D. Vollath, *Nanoparticles, nanocomposites, nanomaterials : an introduction for beginners*, First edit. Wiley, 2013.

[98] C. A. Cooper, D. Ravich, D. Lips, J. Mayer, and H. D. Wagner, "Distribution and alignment of carbon nanotubes and nanofibrils in a polymer matrix," vol. 62, pp. 1105–1112, 2002.

[99] C. Park *et al.*, "Aligned Single Wall Carbon Nanotube Polymer Composites Using an Electric Field," pp. 1–32, 2019.

[100] R. Andrews, A. Berkovich, H. Jc, D. Jacques, and T. Rantell, "Fabrication of carbon multiwall nanotube / polymer composites by shear mixing."

[101] Wilailak Chanklin, "Electrical properties study of carbon fillers in polymer nanocomposites," the university of new brunswick, 2016.

[102] Peng-ChengMa, N. A.Siddiquia, GadMarom, and Jang-KyoKim, "Dispersion and functionalization of carbon nanotubes for polymer-based nanocomposites: A review," *Compos. Part A Appl. Sci. Manuf.*, vol. 41, no. 10, pp. 1345–1367, 2010.

[103] M. L. Clingerman, E. H. Weber, K. H. Schulz, and J. A. King, "Tensile, Thermal, and Electrical Properties of Carbon Filled Nylon 6,6 Conductive Resins," pp. 262–263.

[104] F. Du and J. E. Fischer, "Effect of nanotube alignment on percolation conductivity in carbon nanotube / polymer composites," vol. 72, no. 12, 2005.

[105] Z. Spitalsky, D. Tasis, K. Papagelis, and C. Galiotis, "Carbon nanotube-polymer composites: Chemistry, processing, mechanical and electrical properties," *Prog. Polym. Sci.*, vol. 35, no. 3, pp. 357–401, 2010.

[106] M. Narkis, G. Lidor, A. Vaxman, and L. Zuri, "Innovative ESD thermoplastic composites structured through melt flow processing," *Electr. Overstress/Electrostatic Disch. Symp. Proceedings, 1999*, pp. 251–259, 1999.

[107] G. Wypych, *Handbook of Fillers*, 4th Editio. Ontario, Canada: ChemTec Publishingr, 2016.

[108] A. S. Hoang, "Electrical conductivity and electromagnetic interference shielding characteristics of multiwalled carbon nanotube filled polyurethane composite films," *Adv. Nat. Sci. Nanosci. Nanotechnol.*, vol. 2, no. 2, p. 025007, 2011.

[109] J. X. J. Xu, M. Wong, and C. P. Wong, "Super high dielectric constant carbon black-filled polymer composites as integral capacitor dielectrics," *2004 Proceedings. 54th Electron. Components Technol. Conf. (IEEE Cat. No.04CH37546)*, vol. 1, pp. 536–541, 2004.

[110] P. Verma, P. Saini, R. S. Malik, and V. Choudhary, "Excellent electromagnetic interference shielding and mechanical properties of high loading carbon-nanotubes/polymer composites designed using melt recirculation equipped twin-screw extruder," *Carbon N. Y.*, vol. 89, pp. 308–317, 2015.

[111] M. S. Han, Y. K. Lee, H. S. Lee, C. H. Yun, and W. N. Kim, "Electrical, morphological and rheological properties of carbon nanotube composites with polyethylene and poly(phenylene sulfide) by melt mixing," *Chem. Eng. Sci.*, 2009.

[112] Y. Shi, J. Li, Y. Tan, Y. Chen, and M. Wang, "Percolation behavior of electromagnetic

interference shielding in polymer / multi-walled carbon nanotube nanocomposites," *Compos. Sci. Technol.*, vol. 170, no. July 2018, pp. 70–76, 2019.

[113] D. D. . Chung, "Electromagnetic interference shielding effectiveness of carbon materials," *Carbon N. Y.*, vol. 39, no. 2, pp. 279–285, 2001.

[114] S. M. Zhang *et al.*, "Synergistic effect in conductive networks constructed with carbon nanofillers in different dimensions," *Express Polym. Lett.*, vol. 6, no. 2, pp. 159–168, 2012.

[115] A. Dorigato, M. Brugnara, and A. Pegoretti, "Synergistic effects of carbon black and carbon nanotubes on the electrical resistivity of poly(butylene-terephthalate) nanocomposites," *Adv. Polym. Technol.*, no. March, pp. 1–11, 2017.

[116] A. Motaghi, A. Hrymak, and G. H. Motlagh, "Electrical conductivity and percolation threshold of hybrid carbon/polymer composites," *J. Appl. Polym. Sci.*, vol. 132, no. 13, pp. 1–9, 2015.

[117] I. Kranauskaitė *et al.*, "Enhancing electrical conductivity of multiwalled carbon nanotube/epoxy composites by graphene nanoplatelets," *Lith. J. Phys.*, vol. 57, no. 4, pp. 232–242, 2017.

[118] M. Safdari and M. Al-haik, "5 - A Review on Polymeric Nanocomposites: Effect of Hybridization and Synergy on Electrical Properties," in *Carbon-Based Polymer Nanocomposites for Environmental and Energy Applications*, A. F. Ismail and P. S. Goh, Eds. Elsevier, 2018, pp. 113–146.

[119] H. Zhang *et al.*, "Synergistic e ff ect of carbon nanotube and graphene nanoplates on the mechanical , electrical and electromagnetic interference shielding properties of polymer composites and polymer composite foams," *Chem. Eng. J.*, vol. 353, no. July, pp. 381–393, 2018.

[120] Z. Sun, "Synergistic effects of conductive carbon nano fi llers based on the ultrahigh-molecular-weight polyethylene with uniform and segregated structures," vol. 47317, pp. 1–8, 2019.

[121] Z. A. Ghaleb, M. Mariatti, and Z. M. Ariff, "Synergy effects of graphene and multiwalled carbon nanotubes hybrid system on properties of epoxy nanocomposites," 2017.

[122] H. Ismail, A. F. Ramly, and N. Othman, "The Effect of Carbon Black/Multiwall Carbon Nanotube Hybrid Fillers on the Properties of Natural Rubber Nanocomposites," *Polym. Plast. Technol. Eng.*, vol. 50, no. 7, pp. 660–666, 2011.

[123] P. C. Ma, H. Zhang, S. Q. Wang, Y. K. Wong, B. Z. Tang, and S. H. Hong, “Electrical Conducting Behavior of Hybrid Nanocomposites Containing Carbon Nanotubes and Carbon Black,” *Appl. Mater. interfaces*, vol. 5, no. 1, pp. 1090–1096, 2009.

[124] T. T. Li *et al.*, “Synergistic effects of micro-/nano-fillers on conductive and electromagnetic shielding properties of polypropylene nanocomposites,” *Mater. Manuf. Process.*, vol. 33, no. 2, pp. 149–155, 2018.

[125] D. A. Makeiff and T. Huber, “Microwave absorption by polyaniline-carbon nanotube composites,” *Synth. Met.*, vol. 156, no. 7–8, pp. 497–505, 2006.

[126] C. Y. Huang *et al.*, “The manufacture and investigation of multi-walled carbon nanotube/polypyrrole/EVA nano-polymeric composites for electromagnetic interference shielding,” *Thin Solid Films*, vol. 519, no. 15, pp. 4765–4773, 2011.

[127] Y. K. Hong *et al.*, “Electromagnetic interference shielding characteristics of fabric complexes coated with conductive polypyrrole and thermally evaporated Ag,” *Curr. Appl. Phys.*, 2001.

[128] J. S. Im, J. G. Kim, S. H. Lee, and Y. S. Lee, “Enhanced adhesion and dispersion of carbon nanotube in PANI/PEO electrospun fibers for shielding effectiveness of electromagnetic interference,” *Colloids Surfaces A Physicochem. Eng. Asp.*, vol. 364, no. 1–3, pp. 151–157, 2010.

[129] M. Takeda, M. Ikeda, S. Satoh, H. Dansako, T. Wakita, and N. Kato, “Microwave Dielectric Properties and EMI Shielding Effectiveness of Poly(styrene-b-styrene-butadiene-styrene) Copolymer Filled With PAni.Dodecylbenzenesulfonic Acid and Carbon Black Anderson,” *Acta Med. Okayama*, vol. 70, no. 2, pp. 111–118, 2016.

[130] T. I. W. Schnoor *et al.*, “The production of aligned MWCNT/polypyrrole composite films,” *Carbon N. Y.*, vol. 60, pp. 229–235, 2013.

[131] K. Ketpang and J. S. Park, “Electrospinning PVDF/PPy/MWCNTs conducting composites,” *Synth. Met.*, vol. 160, no. 15–16, pp. 1603–1608, 2010.

[132] S. Nekouian, M. Sojoodi, and S. Nadri, “Fabrication of conductive fibrous scaffold for photoreceptor differentiation of mesenchymal stem cell,” *J. Cell. Biol.*, 2019.

[133] M. Paligová, J. Vilčákova, P. Sáha, V. Křesálek, J. Stejskal, and O. Quadrat, “Electromagnetic shielding of epoxy resin composites containing carbon fibers coated with polyaniline base,” *Phys. A Stat. Mech. its Appl.*, vol. 335, no. 3–4, pp. 421–429, 2004.

[134] T. H. Ting, Y. N. Jau, and R. P. Yu, “Microwave absorbing properties of polyaniline/multi-walled carbon nanotube composites with various polyaniline contents,” *Appl. Surf. Sci.*, vol. 258, no. 7, pp. 3184–3190, 2012.

[135] A. R.A., Schettini, D. Khastgir, and B. G. Soares, “Microwave Dielectric Properties and EMI Shielding Effectiveness of Poly(styrene-b-styrene- butadiene-styrene) Copolymer Filled With PAni.Dodecylbenzenesulfonic Acid and Carbon Black Anderson,” *Polym. Eng. Sci.*, pp. 2041–2048, 2012.

[136] Y. Huangfu *et al.*, “Fabrication and investigation on the PANI/MWCNT/thermally annealed graphene aerogel/epoxy electromagnetic interference shielding nanocomposites,” *Compos. Part A Appl. Sci. Manuf.*, vol. 121, pp. 265–272, 2019.

[137] J. Yun, J. S. Im, H. Il Kim, and Y. S. Lee, “Effect of oxyfluorination on electromagnetic interference shielding of polyaniline-coated multi-walled carbon nanotubes,” *Colloid Polym. Sci.*, vol. 289, no. 15–16, pp. 1749–1755, 2011.

[138] M. Vosgueritchian, D. J. Lipomi, and Z. Bao, “Highly conductive and transparent PEDOT:PSS films with a fluorosurfactant for stretchable and flexible transparent electrodes,” *Adv. Funct. Mater.*, vol. 22, no. 2, pp. 421–428, 2012.

[139] B. Kim, V. Koncar, and C. Dufour, “Polyaniline-coated PET conductive yarns: Study of electrical, mechanical, and electro-mechanical properties,” *J. Appl. Polym. Sci.*, vol. 101, no. 3, pp. 1252–1256, 2006.

[140] Y. Sun, H. Da Bao, Z. X. Guo, and J. Yu, “Modeling of the electrical percolation of mixed carbon fillers in polymer-based composites,” *Macromolecules*, vol. 42, no. 1, pp. 459–463, 2009.

[141] A. Celzard, E. McRae, C. Deleuze, M. Dufort, G. Furdin, and J. F. Marêché, “Critical concentration in percolating systems containing a high-aspect-ratio filler,” *Phys. Rev. B - Condens. Matter Mater. Phys.*, vol. 53, 1996.

[142] I. Balberg, C. H. Anderson, S. Alexander, and N. Wagner, “Excluded volume and its relation to the onset of percolation,” *Phys. Rev. B - Condens. Matter Mater. Phys.*, vol. 30, no. 7, p. 3933, 1985.

[143] L. M. Castano and A. B. Flatau, “Smart fabric sensors and e-textile technologies: a review,” *Smart Mater. Struct.*, vol. 23, no. 5, p. 053001, 2014.

[144] H. Pang, L. Xu, D. Yan, and Z. Li, “Progress in Polymer Science Conductive polymer

composites with segregated structures," *Prog. Polym. Sci.*, vol. 39, no. 11, pp. 1908–1933, 2014.

[145] A. Kolanowska, D. Janas, A. P. Herman, R. G. Jędrysiak, T. Giżewski, and S. Boncel, "From blackness to invisibility – Carbon nanotubes role in the attenuation of and shielding from radio waves for stealth technology," *Carbon N. Y.*, vol. 126, no. September, pp. 31–52, 2018.

[146] H. G. Ortlek, O. G. Saracoglu, O. Saritas, and S. Bilgin, "Electromagnetic shielding characteristics of woven fabrics made of hybrid yarns containing metal wire," *Fibers Polym.*, vol. 13, no. 1, pp. 63–67, 2012.

[147] T. K;, I. N;"Metal allergy to stainless steel wire after coronary artery bypass grafting," *J. Artif. Organs*, vol. 6, no. 1, pp. 71–72, 2003.

[148] G. N. Flint, "A metallurgical approach to metal contact dermatitis," , *Metall. Contact Dermatitis,* vol. 39, pp. 213–221, 1998.

[149] W. R. Schriver;, R. H. Shereff;, J. Domnitz;, and S. S. E. Swintak, ", Allergic response to stainless steel wire, Oral Surgery," *Oral Med. Oral Pathol.*, vol. 42, no. 5, pp. 578–581, 1976.

[150] B. Weng, F. Xu, and K. Lozano, "Development of hierarchical structured carbon nanotube-nylon nanofiber mats," *J. Appl. Polym. Sci.*, vol. 132, no. 38, pp. 3–9, 2015.

[151] R. R. Bonaldi, E. Siores, and T. Shah, "Characterization of electromagnetic shielding fabrics obtained from carbon nanotube composite coatings," *Synth. Met.*, vol. 187, no. 1, pp. 1–8, 2014.

[152] B. Shen, Y. Li, D. Yi, W. Zhai, X. Wei, and W. Zheng, "Strong flexible polymer/graphene composite films with 3D saw-tooth folding for enhanced and tunable electromagnetic shielding," *Carbon N. Y.*, vol. 113, pp. 55–62, 2017.

[153] D. Negru and C. Buda, "Electrical Conductivity of Woven Fabrics Coated with Carbon Black Particles," *FIBRES Text. East. Eur.*, vol. 1, no. 90, pp. 53–56, 2012.

[154] D. J. Thomas, "Ultrafine graphitised MWCNT nanostructured yarn for the manufacture of electrically conductive fabric," pp. 1–4, 2017.

[155] G. H. Motlagh and M. R. T. A.N. Hrymak, "Improved Through-Plane Electrical Conductivity in a Carbon-Filled Thermoplastic via Foaming," *Polym. Eng. Sci.*, vol. 48, no. 4, pp. 687–696, 2008.

[156] M. B. J. B. J. A. J.SchulzfVesselinShanove, “Thermal and electrical conductivity of array-spun multi-walled carbon nanotube yarns,” *Carbon N. Y.*, vol. 50, no. 1, pp. 244–248, 2012.

[157] S. A. Hashemi, S. M. Mousavi, M. Arjmand, N. Yan, and U. Sundararaj, “Electrified single-walled carbon nanotube/epoxy nanocomposite via vacuum shock technique: Effect of alignment on electrical conductivity and electromagnetic interference shielding,” *Polym. Compos.*, vol. 39, pp. E1139–E1148, 2018.

[158] L. Wang, H. Qiu, C. Liang, P. Song, Y. Han, and Y. Han, “Electromagnetic interference shielding MWCNT-Fe 3 O 4 @ Ag / epoxy nanocomposites with satisfactory thermal conductivity and high thermal stability,” *Carbon N. Y.*, vol. 141, pp. 506–514, 2019.

[159] X. Ma, B. Shen, L. Zhang, Y. Liu, and W. Zhai, “Porous superhydrophobic polymer / carbon composites for lightweight and self-cleaning EMI shielding application,” *Compos. Sci. Technol.*, vol. 158, pp. 86–93, 2018.

[160] W. L. Song *et al.*, “Flexible graphene/polymer composite films in sandwich structures for effective electromagnetic interference shielding,” *Carbon N. Y.*, 2014.

[161] M. González, J. Pozuelo, and J. Baselga, “Electromagnetic Shielding Materials in GHz Range,” *Chem. Rec.*, vol. 18, no. 7, pp. 1000–1009, 2018.

[162] X. Ji, D. Chen, Q. Wang, J. Shen, and S. Guo, “Synergistic effect of flame retardants and carbon nanotubes on flame retarding and electromagnetic shielding properties of thermoplastic polyurethane,” *Compos. Sci. Technol.*, vol. 163, pp. 49–55, 2018.

[163] S. Park and J. Ha, “Improved Electromagnetic Interference Shielding Properties Through the Use of Segregate Carbon Nanotube Network,” *Materials (Basel).*, no. 12, pp. 6–13, 2019.

[164] G. Wang *et al.*, “Ultralow-threshold and lightweight biodegradable porous pla/mwcnt with segregated conductive networks for high-performance thermal insulation and electromagnetic interference shielding applications,” *ACS Appl. Mater. Interfaces*, vol. 10, no. 1, pp. 1195–1203, 2018.

[165] S. P. Pawar, P. Rzeczkowski, P. Pötschke, B. Krause, and S. Bose, “Does the Processing Method Resulting in Different States of an Interconnected Network of Multiwalled Carbon Nanotubes in Polymeric Blend Nanocomposites Affect EMI Shielding Properties?,” *ACS Omega*, vol. 3, no. 5, pp. 5771–5782, 2018.

[166] J. K. Yuan, S. H. Yao, A. Sylvestre, and J. Bai, "Biphasic polymer blends containing carbon nanotubes: Heterogeneous nanotube distribution and its influence on the dielectric properties," *J. Phys. Chem. C*, vol. 116, no. 2, pp. 2051–2058, 2012.

[167] Z. Wang, R. Wei, and X. Liu, "Fluffy and Ordered Graphene Multilayer Films with Improved Electromagnetic Interference Shielding over X-Band," *ACS Appl. Mater. Interfaces*, vol. 9, no. 27, pp. 22408–22419, 2017.

[168] Y. Wang, X.-D. Cheng, W.-L. Song, C.-J. Ma, X.-M. Bian, and M. Che, "Hydro-sensitive sandwich structures for self-tunable smart electromagnetic shielding," *Chem. Eng. J.*, vol. 344, pp. 342–352, 2018.

[169] K. Zhang *et al.*, "A facile approach to constructing efficiently segregated conductive networks in poly(lactic acid)/silver nanocomposites via silver plating on microfibers for electromagnetic interference shielding," *Compos. Sci. Technol.*, vol. 156, pp. 136–143, 2018.

[170] B. Weng, F. Xu, A. Salinas, and K. Lozano, "Mass production of carbon nanotube reinforced poly(methyl methacrylate) nonwoven nanofiber mats," *Carbon N. Y.*, vol. 75, pp. 217–226, 2014.

[171] A. Ferreira, F. Ferreira, and M. C. Paiva, "Textile Sensor Applications with Composite Monofilaments of Polymer / Carbon Nanotubes," *Adv. Sci. Technol.*, vol. 80, pp. 65–70, 2013.

[172] Michele T. Byrne and Y. K. Gun'ko, "Recent Advances in Research on Carbon Nanotube–Polymer Composites," *Adv. Mater.*, vol. 22, no. 15, pp. 1672–1688, 2010.

[173] K. Liu *et al.*, "Scratch-Resistant, Highly Conductive, and High-Strength Carbon Nanotube-Based Composite Yarns," *Am. Chem. Soc.*, vol. 4, no. 10, pp. 5827–5843, 2010.

[174] Rafiq I. Noorani, *Rapid prototyping: principles and applications*. 2005.

[175] T. Swetham, K. Madhana, M. Reddy, A. Huggi, and M. N. Kumar, "A Critical Review on of 3D Printing Materials and Details of Materials used in FDM," *Int. J. Sci. Res. Sci. Eng. Technol.*, vol. 3, no. 2, pp. 353–361, 2017.

[176] T. Spahiu, S. Fafenrot, N. Grimmelsmann, E. Piperi, E. Shehi, and A. Ehrmann, "Varying fabric drape by 3D-imprinted patterns for garment design," *IOP Conf. Ser. Mater. Sci. Eng.*, vol. 254, no. 17, 2017.

[177] B. Malengier, C. Hertleer, L. Cardon, and V. L. L, "3D Printing on Textiles : Testing of

Adhesion," *ITMC2017 - Int. Conf. Intell. Text. Mass Cust. 3D*, vol. 1, pp. 1–6, 2017.

[178] A. E. Nils Grimmelsmann, Mirja Lutz, Michael Korger, Hubert Meissner, "Adhesion of 3D printed material on textile substrates Introduction," *Rapid Prototyp. J.*, pp. 7–10, 2014.

[179] E. Pei, J. Shen, and J. Watling, "Direct 3D printing of polymers onto textiles: Experimental studies and applications," *Rapid Prototyp. J.*, vol. 21, no. 5, pp. 556–571, 2015.

[180] R. H. Sanatgar, A. Cayla, C. Campagne, and V. Nierstrasz, "Morphological and electrical characterization of conductive polylactic acid based nanocomposite before and after FDM 3D printing," *J. Appl. Polym. Sci.*, vol. 47040, pp. 1–11, 2018.

[181] C. C. L. Wang, Y. Wang, and M. M. F. Yuen, "Design automation for customized apparel products," *CAD Comput. Aided Des.*, vol. 37, no. 7, pp. 675–691, 2005.

[182] C. C. L. Wang and M. M. F. Yuen, "Editorial: CAD methods in garment design," *CAD Comput. Aided Des.*, vol. 37, no. 6, pp. 583–584, 2005.

[183] A. Cichocka, P. Bruniaux, and I. Frydrych, "3D Garment Modelling - Creation of a virtual mannequin of the human body," *Fibres Text. East. Eur.*, vol. 22, no. 6, pp. 123–131, 2014.

[184] J. McCartney, B. K. Hinds, B. L. Seow, and D. Gong, "Dedicated 3D CAD for garment modelling," *J. Mater. Process. Technol.*, vol. 107, no. 1–3, pp. 31–36, 2000.

[185] J. Wang, G. Lu, W. Li, L. Chen, and Y. Sakaguti, "Computer-Aided Design Interactive 3D garment design with constrained contour curves and style curves," *Comput. Des.*, vol. 41, no. 9, pp. 614–625, 2009.

[186] L. Duan, Z. Yueqi, W. Ge, and H. Pengpeng, "Automatic three-dimensional-scanned garment fitting based on virtual tailoring and geometric sewing," no. 2999, 2019.

[187] Y. Liu, D. Zhang, and M. M. Yuen, "A survey on CAD methods in 3D garment design," *Comput. Ind.*, vol. 61, no. 6, pp. 576–593, 2010.

[188] K. L. LaBat and K. S. Ryan, *Human Body: A Wearable Product Designer's Guide*, 1st ed. CRC Press, 2019.

[189] J. Li and Y. Wang, "Automatically Constructing Skeletons and Parametric Structures for Polygonal Human Bodies," *Digit. Interact. Media Lab, Inst. Autom. Acad. Chinese Sci. Beijing*, 2007.

[190] C. C. L. Wang, "Parameterization and parametric design of mannequins," *CAD Comput. Aided Des.*, vol. 37, no. 1, pp. 83–98, 2005.

[191] B. Allen, B. Curless, and Z. Popović, "The space of human body shapes," *ACM Trans.*

Graph., vol. 22, no. 3, p. 587, 2003.

[192] M. A. Abtew *et al.*, "Female seamless soft body armor pattern design system with innovative reverse engineering approaches," pp. 2271–2285, 2018.

[193] M. Hamad, S. Thomassey, and P. Bruniaux, "A new sizing system based on 3D shape descriptor for morphology clustering," *Comput. Ind. Eng.*, vol. 113, pp. 683–692, 2017.

[194] Y. Hong, X. Zeng, P. Bruniaux, and K. Liu, "Interactive virtual try-on based three-dimensional garment block," *Text. Res. J.*, no. October, 2016.

[195] A. Rudolf, A. Cupar, T. Kozar, and Z. Stjepanović, "Study Regarding the Virtual Prototyping of Garments for Paraplegics," *Fibers Polym.*, vol. 16, no. 5, pp. 1177–1192, 2015.

[196] Z. STJEPANOVIČ, A. Cupar, A. Rudolf, S. JEVŠNIK, and T. K. STJEPANOVIČ, "Construction of adapted garments for people with scoliosis using virtual prototyping and CASP method," *Ind. Textila*, vol. 67, no. 2, pp. 141–149, 2016.

[197] F. Cordier, H. Seo, and N. Magnenat-Thalmann, "Made-to-measure technologies for an online clothing store," *IEEE Comput. Graph. Appl.*, vol. 23, no. 1, pp. 38–48, 2003.

[198] A. Rudolf and A. Cupar, "Designing an adaptive 3D body model suitable for people with limited body abilities Textile Science & Engineering Designing an Adaptive 3D Body Model Suitable for People with Limited Body Abilities," no. August, 2014.

[199] C. Groß, A. Fuhrmann, and V. Luckas, "Automatic pre-positioning of virtual clothing," *Proc. 18th spring Conf. Comput. Graph. - SCCG '03*, vol. 1, no. 212, p. 99, 2003.

[200] S. S. M. Ho, W. W. M. Yu, T. T. Lao, D. H. K. Chow, J. W. Y. Chung, and Y. Li, "Garment needs of pregnant women based on content analysis of in-depth interviews," no. 852, pp. 2426–2435, 2009.

[201] S. A. Lederman, A. Paxton, S. B. Heymsfield, J. Wang, J. Thornton, and R. N. P. Jr, "Body fat and water changes during pregnancy in women with different body weight and weight gain," *Obstet. Gynecol.*, vol. 90, no. 4, pp. 483–488, 1997.

[202] E. B. Calvo *et al.*, "Reference charts for weight gain and body mass index during pregnancy obtained from a healthy cohort," *J. Matern. Neonatal Med.*, vol. 22, no. 1, pp. 36–42, 2009.

[203] G. Wu, S. Liu, X. Wu, and X. Ding, "Research on lower body shape of late pregnant women in Shanghai area of China," *Int. J. Ind. Ergon.*, vol. 46, pp. 69–75, 2015.

[204] P. Georgeta, M. Alexandra, and O. Sabina, "Innovative clothing design for women during pregnancy," *Ann. Univ. Oradea Fascicle Text. Innov.*, pp. 67–72.

[205] C. Quintero Rodriguez, A. Anisimova, S. Ryan, and O. Troynikov, "Critical design aspects of maternity support-garments and its contemporary perspective," *KnE Eng.*, vol. 2, no. 2, p. 91, 2017.

[206] M. Sohn and E. Bye, "Visual analysis of body shape changes during pregnancy," *Int. J. Fash. Des. Technol. Educ.*, vol. 5, no. February, pp. 117–128, 2012.

[207] Y.E.El Mogahzy, "Types of fabric for textile product design," in *Engineering Textiles*, no. 1, Woodhead Publishing, 2009, pp. 271–299.

[208] "ASTM D3883 - 04 (Standard Test Method for Yarn Crimp and Yarn Take-up in Woven Fabrics)," 2008.

[209] P. D. Dubrovski, "Volume porosity of Woven Fabrics," *Text. Res. J.*, vol. 70, no. 10, pp. 915–919, 2000.

[210] F. T. Peirce and J. R. Womersley, *Cloth Geometry*. Manchester, UK: The Textile Institute, 1978.

[211] STandard by ASTM Internationa, *Standard Test Method for D-C Resistance or Conductance of Moderately Conductive Materials*. .

[212] M. González, G. Mokry, M. De Nicolás, J. Baselga, and J. Pozuelo, "Carbon nanotube composites as electromagnetic shielding materials in GHz range," in *Carbon Nanotubes - Current Progress of their Polymer Composites*, 2016.

[213] V. David, E. Vremera, A. Salceanu, I. Nica, and O. Baltag, "On the characterization of electromagnetic shielding effectiveness of materials," no. 4.

[214] E. R. C. Report, Electronic Communications office, Electronic Communications Comitte, European Conference, and Telecommunications Administrations, "The European Table Of Frequency Allocations And Applications In The Frequency Range 8 . 3 Khz To 3000 Ghz (ECA Table)," *Eur. Conf. Post. Telecommun. Adm.*, no. May, 2015.

[215] M. J. Toghchi *et al.*, "The effects of the structural parameters of three-dimensional warp interlock woven fabrics with silver-based hybrid yarns on electromagnetic shielding behavior," *Text. Res. J.*, 2019.

[216] H. OZdemir, S. Ugurlu, and A. Ozkurt, "The electromagnetic shielding of textured steel yarn based woven fabrics used for clothing," *J. Ind. Text.*, vol. 45, no. 3, pp. 416–436,

2015.

[217] U. Szeluga, B. Kumanek, and B. Trzebicka, “Synergy in hybrid polymer/nanocarbon composites. A review,” *Compos. Part A Appl. Sci. Manuf.*, vol. 73, pp. 204–231, 2015.

[218] W. De Zhang, L. Shen, I. Y. Phang, and T. Liu, “Carbon nanotubes reinforced nylon-6 composite prepared by simple melt-compounding,” *Macromolecules*, vol. 37, no. 2, pp. 256–259, 2004.

[219] P. C. Ma *et al.*, “Electrical conducting behavior of hybrid nanocomposites containing carbon nanotubes and carbon black,” *2007 Int. Conf. Electron. Mater. Packag.*, no. December 2007, pp. 1–4, 2007.

[220] *Product Information TORZEN ® U4803 NC01 PA66 Resin*. 2011, p. 4803.

[221] E. P. T. Spahiu, N. Grimmelsmann, A. Ehrmann and E. Shehi, “Effect of 3D printing on textile fabric,” no. November, 2017.

[222] IEC, “62220-1-2 Internationale International Standard Internationale International Standard,” no. 124211, 2006.

[223] “FTTS-FA-003: Test Method of Specified Requirements of Electromagnetic Shielding Textiles.,” Taiwan, 2003.

[224] M. Javadi Toghchi *et al.*, “Virtual Mannequin Simulation for Customized Garment Manufacturing,” *Designs*, vol. 3, no. 53, pp. 1–17, 2019.

[225] M. De Onis, C. Garza, A. W. Onyango, and E. Borghi, “Comparison of the WHO Child Growth Standards and the CDC 2000 Growth Charts 1,” pp. 144–148, 2006.

[226] A. Ölin and S. Rössner, “Factors Related to Body Weight Changes During and After Pregnancy: The Stockholm Pregnancy and Weight Development Study,” *Obes. Res.*, vol. 4, no. 3, pp. 271–276, 1996.

[227] W. E.Brenner, D. A. Edelman, and C. H. Hendricks, “A standard of fetal growth for the united states of America,” *Am. J. Obstet. Gynecol.*, vol. 126, no. 5, pp. 555–564, 1976.

[228] A. F Barbara and R. K. L. Jr., “Prepregnancy weight, weight gain, and birth weight,” *Am. J. Obstet. Gynecol.*, vol. 154, no. 3, pp. 503–509, 1986.

[229] B. Hamad, M. Hamad, S. Thomassey, and P. Bruniaux, “3D Adaptive Morphotype Mannequin for Target Population,” *J. Ergon.*, vol. 8, no. 2, 2018.

[230] S. Efrat, “The development of a method for generating patterns for garments that conform to the shape of the human body.,” De Montfort University-PhD thesis, 1982.

[231] S. Thomassey and P. Bruniaux, "A template of ease allowance for garments based on a 3D reverse methodology," *Int. J. Ind. Ergon.*, vol. 43, no. 5, pp. 406–416, 2013.

[232] Y. Chen *et al.*, "A new method of ease allowance generation for personalization of garment design," 2008.

[233] M. Kulinska, "Digital tools for developing customized co-design platform with integration of comfort and fashion," 2018.